Constraints on the Reactivity and Components of Nocturnal Nitrogen Oxides

Theran P. Riedel

A dissertation
submitted in partial fulfillment of the
requirements for the degree of

Doctor of Philosophy

University of Washington

2013

Reading Committee:

Joel A. Thornton, Chair
Philip J. Reid
Becky Alexander

Program Authorized to Offer Degree:
Department of Chemistry

University of Washington

Abstract

Constraints on Reactivity and Components of Nocturnal Nitrogen Oxides

Theran P. Riedel

Chair of the Supervisory Committee:
Associate Professor Joel Thornton
Department of Atmospheric Sciences

NO and NO_2 (NO_x) are fundamentally important species to tropospheric chemistry. NO_x abundances are tied to ozone production and thus determine the oxidizing capacity of the troposphere. Nocturnal reactions of NO_x are often considered a major loss pathway for NO_x and ozone. Recent measurements have shown that nitryl chloride ($ClNO_2$) is produced at night by reactions of dinitrogen pentoxide (N_2O_5) on chloride containing particles. $ClNO_2$ is photolyzed during the morning hours after sunrise to liberate highly reactive chlorine atoms. This chemistry takes place primarily in polluted environments where the concentrations of N_2O_5 precursors, NO_x, and ozone, are high, though it can likely occur in remote regions at lower intensities. The following describes estimates and ambient measurements of the reactive processes central to $ClNO_2$ formation and field measurements illustrating the potential importance of $ClNO_2$ as a NO_x reservoir and as a chlorine atom source.

The nocturnal reactions of N_2O_5 to form $ClNO_2$ were traditionally thought of as marine phenomena given the more obvious source of particle-phase chloride offered by sea spray emissions. However, long term chemical measurement databases and aerosol thermodynamic models are employed to show that this chemistry is likely widespread as is suggested by recent

field measurements of $ClNO_2$ in Boulder, CO, a site far removed from local sea salt aerosol sources.

Direct measurements of N_2O_5 reaction probability on ambient aerosol particles were made in La Jolla, CA, using a custom flow reactor alongside measurements of aerosol particle size distributions and non-refractory composition. The largest apparent driver of day-to-day variability in the measured reaction probabilities at this site was the particle nitrate loading. The relative change as a function of particle nitrate illustrates the atmospheric importance of the so-called "nitrate effect" on N_2O_5 heterogeneous reactions that lead to the formation of $ClNO_2$.

The magnitude and sources of chlorine atoms in marine air remain highly uncertain but have potentially important consequences for air quality in polluted coastal regions. Continuous measurements of ambient nitryl chloride and molecular chlorine concentrations were made in southern California. In the Los Angeles region, $ClNO_2$ was more ubiquitous than Cl_2 during most nights of the study period. These observations are used to estimate the relative importance of chlorine atom sources in the polluted marine boundary layer. In contrast to the emphasis in previous studies, $ClNO_2$ and hydrochloric acid are likely the dominant primary chlorine atom sources for the Los Angeles basin.

As part of a wintertime field study in Weld County, CO, vertically resolved $ClNO_2$ and Cl_2 measurements taken on a 300 meter tall tower are reported. Gas and particle phase measurements aboard a moveable tower carriage allowed for a detailed description of the chemical state of the nocturnal atmosphere as a function of height. These observations show significant vertical structure in $ClNO_2$ and Cl_2 mixing ratios that undergo dynamic changes over the course of a night. From these measurements $ClNO_2$ yields from N_2O_5-aerosol reactions are inferred. The derived yields in these plumes suggest efficient $ClNO_2$ production within distinct combustion plumes originating from the Denver-Boulder urban corridor.

Finally, the effects of $ClNO_2$ production, photolysis, and subsequent chlorine atom reactions on chemical species relevant to air quality are examined. $ClNO_2$ formation is incorporated into an existing Master Chemical Mechanism box model framework constrained by a large number of measurements taken during field studies in a polluted coastal environment. These results are compared to model runs excluding $ClNO_2$ formation to assess the effects of $ClNO_2$ on tropospheric oxidants, ozone, and nitrogen oxide partitioning.

TABLE OF CONTENTS

LIST OF FIGURES

Chapter 5

Chapter 6

LIST OF TABLES

Acknowledgements

First and foremost I wish to thank my advisor Joel Thornton who has patiently and expertly guided me through this part of my life and instilled in me a great appreciation for understanding the complete story behind the observations. His passion for atmospheric chemistry is only surpassed by his ability to teach it. Taking your introductory course in atmospheric chemistry has turned into one of the best decisions I have made. It has brought me to where I am today, and I am thankful and in debt to you for that and so many other things.

I am also grateful to the other members of the Thornton research group: Glenn Wolfe, Reddy Yatavelli, Sara Harrold, Beth Friedman, Felipe Lopez-Hilfiker, Julia Wargo, Claudia Mohr, Cassandra Gaston, Ben Lee, Jim Kercher, and Tim Bertram. I will always value our time together and how much I have learned from each of you.

All of the work described in this dissertation could not have been accomplished without the help of a countless number of coauthors and contributors. As such I am indebted to all them for their vital involvement. Additionally, I acknowledge the financial support provided by the NASA Earth and Space Science Fellowship NNX10AN48H.

Finally, I must thank my family and friends. I cannot help but feel blessed to know such wonderful people. Chiefly among them I wish to thank my parents, Tom and Therese. Throughout my life your support and love has been unyielding. I am so proud to have you as parents. And to Anna, my sister, I'm sorry for breaking your tooth when we were kids and thank you for the Nutri-Grain bar.

Chapter 1

Introduction

1.1 NO_x and NO_x Reservoirs in the Troposphere

Nitrogen oxide radicals ($NO_x \equiv NO + NO_2$) influence air quality and climate by regulating tropospheric ozone (O_3) production and hydroxyl radical (OH) abundances. These influences in turn affect the lifetime of the greenhouse gas methane, a volatile organic compound (VOC), and aerosol mass formation by the formation of oxidized VOC that can condense to the particle phase, often referred to as secondary organic aerosol or SOA (Fry et al., 2009; Jacob, 2000; Osthoff et al., 2008; Shindell et al., 2009). Ozone and aerosol particles can influence Earth's radiation budget and also cause adverse health effects and are therefore regulated by the Environmental Protection Agency. NO_x is present largely through emissions from anthropogenic activities such as motor vehicle use, industrial processes, agriculture, biomass burning, and power generation. Anthropogenic NO_x emissions have been increasing since pre-industrial times and are expected to continue to increase globally, especially in developing regions with high population densities (Ohara et al., 2007; Streets and Waldhoff, 2000; Yienger et al., 1999).

Figure 1 illustrates how the rapid daytime cycling between NO_2 and NO catalytically produces ozone in the troposphere. At night, however, this ozone production engine stops and the ozone formed during the day converts NO_x to the nitrate radical (NO_3) by the reaction of NO_2 with O_3. The nitrate radical can react with VOC or with NO_2 to form dinitrogen pentoxide (N_2O_5) which can react on particles with some reaction probability (γ_{N2O5}) to form highly soluble nitric acid (HNO_3) which is efficiently removed from the atmosphere through deposition on a

timescale of a few hours, or, if there is ample chloride available in the aerosols, nitryl chloride ($ClNO_2$). These reactions are summarized in Figure 2. Reactions of NO_3 with VOC and of N_2O_5 with aerosol particles are thought to account for ~50% of NO_x removal in polluted regions, thereby exerting a potentially strong influence on ozone production and oxidant levels (Brown et al., 2004; Dentener and Crutzen, 1993).

Despite the aforementioned importance of NO_x, our current quantitative understanding of nocturnal NO_x chemistry remains incomplete. In particular, the rates and products of N_2O_5 reactions with aerosol particles are poorly quantified under conditions and compositions typical of the nocturnal atmosphere. In addition, we have only recently begun to assess the branching (shown in Figure 2 as ϕ; also commonly referred to as the $ClNO_2$ yield) between permanent NO_x reservoirs (e.g. HNO_3) and temporary ones such as and $ClNO_2$ under atmospheric conditions. It is well known that the reaction of N_2O_5 with chloride containing mixtures (sea spray, brine solutions, etc.) produces $ClNO_2$ (Behnke et al., 1997; Thornton and Abbatt, 2005). The nitryl chloride production channel is of interest since during the night $ClNO_2$ remains largely unreactive but undergoes photolysis during the daytime during which NO_2 and Cl are liberated. Thus $ClNO_2$ is a nighttime NO_x reservoir, the formation of which may reduce the efficiency of NO_x removal by nighttime reactions of NO_3 and N_2O_5 described above. Additionally, atomic chlorine is known to be an extremely strong oxidant, with rate constants for VOC reactions 10 – 100 times larger than that of OH, the major tropospheric oxidant. Given this information chlorine atoms could represent an important oxidant source in regions where they form in appreciable quantities.

The research described hereafter addresses the lack of quantitative understanding in abovementioned areas and focuses on developing and applying novel experimental techniques to

determine through *in situ* observations the rates and products of N_2O_5 reactions on particles, and ultimately the effect of these reactions on tropospheric chemistry.

1.2 CIMS Measurement of Nocturnal NO_x Reservoirs

Chemical Ionization Mass Spectrometry (CIMS) is the core analytical technique used here to detect these nocturnal NO_x species. In particular, a quadrupole-based mass spectrometer with the iodide (I^-) reagent ion is used to make measurements of N_2O_5 and $ClNO_2$ concentrations in ambient air and of the N_2O_5 reactive uptake rate to atmospheric particles. The custom-built CIMS shown in Figure 3 is composed of three main regions: i) an ion-molecule reaction region, ii) a collisional dissociation chamber (CDC), iii) and a differentially pumped vacuum chamber housing an octupole ion guide and quadrupole mass spectrometer. A more complete discussion of the instrumental details can be found in other publications (Bertram et al., 2009a; Kercher et al., 2009). The operation and capabilities are briefly summarized below.

Ambient air is sampled through a critical orifice (pinhole) at ~2 standard liters per minute (slpm) and into the ion-molecule reaction region (IMR). The ion-molecule reaction region is a stainless steel tube, 8 cm long, 4 cm ID, held at 60 Torr. Iodide reagent ions are generated and introduced into the IMR region perpendicular to the main flow axis by passing dilute methyl iodide (CH_3I) in a nitrogen (N_2) carrier flow through a commercial ^{210}Po ion source.

A fraction of the reagent ion gas mixture passes through another critical orifice into the 1.5 Torr collisional dissociation chamber (CDC) which is made up of a series of 4 differentially biased static lenses. Here the electric field is maintained to effectively break apart water-analyte clusters while keeping the iodide-analyte clusters intact, effectively maximizing the analyte signal.

The ions exit the CDC through another critical orifice and enter the 3 mTorr octupole region. The octupole itself is made up of 8 stainless steel rods (3.175 mm OD, 4 cm length). It uses a radio frequency (RF) to focus the ions into a narrow beam prior to passing through another critical orifice for mass selection by the quadrupole and detection by a dynode and an off-axis electron multiplier. The species under investigation are detected as ion clusters with high sensitivity (~5 Hz/pptv) and relatively low background (~10 Hz), an ideal situation for measuring small changes in trace gases present in the atmosphere.

Ambient N_2O_5, $ClNO_2$ and Cl_2 concentration measurements are obtained by directly sampling air into the CIMS where the species are detected as ion clusters, $I\cdot(N_2O_5)^-$, $I\cdot(ClNO_2)^-$, and $I\cdot(Cl_2)^-$. Measured ion signals are converted to ambient air concentrations by calibration factors which are dependent on atmospheric water vapor concentrations, flow and pressure regulation, and detector age among other things. For $ClNO_2$ calibrations, a known concentration of N_2O_5, typically provided by a cavity ring-down measurement based on the known NO_3 absorption cross-section, is passed over a wetted NaCl bed converting the N_2O_5 to $ClNO_2$ by reaction R1 with near unit yield (Kercher et al., 2009). Cl_2 calibration factors are obtained from standard concentrations of Cl_2 delivered to the CIMS by a standard permeation source. For further independent confirmation of our $ClNO_2$ sensitivity, we also convert Cl_2 to $ClNO_2$ on an $NaNO_2$ salt bed via reaction R2 (Schweitzer et al., 1998). This approach is beneficial as it does not require an external measurement of N_2O_5 concentration which is difficult to synthesize, store, and deliver. This latter approach also allows for the calibration factors to be determined at higher time resolution, thus having a higher probability to capture any variability in the instrumental sensitivity. However, the yield of $ClNO_2$ from reaction R2 is not as well characterized as that for reaction R1, so the calibration factors from this approach are more uncertain as a result.

$$N_2O_5(g) + NaCl(aq) \longrightarrow ClNO_2(g) + NaNO_3(aq) \quad \text{(R1)}$$

$$Cl_2(g) + NaNO_2(s) \longrightarrow ClNO_2 + NaCl \quad \text{(R2)}$$

During field deployments it is also important to perform frequent assessments of inlet transmission and potential artifact generation on sampling tube walls. This is typically done by adding a small flow of nitrogen carrying N_2O_5 to the tip of the sampling inlet using ambient air as dilution and monitoring the $ClNO_2$ and Cl_2 signals. Finally, the instrumental zero for N_2O_5, $ClNO_2$, and Cl_2 is determined by passing sampled air over a hot (200°C) stainless steel mesh prior to detection which catalytically destroys $ClNO_2$.

1.3 Measuring N_2O_5 Reactivity

To assess the reactivity of N_2O_5 on different aerosol compositions, we use the CIMS and a cylindrical flow reactor that previously has been used for the first-ever direct measurements of N_2O_5 reactivity on ambient aerosol particles (Bertram et al., 2009a; Bertram et al., 2009b). Ambient air is sampled at 2 standard liters per minute (slpm) into a conical aluminum inlet either directly or first through a glass woven filter that removes ~99% of the aerosol surface area. The reaction of excess NO_2 with ozone, produced from the photolysis of O_2 in high purity air, serves as the N_2O_5 and NO_3 source. A small flow of N_2 containing the N_2O_5 and NO_3 in a fixed ratio from the relatively constant source is then added to the ambient air stream. The main body of the flow reactor is a 15 cm inner diameter, 90 cm long stainless-steel tube which is coated with a halocarbon wax to suppress wall reactions. The dimensions and flow rate give a residence time (t_{res}) of ~8 minutes. The flow reactor setup is shown in Figure 4.

The heterogeneous reaction rate of N_2O_5 on aerosol particles is determined by the product of two quantities, the collision frequency between N_2O_5 molecules and particle surface area in a volume of air and the probability that N_2O_5 reacts given a collision (γ_{N2O5}), as shown in Eq. 1. By monitoring the constant source of N_2O_5 and cycling between filter states, the reactive uptake coefficient for N_2O_5 can be directly retrieved. Under constant wall loss conditions, the relative changes in the N_2O_5 signal between the filter on/off states can be used to extract desired kinetic information such as the N_2O_5 reactive uptake coefficient. This technique has demonstrated a single-point precision of ± 0.01 for the reaction probability measurement at a particle surface area concentration of 100 $\mu m^2 m^{-3}$. In polluted regions, we have routinely sampled air with surface area concentrations approaching 300 μm^2 m^{-3} for which the precision improves to ±0.003 (Bertram et al., 2009a).

$$\frac{d[N_2O_5]}{dt} = -\frac{\gamma_{N_2O_5}[N_2O_5]SA\omega}{4} \quad (1)$$

It is well known from nearly two decades of laboratory studies that γ_{N2O5} is a strong function particle composition. Due to the highly complex and poorly constrained nature of particle composition, there are significant challenges for accurately incorporating N_2O_5 reactions into atmospheric chemical models. Regional air quality models and research-grade chemical-transport models must therefore parameterize quantities like the N_2O_5-particle reaction probability and $ClNO_2$ branching to facilitate rapid computations. For the most part these parameterizations are based on laboratory studies of N_2O_5 reactions on highly simplified aerosol compositions which have only recently begun to be tested with field observations (Bertram et al.,

2009b; Brown et al., 2006), thus illustrating the need for supporting measurements on ambient aerosols.

1.4 Box Model Analysis

A number of the previously mentioned chemical processes can be addressed by using an observationally constrained 0-D time-dependent chemical box model. For example:

1) Are laboratory-derived parameterizations of the N_2O_5 reactivity and aerosol composition measurements capable of reproducing observed N_2O_5 reactivity?

2) Are $ClNO_2$ yields from N_2O_5 reactions predicted by laboratory studies consistent with those inferred from *in situ* observations?

A box model approach essentially treats the atmosphere as a static reactor that freely evolves over a predefined period of time. Initial model inputs are often a simplified set of chemical concentrations and conditions representative of the atmosphere at a particular time. Observations of NO, NO_2, O_3, VOC, aerosol surface area, particulate chloride content, relative humidity, and temperature taken during a particular event are used as fixed model constraints. More poorly constrained quantities such as reaction time, aerosol pH, the N_2O_5 reaction probability, and the $ClNO_2$ yield can be used as adjustable parameters that are varied in order to bring the best possible agreement between model output and actual observations. Finally, rate equations corresponding to the production and loss of a chemical species, *X*, (see Eq. 2 for

example) are integrated using an ordinary differential equation (ODE) solver to determine the time-dependent concentrations ($d[X]/dt$) of all of the chemical species tracked in the model.

$$\frac{d[X]}{dt} = \sum \text{source reaction rates} - \sum \text{sink reaction rates} \quad (2)$$

References

Behnke, W., George, C., Scheer, V., and Zetzsch, C.: Production and decay of ClNO2 from the reaction of gaseous N2O5 with NaCl solution: Bulk and aerosol experiments Journal of Geophysical Research-Atmospheres, 102, 3795-3804, 1997.

Bertram, T. H., Riedel, T. P., and Thornton, J. A.: An experimental technique for the direct measurement of N_2O_5 reactivity on ambient particles, AMT, 2, 193-204, 2009a.

Bertram, T. H., Thornton, J. A., Riedel, T. P., Middlebrook, A. M., Bahreini, R., Bates, T. S., Quinn, P. K., and Coffman, D. J.: Direct observations of N_2O_5 reactivity on ambient aerosol, GRL, 36, 2009b.

Brown, S. S., Dibb, J. E., Stark, H., Aldener, M., Vozella, M., Whitlow, S., Williams, E. J., Lerner, B. M., and Jakoubek, R.: Nighttime removal of NO_x in the summer marine boundary layer, GRL, 31, 2004.

Brown, S. S., Ryerson, T. B., Wollny, A. G., Brock, C. A., Peltier, R., Sullivan, A. P., Weber, R. J., Dube, W. P., Trainer, M., Meagher, J. F., Fehsenfeld, F. C., and Ravishankara, A. R.: Variability in Nocturnal Nitrogen Oxide Processing and Its Role in Regional Air Quality, Science, 311, 67-70, 2006.

Dentener, F. J., and Crutzen, P. J.: Reaction of N2O5 on Tropospheric Aerosols: Impact on the Global Distributions of NO_x, O_3, and OH JGR, 98, 7149-7163, 1993.

Fry, J. L., Keindler-Scharr, A., Rollins, A. W., Wooldridge, P. J., Brown, S. S., Fuchs, H., Dube, W., Mensah, A., Maso, M. d., Tillmann, R., Dorn, H.-P., Brauers, T., and Cohen, R. C.: Organic nitrate and secondary organic aerosol yield from NO_3 oxidation of beta-pinene evaluated using a gas-phase kinetics/aerosol partitioning model, ACP, 9, 1431–1449, 2009.

Jacob, D. J.: Heterogeneous chemistry and tropospheric ozone, Atmospheric Environment, 34, 2131, 2000.

Kercher, J. P., Riedel, T. P., and Thornton, J. A.: Chlorine activation by N_2O_5: simultaneous, in situ detection of $ClNO_2$ and N_2O_5 by chemical ionization mass spectrometry, AMT 2, 193-204, 2009.

Ohara, T., Akimoto, H., Kurokawa, J., Horii, N., Yamaji, K., Yan, X., and Hayasaka, T.: An Asian emission inventory of anthropogenic emission sources for the period 1980-2020, Atmospheric Chemistry and Physics, 7, 4419-4444, doi: 10.5194/acp-7-4419-2007, 2007.

Osthoff, H. D., Roberts, J. M., Ravishankara, A. R., Williams, E. J., Lerner, B. M., Sommariva, R., Bates, T. S., Coffman, D., Quinn, P. K., Dibb, J. E., Stark, H., Burkholder, J. B., Talukdar, R. K., Meagher, J., Fehnsenfeld, F. C., and Brown, S. S.: High levels of nitryl chloride in the polluted subtropical marine boundary layer Nature Geoscience, 1, 2008.

Schweitzer, F., Mirabel, P., and George, C.: Multiphase Chemistry of N_2O_5, $ClNO_2$, and $BrNO_2$, J. Phys. Chem. A, 102, 3942-3952, 1998.

Shindell, D. T., Faluvegi, G., Koch, D. M., Schmidt, G. A., Unger, N., and Bauer, S. E.: Improved Attribution of Climate Forcing to Emissions, Science, 326, 716-718, 2009.

Streets, D. G., and Waldhoff, S. T.: Present and future emissions of air pollutants in China:: SO_2, NO_x, and CO, Atmospheric Environment, 34, 363-374, doi: http://dx.doi.org/10.1016/S1352-2310(99)00167-3, 2000.

Thornton, J. A., and Abbatt, J. P. D.: N_2O_5 Reaction on Submicron Sea Salt Aerosol: Kinetics, Products, and the Effect of Surface Active Organics, Journal of Physical Chemistry A, 109, 10004-10012, 2005.

Yienger, J. J., Klonecki, A. A., Levy, H., Moxim, W. J., and Carmichael, G. R.: An evaluation of chemistry's role in the winter-spring ozone maximum found in the northern midlatitude free troposphere, JGR-Atmospheres, 104, 3655, 1999.

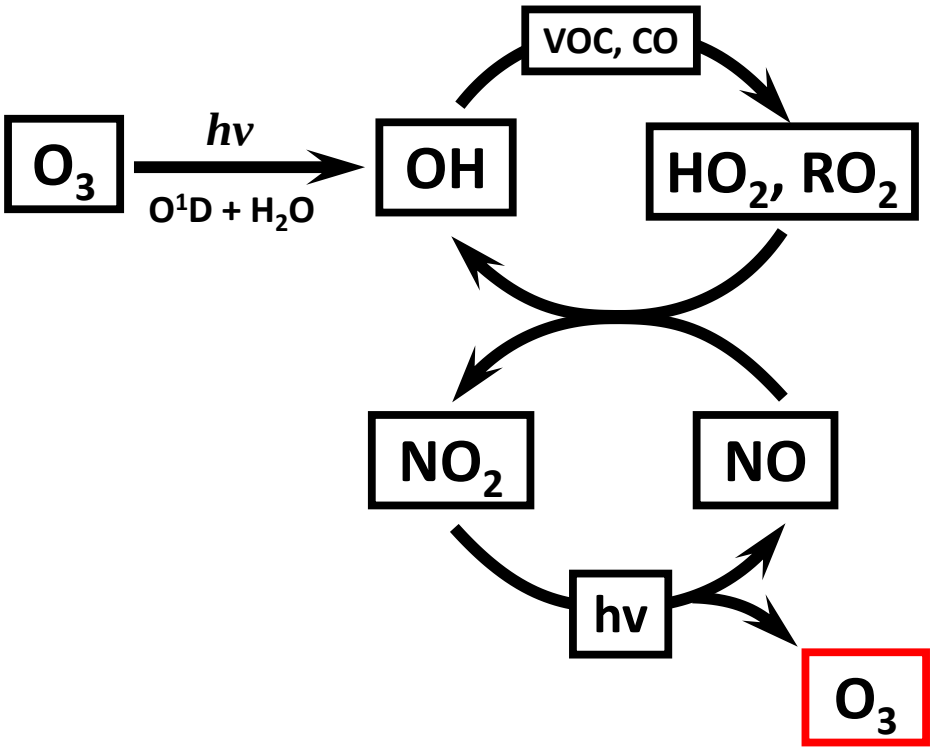

Figure 1.1 Catalytic ozone production mechanism in the troposphere.

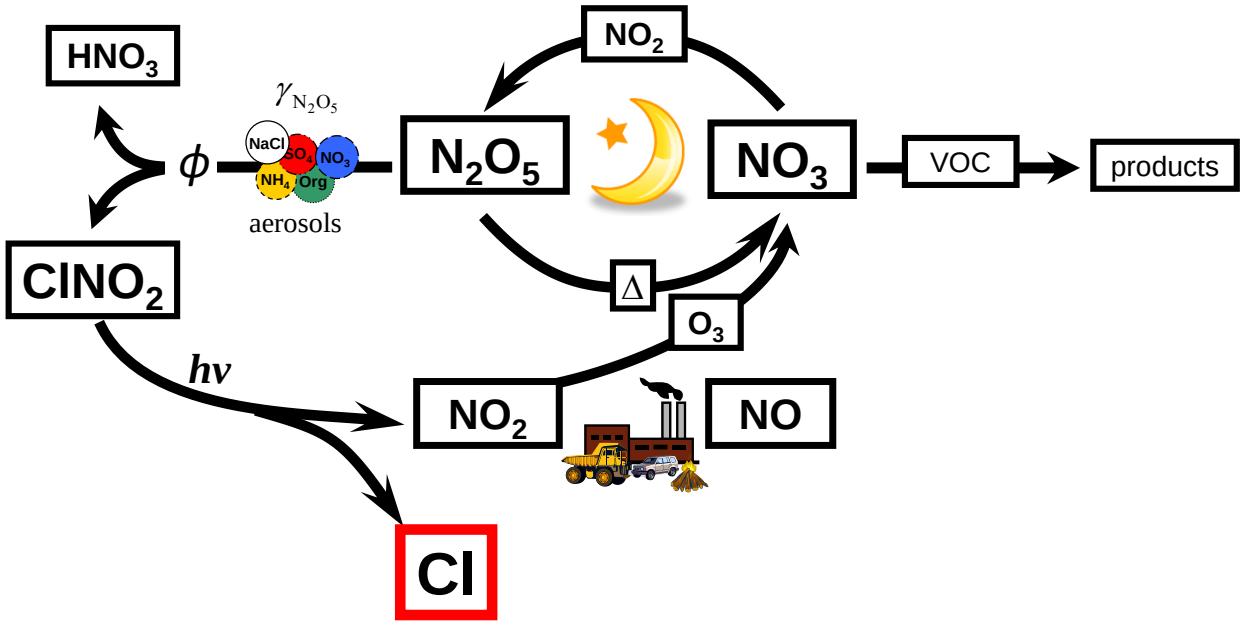

Figure 1.2 Summary of nocturnal NO_x reactions and potential for halogen atom generation with sunrise.

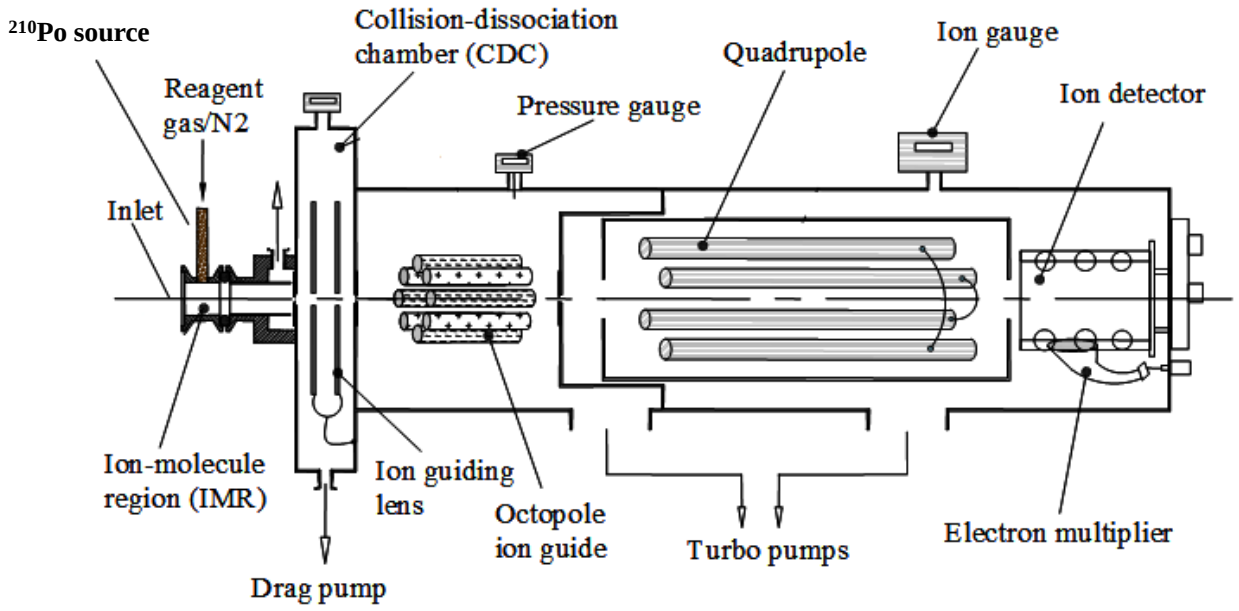

Figure 1.3 Schematic of the chemical ionization mass spectrometer (CIMS) used to measure N_2O_5, $ClNO_2$, and other relevant atmospheric chemical species.

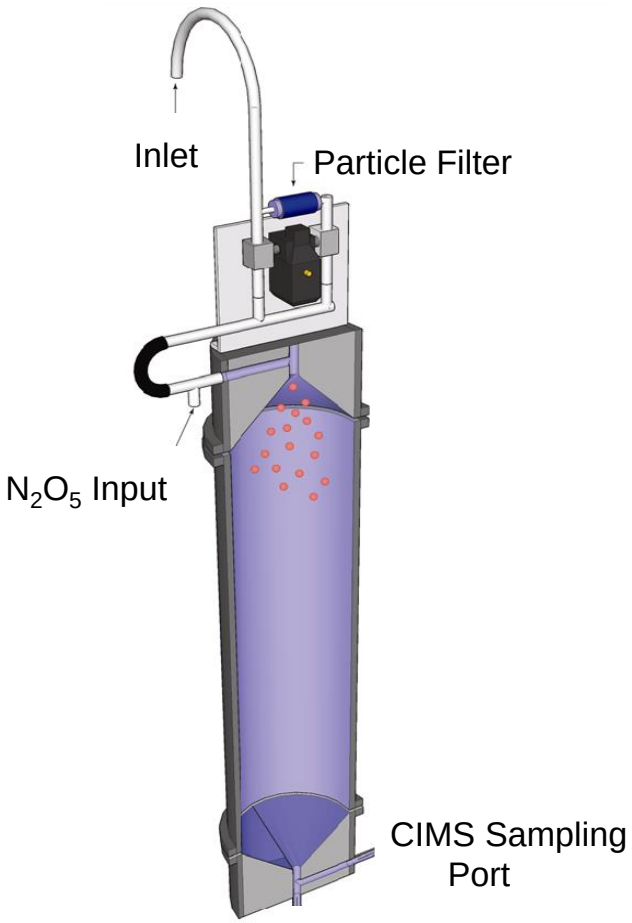

Figure 1.4 Illustration of the flow reactor setup used to obtain *in situ* measurements of the N_2O_5-aerosol reaction probability.

Chapter 2

Observationally Constrained Estimates of Nitryl Chloride Production on Regional and Global Scales

2.1 Introduction

During the nighttime, in the presence of ozone, NO_x is converted into the nitrate radical, NO_3, and dinitrogen pentoxide, N_2O_5, through reactions R1 – R3. Heterogeneous reactions of N_2O_5 with chloride containing mixtures have been shown to produce nitryl chloride, $ClNO_2$, with high yields, and recently this process has been shown to occur in ambient air on chloride containing aerosols (reaction R4) (Finlayson-Pitts et al., 1989; Osthoff et al., 2008). The importance of the $ClNO_2$ formation channel is multifold. In the absence of $ClNO_2$ production, N_2O_5 reactions produce exclusively HNO_3 via reaction R5, which, due to the efficient deposition to surfaces and scavenging by precipitation of HNO_3, is a terminal sink for NO_x, and its formation therefore acts to decrease the atmosphere's oxidizing capacity. $ClNO_2$, on the other hand, is largely unreactive during the night and is quantitatively photolyzed during the first few hours of the morning, recycling NO_2 and liberating atomic chlorine (reaction R6). Atomic chlorine is a powerful oxidant, often having reaction rate constants with tropospheric organic species that are orders of magnitude larger than that of the hydroxyl radical, OH. Thus, the production of $ClNO_2$ potentially reduces the efficiency of NO_x removal by N_2O_5 reactions to form HNO_3 while simultaneously introducing a strong morning oxidant source (Osthoff et al., 2008). Additionally, it has been shown that $ClNO_2$ may react on acidic chloride-containing aerosol to form Cl_2 which also photolyzes during the daytime to liberate Cl-atoms (Roberts et al.,

2008). Such a pathway would potentially increase the morning oxidant source from nighttime NO_x chemistry.

$$NO + O_3 \rightarrow NO_2 + O_2 \quad \text{(R1)}$$

$$NO_2 + O_3 \rightarrow NO_3 + O_2 \quad \text{(R2)}$$

$$NO_3 + NO_2 + M \underset{\Delta}{\rightleftharpoons} N_2O_5 + M \quad \text{(R3)}$$

$$N_2O_5 + Cl^-(aq) \rightarrow ClNO_2 + NO_3^-(aq) \quad \text{(R4)}$$

$$N_2O_5 + H_2O(l) \rightarrow 2HNO_3 \quad \text{(R5)}$$

$$ClNO_2 + h\nu \rightarrow Cl\bullet + NO_2 \quad \text{(R6)}$$

The dominant global source of chloride is wind and wave generated sea spray (Graedel and Keene, 1995). It has thus long been expected that $ClNO_2$ production would only occur in polluted coastal or marine air (Finlayson-Pitts et al., 1989; Knipping and Dabdub, 2003), but through the use of long term chemical measurement databases and aerosol thermodynamic models described below, we show that this chemistry is likely widespread as suggested by recent field measurements of $ClNO_2$ in Boulder, CO (Thornton et al., 2010).

2.2 Particle Phase $ClNO_2$ Formation Mechanism

In the currently accepted mechanism for N_2O_5 reactions on aqueous solutions (R7 – R10), the instantaneous branching between HNO_3 formation (R10) and $ClNO_2$ production (R9) is determined by the competition between liquid water, H_2O, and chloride for the electron deficient intermediate presumed to be similar to solvated NO_2^+ (shown as $H_2ONO_2^+$). Based on this

mechanism and laboratory measurements of the branching between R9 and R10, the instantaneous $ClNO_2$ yield (ϕ_{ClNO_2}) can be estimated by Eq. 1 shown below. Laboratory studies infer that the ratio of the reaction rate constants of R10 and R9 (k_{R10}/k_{R9}) to be 1/450 – 1/890 (Behnke et al., 1997; Roberts et al., 2009). Herein, we use the more recent 1/450 which leads to lower $ClNO_2$ yields for the same $[H_2O]/[Cl^-]$ than the previous estimate. Calculating ϕ_{ClNO2} thus requires knowledge of the particle liquid water content, which is a function of the ambient relative humidity (RH) and particle composition, and the particulate chloride concentration. Assuming the chloride mass fraction is constant across the particle surface area distribution simplifies the calculation in that only the mole ratio of H_2O to Cl^- is needed. Below we describe how ϕ_{ClNO2} can be estimated under this simplifying assumption using a thermodynamic model, RH, and aerosol composition.

$$N_2O_5(g) \longrightarrow N_2O_5(aq) \quad \text{(R7)}$$

$$N_2O_5(aq) + H_2O \rightleftharpoons H_2ONO_2^+(aq) + NO_3^- \quad \text{(R8)}$$

$$H_2ONO_2^+(aq) + Cl^-(aq) \xrightarrow{k_{R9}} ClNO_2 + H_2O \quad \text{(R9)}$$

$$H_2ONO_2^+(aq) + H_2O \xrightarrow{k_{R10}} HNO_3 + H_3O^+ \quad \text{(R10)}$$

$$\phi_{ClNO_2} = \frac{k_c[H_2ONO_2^+][Cl^-]}{k_c[H_2ONO_2^+][Cl^-] + k_d[H_2ONO_2^+][H_2O]} = \frac{1}{1 + \frac{k_d[H_2O]}{k_c[Cl^-]}} \simeq \frac{1}{1 + \frac{[H_2O]}{450[Cl^-]}} \quad (1)$$

2.3 Aerosol Thermodynamic Modeling

As stated above estimates of particle water content, [H_2O], are needed in order to estimate the expected $ClNO_2$ yield. Aerosol particles can exist as solid particles, metastable solutions free of solids, or as aqueous mixtures depending on the composition and humidity history experienced by the particles. However, the phase state (i.e. solid or liquid) of ambient atmospheric aerosols remains uncertain (Martin, 2000). Here we assume, as is conventional in many atmospheric models, that the aerosol particles are metastable solutions, and the precipitation of commonly formed solids is suppressed for all of the following thermodynamic calculations. We use the online thermodynamic equilibrium Aerosol Inorganics Model (AIM - http://www.aim.env.uea.ac.uk/aim/aim.php) to calculate the particulate water content based on the RH and measured aerosol inorganic composition (Wexler and Clegg, 2002). The model output also allows us to infer additional aerosol parameters such as pH and to assess the equilibrium partitioning between aerosol chloride and gas phase HCl for the given aerosol composition and meteorological conditions.

The AIM model is used to explore ϕ_{ClNO2} across a range of RH and chloride mass loadings. The AIM model provides a calculated aerosol water content given relative humidity (RH) and aerosol composition as inputs. For these calculations, we chose ammonium sulfate as the dominant particle component which is broadly consistent with inorganic particle composition observations made worldwide (Zhang et al., 2007). No significant differences were found in terms of the $ClNO_2$ yield if a different aerosol substrate like ammonium nitrate was used. The particle chloride dry mass mole fraction is varied from $<1x10^{-5}$ to 0.25 while keeping the RH constant in order to assess the dependence of ϕ_{ClNO2} on aerosol chloride content. NH_4^+ was increased with Cl^- in order to maintain overall charge balance. As stated above all potential solid

precipitates were suppressed, and finally ϕ_{ClNO2} was then calculated for each Cl^- value based on the particle water content reported by AIM and Eq. 1. The same procedure was repeated for different RH, ranging from 30% to 90%.

In order to facilitate rapid, online calculation of ϕ_{ClNO2}, for use in box modeling and calculations involving large datasets where discrete AIM model runs would be prohibitively difficult, we parameterize ϕ_{ClNO2} to be a function of RH and the particulate chloride dry mass fraction (MF_{Cl^-}) as shown in Eq. 2 which is of the same form as the original yield expression given in Eq. 1.

$$\phi_{ClNO_2} = \frac{1}{1+\left(\frac{Y_{fit}}{MF_{Cl^-}}\right)} \quad (2)$$

$$Y_{fit} = \sum a_n RH^n \quad (3)$$

Y_{fit} is a polynomial fit which incorporates the AIM predicted particle water content as a function of RH and the ratio of the two rate constants, k_c and k_d in reactions R9 and R10. Y_{fit}, as shown in Eq. 3, is obtained by fitting individual ϕ_{ClNO2} vs. MF_{Cl^-} curves obtained for different RH values to Eq. 2. A different fitting parameter is obtained for each RH, and the resulting RH-dependent parameters can then be fit to Eq. 3. The results of these estimates are shown in Figure 1 which shows ϕ_{ClNO2} vs. MF_{Cl^-} curve over a range of different RH.

The major assumptions when employing this parameterization are that, (1) the aerosol particles are aqueous solution droplets with the hygroscopicity of ammonium sulfate, and (2) the

particle chloride mass fraction is constant across the surface-area distribution of the particle population. We expect the first assumption leads to underestimates of ϕ_{ClNO2}, while the second assumption leads to overestimates of ϕ_{ClNO2}. Field measurements tend to show that the water content of ambient particles in the polluted boundary layer increases with RH, but usually not substantially more than pure ammonium sulfate particles between RH 30 – 90%; while particle phase remains highly uncertain (Dick et al., 2000; Martin, 2000). Thus, if particles are less hygroscopic than ammonium sulfate or are crystalline solids, we overestimate liquid water content, which in turn causes an underestimate of the competition of reaction R9 with R10 (i.e. $ClNO_2$ formation) (Finlayson-Pitts et al., 1989; Thornton and Abbatt, 2005). It should also be noted that recent experiments show that $ClNO_2$ is produced from surface reactions of N_2O_5 with HCl (Raff et al., 2009). Our assumption of constant chloride mass fraction across the size distribution likely overestimates ϕ_{ClNO2} on a population average, because if the chloride is confined to a small fraction of the surface area, then only a small fraction of N_2O_5 reactions will result in $ClNO_2$ production. There is too little data on this question at present to allow a more refined approach to calculating ϕ_{ClNO2} from large datasets of particulate chloride observations. Thus, we rely on observations taken in Boulder, CO, described below as well as those made in the Long Island Sound and the Gulf of Mexico to provide additional constraints on the amount of $ClNO_2$ that can be formed (Kercher et al., 2009; Osthoff et al., 2008).

2.4 Estimating Continental $ClNO_2$ Production

The $ClNO_2$ production rate, P_{ClNO2}, can be determined as the product of the yield, ϕ_{ClNO2}, and the gross N_2O_5 reaction rate which, assuming NO_x is in steady state (loss rates ≈ source rates) (Brown et al., 2003), we define as the product of the fraction of NO_x oxidized at night by

N_2O_5 reactions on aerosol particles, f_{N2O5}, and the NO_x emission rate, E_{NOx}. Eq. 4 illustrates this approach.

$$P_{ClNO_2} = E_{NOx} f_{N_2O_5} \phi_{ClNO_2} \quad (4)$$

2.4.1 Continental NO_x Emission Rates

As stated above, assuming NO_x is in steady-state, the local mass flux of NO_x through N_2O_5 heterogeneous chemistry can be determined by the product of the NO_x emission rate and the fraction of the NO_x loss rate caused by N_2O_5 chemistry. Annual NO_x emissions (E_{NOx}) with 1° x 1° resolution were obtained from the Emission Database for Global Atmospheric Research (EDGAR - http://edgar.jrc.ec.europa.eu). The continental United States NO_x emissions (E_{NOx}) were reflective of the year 2000 and reported in kg NO_2 per year as shown in Figure 2, which we converted to moles of nitrogen per year. For seasonal calculations, we simply divide the annual values from the EDGAR database by 4. The seasonal cycle in total U.S. NO_x emissions is small, but a more refined approach could adjust for seasonal variations at the regional scale (Jaegle et al., 2005).

2.4.2 Fraction of NO_x reacted as N_2O_5

The fraction of NO_x oxidized to nitrate by N_2O_5 chemistry (f_{N2O5}) is illustrated in Eq. 5 and represents the nitrate formed by nighttime reactions of N_2O_5 on aerosols (numerator) relative to all other nitrate producing reactions of NO_x (denominator). This parameter was obtained from the 0 – 2 km altitude output of a GEOS-Chem chemical transport model run for the year 2005 and projected onto a 1° x 1° grid (Alexander et al., 2009). The model uses a recent N_2O_5-aerosol

reaction probability parameterization which includes different reaction probabilities for different particle types and RH and temperature dependences based on available experimental data (Evans and Jacob, 2005). Seasonal values of f_{N2O5}, which range from 0 to 1, are shown in Figure 3. Significant seasonal cycles in OH production, temperature, and RH lead to strong seasonality in the predicted f_{N2O5}. Maximum values are during the winter months, when the lower temperatures push the N_2O_5/NO_3 equilibrium toward N_2O_5 and reduce the importance of NO_3 reactions with biogenic hydrocarbons, and in the Northeastern United States in areas of high NO_x emissions. The annual mean f_{N2O5} averaged over the continental U.S. is 0.38.

$$f_{N_2O_5} = \frac{\frac{2\gamma SA\omega[N_2O_5]}{4}}{\frac{2\gamma SA\omega[N_2O_5]}{4} + k[NO_3][VOC] + k[OH][NO_2] + ...} \quad (5)$$

2.4.3 Continental $ClNO_2$ yield estimates

A combination of aerosol and precipitation composition data from the long term (continuous measurements over the past 10 years) networks is used to estimate the fraction of N_2O_5 reactions that lead to $ClNO_2$, i.e. ϕ_{ClNO2}. The goal is to provide estimates of ϕ_{ClNO2} that are consistent with all available $ClNO_2$ observations and that faithfully reconstruct the likely spatial variation in the availability of chloride, i.e. increasing with proximity to coastal regions. We use a combination of IMPROVE network (http://vista.cira.colostate.edu/improve/) measurements of the fine mode chloride mass fraction and our parameterization of the $ClNO_2$ yield (Eq. 2) together with the wet deposition data of chloride and nitrate provided by the National Atmospheric Deposition Program (NADP - http://nadp.sws.uiuc.edu/) (Malm et al., 1994;

NADP, 2010). From each of these two data sets, we created gridded fields of ϕ_{ClNO2} approximations.

The $ClNO_2$ yield estimates for the U.S. were based, in part, on aerosol chloride data from the Interagency Monitoring of PROtected Visual Environments (IMPROVE) (Malm et al., 1994). A map of the distribution of IMPROVE sites across the continental United State is shown in Figure 4. Dry, fine mode total and chloride mass concentrations ($\mu g/m^3$), reported as a 24-hour average every three days for each IMPROVE site, were used from the period covering January 2001 to December 2008. This period was chosen because the data is relatively recent, and there is a noticeable improvement in particulate chloride detection limits occurring in data reported after 2000. That said, negative chloride values still exist in the data set in certain regions, especially between 2001 and 2003. We treat these values as arising from statistical fluctuations about a measurement of zero, and thus include them in the averaging. The median chloride mass fraction values for each site over the 7-year period were assumed to represent the typical annual or seasonal average and were gridded to 1° x 1° over the contiguous United States. Standard deviations were on the order of the medians indicating high inter-annual variability. The differences between using means or medians were negligible.

We input the IMPROVE fine-mode chloride mass fraction data into Eq. 2, assuming 80% RH in every grid cell to produce $\phi_{ClNO_2}^{IMP}$. The higher RH is meant to produce accurate yields near the coast where there is sufficient chloride. We take this quantity as the average instantaneous branching between reactions R9 and R10. Use of $\phi_{ClNO_2}^{IMP}$ alone in equation E1, without adjustments to match yields inferred from observations would imply that $ClNO_2$ production is only limited by the competition between R9 and R10 and NO_x abundance, and not by chloride availability either in total or in terms of its distribution across the particle size distribution.

Hence, estimates based on IMPROVE data alone and the above equations significantly over predict the yields for mid-continent grid cells, likely due to these limitations. Thus, we use the NADP precipitation composition data described below to place a limit on the total amount of soluble chloride that could be activated by nighttime N_2O_5 chemistry.

Relatively recent NADP data was chosen in order for estimates to more accurately represent current conditions and to avoid using data prior to the implementation of improved sampling designs that minimize ion artifacts (NADP, 2010). NADP reports total wet deposition of nitrate and chloride in kg/ha for each site on a seasonal basis. The distribution of NAPD sites across the United States is shown in Figure 5. Assuming that essentially all NO_x emissions are converted to HNO_3 or particulate NO_3^- and deposited by either dry or wet deposition, and that all inorganic chlorine (HCl + particulate) is similarly lost to deposition, then the ratio of chloride to nitrate measured in precipitation should equal the ratio of these species in the atmospheric column from which they precipitated. The fraction of the nitrate attributable to nighttime oxidation of NO_x through N_2O_5 for each site location can be calculated by scaling the measured nitrate by the appropriate f_{N2O5}. We then derive an estimate of the chloride availability for $ClNO_2$ production, $\phi_{ClNO_2}^{NADP}$, from the mole ratio of chloride to nitrate measured contemporaneously in precipitation as shown in Eq. 6.

$$\phi_{ClNO_2}^{NADP} = \frac{mol_{Cl^-}}{f_{N_2O_5} mol_{NO_3^-}} \tag{6}$$

The $\phi_{ClNO_2}^{NADP}$ values carry the seasonal dependence in f_{N2O5} (see below), in addition to any seasonal dependence in the deposition patterns, and represents an upper-limit to the potential $ClNO_2$ yield

as we assume that all chloride in precipitation is in a form that can be activated to $ClNO_2$ by N_2O_5.

The seasonal mean $\phi_{ClNO_2}^{NADP}$ of each site was taken as representative for that site. Standard deviations were typically about half of the mean. However, sites near the coast, or near large NO_x emissions, did exhibit standard deviations slightly larger than the mean values. Thus, we expect significant year-to-year variability in chloride availability. The resulting site-specific $\phi_{ClNO_2}^{NADP}$ values were then gridded to 1° x 1° over the contiguous United States.

For use in Eq. 4 estimate, we then created ϕ_{ClNO_2} fields, where, for each grid cell, we used the lesser of the two quantities, $\phi_{ClNO_2}^{IMP}$ or $\phi_{ClNO_2}^{NADP}$. For comparison, in Figure 6, we show the annual mean fields of $\phi_{ClNO_2}^{IMP}$ and $\phi_{ClNO_2}^{NADP}$. We infer from this figure that the central and north-central U.S. exhibits high chloride mass fractions, but low total chloride relative to the fraction of NO_x that reacts as N_2O_5. Seasonal fields of ϕ_{ClNO2} from the melding of $\phi_{ClNO_2}^{IMP}$ and $\phi_{ClNO_2}^{NADP}$ are shown in Figure 7.

2.4.4 Seasonal and Annual $ClNO_2$ Production

Finally, we estimate seasonal and annual nitryl chloride production over the contiguous United States using Eq. 4. Summing over all 1° x 1° grid cells and over all seasons we estimate an annual total P_{ClNO2} of 3.6 Tg Cl yr^{-1}. In Figure 8 we show the seasonal components of P_{ClNO2}. The corresponding values of these seasonal estimate, i.e. the spatial integral of the fields shown in Figure 7, are 1.35, 0.89, 0.45, 0.89 Tg Cl, for winter, spring, summer, and fall, respectively.

2.5 Observational Support and Conclusions

During a February 2009 field study (Activation of Continental Chloride by Reactive Oxides of Nitrogen in winterIMe – ACCRONIM) that took place in Boulder, CO, $ClNO_2$ was routinely measured with mixing ratios in excess of 100 pttv when the Denver-Boulder urban plume was sampled. Shown in Figure 9 with N_2O_5, these observations represented the first observations of $ClNO_2$ well removed from coastal areas and support the P_{ClNO2} estimates described above where significant $ClNO_2$ production was predicted to occur inland of coastal regions. While our estimates likely represent an upper-limit to P_{ClNO2} as we implicitly assume that all available chloride can be activated to $ClNO_2$ by N_2O_5, we also can't rule out that the actual value may be close to this limit, particularly in mid-continent regions, where chloride is probably a limiting reagent, as evidenced by the good agreement between the our estimates and measurements in Boulder, CO.

The 3.6 Tg Cl yr^{-1} estimate of $ClNO_2$ production over the United States is on the order of other global estimates and represents about 20% of the U.S. NO_x emissions proceeding through the $N_2O_5/ClNO_2$ reaction pathway (Erickson et al., 1999; Osthoff et al., 2008). Given global NO_x emissions reported by the EDGAR database and assuming a similar NO_x to $ClNO_2$ conversion percentage, we can extend our $ClNO_2$ production estimate to obtain a global estimate of $ClNO_2$ production. This approach produces a global estimate of 22 Tg Cl yr^{-1} from $ClNO_2$. This estimate would represent a significant and potentially unaccounted fraction of the total global chlorine atom budget of 35 Tg Cl yr^{-1} estimated from methane isotope data (Platt et al., 2004).

More support for the ubiquity of $ClNO_2$ formation can be found in reported aerosol chloride content as measured by an Aerosol Mass Spectrometer (AMS) at a number of different measurement sites worldwide and shown in Figure 10 (Zhang et al., 2007). The chloride mass

fractions reported from these studies are of similar magnitude to those reported for the ACCRONIM field study (also shown in Figure 10), illustrating the potential significance of this chemistry on a global scale.

References

Alexander, B., Hastings, M. G., Allman, D. J., Dachs, J., Thornton, J. A., and Kunasek, S. A.: Quantifying atmospheric nitrate formation pathways based on a global model of the oxygen isotopic composition (delta(17)O) of atmospheric nitrate, Atmospheric Chemistry and Physics, 9, 5043-5056, doi: 10.5194/acp-9-5043-2009, 2009.

Behnke, W., George, C., Scheer, V., and Zetzsch, C.: Production and decay of $ClNO_2$, from the reaction of gaseous N_2O_5 with NaCl solution: Bulk and aerosol experiments, Journal of Geophysical Research-Atmospheres, 102, 3795-3804, doi: 10.1029/96jd03057, 1997.

Brown, S. S., Stark, H., and Ravishankara, A. R.: Applicability of the steady state approximation to the interpretation of atmospheric observations of NO_3 and N_2O_5, Journal of Geophysical Research: Atmospheres, 108, 4539, doi: 10.1029/2003jd003407, 2003.

Dick, W. D., Saxena, P., and McMurry, P. H.: Estimation of water uptake by organic compounds in submicron aerosols measured during the Southeastern Aerosol and Visibility Study, Journal of Geophysical Research: Atmospheres, 105, 1471-1479, doi: 10.1029/1999jd901001, 2000.

Erickson, D. J., Seuzaret, C., Keene, W. C., and Gong, S. L.: A general circulation model based calculation of HCl and $ClNO_2$ production from sea salt dechlorination: Reactive Chlorine Emissions Inventory, Journal of Geophysical Research: Atmospheres, 104, 8347-8372, doi: 10.1029/98jd01384, 1999.

Evans, M. J., and Jacob, D. J.: Impact of new laboratory studies of N_2O_5 hydrolysis on global model budgets of tropospheric nitrogen oxides, ozone, and OH, Geophysical Research Letters, 32, doi: 10.1029/2005gl022469, 2005.

Finlayson-Pitts, B. J., Ezell, M. J., and Pitts, J. N.: Formation of chemically active chlorine compounds by reactions of atmospheric NaCl particles with gaseous N_2O_5 and $ClONO_2$, Nature, 337, 241-244, doi: 10.1038/337241a0, 1989.

Graedel, T. E., and Keene, W. C.: Tropospheric budget of reactive chlorine, Glob. Biogeochem. Cycles, 9, 44-77, 1995.

Jaegle, L., Steinberger, L., Martin, R. V., and Chance, K.: Global partitioning of NO sources using satellite observations: Relative roles of fossil fuel combustion, biomass burning and soil emissions, Faraday Discussions, 130, 407-423, doi: 10.1039/b502128f, 2005.

Kercher, J. P., Riedel, T. P., and Thornton, J. A.: Chlorine activation by N_2O_5: simultaneous, in situ detection of $ClNO_2$ and N_2O_5 by chemical ionization mass spectrometry, Atmospheric Measurement Techniques, 2, 193-204, doi: 10.5194/amt-2-193-2009, 2009.

Knipping, E. M., and Dabdub, D.: Impact of chlorine emissions from sea-salt aerosol on coastal urban ozone, Environmental Science & Technology, 37, 275-284, doi: 10.1021/es025793z, 2003.

Malm, W. C., Sisler, J. F., Huffman, D., Eldred, R. A., and Cahill, T. A.: Spatial and seasonal trends in particle concentration and optical extinction in the United States, Journal of Geophysical Research: Atmospheres, 99, 1347-1370, doi: 10.1029/93jd02916, 1994.

Martin, S. T.: Phase Transitions of Aqueous Atmospheric Particles, Chemical Reviews, 100, 3403-3454, doi: 10.1021/cr990034t, 2000.

NADP: National Atmospheric Deposition Program (NRSP-3), Illinois State Water Survey, Champaign, Illinois, 2010.

Osthoff, H. D., Roberts, J. M., Ravishankara, A. R., Williams, E. J., Lerner, B. M., Sommariva, R., Bates, T. S., Coffman, D., Quinn, P. K., Dibb, J. E., Stark, H., Burkholder, J. B.,

Talukdar, R. K., Meagher, J., Fehnsenfeld, F. C., and Brown, S. S.: High levels of nitryl chloride in the polluted subtropical marine boundary layer Nature Geoscience, 1, 2008.

Platt, U., Allan, W., and Lowe, D.: Hemispheric average Cl atom concentration from $^{13}C/^{12}C$ ratios in atmospheric methane, Atmos. Chem. Phys., 4, 2393-2399, doi: 10.5194/acp-4-2393-2004, 2004.

Raff, J. D., Njegic, B., Chang, W. L., Gordon, M. S., Dabdub, D., Gerber, R. B., and Finlayson-Pitts, B. J.: Chlorine activation indoors and outdoors via surface-mediated reactions of nitrogen oxides with hydrogen chloride, Proceedings of the National Academy of Sciences of the United States of America, 106, 13647-13654, doi: 10.1073/pnas.0904195106, 2009.

Roberts, J. M., Osthoff, H. D., Brown, S. S., and Ravishankara, A. R.: N_2O_5 Oxidizes Chloride to Cl_2 in Acidic Atmospheric Aerosol, Science, 321, 1059, 2008.

Roberts, J. M., Osthoff, H. D., Brown, S. S., Ravishankara, A. R., Coffman, D., Quinn, P., and Bates, T.: Laboratory studies of products of N_2O_5 uptake on Cl^- containing substrates, Geophysical Research Letters, 36, doi: 10.1029/2009gl040448, 2009.

Thornton, J. A., and Abbatt, J. P. D.: N_2O_5 reaction on submicron sea salt aerosol: Kinetics, products, and the effect of surface active organics, Journal of Physical Chemistry A, 109, 10004-10012, doi: 10.1021/jp054183t, 2005.

Thornton, J. A., Kercher, J. P., Riedel, T. P., Wagner, N. L., Cozic, J., Holloway, J. S., Dube, W. P., Wolfe, G. M., Quinn, P. K., Middlebrook, A. M., Alexander, B., and Brown, S. S.: A large atomic chlorine source inferred from mid-continental reactive nitrogen chemistry, Nature, 464, 271-274, doi: 10.1038/nature08905, 2010.

Wexler, A. S., and Clegg, S. L.: Atmospheric aerosol models for systems including the ions H^+, NH_4^+, Na^+, SO_4^{2-}, NO_3^-,Cl^-, Br^-, and H_2O, Journal of Geophysical Research-Atmospheres, 107, doi: 10.1029/2001jd000451, 2002.

Zhang, Q., Jimenez, J. L., Canagaratna, M. R., Allan, J. D., Coe, H., Ulbrich, I., Alfarra, M. R., Takami, A., Middlebrook, A. M., Sun, Y. L., Dzepina, K., Dunlea, E., Docherty, K., DeCarlo, P. F., Salcedo, D., Onasch, T., Jayne, J. T., Miyoshi, T., Shimono, A., Hatakeyama, S., Takegawa, N., Kondo, Y., Schneider, J., Drewnick, F., Borrmann, S., Weimer, S., Demerjian, K., Williams, P., Bower, K., Bahreini, R., Cottrell, L., Griffin, R. J., Rautiainen, J., Sun, J. Y., Zhang, Y. M., and Worsnop, D. R.: Ubiquity and dominance of oxygenated species in organic aerosols in anthropogenically-influenced Northern Hemisphere midlatitudes, Geophysical Research Letters, 34, doi: 10.1029/2007gl029979, 2007.

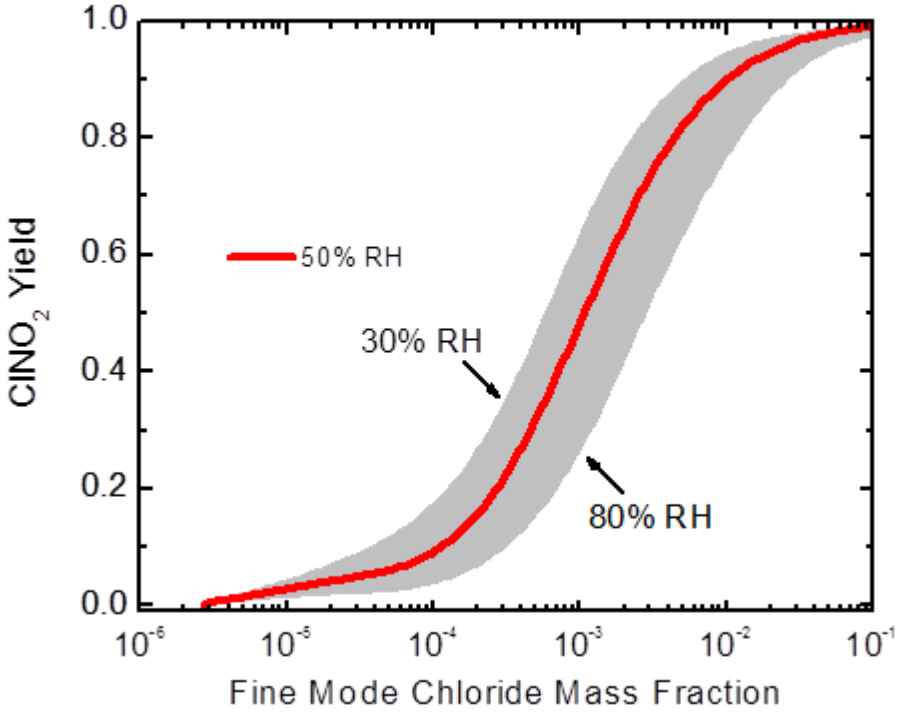

Figure 1 Predicted $ClNO_2$ yield vs. particulate chloride mass fraction from aerosol thermodynamic modeling. The grey area corresponds to effects from varying relative humidities.

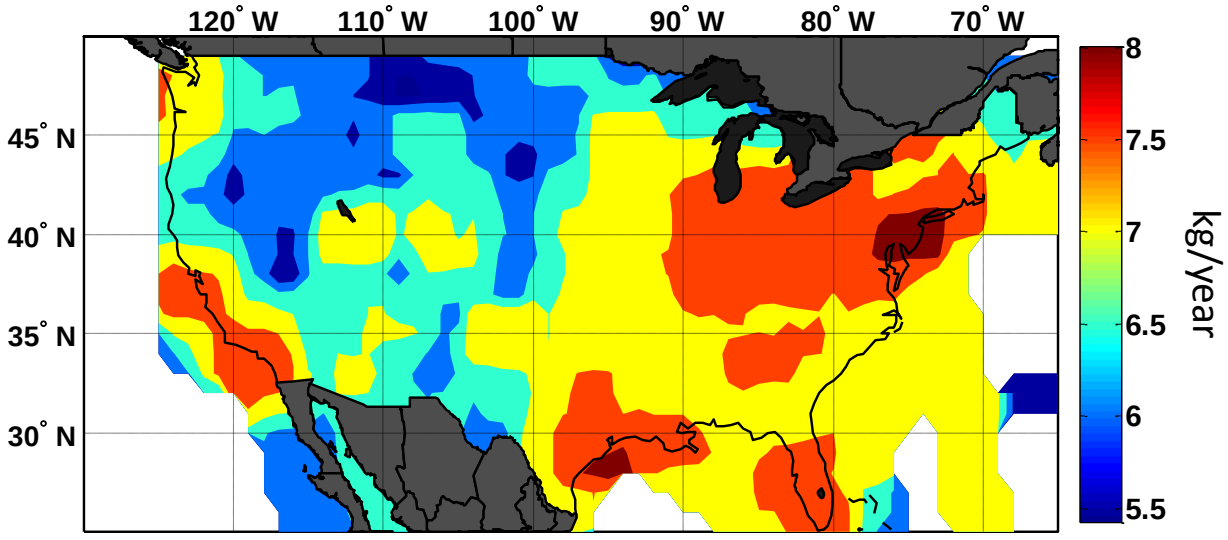

Figure 2 Annual U.S. NO_x emissions as reported by the EDGAR database for the year 2000.

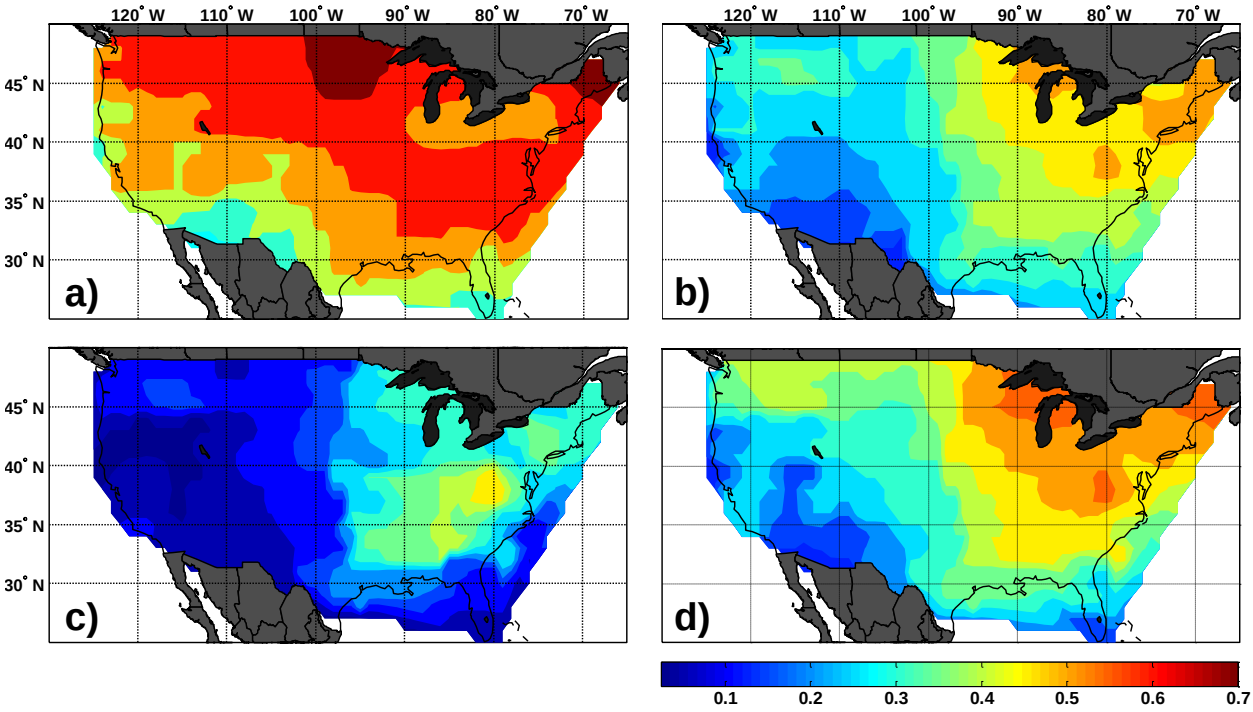

Figure 3 Seasonal fraction of nitrate attributed to N_2O_5 reactions as predicted by the GEOS-Chem global chemical transport model for a) winter: DJF b) spring: MAM c) summer: JJA d) fall: SON.

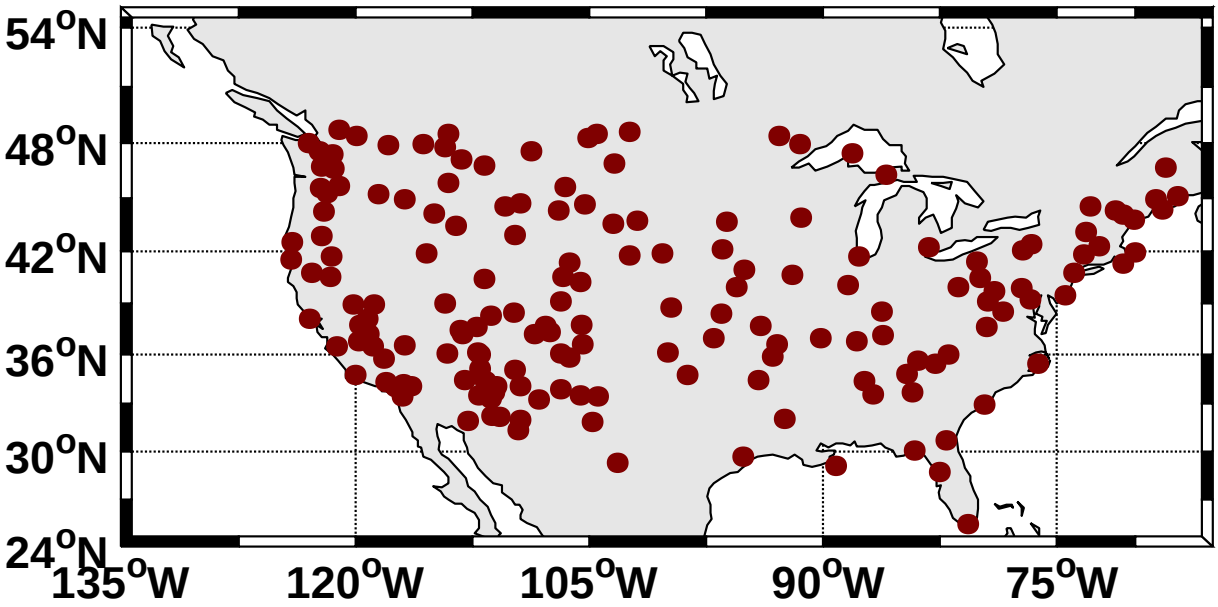

Figure 4 IMPROVE network site locations.

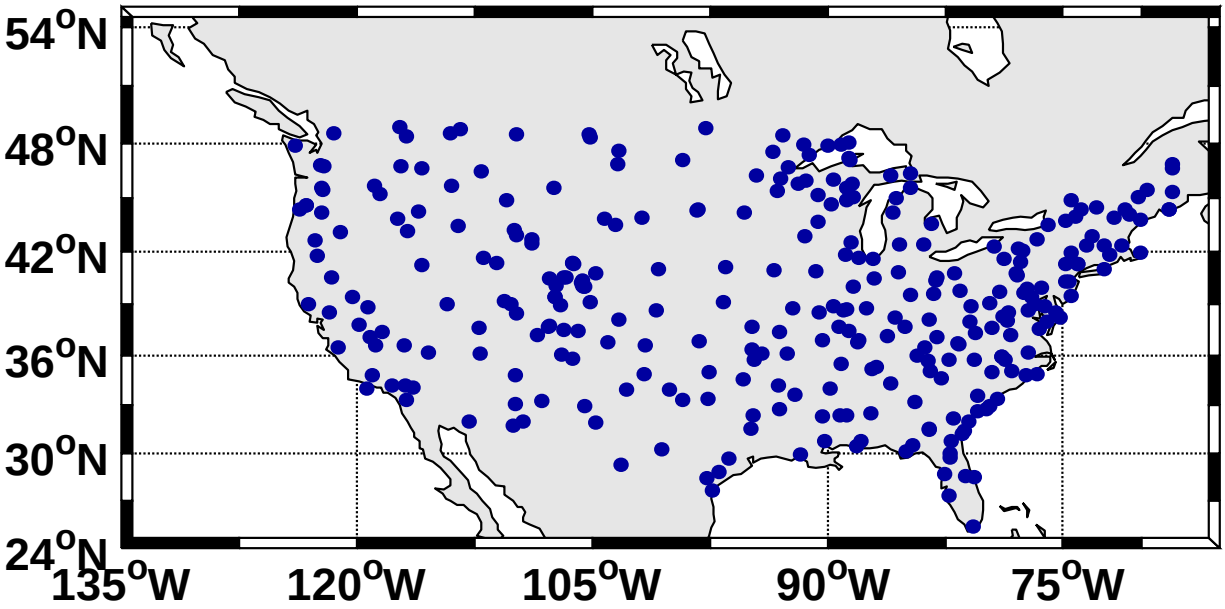

Figure 5 NADP site locations.

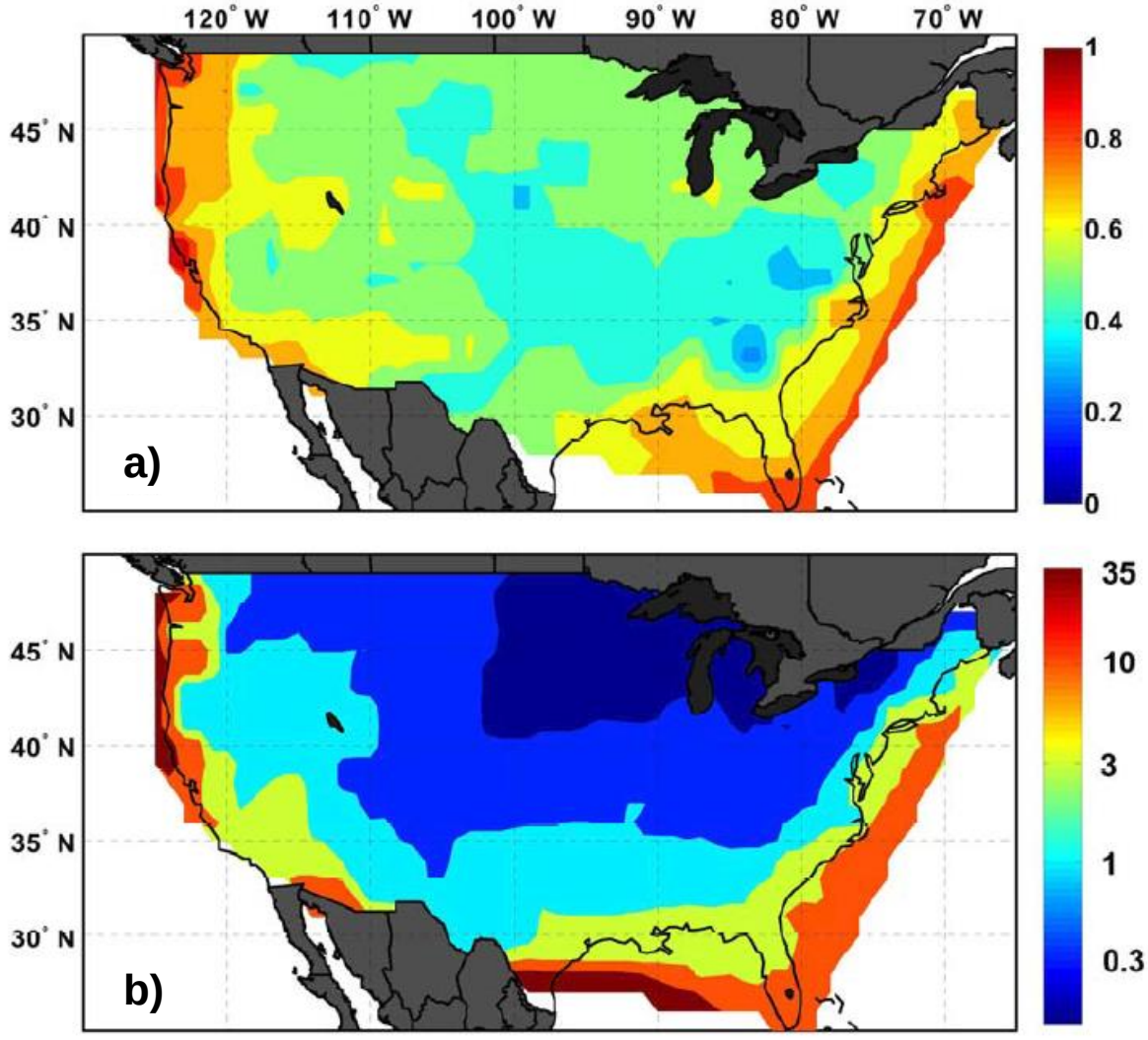

Figure 6 a) Estimated annual branching between reactions R9 and R10 from the IMPROVE network fine mode chloride mass fraction. b) Chloride availability relative to nitrate measured in precipitation by the NADP. Note the color scales are different for the two panels.

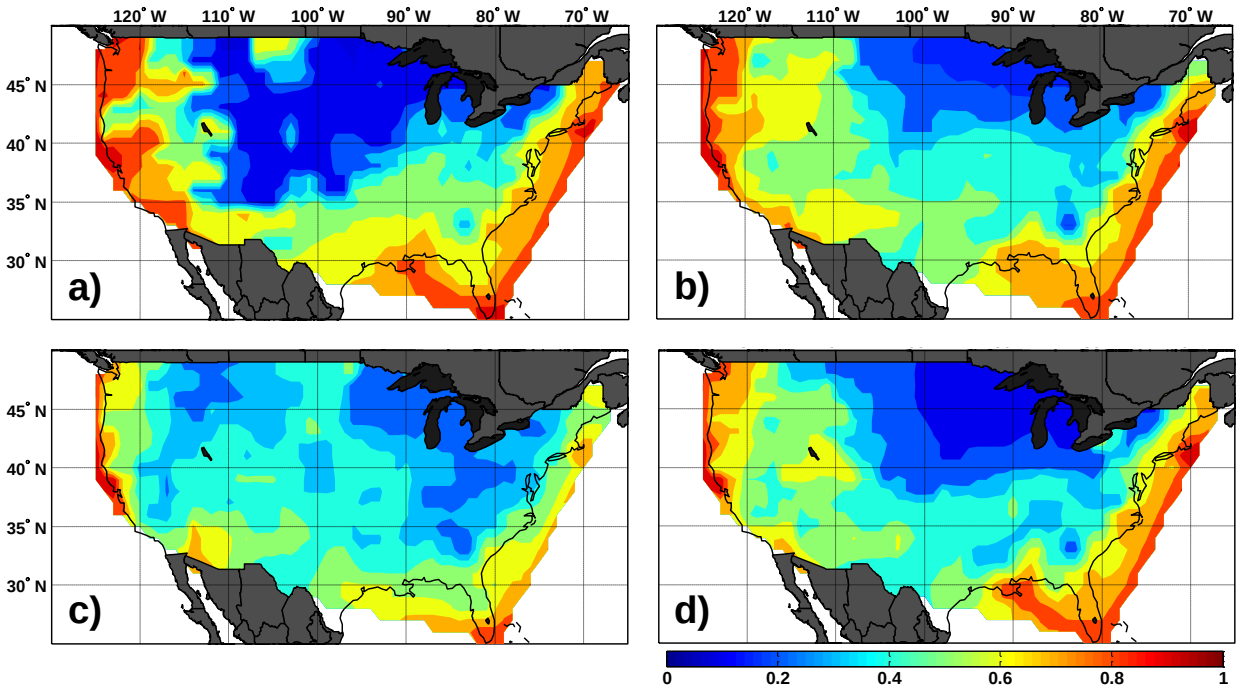

Figure 7 Seasonal $ClNO_2$ yields estimated from IMPROVE network and NADP data for a) winter: DJF b) spring: MAM c) summer: JJA d) fall: SON.

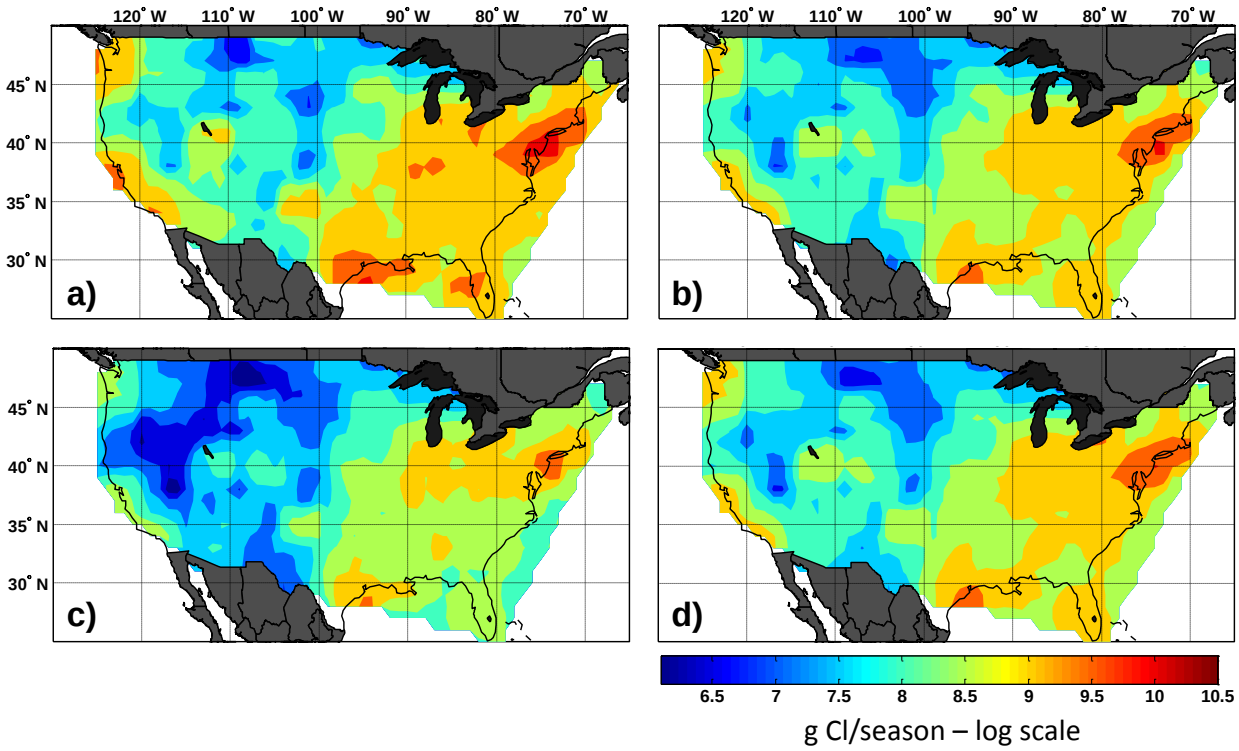

Figure 8 Seasonal $ClNO_2$ production rates over the continental U.S. for a) winter: DJF b) spring: MAM c) summer: JJA d) fall: SON. Note the color scale is logarithmic with a minimum value of 10^6 g Cl/season and a maximum value of $10^{10.5}$ g Cl/season.

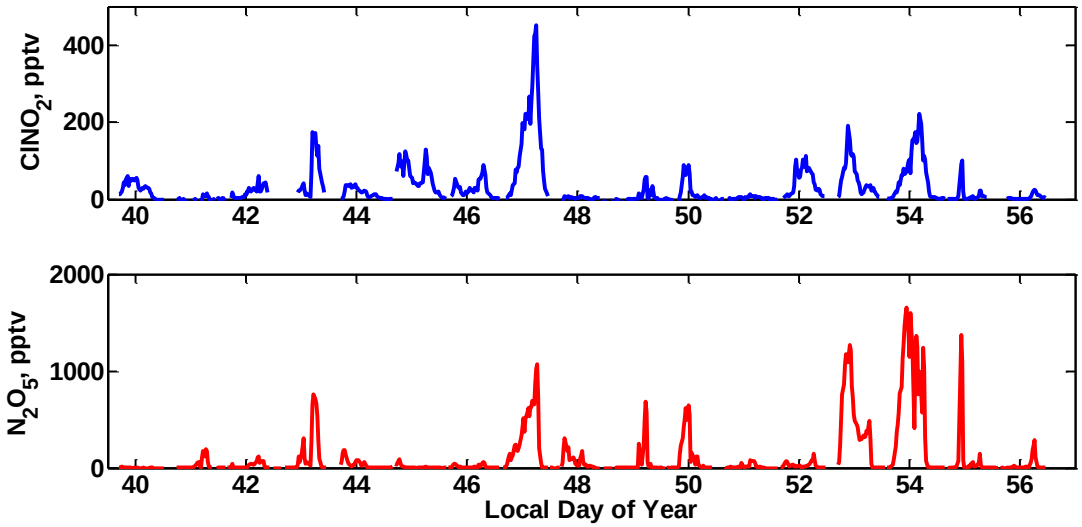

Figure 9 Observations of ambient $ClNO_2$ and N_2O_5 mixing ratios from the ACCRONIM study in Boulder, CO.

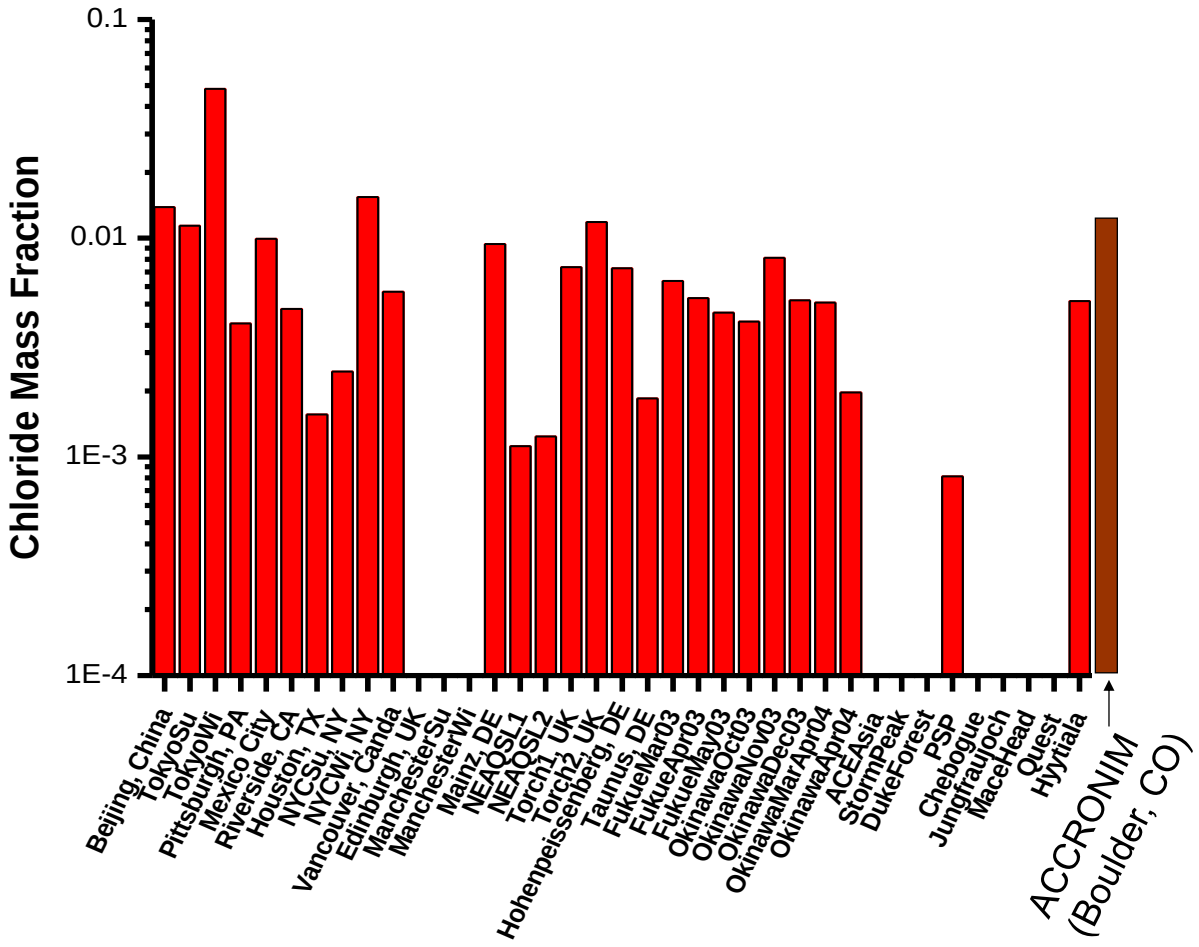

Figure 10 Non-refractory aerosol chloride mass fraction data from Zhang, et al., 2007 and from the ACCRONIM study in Boulder, CO.

Chapter 3

Direct N_2O_5 Reactivity Measurements at a Polluted Coastal Site

3.1 Introduction

Nitrogen oxides ($NO_x \equiv NO + NO_2$) influence air quality and climate by regulating tropospheric ozone (O_3) production and hydroxyl radical (OH) abundances which in turn affect aerosol mass formation and the lifetime of the greenhouse gases such as methane (Jacob, 2000; Logan et al., 1981; Shindell et al., 2009). NO_x is present largely through emissions from anthropogenic activities such as motor vehicle use, industrial processes, agriculture, and power generation. These emissions have steadily increased since pre-industrial times and are expected to continue increasing globally (Ohara et al., 2007; Yienger, 1999).

Understanding NO_x removal pathways is crucial to accurately assessing its impacts. In the troposphere, conversion of NO_x to HNO_3 is the dominant removal process due to the efficient wet and dry deposition of HNO_3. During the daytime, NO_x is converted to HNO_3 by OH. At night in the presence of ozone, NO_x is converted into the nitrate radical, NO_3, by reaction of NO_2 with O_3. The nitrate radical can react with a variety of different volatile organic compounds (VOC) or again with NO_2 to form dinitrogen pentoxide, N_2O_5, which can react on aerosol particles. Nocturnal reactions of NO_3 and N_2O_5 to terminal products such as alkyl nitrates and nitric acid are thought to account for 20 - 80% of NO_x removal in polluted regions (Alexander et al., 2009; Brown et al., 2004; Dentener and Crutzen, 1993). These previous studies have assumed that N_2O_5 reactions on particles proceed solely via a hydrolysis channel to form two HNO_3 molecules. Laboratory studies and recent field work has shown that N_2O_5 reactions on chloride

containing aerosol particles can efficiently proceed through a second channel to form nitryl chloride, $ClNO_2$, in both continental and marine locations (Behnke et al., 1997; Finlayson-Pitts et al., 1989; Osthoff et al., 2008; Roberts et al., 2009; Thornton et al., 2010). $ClNO_2$ is a photolabile compound that releases atomic chlorine and NO_x upon photolysis, its formation thereby decreases nocturnal NO_x losses due to HNO_3 formation while liberating a strong oxidant. The importance of this second channel has implications for both the reactive halogen budget and the efficiency of photochemical ozone production. Moreover, there remains significant uncertainty in the efficiency of N_2O_5 reactions on atmospheric particles.

The heterogeneous reaction rate of N_2O_5 on aerosol particles is calculated from the product of two quantities, the collision frequency between N_2O_5 molecules with particle surface area in a volume of air and the probability that N_2O_5 reacts given a collision, $\gamma(N_2O_5)$, also called the reactive uptake coefficient. This relationship is shown in Eq. 1 where ω is the average molecular speed of an N_2O_5 molecule (m sec^{-1}) and SA is the surface area concentration of aerosol particles (m^2m^{-3}).

$$\frac{d[N_2O_5]}{dt} = -\frac{\gamma(N_2O_5)[N_2O_5]SA\omega}{4} \quad (1)$$

Eq. 1 neglects any limitations resulting from gas-phase diffusion to the particle surfaces which are likely negligible under our measurement conditions ($\gamma(N_2O_5)<0.05$ and $r_p<2\mu m$). $\gamma(N_2O_5)$ represents the net result of multiphase chemistry that is a complex function of various particle properties including chemical composition, liquid water content, particle phase state (solid vs. liquid), mixing state, morphology of particle constituents across the size distribution, and pH. Routine, quantitative measurements of the aforementioned particle properties in ambient air are

rare at best, and the fundamental dependence of $\gamma(N_2O_5)$ on some of these properties, in particular organic composition and mixing state is lacking. Therefore, our understanding of the absolute and relative rates of N_2O_5 reaction channels in ambient particles remains poor. These issues also pose significant challenges for accurately incorporating these processes in atmospheric chemical models. Models must parameterize the reaction probability based on laboratory studies that use highly idealized particle compositions, and then also make assumptions about the mixing state of atmospheric particles.

Laboratory studies have shown that $\gamma(N_2O_5)$ can span several orders of magnitude depending upon particle composition and phase state (Hallquist et al., 2003; Hu and Abbatt, 1997; Kane et al., 2001; McNeill et al., 2006; Mozurkewich and Calvert, 1988; Robinson et al., 1997). Particulate water, chloride, nitrate, and organic particle coatings can all have effects on the N_2O_5 reaction probability (Bertram and Thornton, 2009; Bertram et al., 2009b; Cosman and Bertram, 2008; Folkers et al., 2003; Mentel et al., 1999; Park et al., 2007; Thornton et al., 2003; Thornton and Abbatt, 2005; Wahner et al., 1998). These findings have led to the development of a working mechanism, Reactions R1-R4.

$$N_2O_5(g) \longleftrightarrow N_2O_5(aq) \quad \text{(R1)}$$

$$N_2O_5(aq) + H_2O(l) \longrightarrow H_2ONO_2^+(aq) + NO_3^-(aq) \quad \text{(R2a)}$$

$$H_2ONO_2^+(aq) + NO_3^-(aq) \longrightarrow N_2O_5(aq) + H_2O(l) \quad \text{(R2b)}$$

$$H_2ONO_2^+(aq) + H_2O(l) \longrightarrow H_3O^+(aq) + HNO_3(aq) \quad \text{(R3)}$$

$$H_2ONO_2^+(aq) + Cl^-(aq) \longrightarrow ClNO_2(aq) + H_2O(l) \quad \text{(R4)}$$

Increases in particulate liquid water enhance $\gamma(N_2O_5)$, ultimately up to a value limited by Reaction R1, by increasing the rates of solvation and hydrolysis reactions of accommodated N_2O_5 molecules (R2 and R3) (Bertram and Thornton, 2009; Thornton et al., 2003). The presence of particulate nitrate hinders N_2O_5 uptake, commonly called the "nitrate effect", presumably by forcing the solvated N_2O_5 intermediate back to reactants (R2b) (Wahner et al., 1998). The presence of particulate chloride provides an additional reaction channel for the solvated N_2O_5 intermediate (R4) (Behnke et al., 1997; Finlayson-Pitts et al., 1989; Roberts et al., 2009). This additional nucleophile can change the product distributions and increase the rate of N_2O_5 uptake in particles by overcoming the nitrate effect (Bertram and Thornton, 2009). That is, there is a connection, in terms of particle chloride content, between $\gamma(N_2O_5)$ and the branching ratio that predicts the $ClNO_2$ produced per reaction of N_2O_5 on aerosol particles (ϕ).

$$\phi(ClNO_2) = \frac{Rate_{R4}}{Rate_{R3} + Rate_{R4}} \quad (2)$$

The presence of organic compounds and their effect on the reaction probability remain a particular challenge to assess. Surface active organics and organic coatings generally appear to lower $\gamma(N_2O_5)$ (Cosman et al., 2008; Folkers et al., 2003; McNeill et al., 2006; Park et al., 2007; Thornton and Abbatt, 2005).

Parameterizations of $\gamma(N_2O_5)$ as a function of particle composition, based on the above laboratory findings, have only recently begun to be tested with field observations, a step that is ultimately necessary for accurate representation of nocturnal NO_x processes in large-scale chemical transport models (Bertram and Thornton, 2009; Brown et al., 2009). Bertram et al. (2009b) using the same direct reactivity approach described here, illustrated that $\gamma(N_2O_5)$

depended strongly on particulate organic matter loading during a stagnation event in which SOA mass increased substantially relative to inorganic components. The $\gamma(N_2O_5)$ decreased with increasing particulate organic mass fraction, which would be inconsistent with a purely hygroscopic organic aerosol.

Brown et al. (2006) used observations of NO_2, O_3, NO_3 and N_2O_5 to determine the steady state lifetime of N_2O_5 from which they estimated $\gamma(N_2O_5)$. In that study, and more recently, they demonstrated high spatial variability in $\gamma(N_2O_5)$, but a specific cause or causes in the variability were not clear from the available data (Brown et al., 2006; Brown et al., 2009).

We used the direct reactivity approach described in Bertram et al. (2009a) to make *in situ* measurements of the N_2O_5 reactivity on ambient aerosol particles over the course of two and a half weeks in a polluted coastal environment (La Jolla, CA, USA). These data represent the first such measurements in a coastal region. This region routinely receives fresh and aged sea spray as well as particles associated with urban pollution, and therefore provides a broad range of particle types over which to study the response of $\gamma(N_2O_5)$. Using aerosol composition and meteorological measurements, we illustrate a strong influence of particulate nitrate on the observed $\gamma(N_2O_5)$ over the course of the study that is quantitatively consistent with that expected from laboratory studies. Other mechanisms of suppression are also apparent, but remain to be conclusively identified.

3.2 Site Description and Methods

Measurements of N_2O_5 reactivity and other variables were made continuously from September 11-28, 2009, at the Scripps Pier (32.867°, -117.257°) located on the Scripps Institution of Oceanography on the UC San Diego campus in La Jolla, CA. Supporting

measurements included size-resolved non-refractory aerosol composition from an Aerosol Mass Spectrometer (AMS), aerosol size distributions, NO_x, O_3, and meteorological measurements such as temperature, relative humidity, pressure, wind speed and direction.

Ambient temperature (T), relative humidity (RH), and wind speed and direction measurements were obtained from an existing weather station operated by SIO (archived data can be found at http://meteora.ucsd.edu/wx_pages/scripps.html). RH governs particle water content as well as the reaction efficiency of N_2O_5 on the flow reactor walls and is thus an important variable both in ambient air and within the flow reactor. We determined the RH within the flow reactor from the ambient RH and T by assuming constant water vapor mixing ratio between ambient air and the air sampled into the flow reactor. A high time resolution temperature measurement taken in the instrument trailer adjacent to the flow reactor apparatus was used with ambient RH and T to calculate a flow reactor RH. The ambient and flow reactor RH are shown in Figure 1a for the entirety of the study. Characteristic of a coastal setting, ambient RH was typically about 70% with little diurnal cycle except for a few days during which continental flow dominated bringing low RH. Due to persistently warmer conditions within the trailer compared to ambient air, RH within the flow reactor was consistently lower than that outside. This condition suggests a possible biasing of $\gamma(N_2O_5)$ low relative to its actual value in ambient air, though most recent laboratory studies illustrate only a weak $\gamma(N_2O_5)$ dependence on RH for aqueous solution particles at RH > 50% (Davis et al., 2008; Folkers et al., 2003; Thornton et al., 2003).

As illustrated in Figure 1b, a range of air mass source regions were sampled during the campaign. The wind rose represents only wind direction and speeds for the periods between 9:00 PM – 6:30 AM local time, when the bulk of the N_2O_5 reactivity measurements were obtained, so

it is a subsample of all conditions experienced during the campaign. Nonetheless, clean marine air, marine air mixed with coastal urban pollution, and continental air were sampled during the campaign providing a variety of particle types and histories which are described in detail elsewhere (Liu et al., 2011).

Number size distributions were measured from 0.01 – 0.6 μm at ambient RH with a Scanning Mobility Particle Sizer (SMPS) (TSI Inc. 3010 CPC & TSI Inc. 3081 DMA) and from 0.6 – 20 μm at 15-30% RH using an Aerodynamic Particle Sizer (APS) (TSI Inc. 3321). Aerosols sampled into the SMPS were drawn through a short length of insulated tubing to maintain the RH at near ambient levels. These distributions were then converted to surface area concentrations (SA). The SMPS derived surface areas were not corrected for the lower RH in the flow reactor compared to ambient, and therefore represent an overestimate of the SA in this size range contributing to observed N_2O_5 reactivity. This overestimate would lead to $\gamma(N_2O_5)$ observations that are biased low depending on the actual hygroscopic growth factor of these particles. Assuming the particles are pure ammonium sulfate, our reported $\gamma(N_2O_5)$ values may be biased low by at most 50%. The sampling configuration of the inlet and the reactivity apparatus (described below) was such that large particles were unlikely to efficiently transit to the flow reactor due to inertial impaction. Using the APS measured surface area distribution, scaled by a pure ammonium sulfate hygroscopic growth factor, we estimate that on average, approximately 60% of the supermicron surface area is lost in transit to the flow reactor (Baron and Willeke, 2001). Much of the supermicron surface area is lost when sampling at 2 slpm through the 90 degree tee from the 14 slpm flow which results in a d_{50} ~2.5 μm. Moreover, during actual $\gamma(N_2O_5)$ measurements, the fraction of the scaled APS surface area estimated to reach the flow reactor was found to be on the order of 13% (±10%) of the SMPS reported surface

area. Therefore, we neglected it in the analyses performed here, leading to population average $\gamma(N_2O_5)$ that are possibly biased slightly high as a result. Neglecting this may also induce some variability in the agreement between observations and predictions due to a varying contribution of the supermicron particles to N_2O_5 reactivity. The focus here is on the submicron particle contribution to N_2O_5 reactivity.

Non-refractory size-resolved particle composition over the size range of 0.01 – 1 μm was measured using an Aerodyne quadrupole aerosol mass spectrometer (AMS). The AMS co-sampled from the same inlet as the N_2O_5 reactivity apparatus described below. Mass concentrations of organics, sulfate, ammonium, nitrate, and chloride were obtained at five minute time resolution. In addition, post-campaign positive matrix factorization (PMF) analysis separated the organic mass concentration into three factors: oxidized (aged combustion and biogenic SOA), biomass burning, and marine organic aerosol; OOA, BBOA, and MOA, respectively (Liu et al., 2011). These factors illustrate the variety of air masses sampled during the study period. Collectively we refer to the organic species as particulate organic mass (POM). These aerosol composition measurements and a recently developed N_2O_5 reaction probability parameterization were used to derive predictions of the N_2O_5 reaction probability for comparison with measurements. The parameterization estimates the reaction probability given the aerosol nitrate, chloride, and liquid water content (Bertram and Thornton, 2009). The latter were obtained using an online aerosol thermodynamic equilibrium model (AIM) (Wexler and Clegg, 2002) with the measured non-refractory ammonium, sulfate, nitrate, and chloride mass loadings, and flow reactor RH as inputs. Non-refractory chloride does not include chloride from sea salt, which is not quantitatively measured by the AMS. Organic species were assumed to not contribute to the overall particle water content and were not included in the aerosol modeling.

This assumption is appropriate if organics are indeed hydrophobic and do not inhibit water uptake. Over the course of this study, there was significant alkane character to the organic mass which would support the assumption that organic species were hydrophobic (Liu et al., 2011), but we do not have direct knowledge of the particle hygroscopicity. We also used the AMS size-resolved particle composition to calculate surface area weighted N_2O_5 reaction probabilities. The net result was not substantially different to the simpler approach using the bulk mass composition, which we report here.

N_2O_5 reactivity was measured using a similar version of the flow reactor apparatus described previously (Bertram et al. 2009). Briefly, ambient air was sampled from 4 m above the pier (15 m above sea level) at 14 standard liters per minute (slpm) through a 6 mm inner diameter (ID) stainless steel tube. 2 slpm was drawn through a 90° tee from the main 14 slpm flow and sent through a 1 meter long, 6 mm ID stainless steel tube to the flow reactor. Air then passed into a conical aluminum entrance to the flow reactor, either directly or first through a glass woven filter that removed ~99% of the aerosol surface area. The reaction of excess NO_2 with ozone, produced from the photolysis of O_2 in high purity air, served as the N_2O_5 source. A 40 standard cubic centimeters per minute (sccm) flow of N_2 containing the N_2O_5 from the relatively constant (± 2%) source was then added to the ambient air stream. The main body of the flow reactor is a 15 cm inner diameter, 90 cm long stainless-steel tube which was coated with a halocarbon wax to suppress wall reactions. The dimensions and flow rate gave a residence time (t_{res}) of ~8 minutes. N_2O_5 eluting from the flow reactor was monitored using an iodide ion (I^-) chemical ionization mass spectrometer (CIMS) described previously (Kercher et al., 2009).

By monitoring the N_2O_5 source output with the CIMS and periodically filtering out aerosol particles, the N_2O_5-particle reaction probability was retrieved by the so-called particle

modulation technique. A representative measurement cycle is shown in Figure 2. Under an assumption of constant wall loss conditions between filter on/off states, the relative changes in the N_2O_5 signal (SIG) between the filter on/off states was used to extract the pseudo first order rate constant for N_2O_5-particle reactions (k_{het}) about every 50 minutes. We allowed 15 minutes of equilibration time between filter states and then averaged the N_2O_5 signal for 10 minutes. The resulting k_{het} was then used along with the measured particle surface area concentration (SA) to calculate the reaction probability, as shown in Eq. 3 and Eq. 4. The single-point precision for a reaction probability measurement at a particle surface area concentration of 100 $\mu m^2 m^{-3}$ is ±0.01 and decreases to ±0.003 with a surface area concentration of 300 $\mu m^2 m^{-3}$. This imprecision is driven primarily by random variations in source output and detector noise and thus adjacent measurements can be averaged to reduce the scatter. A more complete discussion of the reactivity apparatus and its capabilities can be found in other publications (Bertram et al., 2009a; Bertram et al., 2009b).

$$k_{het} = -\frac{\ln\left(\frac{sig^{w/}}{sig^{w/o}}\right)}{t_{res}} \quad (3)$$

$$\gamma(N_2O_5) \approx \frac{4k_{het}}{\omega SA} \quad (4)$$

3.2.1 Data Quality and Averaging

The most significant challenge to obtaining meaningful reactivity measurements was maintaining a relatively constant temperature within the instrument trailer over the course of a filter on/off/on cycle. Large temperature swings affect the relative humidity, and fluctuations in RH change the wall loss rate within the flow reactor (Bertram et al., 2009a).

In light of these effects, we instituted a fairly rigorous data quality filter. We reject any reaction probabilities obtained when the RH in the flow reactor measured at the end of a filter on/off/on cycle was more than 2% different from that measured at the start. Large variations in flow reactor RH, inferred from trailer temperature swings, were most evident during the daytime hours as the instrument trailer heated up and personnel entered and exited the trailer. The nighttime temperatures were much more stable. Therefore 72% of the 106 reaction probabilities that passed the quality assurance checks occurred at night between 9:00 PM and 6:30 AM local time. During these time periods the winds (shown in Figure 1b) came predominantly from the SSE, corresponding to urban San Diego and La Jolla, CA, and the NNW potentially bringing air from the Los Angles urban area. Additionally, we reject any data where NO concentrations exceeded 750 pptv to avoid artificial reactivity changes caused by the NO_3/N_2O_5 equilibrium (Bertram et al., 2009b).

Reactivity measurements that passed the above criteria were then averaged into 24 hr bins, primarily to reduce point-to-point variation in the data caused by measurement imprecision. For figures showing $\gamma(N_2O_5)$, we report the bin mean as points, the standard deviation (1σ) to illustrate point-to-point variability within the bin as vertical bars, and the measurement error obtained by error propagation using the SA precision dependence discussed above as gray shading. For comparison purposes, predictions of $\gamma(N_2O_5)$ from the parameterization were similarly averaged using only values generated from data obtained coincident with each individual reactivity measurement.

3.3 Results and Discussion

The surface area concentration contributed by particles less than 0.6 μm in diameter is shown in Figure 3b, and the AMS reported non-refractory aerosol composition is shown in Figure 3b. In general, over the course of the study, particle surface area correlated well with aerosol mass loadings. In terms of particle composition, two distinct periods are apparent over the study. The first period (days 254 – 260) was marked by high sulfate loadings with comparatively low POM and nitrate loadings. The bulk of the particle composition for this period is likely ammonium sulfate or ammonium bisulfate. Ammonium loadings largely followed sulfate trends. Ammonium sulfate aerosol is hygroscopic and an efficient substrate for N_2O_5-particle reactions, so $\gamma(N_2O_5)$ for this period are expected to be relatively high. The second period (days 261 – 272) has a notable drop in sulfate loadings and a substantial increase in particulate nitrate accompanied by an increase in POM. The largest nitrate loadings occurred when winds were out of the NNW, and the air may have originated from the Los Angeles area as noted above. Compared to the first period, $\gamma(N_2O_5)$ is expected to be relatively low in the second period due to an increase in the nitrate effect and the potential for non-hygroscopic organic species to lower, in a relative sense, the liquid water content or form coatings.

Sea salt chloride mass is not measured efficiently by the AMS, so the reported non-refractory chloride data represent a lower limit to actual particulate chloride loadings. Small chloride loadings relative to nitrate (Cl^-moles/NO_3^-moles ~ 0.1) have been shown to be able to negate the nitrate effect in laboratory studies (Bertram and Thornton, 2009). If the particles are internally mixed, then, in some instances during this study, the non-refractory chloride measured by the AMS, while a lower limit, is still large enough to overcome the nitrate effect and presumably drive $\gamma(N_2O_5)$ higher.

The mean of all $\gamma(N_2O_5)$ measured during the Pier study was 0.0054 with a standard deviation of 0.005, and the measurements ranged from a minimum of $3x10^{-5}$ to a maximum of 0.029. We bin and average the 106 reaction probabilities into daily (24-hour) bins requiring at least 3 reaction probability measurements per bin. The time series is shown in Figure 4a as black squares. The vertical lines indicate the 1σ variation of points within the bin. The gray shading represents the instrumental error obtained by propagating the SA-dependent precision (see above) through the averaging.

As seen in Figure 4a, $\gamma(N_2O_5)$ during the early portion of the study (days 254 - 260) was relatively high, indicating efficient hydrolysis of N_2O_5 consistent with the high sulfate mass loadings relative to nitrate loadings. The mean $\gamma(N_2O_5)$ for this first period was 0.008. This period also included the campaign maximum $\gamma(N_2O_5)$ of 0.029. After day 260, the increase in the nitrate mass fraction coincides with a drop in $\gamma(N_2O_5)$ to a mean of 0.004 for this period. Figure 4b shows the mole ratio of particulate water to particulate nitrate. Particulate water estimates are predicted from the thermodynamic aerosol equilibrium model. The two have competing effects on $\gamma(N_2O_5)$ as described above, and these effects are most apparent in the binned $\gamma(N_2O_5)$ values when the nitrate loadings increase after day 260. During the early portion the mole ratio is biased toward H_2O with values near 75, but as the study progresses the ratio changes toward nitrate with mean values near 12, and $\gamma(N_2O_5)$ drops accordingly. The nitrate effect is most obvious in the period between days 260 and 262 where the binned $\gamma(N_2O_5)$ drops from 0.005 to 0.001 as the water to nitrate mole ratio drops from 20 to 6. Starting at day 262, the rise in the water to nitrate ratio coincides with increases in $\gamma(N_2O_5)$. Additionally, on day 269 the water to nitrate ratio shows a campaign minimum which also aligns with the minimum in $\gamma(N_2O_5)$.

Daily parameterized reaction probabilities are also calculated using the Bertram and Thornton (2009) parameterization with reported aerosol mass loadings and estimated particulate water from the AIM thermodynamic equilibrium model. The AIM model has been shown in other publications to reasonably estimate the particulate water content based on the inorganic particle composition (Engelhart et al., 2011). These predictions are shown with the 24-hour binned $\gamma(N_2O_5)$ values in Figure 4a. Predictions from the parameterizations were averaged using only output from the time periods for which a valid $\gamma(N_2O_5)$ measurement existed. The full reaction probability parameterization includes a chloride dependence, and predictions from this full parameterization are shown as red circles. The full parameterization estimates are consistently higher than the observed $\gamma(N_2O_5)$. Given the uncertainty in how chloride mass is distributed throughout the particle surface area distribution based on the AMS measurement, we also test the other extreme by neglecting the presence of particulate chloride in the parameterization. The estimates from the parameterization with chloride set equal to zero are also shown in Figure 4a as blue squares. Even when neglecting aerosol chloride, the parameterized reaction probabilities remain on average 1.5 to 3 times larger than the observed. This result indicates either that there are deficiencies in the parameterizations when applied to ambient aerosols, such as a neglected form of N_2O_5 reactivity suppression, or alternatively, that there is a systematic bias in the field measurements. That said, both parameterized reaction probabilities broadly correlate with observed N_2O_5 reaction probabilities on average, showing maximum values in the early part of the study and depressions between day 260 -262 and on day 269. Indeed, the parameterizations even show similar day-to-day variations, except the variations are much less pronounced in the parameterizations than in the observations.

The overestimates of the parameterizations are especially large during the first period of the study when particulate nitrate loadings are low. As noted above, some of the overestimation of the full parameterization may be caused by the assumption that chloride is internally mixed across all particles. The parameterization also has no explicit dependences on POM, the effects of which represent an area requiring more research. Similarly we neglect particle phase transitions and assume all particles are metastable solutions. Thus, if effloresced aerosol components were present in the atmosphere, then the parameterization would likely overestimate $\gamma(N_2O_5)$ given its strong dependence on particle phase (Thornton et al., 2003). Despite these deficiencies, the parameterization still manages to capture much of the day-to-day variability in $\gamma(N_2O_5)$. Moreover, the exclusion of particulate chloride from the parameterization doesn't vastly change the day-to-day behavior in the predictions relative to the observations. This result implies that nitrate concentrations relative to water must explain a significant amount of this variation in the parameterizations, and presumably that in the observations as well.

In Figure 5 we illustrate the extent to which the nitrate effect can explain the observed variations in $\gamma(N_2O_5)$ by binning the 24 hour reaction probabilities (measured and parameterized) as a function of the corresponding particulate water to nitrate ratios. We chose the water to nitrate bin widths such that the bins covered an appropriately large span of mole ratios over which the nitrate effect is apparent. Each bin has a minimum of three 24-hour average points (corresponding to at least 9 raw observations). Figure 5a shows that the parameterization estimates follow the overall shape in the observed $\gamma(N_2O_5)$ relative to the water to nitrate mole ratio. However, in an absolute sense, the persistent overestimate of the observed data is also clear. When the observations and predictions are normalized to their respective maximum values in Figure 5b, the agreement between the binned observations and the parameterization becomes

most apparent. Here the observations follow quite well the functional dependence on the water to nitrate mole ratio as predicted by the parameterization. The Scripps Pier observations therefore suggest that the magnitude of the nitrate effect found in laboratory studies and recent parameterizations (e.g. Wahner et al. (1998), Bertram and Thornton (2009)) is consistent with that found in the atmosphere at least for the range of conditions sampled.

Using *in situ* measurements made in Seattle, WA, Bertram et al. (2009b) found $\gamma(N_2O_5)$ was suppressed with increasing POM to sulfate mass ratios. The POM/SO_4 ratios in that study spanned a range of approximately 2 – 12. In contrast, over the course of the Scripps Pier study, 90% of the POM/SO_4 ratios were below 2. The Seattle observations showed an appreciable suppression of $\gamma(N_2O_5)$ at POM/SO_4 ratios above 6, whereas our observations exhibit similar $\gamma(N_2O_5)$ values but at the significantly lower POM/SO_4 ratios. Bertram et al. (2009b) argued that the decreasing trend in $\gamma(N_2O_5)$ with increasing POM/SO_4 in Seattle could be partly explained by a correlated increase in the nitrate effect if the increasing POM did not significantly contribute to liquid water content. Indeed, such a correlated impact between POM and nitrate appears in the Scripps Pier dataset as well. However, the differences in POM/SO_4 between these two locations indicate that either the organic components in the particles sampled at the Scripps Pier were substantially more effective at lowering $\gamma(N_2O_5)$ per contribution to particle mass than those in Seattle, or still another driver of $\gamma(N_2O_5)$ variability is operating at the Scripps Pier location. The explicit role of organics species on $\gamma(N_2O_5)$ remains to be determined and should be a topic of future investigations.

Additionally we estimated the $ClNO_2$ branching ratio ($\phi(ClNO_2)$ - also referred to as the yield) using the reactivity apparatus. Uncalibrated $ClNO_2$ signals were monitored by the CIMS during the N_2O_5 uptake experiments. Despite the uncertainties resulting from the uncalibrated

signals, $\phi(ClNO_2)$ values obtained are consistent with the low $\gamma(N_2O_5)$ values. The mean $\phi(ClNO_2)$ was ~10% with a standard deviation of ~10%. It should be stated that under atmospheric conditions it is likely that significant ClNO2 formation occurs on supermicron particle surface area, the majority of which is likely lost in transit to the flow reactor as we describe above. Therefore these yield estimates are likely lower limits. With this in mind, the $ClNO_2$ yields show no appreciable trend with AMS measured chloride, H_2O/NO_3, or POM/SO_4. Experiments of this type certainly warrant additional investigations.

3.4 Conclusions

We report direct *in situ* measurements of the N_2O_5-aerosol reaction probability taken in the late summer in La Jolla, CA, using a recently developed heterogeneous reactivity apparatus. Particulate nitrate appears to have the most important day-to-day influence on the measured reaction probabilities during the study. The suppression effect of nitrate can be clearly seen in daily averages, and the observed dependence on the water to nitrate ratio within ambient particles closely resembles the expected relationship based on previous laboratory studies. Given the prevalence of particulate nitrate in polluted urban areas, especially during winter when N_2O_5 chemistry is likely to be most important, chemical transport models should incorporate the nitrate effect into N_2O_5 reaction probabilities used therein. Our results suggest the existing parameterizations adequately capture the nitrate effect for the conditions sampled at the Scripps Pier. While the nitrate effect is likely a significant contributor to the variations in the Scripps Pier $\gamma(N_2O_5)$ measurements, the data also illustrate that an unidentified, yet persistent, means of suppression exists in addition to the nitrate effect, perhaps connected to POM but the mechanism remains unclear.

Though chloride is expected to be an important driver of the N_2O_5 reaction probability, it does not appear to play a large role in the reaction probabilities reported here. This conclusion is based on the fact that predictions which include the expected chloride effect in a bulk sense have worse agreement with observations compared to those which assume particulate chloride is negligible in the particles that dominate the surface area of the submicron mode. This finding has important implications not only for accurately predicting $\gamma(N_2O_5)$ in models, but also for determining the efficiency of halogen activation by N_2O_5. Assuming chloride was internally mixed across the submicron particle size distribution, and importantly, in particles containing nitrate, led to a large overestimate of $\gamma(N_2O_5)$ compared to observations. Given the connection between the $\gamma(N_2O_5)$ and the branching ratio to $ClNO_2$ production (see Eq. 2), these results imply that $ClNO_2$ production in this coastal environment may not be 100% efficient. Thus, to further our understanding of $ClNO_2$ production efficiencies, closure experiments that utilize simultaneous quantitative measurements of size-resolved inorganic particle composition and $\gamma(N_2O_5)$ alongside the suite of important nighttime constituents will be necessary.

References

Alexander, B., Hastings, M. G., Allman, D. J., Dachs, J., Thornton, J. A., and Kunasek, S. A.: Quantifying atmospheric nitrate formation pathways based on a global model of the oxygen isotopic composition (delta(17)O) of atmospheric nitrate, Atmospheric Chemistry and Physics, 9, 5043-5056, doi: 10.5194/acp-9-5043-2009, 2009.

Baron, P. A., and Willeke, K.: Aerosol Measurement: Principles, Techniques, and Applications, 2 ed., Wiley-Interscience, New York, 2001.

Behnke, W., George, C., Scheer, V., and Zetzsch, C.: Production and decay of $ClNO_2$, from the reaction of gaseous N_2O_5 with NaCl solution: Bulk and aerosol experiments, Journal of Geophysical Research-Atmospheres, 102, 3795-3804, doi: 10.1029/96jd03057, 1997.

Bertram, T. H., and Thornton, J. A.: Toward a general parameterization of N_2O_5 reactivity on aqueous particles: the competing effects of particle liquid water, nitrate and chloride, Atmospheric Chemistry and Physics, 9, 8351-8363, doi: 10.5194/acp-9-8351-2009, 2009.

Bertram, T. H., Thornton, J. A., and Riedel, T. P.: An experimental technique for the direct measurement of N_2O_5 reactivity on ambient particles, Atmospheric Measurement Techniques, 2, 231-242, doi: 10.5194/amt-2-231-2009, 2009a.

Bertram, T. H., Thornton, J. A., Riedel, T. P., Middlebrook, A. M., Bahreini, R., Bates, T. S., Quinn, P. K., and Coffman, D. J.: Direct observations of N_2O_5 reactivity on ambient aerosol particles, Geophysical Research Letters, 36, doi: 10.1029/2009gl040248, 2009b.

Brown, S. S., Dibb, J. E., Stark, H., Aldener, M., Vozella, M., Whitlow, S., Williams, E. J., Lerner, B. M., Jakoubek, R., Middlebrook, A. M., DeGouw, J. A., Warneke, C., Goldan, P. D., Kuster, W. C., Angevine, W. M., Sueper, D. T., Quinn, P. K., Bates, T. S., Meagher, J. F., Fehsenfeld, F. C., and Ravishankara, A. R.: Nighttime removal of NO_x in the summer marine boundary layer, Geophysical Research Letters, 31, doi: 10.1029/2004gl019412, 2004.

Brown, S. S., Ryerson, T. B., Wollny, A. G., Brock, C. A., Peltier, R., Sullivan, A. P., Weber, R. J., Dube, W. P., Trainer, M., Meagher, J. F., Fehsenfeld, F. C., and Ravishankara, A. R.: Variability in nocturnal nitrogen oxide processing and its role in regional air quality, Science, 311, 67-70, doi: 10.1126/science.1120120, 2006.

Brown, S. S., Dube, W. P., Fuchs, H., Ryerson, T. B., Wollny, A. G., Brock, C. A., Bahreini, R., Middlebrook, A. M., Neuman, J. A., Atlas, E., Roberts, J. M., Osthoff, H. D., Trainer, M., Fehsenfeld, F. C., and Ravishankara, A. R.: Reactive uptake coefficients for N_2O_5 determined from aircraft measurements during the Second Texas Air Quality Study: Comparison to current model parameterizations, Journal of Geophysical Research-Atmospheres, 114, doi: 10.1029/2008jd011679, 2009.

Cosman, L. M., and Bertram, A. K.: Reactive uptake of N_2O_5 on aqueous H_2SO_4 solutions coated with 1-component and 2-component monolayers, Journal of Physical Chemistry A, 112, 4625-4635, doi: 10.1021/jp8005469, 2008.

Cosman, L. M., Knopf, D. A., and Bertram, A. K.: N_2O_5 reactive uptake on aqueous sulfuric acid solutions coated with branched and straight-chain insoluble organic surfactants, Journal of Physical Chemistry A, 112, 2386-2396, doi: 10.1021/jp710685r, 2008.

Davis, J. M., Bhave, P. V., and Foley, K. M.: Parameterization of N_2O_5 reaction probabilities on the surface of particles containing ammonium, sulfate, and nitrate, Atmospheric Chemistry and Physics, 8, 5295-5311, doi: 10.5194/acp-8-5295-2008, 2008.

Dentener, F. J., and Crutzen, P. J.: Reaction of N_2O_5 on tropospheric aerosols - Impacts on the global distributions of NO_X, O_3, AND OH, Journal of Geophysical Research-Atmospheres, 98, 7149-7163, doi: 10.1029/92jd02979, 1993.

Engelhart, G. J., Hildebrandt, L., Kostenidou, E., Mihalopoulos, N., Donahue, N. M., and Pandis, S. N.: Water content of aged aerosol, Atmospheric Chemistry and Physics, 11, 911-920, doi: 10.5194/acp-11-911-2011, 2011.

Finlayson-Pitts, B. J., Ezell, M. J., and Pitts, J. N.: Formation of chemically active chlorine compounds by reactions of atmospheric NaCl particles with gaseous N_2O_5 and $ClONO_2$, Nature, 337, 241-244, doi: 10.1038/337241a0, 1989.

Folkers, M., Mentel, T. F., and Wahner, A.: Influence of an organic coating on the reactivity of aqueous aerosols probed by the heterogeneous hydrolysis of N_2O_5, Geophysical Research Letters, 30, doi: 10.1029/2003gl017168, 2003.

Hallquist, M., Stewart, D. J., Stephenson, S. K., and Cox, R. A.: Hydrolysis of N_2O_5 on sub-micron sulfate aerosols, Physical Chemistry Chemical Physics, 5, 3453-3463, doi: 10.1039/b301827j, 2003.

Hu, J. H., and Abbatt, J. P. D.: Reaction probabilities for N_2O_5 hydrolysis on sulfuric acid and ammonium sulfate aerosols at room temperature, Journal of Physical Chemistry A, 101, 871-878, doi: 10.1021/jp9627436, 1997.

Jacob, D. J.: Heterogeneous chemistry and tropospheric ozone, Atmospheric Environment, 34, 2131-2159, doi: 10.1016/s1352-2310(99)00462-8, 2000.

Kane, S. M., Caloz, F., and Leu, M. T.: Heterogeneous uptake of gaseous N_2O_5 by $(NH_4)_2SO_4$, NH_4HSO_4, and H_2SO_4 aerosols, Journal of Physical Chemistry A, 105, 6465-6470, doi: 10.1021/jp010490x, 2001.

Kercher, J. P., Riedel, T. P., and Thornton, J. A.: Chlorine activation by N_2O_5: simultaneous, in situ detection of $ClNO_2$ and N_2O_5 by chemical ionization mass spectrometry, Atmospheric Measurement Techniques, 2, 193-204, doi: 10.5194/amt-2-193-2009, 2009.

Liu, S., Day, D. A., Shields, J. E., and Russell, L. M.: Ozone-driven photochemical formation of carboxylic acid groups from alkane groups, Atmos. Chem. Phys. Discuss., 11, 7189-7233, doi: 10.5194/acpd-11-7189-2011, 2011.

Logan, J. A., Prather, M. J., Wofsy, S. C., and McElroy, M. B.: TROPOSPHERIC CHEMISTRY - A GLOBAL PERSPECTIVE, Journal of Geophysical Research-Oceans and Atmospheres, 86, 7210-7254, doi: 10.1029/JC086iC08p07210, 1981.

McNeill, V. F., Patterson, J., Wolfe, G. M., and Thornton, J. A.: The effect of varying levels of surfactant on the reactive uptake of N_2O_5 to aqueous aerosol, Atmospheric Chemistry and Physics, 6, 1635-1644, doi: 10.5194/acp-6-1635-2006, 2006.

Mentel, T. F., Sohn, M., and Wahner, A.: Nitrate effect in the heterogeneous hydrolysis of dinitrogen pentoxide on aqueous aerosols, Physical Chemistry Chemical Physics, 1, 5451-5457, doi: 10.1039/a905338g, 1999.

Mozurkewich, M., and Calvert, J. G.: Reaction probability of N_2O_5 on aqueous aerosols, Journal of Geophysical Research-Atmospheres, 93, 15889-15896, doi: 10.1029/JD093iD12p15889, 1988.

Ohara, T., Akimoto, H., Kurokawa, J., Horii, N., Yamaji, K., Yan, X., and Hayasaka, T.: An Asian emission inventory of anthropogenic emission sources for the period 1980-2020, Atmospheric Chemistry and Physics, 7, 4419-4444, doi: 10.5194/acp-7-4419-2007, 2007.

Osthoff, H. D., Roberts, J. M., Ravishankara, A. R., Williams, E. J., Lerner, B. M., Sommariva, R., Bates, T. S., Coffman, D., Quinn, P. K., Dibb, J. E., Stark, H., Burkholder, J. B.,

Talukdar, R. K., Meagher, J., Fehsenfeld, F. C., and Brown, S. S.: High levels of nitryl chloride in the polluted subtropical marine boundary layer, Nature Geoscience, 1, 324-328, doi: 10.1038/ngeo177, 2008.

Park, S.-C., Burden, D. K., and Nathanson, G. M.: The inhibition of N_2O_5 hydrolysis in sulfuric acid by 1-butanol and 1-hexanol surfactant coatings, Journal of Physical Chemistry A, 111, 2921-2929, doi: 10.1021/jp068228h, 2007.

Roberts, J. M., Osthoff, H. D., Brown, S. S., Ravishankara, A. R., Coffman, D., Quinn, P., and Bates, T.: Laboratory studies of products of N_2O_5 uptake on Cl^- containing substrates, Geophysical Research Letters, 36, doi: 10.1029/2009gl040448, 2009.

Robinson, G. N., Worsnop, D. R., Jayne, J. T., Kolb, C. E., and Davidovits, P.: Heterogeneous uptake of $ClONO_2$ and N_2O_5 by sulfuric acid solutions, Journal of Geophysical Research-Atmospheres, 102, 3583-3601, doi: 10.1029/96jd03457, 1997.

Shindell, D. T., Faluvegi, G., Koch, D. M., Schmidt, G. A., Unger, N., and Bauer, S. E.: Improved Attribution of Climate Forcing to Emissions, Science, 326, 716-718, doi: 10.1126/science.1174760, 2009.

Thornton, J. A., Braban, C. F., and Abbatt, J. P. D.: N_2O_5 hydrolysis on sub-micron organic aerosols: the effect of relative humidity, particle phase, and particle size, Physical Chemistry Chemical Physics, 5, 4593-4603, doi: 10.1039/b307498f, 2003.

Thornton, J. A., and Abbatt, J. P. D.: N_2O_5 reaction on submicron sea salt aerosol: Kinetics, products, and the effect of surface active organics, Journal of Physical Chemistry A, 109, 10004-10012, doi: 10.1021/jp054183t, 2005.

Thornton, J. A., Kercher, J. P., Riedel, T. P., Wagner, N. L., Cozic, J., Holloway, J. S., Dube, W. P., Wolfe, G. M., Quinn, P. K., Middlebrook, A. M., Alexander, B., and Brown, S. S.: A large atomic chlorine source inferred from mid-continental reactive nitrogen chemistry, Nature, 464, 271-274, doi: 10.1038/nature08905, 2010.

Wahner, A., Mentel, T. F., Sohn, M., and Stier, J.: Heterogeneous reaction of N_2O_5 on sodium nitrate aerosol, Journal of Geophysical Research-Atmospheres, 103, 31103-31112, doi: 10.1029/1998jd100022, 1998.

Wexler, A. S., and Clegg, S. L.: Atmospheric aerosol models for systems including the ions H^+, NH_4^+, Na^+, SO_4^{2-}, NO_3^-,Cl^-, Br^-, and H_2O, Journal of Geophysical Research-Atmospheres, 107, doi: 10.1029/2001jd000451, 2002.

Yienger, J. J.: An evaluation of chemistry's role in the winter-spring ozone maximum found in the northern midlatitude free troposphere, Journal of Geophysical Research-Atmospheres, 104, 8329-8329, doi: 10.1029/1999jd900140, 1999.

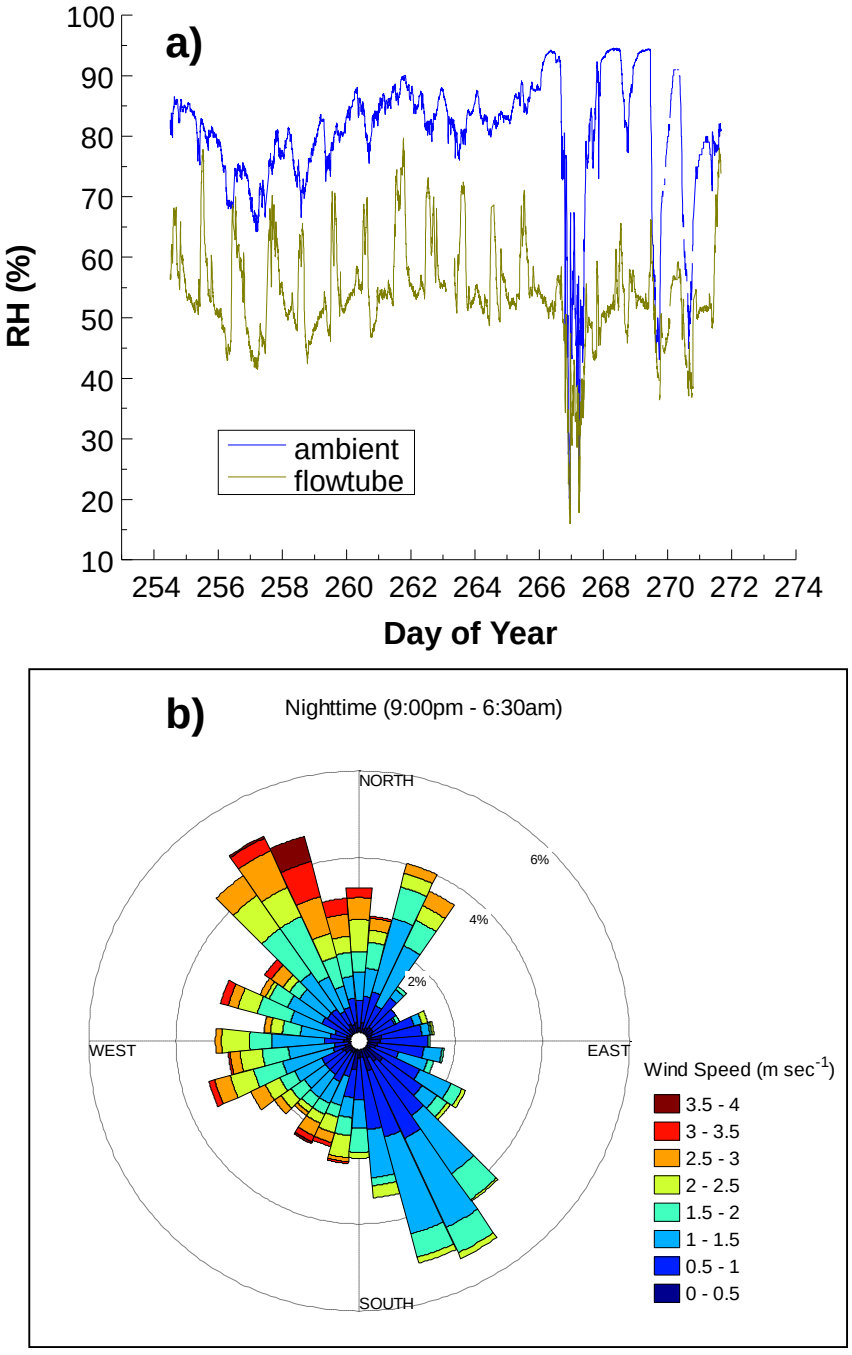

Figure 3.1 Meteorological conditions during the measurement campaign. a) The ambient relative humidity (RH%) is shown in blue. The calculated flow reactor RH is shown in olive. The large swings in flowtube RH accompany rapid temperature swings in the instrument trailer during the daytime. b) A wind rose illustrating the nighttime wind conditions at the measurement site.

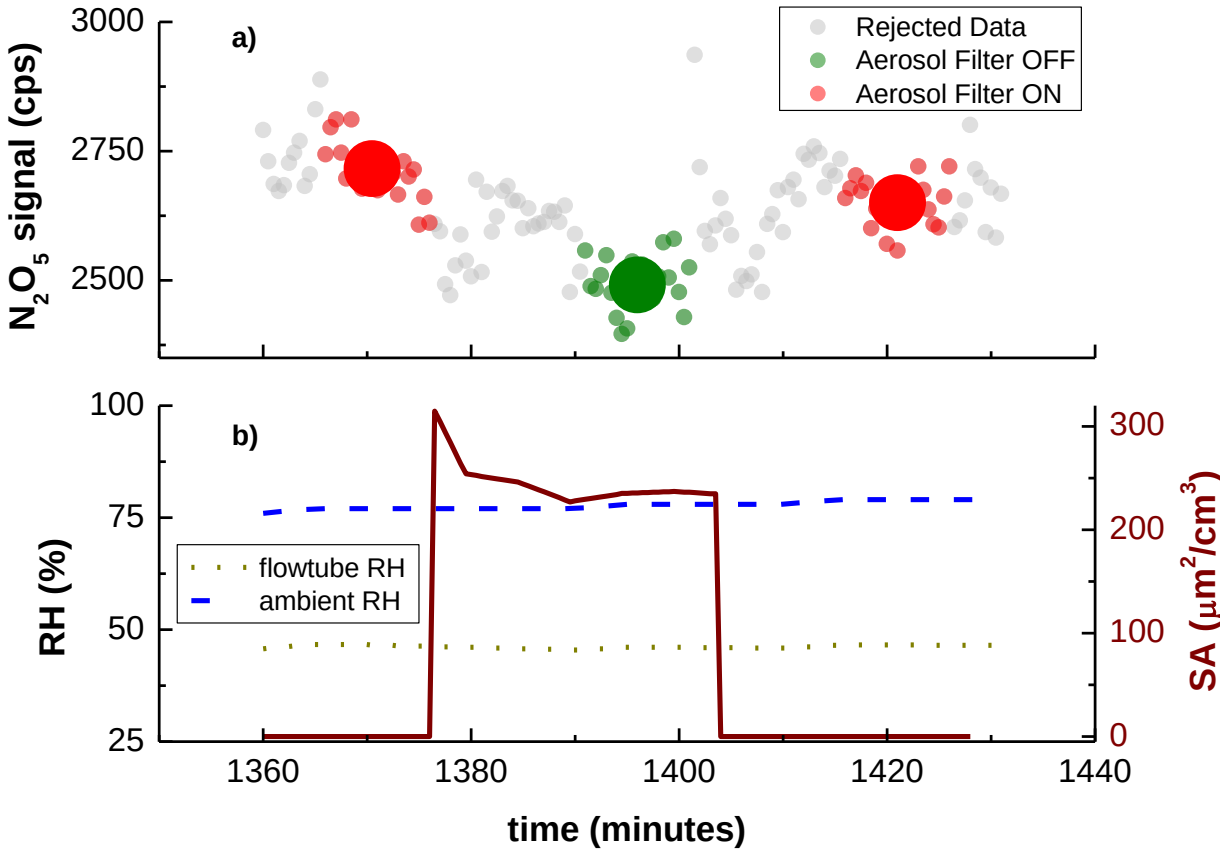

Figure 3.2 a) Select data illustrating the capabilities and precision of the reactivity apparatus over a single aerosol filter ON/OFF/ON cycle. Aerosol Filter ON indicates particles are not present in the flow reactor. Aerosol Filter OFF indicates when the reactor is sampling ambient particles. The size of the three large markers represents the 95% confidence range of signals incorporated in the average. b) Ambient RH (blue dashed line), calculated flow reactor RH (olive dotted line), and particle surface area concentrations are shown for the same period. Surface area is only shown for the Filter OFF status and set to zero for the Filter ON status to illustrate the particle surface areas within the flow reactor.

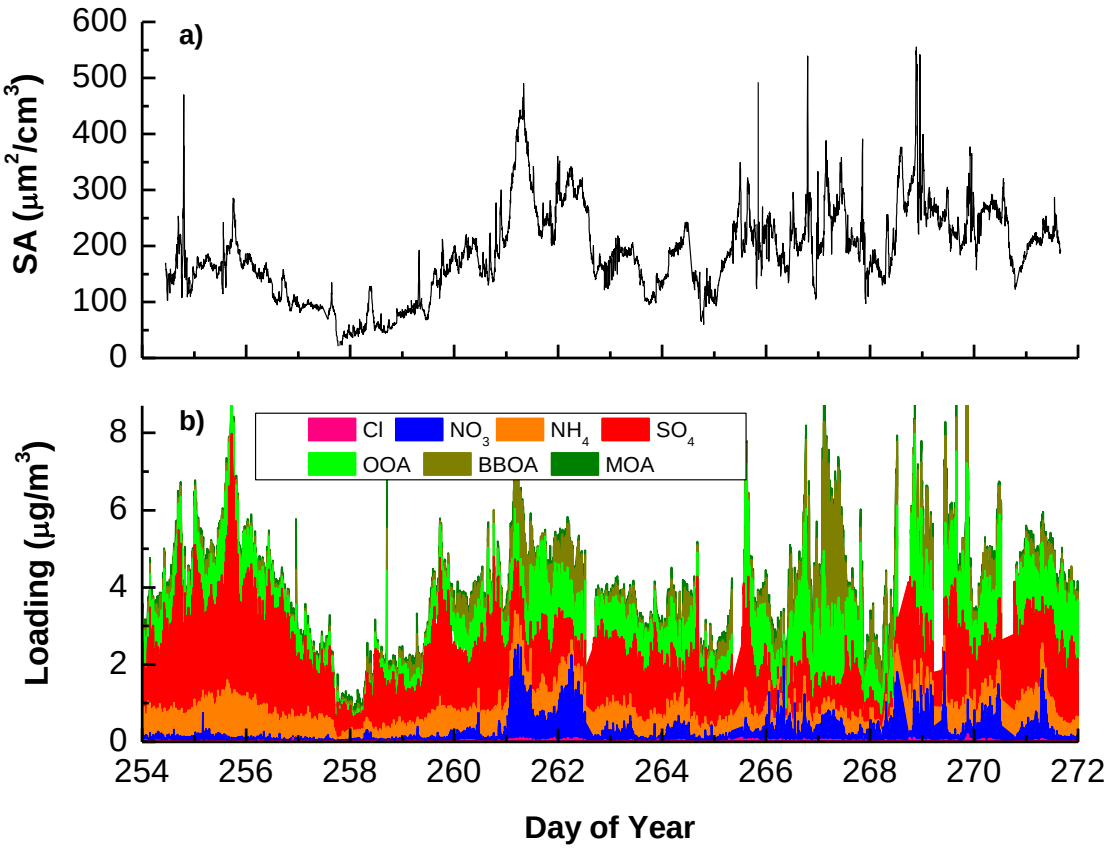

Figure 3.3 a) A full time series of measured particle surface area concentrations (0.01 - 0.6 μm) at ambient RH conditions for the study period. b) A full time series of AMS reported non-refractory particle composition for the study period with organics (shown in greens) differentiated by factor analysis as oxidized organic aerosol (OOA), biomass burning organic aerosol (BBOA), and marine organic aerosol (MOA). In general, high particle surface area correlated well with aerosol mass loadings indicating only a few periods in which submicron particle surface area were influenced by fresh sea salt emissions.

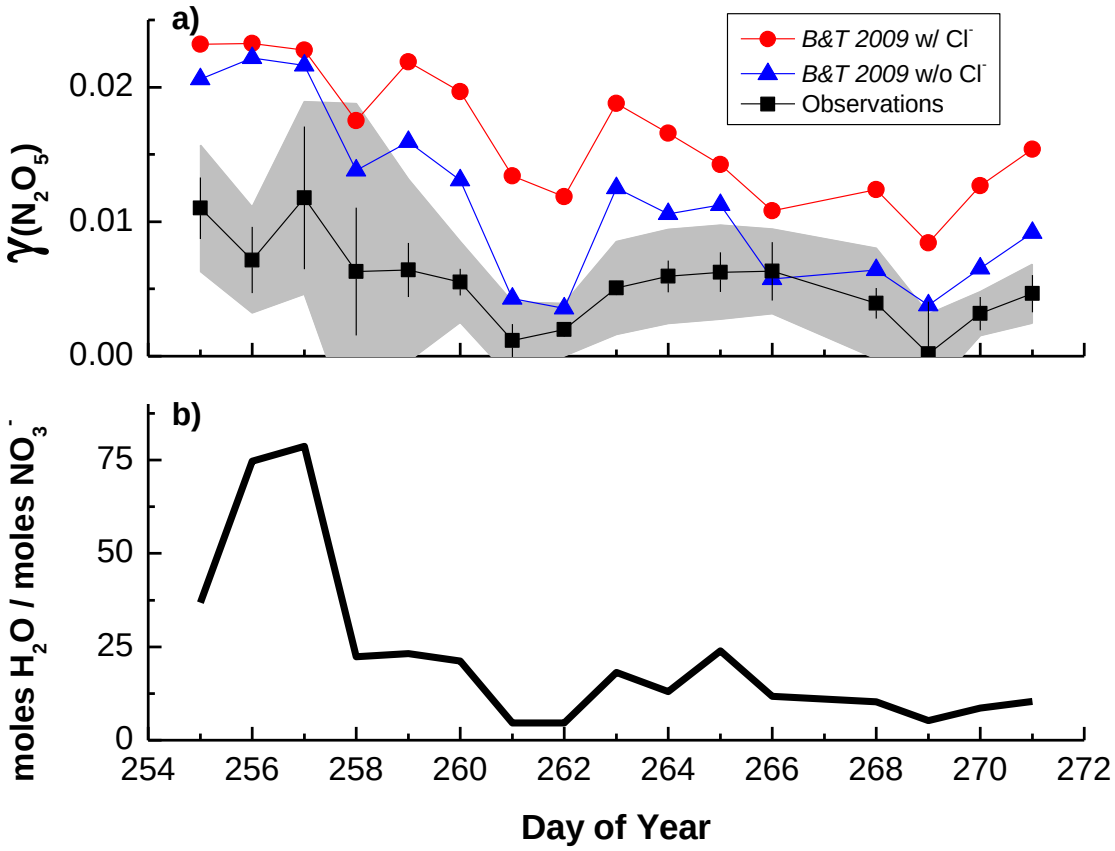

Figure 3.4 a) Observed (black squares) and parameterized (blue triangles and red circles) N_2O_5 reaction probabilities, $\gamma(N_2O_5)$, binned to a 24-hour time base for the entire study. The gray shaded area represents the estimated instrumental error, and the vertical bars represent the standard deviation (1σ) of the points in each bin. The red circles show the predictions of the full parameterization while the blue triangles show the predictions from the parameterization neglecting the chloride dependence. b) 24-hour bins of the mole ratio of particulate water predicted by the AIM model and the AMS reported nitrate loadings.

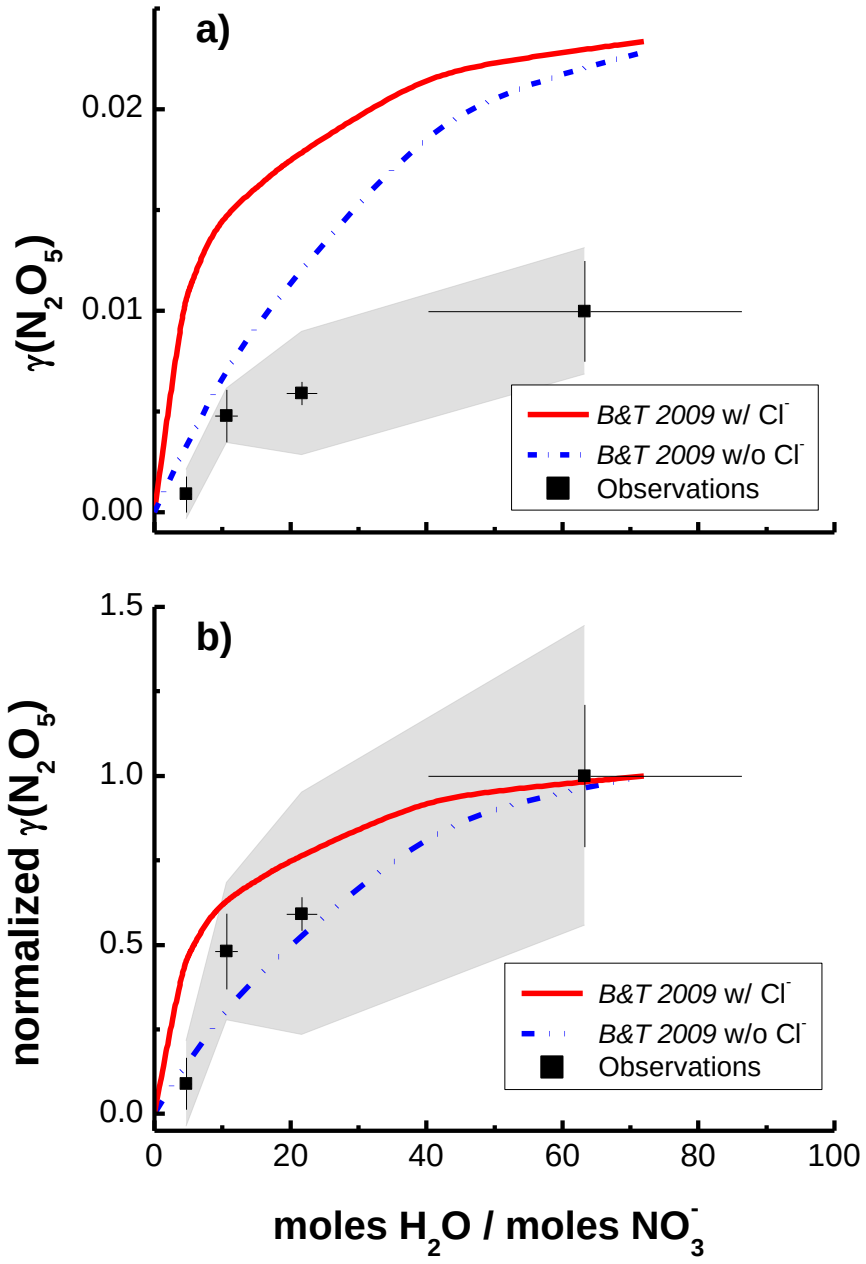

Figure 3.5 a) The observed dependence of N_2O_5 reaction probabilities (black squares) on the water to nitrate mole ratio (i.e. "the nitrate effect"). Parameterized reaction probabilities are also included for comparison. b) Observed (black squares) and parameterized reaction probabilities normalized to maximum values. For both panels, the shaded area represents estimated error from the precision of the measurement technique. The bars represent the 1σ variation of 24-hr averaged points in each bin.

Chapter 4

Nitryl Chloride and Molecular Chlorine in the Coastal Marine Boundary Layer

4.1 Introduction

Emissions of nitrogen oxide radicals ($NO_x \equiv NO + NO_2$) and volatile organic compounds (VOC) can lead to degraded air quality due to enhanced ozone and aerosol particle mass (Sillman, 1999). In coastal areas, the large natural halogen source represented by sea spray coupled with these emissions may further impact coastal air quality through enhanced oxidant sources in the form of chlorine atoms (Knipping and Dabdub, 2003). Atomic chlorine radicals are reactive toward a variety of VOC as well as ozone. For most alkanes, the rate coefficients for reaction with Cl-atoms surpass that of the hydroxyl radical (OH), the major tropospheric oxidant, by one to two orders of magnitude. Until recently, molecular chlorine (Cl_2) has represented a major focus of research into marine Cl-atom sources (Finley and Saltzman, 2006, 2008; Lawler et al., 2011; Spicer et al., 1998), followed by the more ubiquitous but often smaller source from the reaction of hydrochloric acid (HCl) with the hydroxyl radical (Singh and Kasting, 1988). Recently, observations of nitryl chloride, $ClNO_2$, in marine and continental air have illustrated the potential importance of $ClNO_2$ as another source of Cl-atoms (Mielke et al., 2011; Osthoff et al., 2008; Thornton et al., 2010). However, to our knowledge, collocated measurements of HCl, Cl_2, and $ClNO_2$ have not yet been reported, preventing a direct comparison of their relative importance.

Nitryl chloride is formed by nocturnal reactions of NO_x, ozone, and chloride-containing aerosol particles (Behnke et al., 1997; Finlayson-Pitts et al., 1989). NO_2 reacts with O_3 to form the nitrate radical, NO_3 (R1), which photolyzes rapidly during daylight hours, but after sunset can react with another NO_2 molecule to form dinitrogen pentoxide, N_2O_5. The latter typically exists in thermal equilibrium with NO_2 and NO_3 (R2a and R2b). These reactions are most relevant in areas where NO_2 and O_3 are high, such as aloft or downwind of urban areas during winter, where reactions of NO_3 with biogenic VOC or NO are relatively slow. N_2O_5 will react heterogeneously on aerosol particles to form either soluble nitric acid, HNO_3, or, if there is chloride within the particle, $ClNO_2$ (R3 – R4) which partitions to the gas phase. The branching between HNO_3 and $ClNO_2$ production is controlled by the relative abundance of particle chloride and water content, with $ClNO_2$ production generally expected to be efficient in coastal regions (Behnke et al., 1997; Bertram and Thornton, 2009; Finlayson-Pitts et al., 1989; Roberts et al., 2009; Thornton et al., 2003). HNO_3 formation represents a terminal sink for NO_x as it is efficiently removed from the atmosphere through dry and wet deposition. Reactions of N_2O_5 and NO_3 to form HNO_3 or organic nitrates are thought to account for up to ~50% of the removal of NO_x from the atmosphere (Alexander et al., 2009; Dentener and Crutzen, 1993). $ClNO_2$ formation potentially alters such estimates as $ClNO_2$ remains largely unreactive at night and is photolyzed in the morning to liberate NO_2 and Cl-atoms (R5). This process therefore represents an enhancement in the regional oxidizing power of the atmosphere with consequences for ozone formation and trace gas degradation.

$$NO_2 + O_3 \rightarrow NO_3 + O_2 \quad \text{(R1)}$$

$$NO_3 + NO_2 + M \rightarrow N_2O_5 + M \quad \text{(R2a)}$$

$$N_2O_5 \xrightarrow{\Delta} NO_3 + NO_2 \quad \text{(R2b)}$$

$$N_2O_5 + H_2O(l) \rightarrow 2HNO_3 \quad \text{(R3)}$$

$$N_2O_5 + Cl^-(aq) \rightarrow ClNO_2 + NO_3^-(aq) \quad \text{(R4)}$$

$$ClNO_2 + h\nu \rightarrow Cl\bullet + NO_2 \quad \text{(R5)}$$

Similarly, Cl_2 represents a Cl-atom source as it undergoes rapid photolysis in the daytime releasing two Cl-atoms. Cl_2 can be directly emitted from industrial processes associated with power generation, oil and metal refining, or large-scale bleaching processes such as at water treatment plants (Tanaka et al., 2000). Additionally, Cl_2 can be formed *in situ* within the atmosphere. Indeed, there has been a substantial effort to determine chemistry that can lead to elevated Cl_2 in polluted regions since the pioneering measurements of Spicer, et al. showing mixing ratios approaching 150 pptv in Long Island, New York (Spicer et al., 1998). Recent measurements of Cl_2 on the Pacific coast near La Jolla, CA by Finley and Saltzman indicated lower Cl_2 mixing ratios of order 20 pptv, mostly at night, though persistent daytime Cl_2 averaging near 3 pptv was also observed. Sustained daytime Cl_2, even at these small concentrations can be a significant Cl-atom source with implications for VOC degradation (Finley and Saltzman, 2006).

The most commonly inferred mechanisms of Cl_2 production are associated with the autocatalytic halogen activation mechanism (Vogt et al., 1996), which begins with a Cl atom reacting with ozone to form chlorine monoxide (ClO).

$$Cl\bullet + O_3 \rightarrow ClO + O_2 \quad \text{(R6)}$$

$$ClO + NO \rightarrow Cl\bullet + NO_2 \quad \text{(R7)}$$

$$ClO + HO_2 \rightarrow HOCl + O_2 \quad \text{(R8)}$$

$$ClO + NO_2 + M \rightarrow ClONO_2 + M \quad \text{(R9)}$$

ClO that reacts with either HO_2 or NO_2 forms the stable intermediates of hypochlorous acid (HOCl) which has been observed in the marine boundary layer or chlorine nitrate ($ClONO_2$), respectively (Lawler et al., 2011). These compounds can undergo photolysis, deposition, or react on acidic chloride-containing aerosol particles to form Cl_2 that partitions to the gas phase (R10 – R11) (Deiber et al., 2004; Gebel and Finlayson-Pitts, 2001; Vogt et al., 1996).

$$HOCl + Cl^-(aq) + H^+(aq) \rightarrow Cl_2 + H_2O \quad \text{(R10)}$$

$$ClONO_2 + Cl^-(aq) + H^+(aq) \rightarrow Cl_2 + HNO_3 \quad \text{(R11)}$$

These reactions, while carrying uncertainty in terms of their efficiency on atmospheric particles, can occur during both day and night. Thus they may be important for recycling Cl-atoms during the day while leading to the buildup of Cl_2 during the night. Other mechanisms for Cl_2 production have also been proposed, such as, the daytime reaction of OH on particle surfaces (Knipping et al., 2000; Laskin et al., 2003), and the production of bromine chloride (BrCl) via heterogeneous activation of particle bromide (Vogt et al., 1996). Due to a lack of observational evidence in our data set, bromine reactions are not considered in the following analysis. Most relevant to our data presented here is the recently proposed reaction of $ClNO_2$ on acidic chloride-containing particles to form Cl_2 and nitrous acid, HONO (R12) (Roberts et al., 2008).

$$ClNO_2 + H^+(aq) + Cl^-(aq) \rightarrow Cl_2 + HONO \quad \text{(R12)}$$

This mechanism has yet to be validated by field measurements, and the relationships between $ClNO_2$ and Cl_2 we observed during CalNex present an initial opportunity to assess its potential.

Herein, we examine the relative importance of Cl_2, $ClNO_2$, and HCl as Cl-atom sources in the region of Los Angeles urban outflow. We show that during CalNex, $ClNO_2$ was a large and dominant morning-time Cl-atom source that was broadly distributed in the outflow from the Los Angeles vicinity. Only the daytime Cl-atom source from HCl reaction with OH was found to be competitive, though Cl_2 levels below our detection capabilities would still be important at midday if present. In the morning and night, Cl_2 levels were typically minor by comparison, except within confined plumes that likely originated from local anthropogenic Cl_2 point sources. Sustained Cl_2 was observed at times on some nights providing support for *in situ* production, though the exact mechanism remains unclear. The magnitude of the Cl-atom source from $ClNO_2$ and HCl alone, as inferred from our measurements, rivals that previously inferred from Cl_2 in polluted coastal air (Finley and Saltzman, 2006; Pechtl and von Glasow, 2007; Spicer et al., 1998), and suggests that it should be incorporated in air quality models.

4.2 Methods and Campaign Description

CalNex 2010 was a large-scale field measurement campaign that took place throughout southern California during the spring and summer of 2010. This study included multiple ground, airborne, and ship-based measurements (Ryerson, 2012). Specifically, the R/V *Atlantis* offered a unique opportunity to take measurements aboard a mobile platform within the polluted marine boundary layer (MBL) from May 14 to June 8. The analysis reported here concentrates on the Los Angeles portion of the research cruise (May 16 – 31) where the largest concentrations of

$ClNO_2$ and Cl_2 were observed. After May 31 NO_x levels were generally low as the R/V *Atlantis* left the Los Angeles region, and outside of occasional ship plumes and urban outflow, observations of $ClNO_2$ and Cl_2 were often below detection limits. A list of relevant observations can be found in Table 1. Here, we describe in more detail the methods directly relevant to our conclusions.

$ClNO_2$ and Cl_2 mixing ratios were measured at ~0.5 Hz by sampling air at 12 standard liters per minute at 0.5 atm through an inlet composed of a 10 m length of 5 mm I.D. polytetrafluoroethylene (PTFE) tubing collocated with several other trace gas inlets at 17 m above sea level. The inlet setup was similar to those described previously (Kercher et al., 2009; Thornton et al., 2010). A portion of the air flow was directed to the University of Washington chemical ionization mass spectrometer (UW-CIMS), which was configured nearly identically to previous measurements (Kercher et al., 2009; Thornton et al., 2010). Iodide was used as the reagent ion, and $ClNO_2$ and Cl_2 were detected as ion clusters $I\cdot(ClNO_2)^-$ and $I\cdot(Cl_2)^-$. We also monitored ion clusters corresponding to HOCl though we did not attempt to calibrate our signal for this compound as the inlet was optimized for measurements of $ClNO_2$ and its precursor, N_2O_5. In all cases, all naturally occurring isotopes were monitored. For $ClNO_2$ calibrations, a known concentration of N_2O_5 as measured by a cavity ring-down instrument was passed over a wetted NaCl bed converting the N_2O_5 to $ClNO_2$ with near unit yield before being detected by the UW-CIMS. Cl_2 calibrations were performed every 70 minutes by periodically delivering a small flow from a certified Cl_2 permeation tube (KIN-TEK Laboratories, Inc.) to the UW-CIMS inlet. For further independent confirmation of the $ClNO_2$ detection sensitivity, Cl_2 from the permeation tube was converted to $ClNO_2$ on a $NaNO_2$ salt bed at the beginning and end of each Cl_2 calibration (Mielke et al., 2011). Instrumental backgrounds for $ClNO_2$ and Cl_2 were determined

by routinely sampling through a stainless steel tube filled with stainless steel wool heated to 200 °C which satisfactorily scrubs $ClNO_2$ and Cl_2 from ambient air. Assessments of inlet transmission efficiencies for $ClNO_2$ were performed almost daily to check for potential artifacts arising from generation and loss on sampling tube walls. Though inlet effects on $ClNO_2$ were usually negligible, the assembly was replaced almost daily as a precaution.

Cl_2 concentrations reported here likely represent an upper limit on ambient Cl_2 levels for two reasons. First, the distribution of ion signals associated with the $I\cdot(Cl_2)^-$ clusters rarely matched that expected from the isotopic ratios of Cl_2. There were significant interferences resulting in elevated backgrounds at m/z 198.9 and m/z 200.9, making isotopic confirmation of measured Cl_2 difficult except under periods of very elevated signal. These interferences were particularly large during daytime and so we have primarily limited our analysis of Cl_2 to night and early morning. Interferences at m/z 196.9, the major isotopic Cl_2 signal, were generally small as inferred from the difference between signal during sampling and the instrumental background. That said, signal at this m/z was routinely above the instrumental background during the daytime at values equivalent to a few parts per trillion on average; not dissimilar to that reported by Finley and Saltzman (Finley and Saltzman, 2006). Second, while we determined that Cl_2 was efficiently transmitted through our inlet, we could not rule out conversion of other gases such as HOCl or $ClONO_2$ to Cl_2 in the inlet.

Gas-phase acids, including HCl and HONO, were measured using a proof of concept technique with a recently developed chemical ionization compact time of flight mass spectrometer discussed in more detail elsewhere (Bertram et al., 2011). We use calibrated HCl concentrations reported from this instrument to calculate a diurnal average in the vicinity of Los Angeles outflow and to examine its behavior over one specific 2 hour period. A detailed

description of HCl measurements is forthcoming. We also utilize uncalibrated signals corresponding to HONO from the same 2 hour period as it provides a useful, albeit qualitative constraint on the composition of certain plumes.

A suite of VOC concentrations used to constrain Cl-atom loss rates in a 0-D chemical box model (described below) were measured by a Proton Transfer Reaction Time of Flight Mass Spectrometer (PTR-ToF) and a Gas Chromatograph with a Flame Ionization Detector (GC-FID). The PTR-ToF reported acetaldehyde, acetone, acetonitrile, benzene, dimethyl sulfide, 8 carbon containing aromatics, methyl vinyl ketone, methacrolein, methanol, monoterpenes, and toluene every minute. The GC-FID reported benzene, butene, ethane, ethyne, propane, propene, toluene, i-butane, n-butane, and n-pentane.

4.3 Results and Discussion

A time series of $ClNO_2$ and Cl_2 observations obtained in the vicinity of the Los Angeles (LA) basin is shown in Figure 1, along with a map of the ship track. Nighttime data was obtained almost continuously with instrument and inlet maintenance taking place primarily during the late afternoon of each day. $ClNO_2$ was observed on most nights, and always when sampling outflow from the polluted basin, suggesting persistent production of $ClNO_2$ in this region. The observation is consistent with expectations from the above mechanism and that the LA basin has collocated sources of both NO_x and particulate chloride (Thornton et al., 2010). A detailed assessment of $ClNO_2$ production efficiency and its variability in this region is the subject of future manuscripts. The goal here is to establish a baseline understanding of how $ClNO_2$ and Cl_2 are related to each other and of their importance as Cl-atom sources in the polluted marine boundary layer near LA relative to the more ubiquitous source from HCl.

The mean nighttime $ClNO_2$ mixing ratio observed during the cruise was 120 pptv with a large standard deviation of 230 pptv and a maximum of 2150 pptv. The maximum in $ClNO_2$ occurred on day of year 141 (May 21) about 15 kilometers west of Los Angeles International Airport in Santa Monica Bay. In contrast, Cl_2 was almost always lower than $ClNO_2$, at least by the end of the night, with a mean mixing ratio of 10 pptv and a standard deviation of 15 pptv. The maximum value of Cl_2 reached 200 pptv, but that was observed in narrow, abrupt plumes as described below. Averaged over the entire domain, the integrated concentration of $ClNO_2$ over an entire day was 7 times larger than that of Cl_2.

As shown in Figure 2, the actual relationship between Cl_2 and $ClNO_2$ varied night-to-night and even within a night. Daily correlation coefficients range from 0.7 to -0.6 over the course of the study, with an overall value of 0.3. We can conclude from this behavior that the processes which give rise to $ClNO_2$ and Cl_2 vary relative to one another in time and space as might be expected given that several processes can give rise to Cl_2 while, at this time only one reactant, N_2O_5, is known to produce nighttime $ClNO_2$.

To obtain further insights into the relationships between $ClNO_2$ and Cl_2 and their relative abundance in LA outflow, we present case studies from three nights in the Santa Monica Bay (SMB). These case studies include the highest $ClNO_2$ and Cl_2 mixing ratios observed during the study period and provide examples connecting $ClNO_2$ and Cl_2 geographically, as shown in Figure 3. In the left panels of Figure 3, we show time series of both $ClNO_2$ and Cl_2 from specific time periods within a given night. In the right panels we indicate *Atlantis'* position within SMB with a wind rose colored by the Cl_2 mixing ratios detected during those periods. As Cl_2 is classified as a Hazardous Air Pollutant (HAP), the U.S. EPA maintains an inventory of anthropogenic emissions. Therefore, also included in the right panels of Figure 3 are the

locations of documented Cl_2 emitters for a single year between 2000 and 2009 obtained from the South Coast Air Quality Management District (Chico, September 2011). Documented Cl_2 emitters are shown as points with their size proportionate to an annual emission factor in kilograms of Cl_2 emitted per year. The four sites shown in Figure 3 are registered from north to south as Palace Plating (15 kg/yr), LA City Sanitation Bureau (5 kg/yr), Chevron Products Co. (70 kg/yr), and Exxon Mobil Oil Corporation (300 kg/yr).

In Figure 3a, $ClNO_2$ and Cl_2 are both enhanced when the urban outflow is first encountered at approximately 2 AM local time on day 141 as the ship drove into SMB. The highest $ClNO_2$ mixing ratio of the study, 2150 pptv, is reached at 5 AM (141.2), just prior to sunrise. $ClNO_2$ then exhibits its expected decay after sunrise, as it undergoes photolysis. At the intercept of the urban outflow, Cl_2 increases nearly simultaneously as the $ClNO_2$, though perhaps with a slightly slower time constant. During the remainder of the night, $ClNO_2$ and Cl_2 are well correlated although the ratio of $ClNO_2/Cl_2$ decreases substantially towards the end of the night. After sunrise, in contrast to $ClNO_2$, Cl_2 decays slightly but remains elevated throughout the morning, which could be due to an artifact as discussed above, multiphase autocatalytic recycling, or continued sampling of local emission sources (see below). The behavior of Cl_2 on this night compared to others discussed below does seem to imply a more broadly distributed source, such as from *in situ* chemistry, instead of direct emission from a point source based on sampled wind directions. That Cl_2 is correlated to $ClNO_2$ is expected if nighttime heterogeneous conversion of HOCl and $ClONO_2$, either on atmospheric particles or our inlet, is the source of Cl_2. This notion requires that, on the preceding day, a significant fraction of Cl-atoms reacted with ozone to form ClO, and that ClO then formed HOCl or $ClONO_2$. Using observationally constrained model calculations, we find this idea to be plausible but highly sensitive to uncertain

parameters. Alternatively, the correlations could indicate Cl_2 is produced by heterogeneous conversion of $ClNO_2$ albeit at very low efficiency. This possibility seems less plausible, given that aerosol composition measurements taken during the study together with a thermodynamic model indicate submicron particle pH > 4 (Wexler and Clegg, 2002), and Roberts et al report that $ClNO_2$ to Cl_2 conversion occurs only at pH < 2 (Roberts et al., 2008). However, we cannot rule out that the conversion is occurring efficiently on a small fraction of the aerosol particle surface area (~0.1%) with pH < 2.

An additional challenge to inferring the importance of *in situ* chemical production of Cl_2 is the presence of direct emission sources within the SMB and the LA basin (Chico, September 2011). On day 144 (May 24), the *Atlantis* was positioned in the SMB shortly after sunset and stayed within ~2 km of the coast for the entire night. Figure 3b shows $ClNO_2$ increasing throughout this night, as expected in an area like Los Angeles with ubiquitous concentrations of $ClNO_2$ precursors. Contrary to the first case, Cl_2 is observed only in distinct pulses when the wind is from a narrow sector (80° to 100°) east of the R/V *Atlantis'* location. Within these plumes only HCl and HOCl showed correlated increases. Neither $ClNO_2$ nor HONO exhibit noticeable perturbations, ruling out conversion of $ClNO_2$ on acidic particles as being the sole Cl_2 source. Moreover, the plumes arrive from a sector with known reactive chlorine emitters, in particular, a water treatment plant and a complex that includes an electrical power generation plant and a refinery. These potential sources seem to spatially align well with Cl_2 observations, as in Figure 3b and 3c below. Depending upon the nature of dilution during this night and unknown properties of the emission source such as height and average intensity, our observations are roughly consistent with a 1000 lb/yr continuous emission of Cl_2 but almost certainly require a source larger than 10 lb/yr. Clearly, further validation of such emission sources is warranted.

Reactive chlorine point sources are apparently scattered throughout the LA basin (see Figure 4), and likely elsewhere, with implications for the interpretation of Cl_2 measurements in other polluted regions.

In the third and final case (Figure 3c), the *Atlantis* again entered the SMB at ~10 PM and remained 5 km off shore until 9 AM. Similar to the second case, time periods of high $ClNO_2$ existed with little to no Cl_2 such as during the early portion of the night when $ClNO_2$ remained relatively constant around 350 pptv. At the end of the night, ~6 AM, an apparent air mass shift and a decrease in wind speed occurred with $ClNO_2$ mixing ratios increasing to ~700 pptv and Cl_2 reaches values up to ~200 pptv. Flow remains generally out of the east during this event. On the whole, this final case provides further evidence that $ClNO_2$ and Cl_2 are enhanced in urban outflow and that $ClNO_2$ is more ubiquitous whereas Cl_2 is more episodic in space and time. The pulse of Cl_2 mixing ratios on this night exhibited a strong but variable correlation ($r = 0.8$, $p < 0.01$) with nitric oxide (NO), and ozone exhibited correlated decreases in the early half of the plume indicating fresh combustion emissions were simultaneously being sampled (see Figure 5). In addition, the Cl_2 correlated with reactive nitrogen species generally in the early part of the plume, but the changes in Cl_2, $ClNO_2$ and other reactive nitrogen species do not correspond in time perfectly. The initial increase in Cl_2 leads that of the others (see Figure 5). We could not detect an enhancement in HOCl nor HCl in this plume, possibly due to the greater transit time from the inferred source regions, or suggesting we were sampling Cl_2 from a different emission source or a mixture of *in situ* chemical production and emissions.

We finish this section by assessing the importance of $ClNO_2$ and Cl_2 as Cl-atom sources in the polluted marine boundary layer using a simple 0-D diurnal chemical box model. Briefly, the model calculates Cl-atom production from $ClNO_2$ and Cl_2 photolysis, and from the reaction

of HCl with OH. Reaction rate constants at 298 K were obtained from the NIST Chemical Kinetics Database (kinetics.nist.gov), the IUPAC Subcommittee for Gas Kinetic Data Evaluation (www.iupac-kinetic.ch.cam.ac.uk), and JPL's Chemical Kinetics and Photochemical Data for Use in Atmospheric Studies (Sander et al., 2011). Initial model inputs and photolysis frequencies are constrained based on the observations from the R/V *Atlantis*. We select data obtained in regions most likely influenced by Los Angeles outflow: in close proximity to Santa Monica Bay, The Port of Los Angeles, and Palos Verdes Peninsula (see Figure 6). The maximum mixing ratios in the diurnal averages for these data are used as initial inputs for $ClNO_2$, Cl_2, and HCl (275 pptv, 17 pptv, and 2.8 ppbv, respectively). $ClNO_2$ and Cl_2 decay away from their initial concentrations due to photolysis, while HCl concentrations remain relatively constant. This latter assumption masks significant variations in HCl over the course of a day, though the concentration used is consistent with previous measurements in urban outflow (Keene et al., 2007). The concentration of OH was parameterized using the average photolysis rate of O_3 to form $O(^1D)$ from the R/V *Atlantis* such that OH reached a maximum midday concentration of $5x10^6$ molec cm^{-3} and was zero at night. The only losses of Cl-atoms in the model were reaction with the VOCs listed above and with methane. Methane was fixed at 1800 ppbv, and the remaining VOCs were fixed to average concentrations observed during the day 141 Los Angeles outflow event (141.1 – 141.4). These concentrations of hydrocarbons result in a Cl-atom lifetime of 0.04 s.

The observationally constrained model demonstrates that, in the first 5 hours after sunrise, the vast majority of Cl-atom production is driven by $ClNO_2$ photolysis on average. The maximum in the total Cl-atom production rate of $2.5x10^5$ molecules $cm^{-3}sec^{-1}$ is reached at 9 AM which coincides with the maximum contribution by $ClNO_2$ (see Figure 7a). Cl-atom production

from Cl_2 peaks slightly earlier in the day as expected given its stronger absorption cross section in the visible. $ClNO_2$ dominates the morning-time Cl-atom source by more than a factor of 5. As the day progresses and OH concentrations increase, the contribution from HCl + OH expectedly increases and becomes the dominant Cl-atom source at approximately local noon. Over the course of an entire model day, $ClNO_2$ accounts for about 45% of the integrated Cl-atom production compared to 10% from Cl_2 photolysis, while the reaction of HCl with OH accounts for the remaining 45%. If inputs are based only on observations taken in SMB where urban outflow was most persistently observed ($ClNO_2$ = 475 pptv, double that used in Figure 7), the maximum Cl-atom production rate nearly doubles, and the importance of $ClNO_2$ increases to near 60% of the daily total production rate with Cl_2 and HCl producing 3% and 37%, respectively.

These Cl-atom production rates represent a significant contribution to morning-time oxidation, especially of alkanes, and including recycling reactions or incorporating small daytime Cl_2, as observed elsewhere (Finley and Saltzman, 2006), would only further increase the importance of Cl-atom chemistry in this region. In Figure 7b, we use the model predicted Cl-atom and OH concentrations to show the potential effect of Cl-atoms on the oxidation of the alkanes measured during CalNex relative to that of OH. Under an assumption that precursors of OH and Cl-atoms are collocated over the same air mass volume throughout the day, the model predicts that ~25% of total daily alkane oxidation is driven by Cl-atoms, and that Cl-atoms dominate in the early morning oxidation of alkanes before ~10 AM. The additional source of alkyl peroxy radicals from Cl-atom attack of alkanes will necessarily lead to an increase in the ozone production rate in the NO_x-saturated LA Basin and may have implications for the rate of secondary organic aerosol formation as well.

4.4 Conclusions

Within the Los Angeles region and likely other coastal urban areas, $ClNO_2$ dominates the morning-time source of Cl-atoms, while Cl_2 was found to be minor by comparison. Therefore, to assess the impacts of Cl-atom chemistry on urban air quality, it is critical that air quality models accurately incorporate nocturnal NO_x chemistry. That NO_x, O_3 and particle chloride are likely broadly distributed across coastal urban areas, implies $ClNO_2$ formation will be a ubiquitous component of nocturnal urban air masses that flow into the marine boundary layer. Cl_2 may have a greater variety of *in situ* and emission sources, but these sources appeared more sporadic compared to that of $ClNO_2$ in the LA Basin. Clearly, there remains more effort necessary to assess the dominant sources of Cl_2. The sources of $ClNO_2$ and HCl are relatively well understood and their incorporation into air quality models can therefore be an important first step towards accurately representing Cl-atom chemistry, though the potential for recycling should not be neglected. The relatively large early morning Cl-atom source driven by $ClNO_2$ that we estimate based on our observations can affect the chemistry of polluted marine boundary layer air throughout the day, especially that of alkane oxidation where Cl-atoms are often orders of magnitude faster than OH. This enhanced oxidation therefore has implications for coastal urban air quality by altering the total ozone production rate and the rate of anthropogenic secondary organic aerosol formation from alkanes.

References

Alexander, B., Hastings, M. G., Allman, D. J., Dachs, J., Thornton, J. A., and Kunasek, S. A.: Quantifying atmospheric nitrate formation pathways based on a global model of the oxygen isotopic composition (delta(17)O) of atmospheric nitrate, Atmospheric Chemistry and Physics, 9, 5043-5056, doi: 10.5194/acp-9-5043-2009, 2009.

Behnke, W., George, C., Scheer, V., and Zetzsch, C.: Production and decay of $ClNO_2$, from the reaction of gaseous N_2O_5 with NaCl solution: Bulk and aerosol experiments, Journal of Geophysical Research-Atmospheres, 102, 3795-3804, doi: 10.1029/96jd03057, 1997.

Bertram, T. H., and Thornton, J. A.: Toward a general parameterization of N_2O_5 reactivity on aqueous particles: the competing effects of particle liquid water, nitrate and chloride, Atmospheric Chemistry and Physics, 9, 8351-8363, doi: 10.5194/acp-9-8351-2009, 2009.

Bertram, T. H., Kimmel, J. R., Crisp, T. A., Ryder, O. S., Yatavelli, R. L. N., Thornton, J. A., Cubison, M. J., Gonin, M., and Worsnop, D. R.: A field-deployable, chemical ionization time-of-flight mass spectrometer, Atmospheric Measurement Techniques, 4, 1471-1479, doi: 10.5194/amt-4-1471-2011, 2011.

Bon, D. M., Ulbrich, I. M., de Gouw, J. A., Warneke, C., Kuster, W. C., Alexander, M. L., Baker, A., Beyersdorf, A. J., Blake, D., Fall, R., Jimenez, J. L., Herndon, S. C., Huey, L. G., Knighton, W. B., Ortega, J., Springston, S., and Vargas, O.: Measurements of volatile organic compounds at a suburban ground site (T1) in Mexico City during the MILAGRO 2006 campaign: measurement comparison, emission ratios, and source attribution, Atmospheric Chemistry and Physics, 11, 2399-2421, doi: DOI 10.5194/acp-11-2399-2011, 2011.

Chico, T.: personal communication - www.aqmd.gov, September 2011.

Deiber, G., George, C., Le Calve, S., Schweitzer, F., and Mirabel, P.: Uptake study of $ClONO_2$ and $BrONO_2$ by Halide containing droplets, Atmospheric Chemistry and Physics, 4, 1291-1299, doi: 10.5194/acp-4-1291-2004, 2004.

Dentener, F. J., and Crutzen, P. J.: Reaction of N_2O_5 on tropospheric aerosols - Impacts on the global distributions of NO_X, O_3, AND OH, Journal of Geophysical Research-Atmospheres, 98, 7149-7163, doi: 10.1029/92jd02979, 1993.

Finlayson-Pitts, B. J., Ezell, M. J., and Pitts, J. N.: Formation of chemically active chlorine compounds by reactions of atmospheric NaCl particles with gaseous N_2O_5 and $ClONO_2$, Nature, 337, 241-244, doi: 10.1038/337241a0, 1989.

Finley, B. D., and Saltzman, E. S.: Measurement of Cl_2 in coastal urban air, Geophysical Research Letters, 33, doi: 10.1029/2006gl025799, 2006.

Finley, B. D., and Saltzman, E. S.: Observations of Cl_2, Br_2, and I_2 in coastal marine air, Journal of Geophysical Research-Atmospheres, 113, doi: 10.1029/2008jd010269, 2008.

Fuchs, H., Dube, W. P., Cicioira, S. J., and Brown, S. S.: Determination of inlet transmission and conversion efficiencies for in situ measurements of the nocturnal nitrogen oxides, NO3, N2O5 and NO2, via pulsed cavity ring-down spectroscopy, Anal Chem, 80, 6010-6017, doi: Doi 10.1021/Ac8007253, 2008.

Gebel, M. E., and Finlayson-Pitts, B. J.: Uptake and Reaction of ClONO2 on NaCl and Synthetic Sea Salt, The Journal of Physical Chemistry A, 105, 5178-5187, doi: 10.1021/jp0046290, 2001.

Jayne, J. T., Leard, D. C., Zhang, X. F., Davidovits, P., Smith, K. A., Kolb, C. E., and Worsnop, D. R.: Development of an aerosol mass spectrometer for size and composition analysis of submicron particles, Aerosol Sci Tech, 33, 49-70, 2000.

Jordan, A., Haidacher, S., Hanel, G., Hartungen, E., Mark, L., Seehauser, H., Schottkowsky, R., Sulzer, P., and Mark, T. D.: A high resolution and high sensitivity proton-transfer-reaction time-of-flight mass spectrometer (PTR-TOF-MS), Int J Mass Spectrom, 286, 122-128, doi: DOI 10.1016/j.ijms.2009.07.005, 2009.

Keene, W. C., Stutz, J., Pszenny, A. A. P., Maben, J. R., Fischer, E. V., Smith, A. M., von Glasow, R., Pechtl, S., Sive, B. C., and Varner, R. K.: Inorganic chlorine and bromine in coastal New England air during summer, Journal of Geophysical Research-Atmospheres, 112, doi: 10.1029/2006jd007689, 2007.

Kercher, J. P., Riedel, T. P., and Thornton, J. A.: Chlorine activation by N_2O_5: simultaneous, in situ detection of $ClNO_2$ and N_2O_5 by chemical ionization mass spectrometry, Atmospheric Measurement Techniques, 2, 193-204, doi: 10.5194/amt-2-193-2009, 2009.

Knipping, E. M., Lakin, M. J., Foster, K. L., Jungwirth, P., Tobias, D. J., Gerber, R. B., Dabdub, D., and Finlayson-Pitts, B. J.: Experiments and simulations of ion-enhanced interfacial chemistry on aqueous NaCl aerosols, Science, 288, 301-306, 2000.

Knipping, E. M., and Dabdub, D.: Impact of chlorine emissions from sea-salt aerosol on coastal urban ozone, Environmental Science & Technology, 37, 275-284, doi: 10.1021/es025793z, 2003.

Laskin, A., Gaspar, D. J., Wang, W. H., Hunt, S. W., Cowin, J. P., Colson, S. D., and Finlayson-Pitts, B. J.: Reactions at interfaces as a source of sulfate formation in sea-salt particles, Science, 301, 340-344, 2003.

Lawler, M. J., Sander, R., Carpenter, L. J., Lee, J. D., von Glasow, R., Sommariva, R., and Saltzman, E. S.: HOCl and Cl_2 observations in marine air, Atmospheric Chemistry and Physics, 11, 7617-7628, doi: 10.5194/acp-11-7617-2011, 2011.

Lerner, B. M., Murphy, P. C., and Williams, E. J.: Field Measurements of Small Marine Craft Gaseous Emission Factors during NEAQS 2004 and TexAQS 2006, Environmental Science & Technology, 43, 8213-8219, doi: Doi 10.1021/Es901191p, 2009.

Mielke, L. H., Furgeson, A., and Osthoff, H. D.: Observation of $ClNO_2$ in a Mid-Continental Urban Environment, Environmental Science & Technology, 45, 8889-8896, doi: 10.1021/es201955u, 2011.

Osthoff, H. D., Roberts, J. M., Ravishankara, A. R., Williams, E. J., Lerner, B. M., Sommariva, R., Bates, T. S., Coffman, D., Quinn, P. K., Dibb, J. E., Stark, H., Burkholder, J. B., Talukdar, R. K., Meagher, J., Fehsenfeld, F. C., and Brown, S. S.: High levels of nitryl chloride in the polluted subtropical marine boundary layer, Nature Geoscience, 1, 324-328, doi: 10.1038/ngeo177, 2008.

Pechtl, S., and von Glasow, R.: Reactive chlorine in the marine boundary layer in the outflow of polluted continental air: A model study, Geophysical Research Letters, 34, doi: 10.1029/2007gl029761, 2007.

Roberts, J. M., Osthoff, H. D., Brown, S. S., and Ravishankara, A. R.: N_2O_5 oxidizes chloride to Cl_2 in acidic atmospheric aerosol, Science, 321, 1059-1059, doi: 10.1126/science.1158777, 2008.

Roberts, J. M., Osthoff, H. D., Brown, S. S., Ravishankara, A. R., Coffman, D., Quinn, P., and Bates, T.: Laboratory studies of products of N_2O_5 uptake on Cl^- containing substrates, Geophysical Research Letters, 36, doi: 10.1029/2009gl040448, 2009.

Ryerson, T.: Overview of Calnex-2010, in prep., 2012.
Sander, S. P., Abbatt, J., Barker, J. R., Burkholder, J. B., Friedl, R. R., Golden, D. M., Huie, R. E., Kolb, C. E., Kurylo, M. J., Moortgat, G. K., Orkin, V. L., and Wine, P. H.: "Chemical Kinetics and Photochemical Data for Use in Atmospheric Studies, Evaluation No. 17" http://jpldataeval.jpl.nasa.gov., JPL Publication, 10-6, 2011.
Sillman, S.: The relation between ozone, NOx and hydrocarbons in urban and polluted rural environments, Atmospheric Environment, 33, 1821-1845, doi: http://dx.doi.org/10.1016/S1352-2310(98)00345-8, 1999.
Singh, H. B., and Kasting, J. F.: Chlorine-Hydrocarbon Photochemistry in the Marine Troposphere and Lower Stratosphere, Journal of Atmospheric Chemistry, 7, 261-285, doi: 10.1007/bf00130933, 1988.
Spicer, C. W., Chapman, E. G., Finlayson-Pitts, B. J., Plastridge, R. A., Hubbe, J. M., Fast, J. D., and Berkowitz, C. M.: Unexpectedly high concentrations of molecular chlorine in coastal air, Nature, 394, 353-356, doi: 10.1038/28584, 1998.
Stark, H., Lerner, B. M., Schmitt, R., Jakoubek, R., Williams, E. J., Ryerson, T. B., Sueper, D. T., Parrish, D. D., and Fehsenfeld, F. C.: Atmospheric in situ measurement of nitrate radical (NO_3) and other photolysis rates using spectroradiometry and filter radiometry, Journal of Geophysical Research: Atmospheres, 112, D10S04, doi: 10.1029/2006jd007578, 2007.
Tanaka, P. L., Oldfield, S., Neece, J. D., Mullins, C. B., and Allen, D. T.: Anthropogenic sources of chlorine and ozone formation in urban atmospheres, Environmental Science & Technology, 34, 4470-4473, doi: 10.1021/es991380v, 2000.
Thornton, J. A., Braban, C. F., and Abbatt, J. P. D.: N_2O_5 hydrolysis on sub-micron organic aerosols: the effect of relative humidity, particle phase, and particle size, Physical Chemistry Chemical Physics, 5, 4593-4603, doi: 10.1039/b307498f, 2003.
Thornton, J. A., Kercher, J. P., Riedel, T. P., Wagner, N. L., Cozic, J., Holloway, J. S., Dube, W. P., Wolfe, G. M., Quinn, P. K., Middlebrook, A. M., Alexander, B., and Brown, S. S.: A large atomic chlorine source inferred from mid-continental reactive nitrogen chemistry, Nature, 464, 271-274, doi: 10.1038/nature08905, 2010.
Vogt, R., Crutzen, P. J., and Sander, R.: A mechanism for halogen release from sea-salt aerosol in the remote marine boundary layer, Nature, 383, 327-330, doi: 10.1038/383327a0, 1996.
Wexler, A. S., and Clegg, S. L.: Atmospheric aerosol models for systems including the ions H^+, NH_4^+, Na^+, SO_4^{2-}, NO_3^-,Cl^-, Br^-, and H_2O, Journal of Geophysical Research-Atmospheres, 107, doi: 10.1029/2001jd000451, 2002.
Williams, E. J., Fehsenfeld, F. C., Jobson, B. T., Kuster, W. C., Goldan, P. D., Stutz, J., and McCleanny, W. A.: Comparison of ultraviolet absorbance, chemiluminescence, and DOAS instruments for ambient ozone monitoring, Environmental Science & Technology, 40, 5755-5762, doi: Doi 10.1021/Es0523542, 2006.

Observations	Technique	Notes
$ClNO_2$, Cl_2, HOCl	Iodide Cluster CI-QMS (Kercher et al., 2009)	HOCl not calibrated
HCl, HONO	Acetate CI-cToF-MS (Bertram et al., 2011)	HONO not calibrated
VOC	GC-FID (Bon et al., 2011) and PTR-ToF-MS (Jordan et al., 2009)	acetaldehyde, acetone, acetonitrile, benzene, dimethyl sulfide, 8 carbon containing aromatics, methyl vinyl ketone, methacrolein, methanol, monoterpenes, toluene, butene, ethane, ethyne, propane, propene, toluene, i-butane, n-butane, and n-pentane
NO, NO_2	Chemiluminescence/LED photolysis (Lerner et al., 2009)	
O_3	UV absorption/chemiluminescence (Williams et al., 2006)	
N_2O_5	Iodide Cluster CI-QMS[1] and CaRDS (Fuchs et al., 2008)	
SO_2	Pulsed UV fluorescence (Lerner et al., 2009)	
CO	VUV resonance fluorescence (Lerner et al., 2009)	
Non-refractory particle composition	Aerodyne aerosol mass spectrometer (Jayne et al., 2000)	
Wind speed and direction	Standard anemometers	
Temperature and relative humidity	Standard sensors	
Molecular photolysis frequencies	Spectroradiometer (Stark et al., 2007)	

Table 4.1 Supporting measurements and observations used in the analysis.

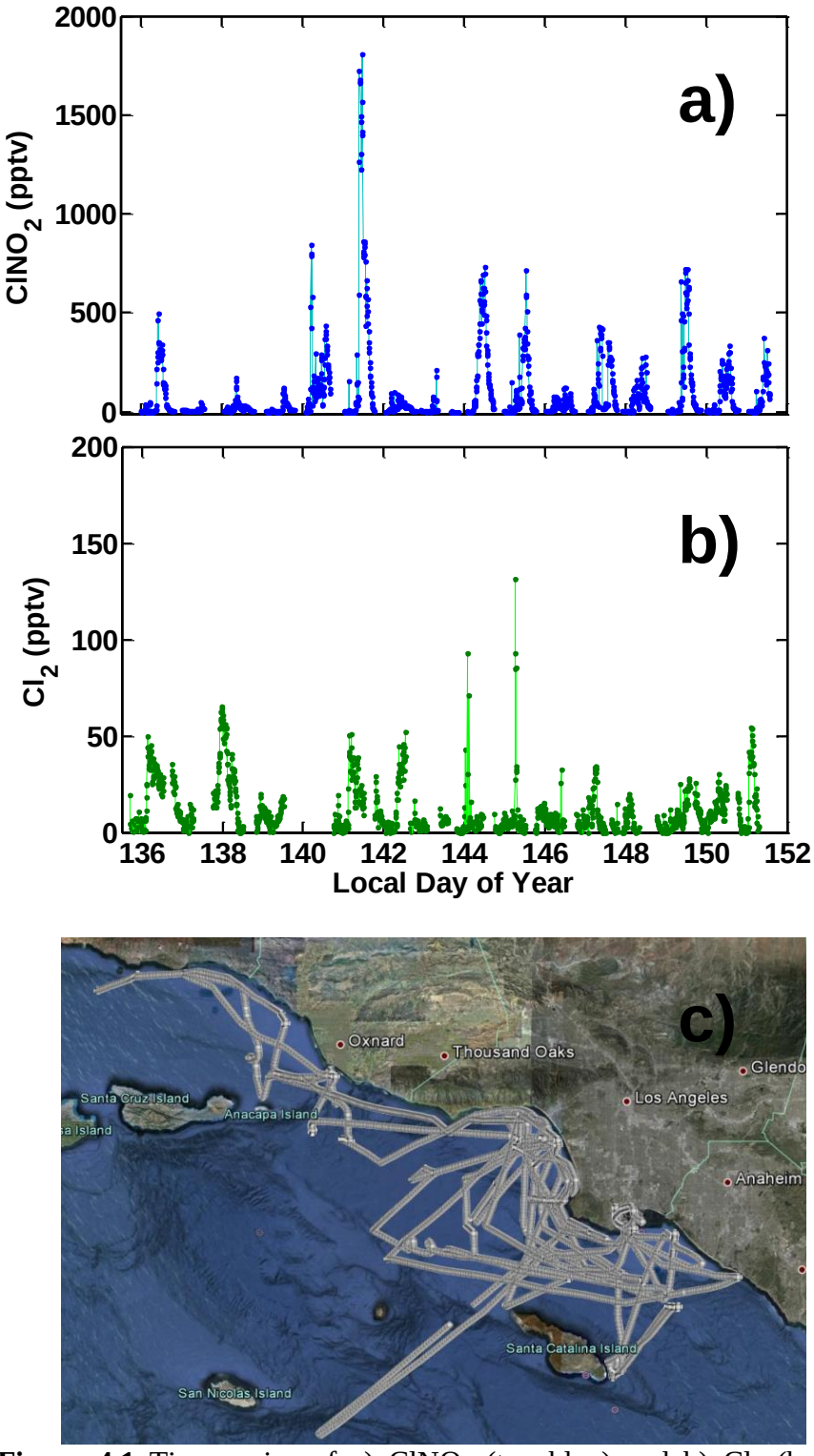

Figure 4.1 Time series of a) $ClNO_2$ (top blue) and b) Cl_2 (bottom green) mixing ratios as measured from the R/V *Atlantis* during CalNex 2010. The observations are averaged to a 10 minute time base. c) Ship track of the R/V *Atlantis* during the Los Angeles portion of the CalNex study.

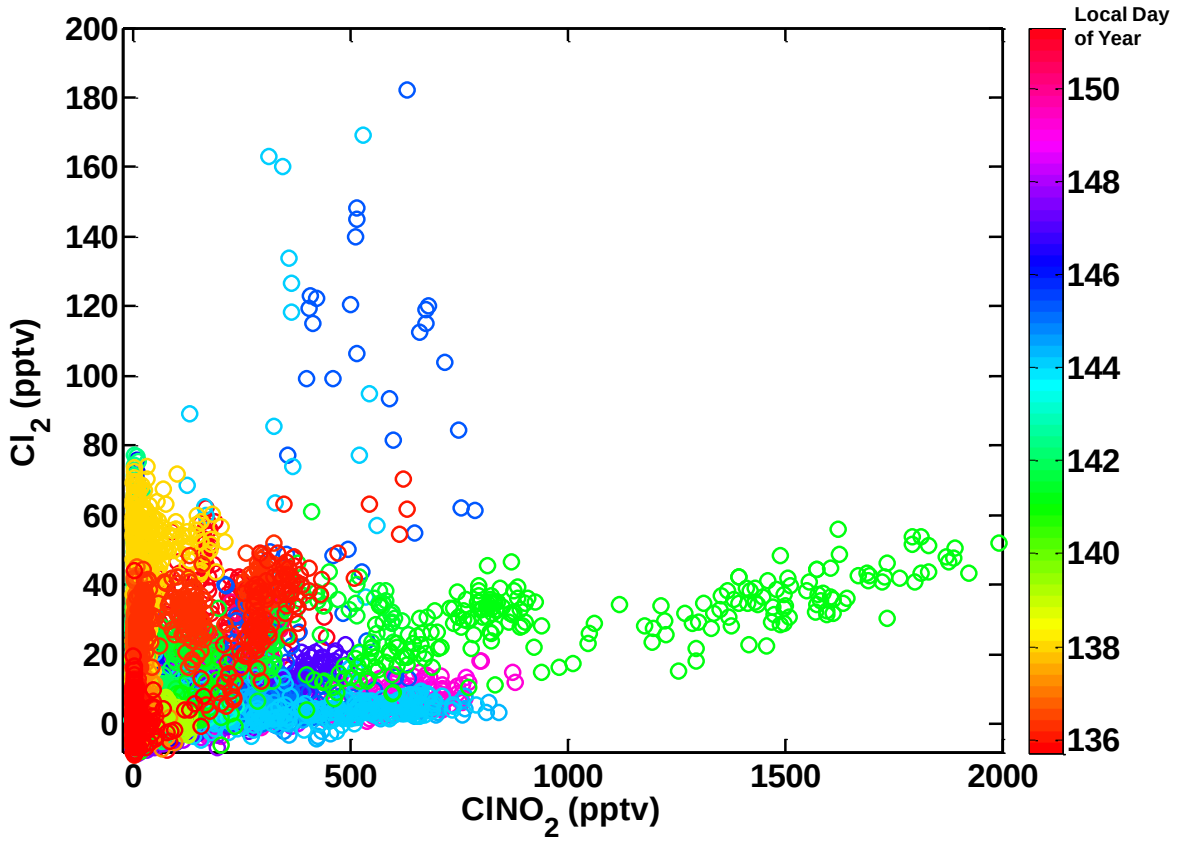

Figure 4.2 A scatter plot of Cl_2 mixing ratios vs. $ClNO_2$ mixing ratios colored by local day of year.

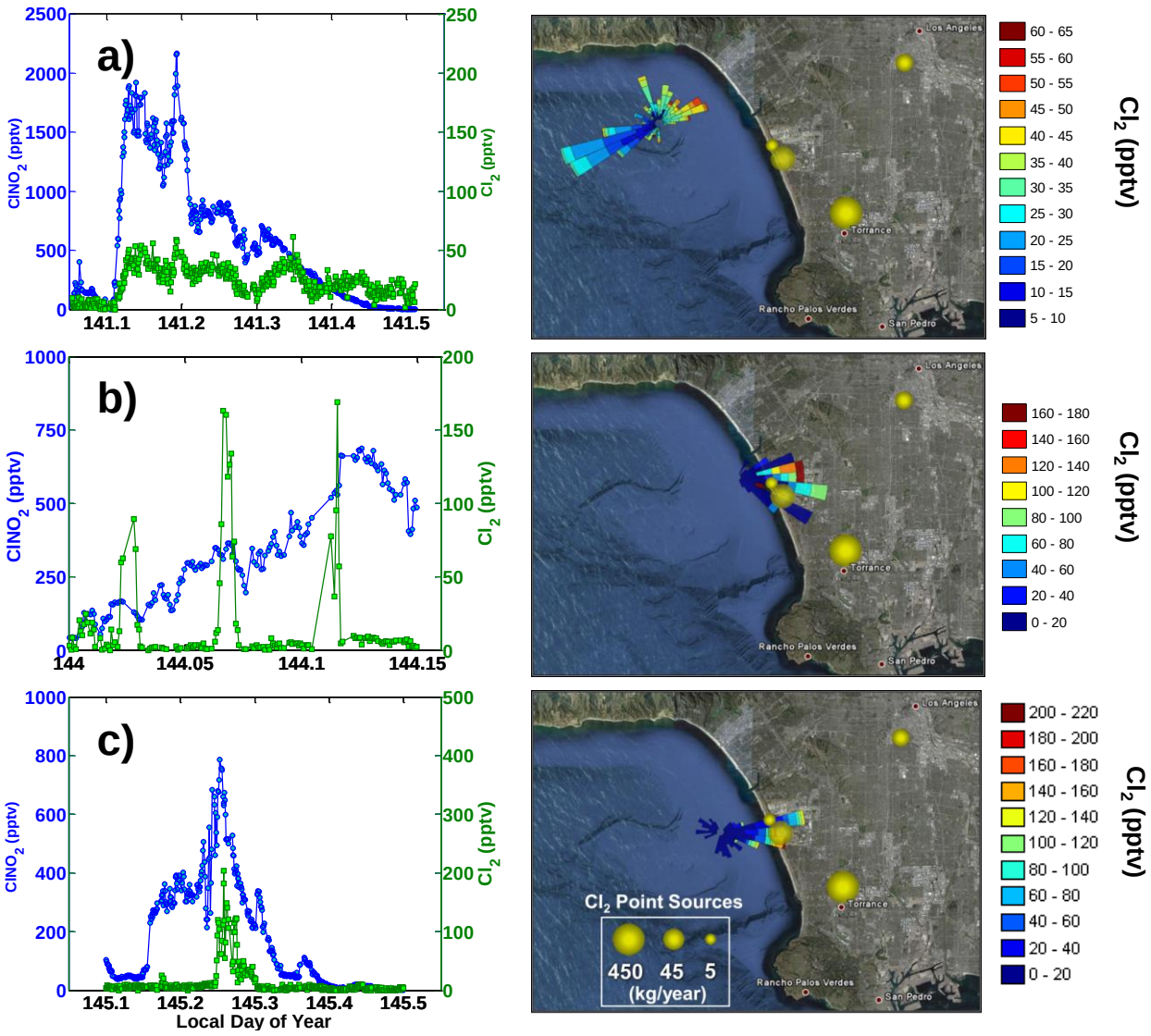

Figure 4.3 A selection of $ClNO_2$ and Cl_2 observations while the *Atlantis* was positioned in the Santa Monica Bay. The left side panels show a $ClNO_2$ and Cl_2 time series for each event. The right side panels show a wind rose for the same time period centered on the R/V *Atlantis* location and colored by the Cl_2 mixing ratios. The rose arm lengths are proportional to the frequency of winds originating from that direction. Also included as yellow dots are documented Cl_2 emission sources for the Los Angeles Basin. The size of the dot is proportional to an annual Cl_2 emission rate between 2000 and 2009 (Chico, September 2011).

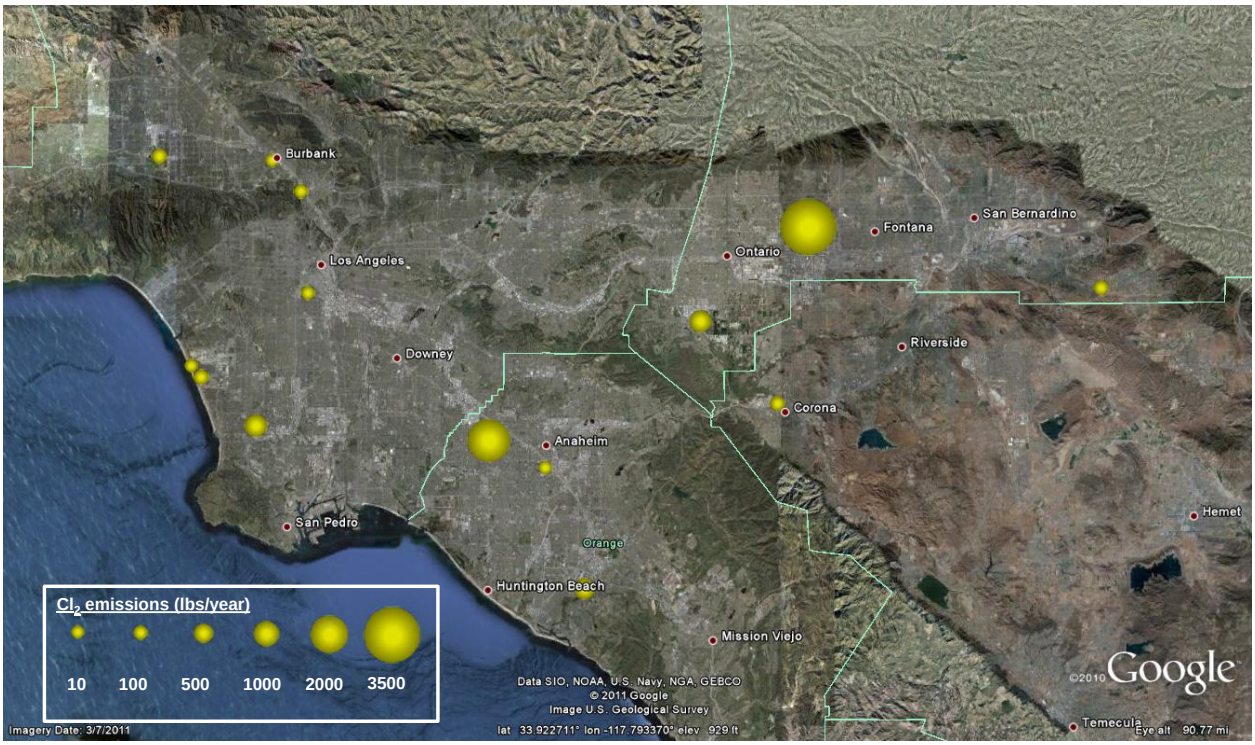

Figure 4.4 Molecular chlorine emissions in and around the Los Angeles basin for a single year between 2000 and 2009 as reported by the South Coast Air Quality Management District.

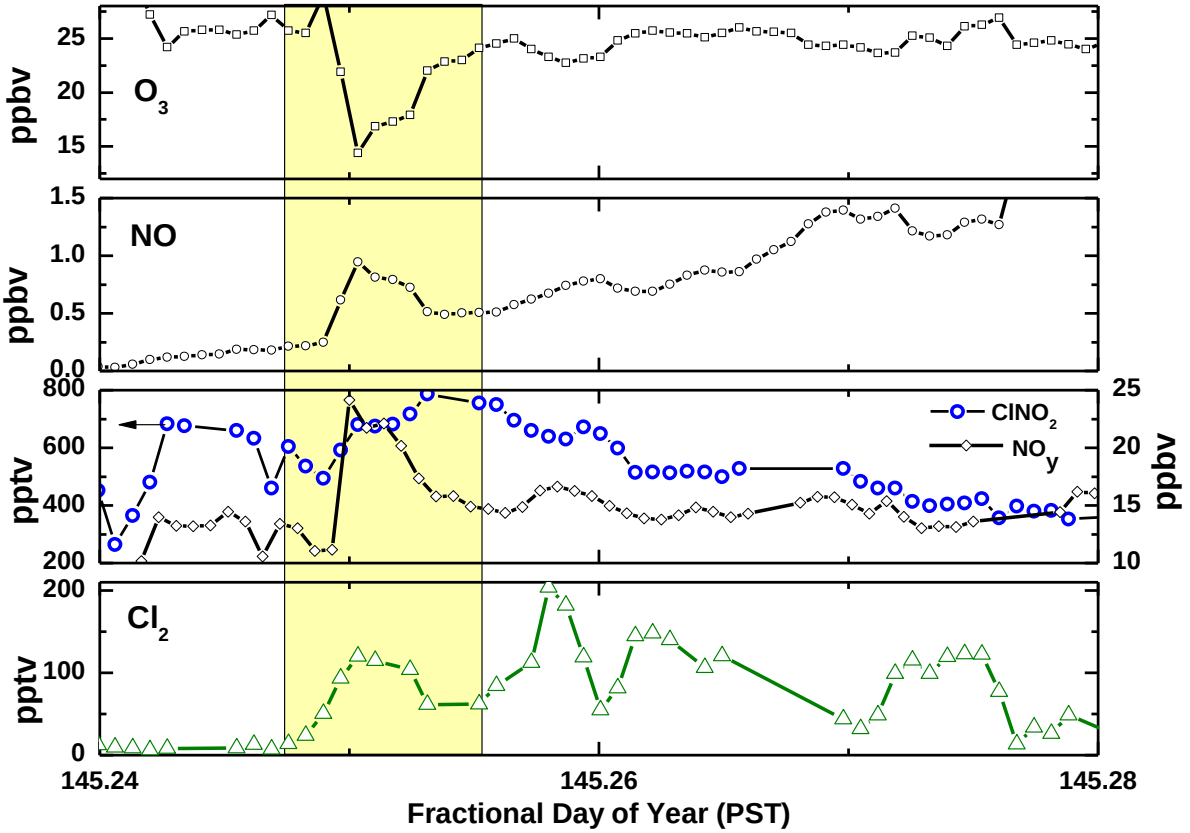

Figure 4.5 Additional information for Day 145 plume that shows Cl_2 and NO, NO_y, and HONO are correlated and O_3 is anti-correlated during the first intercept (highlighted), and some evidence of the same during the second. This plume was intercepted after sunrise, and the NO_2 – NO – O_3 relationship is therefore changing over the period shown. Note that the rise times of $ClNO_2$ and NO_y lag those of Cl_2 in the first intercept.

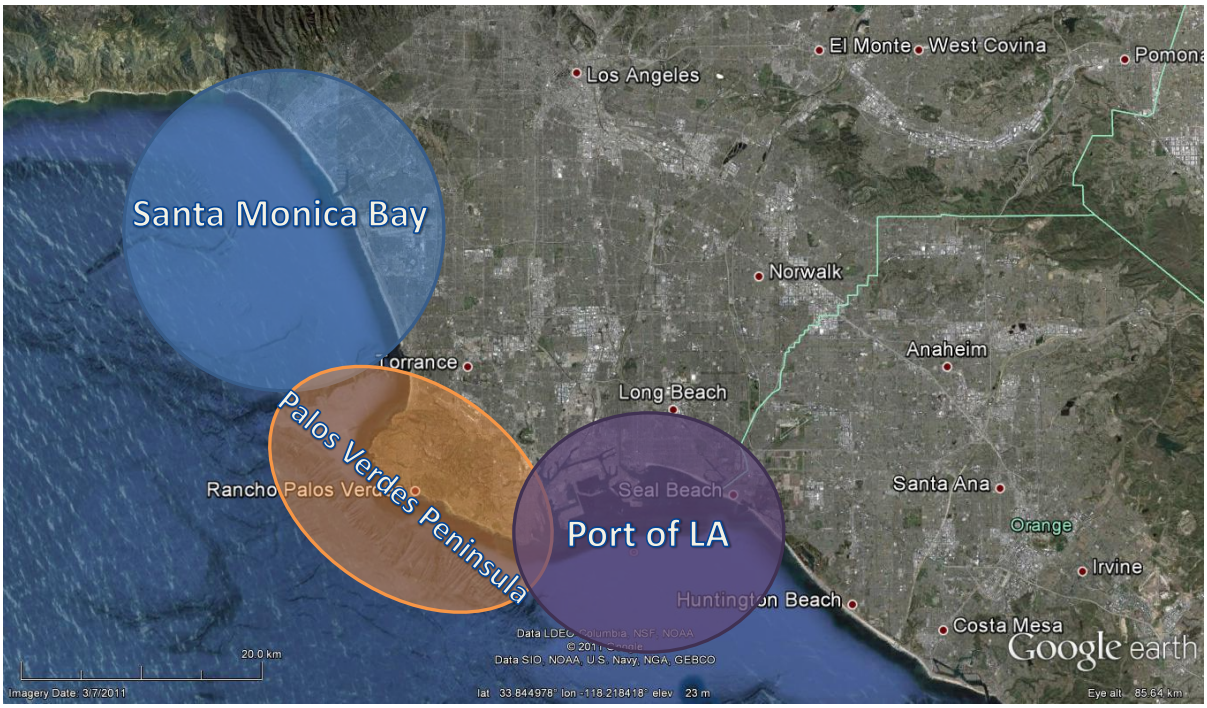

Figure 4.6 Major Los Angeles urban outflow sampling locations during CalNex. The coastal boundarys and southern and western edges of the bubbles indicate the extent of space incorporated into the averages.

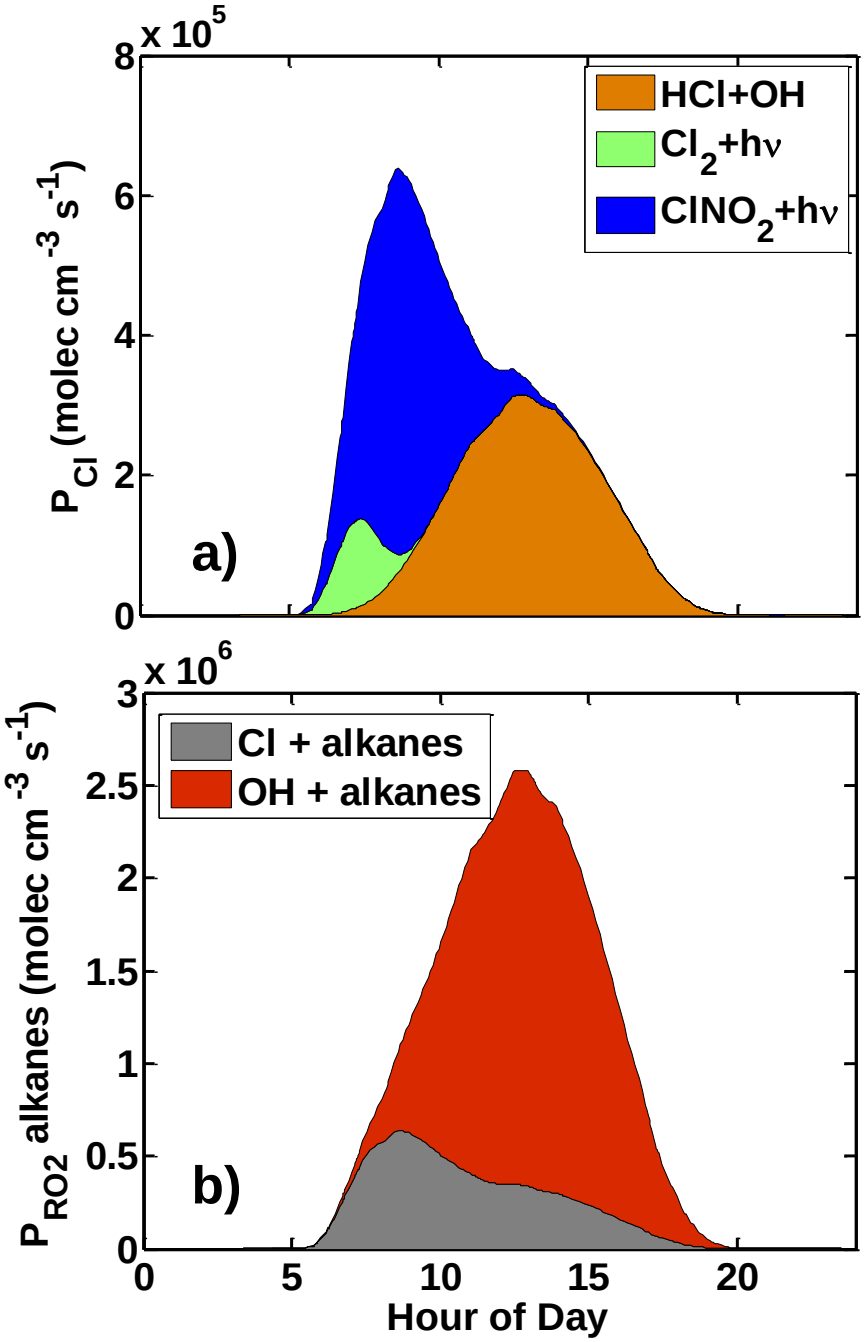

Figure 4.7 a) Total Cl-atom production rates from observationally constrained predictions by a simple pseudo-lagrangian box model. Cl-atom production from the photolysis of $ClNO_2$ is shown in blue, that from Cl_2 photolysis is shown in green and that from HCl + OH is shown in orange. The relative contributions from $ClNO_2$, Cl_2, and HCl are approximately 45%, 10%, and 45%, respectively. b) Model estimates of the alkyl peroxy radical (RO_2) production rate from the Cl-atom and OH based oxidation of alkane species measured during the study period.

Chapter 5

Chlorine Activation Within Urban or Power Plant Plumes: Vertically Resolved $ClNO_2$ and Cl_2 Measurements from a Tall Tower in a Polluted Continental Setting

5.1 Introduction

Chlorine atoms have the potential to impact the oxidative environment of the troposphere due to their large reaction rate constants with most volatile organic compounds (VOC) relative to that of the hydroxyl radical (OH), the dominant tropospheric oxidant. However, both Cl atom concentrations and mechanisms for their generation have been uncertain (Knipping and Dabdub, 2003; Pszenny et al., 2007; Spicer et al., 1998). In the boundary layer of polluted regions, two Cl atom precursors, nitryl chloride ($ClNO_2$) and molecular chlorine (Cl_2) have recently been quantified and shown to play a potentially important role in the evolution of oxidants and primary and secondary pollutants such as OH, O_3 and alkanes (Finley and Saltzman, 2006, 2008; Kercher et al., 2009; Lawler et al., 2011; Mielke et al., 2011; Osthoff et al., 2008; Phillips et al., 2012; Pszenny et al., 1993; Riedel et al., 2012a; Spicer et al., 1998; Thornton et al., 2010; Young et al., 2012). However, in addition to unresolved questions related to formation mechanisms or emission sources, relatively little is known about the vertical distribution of these Cl atom precursors. To date, the only measurements capturing the vertical distribution of $ClNO_2$ are limited to profiles of the Los Angeles basin urban plume by the NOAA P3 aircraft during the CalNex field study in late spring and early summer of 2010 (Young et al., 2012). Mixing ratios of $ClNO_2$ averaged ~1200 parts per trillion by volume (pptv) on individual profiles, and although

there was considerable vertical variability on individual profiles, there was little vertical variability within the planetary boundary layer in an average sense. To our knowledge, there have been no vertically resolved measurements of these species in continental settings, and none during wintertime when the heterogeneous chemistry of N_2O_5, the precursor to $ClNO_2$, is most important (Alexander et al., 2009; Dentener and Crutzen, 1993; Tie et al., 2003). Thus, the information necessary to determine the total impact of this chlorine atom source on regional air quality remains either limited or absent.

$ClNO_2$ is a nocturnal NO_x (NO_2 + NO) reservoir that photolyzes in the morning hours of the day to liberate a highly reactive chlorine atom and an NO_2 molecule. It is produced primarily at night by the reaction of dinitrogen pentoxide (N_2O_5) on chloride containing aerosol particles (Behnke et al., 1997; Bertram and Thornton, 2009; Finlayson-Pitts et al., 1989; Roberts et al., 2009; Thornton and Abbatt, 2005) or potentially ground surfaces (Lopez-Hilfiker et al., 2012), suggesting the potential for vertical gradients to develop overnight depending upon which of these sources is most important. To our knowledge, $ClNO_2$ is produced only from secondary chemistry in the atmosphere, and there is no evidence that $ClNO_2$ is directly emitted. The $ClNO_2$ production channel is in competition with the hydrolysis of N_2O_5 to form two HNO_3 (see R1).

$$N_2O_5 \xrightarrow{\gamma_{N_2O_5}} \phi_{ClNO_2} ClNO_2 + (2-\phi_{ClNO_2}) HNO_3 \qquad \text{(R1)}$$

The yield of $ClNO_2$ from N_2O_5 reactions (ϕ_{ClNO_2}), which varies between 0 – 1, depends upon the particulate chloride and liquid water content; the latter of which is set by the ambient relative humidity (RH). The gross production rate of $ClNO_2$ also depends upon: i) the NO_3 formation rate and the temperature-dependent equilibrium between N_2O_5, NO_3, and NO_2 (R2 and

R3) (Brown et al., 2009), ii) the available aerosol surface area (*SA*), and iii) the overall heterogeneous reaction probability of N_2O_5 ($\gamma_{N_2O_5}$) which in turn is a function of aerosol composition (Anttila et al., 2006; Bertram and Thornton, 2009; Brown et al., 2009; Folkers et al., 2003; Roberts et al., 2009; Thornton et al., 2003).

$$NO_2 + O_3 \longrightarrow NO_3 + O_2 \quad \text{(R2)}$$

$$NO_3 + NO_2 \underset{\Delta}{\rightleftharpoons} N_2O_5 \quad \text{(R3)}$$

$$P_{ClNO_2} \approx \phi_{ClNO_2}(t)\gamma_{N_2O_5}(t)[N_2O_5](t)\left\{\frac{SA(t)\omega}{4}\right\} \quad (1)$$

As illustrated in Eq. 1 the instantaneous $ClNO_2$ production rate (P_{ClNO_2}) varies with time (*t*), both in a seasonal sense and within a night, due to the time dependences of ϕ_{ClNO_2}, $\gamma_{N_2O_5}$, N_2O_5 concentrations, SA and composition. The bracketed portion of Eq. 1 describes the gas-particle collision frequency, where ω is the average molecular speed of an N_2O_5 molecule, in the free molecular regime neglecting gas diffusion limitations. In cases where super-micron SA is significant or reaction probabilities > 0.05, Eq. 1 must be modified to incorporate gas diffusion limitations.

While Cl_2 has been detected in several polluted regions, albeit typically at significantly lower abundances than $ClNO_2$ (Finley and Saltzman, 2006, 2008; Mielke et al., 2011; Riedel et al., 2012a), its sources are less well understood compared to $ClNO_2$. Cl_2 can be directly emitted by industrial processes like incineration and power generation (Sarwar and Bhave, 2007) but is also produced *in situ* via multiphase chemistry of reactive chlorine reservoirs such as $ClONO_2$

and HOCl (Deiber et al., 2004; Gebel and Finlayson-Pitts, 2001; Vogt et al., 1996). In this mechanism, chlorine atoms react with O_3 to form ClO, which reacts with either NO_2 to form $ClONO_2$ or HO_2 to form HOCl. $ClONO_2$ and HOCl then can react on acidic chloride containing particles to produce Cl_2 (R4 – R8), though the efficiency of these reactions in polluted urban regions is unknown (Lawler et al., 2011).

$$Cl\bullet + O_3 \longrightarrow ClO + O_2 \quad \text{(R4)}$$

$$ClO + NO_2 \longrightarrow ClONO_2 \quad \text{(R5)}$$

$$ClO + HO_2 \longrightarrow HOCl + O_2 \quad \text{(R6)}$$

$$ClONO_2 + Cl^-(aq) + H^+(aq) \longrightarrow Cl_2 + HNO_3 \quad \text{(R7)}$$

$$HOCl + Cl^-(aq) + H^+(aq) \longrightarrow Cl_2 + H_2O \quad \text{(R8)}$$

The NACHTT study presented a unique opportunity to measure a number of the chemical species relevant to $ClNO_2$ and Cl_2 chemistry, allowing for the assessment of the $ClNO_2$ yield in a variety of air masses, the role of ground surfaces relative to aerosol particles in the formation of $ClNO_2$, and the relative importance of chemical versus emission sources of Cl_2 in a continental setting. This field study represents the most complete vertical measurements of $ClNO_2$ and Cl_2 in the nocturnal planetary boundary layer to date. We focus much of our analysis here on two representative NO_x-rich plumes; one of which exhibited the deepest vertical extent of enhanced $ClNO_2$ while the other contained the highest $ClNO_2$ mixing ratio of the campaign. One plume is likely a more distributed combustion NO_x source such as motor vehicle traffic and other urban emissions, while the other plume is representative of a large NO_x point source such as that from a

nearby power plant. Although we cannot conclusively identify the sources of either from measurements at a fixed sampling location, their vertical distributions and inferred transport times (see below) are most consistent with these assignments. We compare and contrast $ClNO_2$ yields, N_2O_5-aerosol reaction probabilities, and Cl_2 within these plumes while also providing summary information on the typical characteristics that gave rise to $ClNO_2$ and Cl_2 at this site.

5.2 Methods

Nitrogen, Aerosol Composition, and Halogens on a Tall Tower (NACHTT) was a collaborative research effort that took place in February and March of 2011. Its aim was to assess a number of atmospheric chemical processes including halogen precursor chemistry in the Denver, CO, urban area (Brown et al., 2013). The measurement site (40.05°, -105.004°) was located at NOAA's Boulder Atmospheric Observatory (BAO - http://www.esrl.noaa.gov/psd/technology/bao) in Weld County, CO, which is about 35 km due north of the Denver urban core (see Figure 1). In addition to emissions from the Denver area which are encountered frequently, the site is also a receptor for emissions from nearby Boulder, CO, to the west, and natural gas power plant and oil and gas extraction activities to the northeast. Large local point sources of NO_x, CO_2, SO_2, and other primary pollutants include the Valmont coal and natural gas power plant 17 km west southwest of the site, the Cherokee coal power plant 27 km south of the site, and the Arapahoe coal power plant 40 km south of the site (Figure 1). Commerce City, an area with oil refining operations, is also approximately 27 km south, adjacent to the Cherokee coal power plant. Air largely unaffected by urban emissions is also routinely encountered at the site with downslope flow out of the Rocky Mountains to the west (Wolfe et al., 2013).

A unique feature of this study was the incorporation of BAO's 300 m tall tower to provide vertical measurements of a number of gas phase species (HCl, HONO, HNO_3, HNCO, organic acids, NO_x, O_3, NO_3, N_2O_5, $ClNO_2$, Cl_2, CO_2), particulate properties and composition (surface area, NH_4^+, SO_4^{2-}, NO_3^-, Cl^-, organics), and meteorological data (temperature, pressure, relative humidity, wind speed and direction). Instruments were installed in a temperature-controlled enclosure that was then mounted to the tower's payload elevator which is capable of lifting ~1.5 tons. Instruments sampled through holes in the enclosure walls which allowed for relatively short inlets (e.g., less than 2 m for the $ClNO_2$ instrument, and substantially less than 1 m for instruments mounted near the outside wall of the enclosure), thus minimizing artifacts due to heterogeneous chemistry on inlets. The tower elevator was capable of a single 300 m vertical profile in ~10 minutes and was programmed to be controlled remotely from a nearby building. Nearly continuous vertical profiles were taken over the course of the study except in cases of high winds and snow/ice events that resulted in unsafe conditions. Fixed height measurements of meteorological and less reactive trace gases were also carried out at a number of locations on the tower, and size-resolved aerosol composition and gas-particle partitioning of several inorganic gases were measured on a 22 m scaffold mounted on a different face of the tower (Young et al., 2013). A detailed description of all the measurements taken during the NACHTT study can be found in the overview paper (Brown et al., 2013).

The detection scheme and the calibration setup used to obtain measurements of $ClNO_2$ and Cl_2 are detailed in other publications (Kercher et al., 2009; Riedel et al., 2012a). Briefly, all Cl-isotopomers of $ClNO_2$ and Cl_2 were measured at ~0.36 Hz by a quadrupole chemical ionization mass spectrometer (CIMS) as clusters with the iodide reagent ion, $I\cdot(ClNO_2)^-$ and $I\cdot(Cl_2)^-$, respectively. A 2 m length of 6 mm inner diameter PFA tubing at ambient pressure was

used as the inlet line. A sampling flow rate of 1.5 standard liters per minute (slpm) was maintained through the inlet to the low-pressure (~80 mbar) ionization region by a critical orifice and a vacuum pump. The nitrogen carrier flow through the radioactive ion source was varied by ±15% in order to maintain a constant pressure within the mass spectrometer as the carriage ascended and descended the tower. This variation did not appreciably alter reagent ion signals, and therefore had little to no effect on instrumental sensitivity. Calibrations to both $ClNO_2$ and Cl_2 were performed every 70 minutes, as in Riedel et al. (2012a). Chlorine isotopic ratios matched those expected for the $ClNO_2$ mass-to-charge ratios. A high instrumental background signal at two ($^{35}Cl^{37}Cl$ and $^{37}Cl^{37}Cl$) of the three Cl_2 cluster masses prevented similar isotopic verification for Cl_2 using the raw data. However, we approximated the background interferences at each time point by using the signals present at the contaminated mass-to-charge ratios during a time period when there was no signal at the dominant Cl_2 mass ($^{35}Cl^{35}Cl$). Subtracting these background estimates from the raw data produced good agreement with the expected Cl_2 ratios based on the natural isotope abundances. The raw data were averaged to 10 seconds in order to reduce the uncertainty of each datum due to counting statistics. This resulted in a reported measurement about every 10 m in altitude during a vertical profile with a measurement uncertainty of ~20%. Given the instrument duty cycles, averaging time associated with the CIMS, aerosol composition, and gas phase acid measurements, coupled with the narrow extent of certain plume observations in the vertical and in time, the number of data points available within these plumes can be few. That said, it is important to note that each data point within a plume is precise and not the result of instrumental noise. Inlet transmission tests in which ~2 ppbv N_2O_5 was added to the inlet while sampling ambient air were also routinely performed to ensure that

$ClNO_2$ and Cl_2 were not produced in appreciable quantities by reactions on sampling lines ($ClNO_2$:N_2O_5 < 0.03; Cl_2:N_2O_5 < 0.02).

5.3 Results and Discussion

5.3.1 Overview of observations

Consistent with previous ground-based measurements in this region (Thornton et al., 2010), $ClNO_2$ was routinely observed at night during the entirety of NACHTT (see Figure 2) with the largest mixing ratios occurring when high RH (>50%) plumes enhanced in NO_x and depleted in O_3 were sampled. The study average nighttime maximum $ClNO_2$ mixing ratio was 270 ± 260 pptv (1σ) with a maximum observed mixing ratio of 1300 pptv. $ClNO_2$ mixing ratios were variable in the vertical, with some enhanced layers being less than 50 m in depth and persisting for a few minutes. In other cases $ClNO_2$ mixing ratios were greater than 100 pptv from tens of meters above ground level, extending to and likely beyond the highest point reached by the tower carriage (265 m). Such plumes were also persistent, observed at the measurement site for hours at a time. There does not appear to be one single factor which can explain the night-to-night variability or variability with height in a given night. The most import factors appear to be polluted air from the surrounding urban areas or large combustion sources, relative humidity (RH) greater than 40%, and time since sunset (see Figures 3 – 7). $ClNO_2$ was almost always positively associated with RH and exhibited a local enhancement near ground level where the temperatures were colder and the RH higher. The lowest $ClNO_2$ levels were often observed at higher altitudes when RH was below 40%. Figure 2 shows 15 days' worth of vertically resolved $ClNO_2$ observations during which vertical profiles were continuously taken for >3 hours. Overall there was typically $ClNO_2$ near the surface (~60 pptv nightly maxima) possibly arising from

N_2O_5 deposition to the ground or reaction on aerosol particles, the liquid water content of which in these low altitude, high RH conditions potentially enhances $ClNO_2$ production through a higher N_2O_5 reaction probability (Behnke et al., 1997; Bertram and Thornton, 2009; Raff et al., 2009; Thornton et al., 2003). Importantly, the largest $ClNO_2$ values (>200 pptv) of the study were typically aloft and associated with plumes that were markedly separate from the $ClNO_2$ that appeared associated with the surface layer. Moreover, based on the wind direction at the time of sampling, these plumes are most likely associated with urban and power plant sources. As shown in Figure 8, major $ClNO_2$ events were generally localized to 2 directions relative to the measurement site, south or southwest wind flow (Denver-Boulder urban corridor) and occasionally during north or northeast winds (natural gas extraction fields).

Cl_2 was always less abundant than $ClNO_2$ (see Figure 9) with a study average nighttime mixing ratio within the instrumental error of zero (-2 pptv). On a few occasions, enhanced Cl_2 was detected at night; similar to $ClNO_2$, Cl_2 observations most often occurred when winds were from specific sectors (south-southwest, southeast, and north-northeast – see Figure 8). The maximum observed mixing ratio of 320 pptv, as with all observations greater than 100 pptv, was limited to a few time periods and confined to a few tens of meters in the vertical, consistent with a specific point source. These Cl_2 plumes tended to also be high in NO_x and CO_2, potentially indicating emission from nearby power plants and/or associated cooling towers, or other chlorine emitting processes such as waste disposal or incineration (Chang and Allen, 2006; Reff et al., 2009; Sarwar and Bhave, 2007).

In what follows, we focus on two specific plume intercepts, one that occurred in the early morning of February 26 and the other that occurred in the early morning of March 5. For simplicity we refer to the plume encountered on February 26 as plume 1 and the plume

encountered on March 5 as plume 2. These plumes are subsets of the two classes of air masses which contained elevated $ClNO_2$ or Cl_2, i.e. the broadly polluted urban region and specific combustion point sources.

5.3.2 Plume 1: Diffuse Urban Pollution

The vertical distribution of $ClNO_2$ and Cl_2 mixing ratios observed in plume 1 are shown in Figure 10. The plume is first intercepted around 3:00 AM local time and is continuously sampled for approximately 3.5 hours until sunrise at ~6:30 AM. The $ClNO_2$ color scale in Figure 10a saturates at 500 pptv. Plume 1 represents some of the highest sustained $ClNO_2$ observed during the campaign with an average mixing ratio of 340 ± 120 pptv (1σ) and a maximum value of 640 pptv. It was a relatively deep plume, with depths spanning between 75 m and greater than 150 m and elevated mixing ratios appear to extend beyond the measurement ceiling. During the first 1.5 hours that the plume was sampled, the $ClNO_2$ layer was deep (>100 m) and consistently sampled. At ~5:00 AM the depth of the $ClNO_2$ plume decreases and Cl_2 becomes enhanced to ~140 pptv possibly representing a change in the plume chemistry, the source of the plume, or a mixing of sources. Average Cl_2 mixing ratios in the plume were 30 ± 40 pptv (1σ) with a maximum of 190 pptv. The Cl_2 color scale in Figure 10b saturates at 160 pptv.

Figure 11 illustrates the vertical structure of $ClNO_2$, Cl_2, N_2O_5, aerosol chloride, aerosol nitrate, HNO_3, CO_2, NO_2, O_3, potential temperature (θ), and RH during one of the plume 1 transects that occurred between 4:36 AM and 4:44 AM. Lower mixing ratios of $ClNO_2$ near 100 pptv are present over the first 60 m above the surface. This portion of the average profile had a particularly high RH (>90%) and is representative of the persistent near-surface $ClNO_2$ formation observed throughout the campaign. N_2O_5 is low over the first 60 m, either due to

titration by fresh NO emissions or to efficient uptake onto aerosols and ground surfaces at high RH (Chang et al., 2011). Above 60 m, plume 1 becomes apparent with large increases in $ClNO_2$ and N_2O_5 that persist to the top of the profile. Cl_2 is also elevated within this transect at heights >150 m, with mixing ratios of a few tens of pptv. Aerosol nitrate is largest near the surface (~5 ppbv) and decreases sharply to ~2.5 ppbv at the bottom of the plume, remaining relatively constant until 175 m where it decreases steadily. There is no marked enhancement in aerosol chloride, HNO_3, CO_2, NO_2, or O_3 within the plume, and NO_2 and O_3 are strongly anticorrelated (slope = -0.50, R = -0.95). The RH only falls below 50% during the top 10 m of the profile, between 240 – 250 m above ground level (AGL). Potential temperature gradually increases with height throughout the profile, with steep increases between 50 – 60 m, and again above 180 m. These inversions represent separations between individual layers and are coincident with the changes in the chemical composition described above. The largest $ClNO_2$ observations during this profile occurred when the winds were from 158° (south southeast) relative to the measurement site. In general this corresponds to winds coming from the Denver urban area south of the site. The same was true for maximum Cl_2 observations, indicating a correlation in the source region for these two species.

5.3.3 Plume 2: Combustion Point Source

The largest $ClNO_2$ mixing ratio of the NACHTT study occurred on March 5. For the purpose of comparison, we apply a similar description of the plume that contained this observation (referred to as plume 2) as for plume 1. Multiple $ClNO_2$ and Cl_2 vertical profiles taken during the plume 2 intercept are shown in Figure 12. Plume 2 is likely first sampled at ~3:00 AM and is sampled intermittently until ~4:00 AM. Compared to plume 1, plume 2 is

significantly narrower in depth. $ClNO_2$ enhancements were largely confined to heights between 80 m and 120 m, and the enhancements had distinctly sharp edges. The maximum $ClNO_2$ mixing ratio detected in these intercepts was 1300 pptv, though this maximum was not observed on every transect shown in Figure 12, possibly due to meandering of the plume away from and towards the tower, or time dependent changes in plume composition or chemistry. The color scale in Figure 12a saturates at 500 pptv. Plume 2 had a Cl_2 average mixing ratio of 3 ± 20 pptv (1σ) with a maximum of 120 pptv. As with Figure 10b, shortly prior to sunrise at ~6:30 AM, there is a slight increase in Cl_2 mixing ratios to values near 50 pptv. However, at this point it is likely that plume 2 is no longer being sampled given the stark changes in the $ClNO_2$ and Cl_2 vertical profiles.

As stated above, plume 2 represents a particularly confined plume in terms of $ClNO_2$ and Cl_2. This is apparent in Figure 13 which shows $ClNO_2$, Cl_2, N_2O_5, aerosol chloride, aerosol nitrate, HNO_3, CO_2, NO_2, O_3, potential temperature, and RH for the vertical profile that contained the 1300 pptv $ClNO_2$ observation (4:12 AM – 4:21 AM). The sharpness of the plume in terms of $ClNO_2$ and Cl_2 between 75 m and 110 m, together with coincident enhancements in aerosol chloride, CO_2, and NO_2 indicates that it likely originated from a local point source, possibly from one of the power plants indicated earlier (see Methods section). Aloft of this enhanced $ClNO_2$ layer, RH drops steeply, and θ increases with height. N_2O_5 remains sustained while NO_2 and O_3 decrease above this layer likely due to a smaller reaction probability on aerosols at low RH. The apparent decoupling of $ClNO_2$ and N_2O_5 just above the enhanced $ClNO_2$ layer suggests that the components and/or environmental conditions necessary for $ClNO_2$ production were not fully coincident with NO_x in the vertical. The aerosol chloride measurement (Figure 13b) supports this argument, illustrating that particle phase chloride was present only in

the $ClNO_2$ layer. In general, aerosol chloride showed enrichments during preceding plume 2 intercepts (see Figure 14) that had $ClNO_2$ mixing ratios in excess of 200 pptv and showed similar vertical trends, indicating the plume source emitted significant amount of chloride in addition to the $ClNO_2$ precursor compounds. Additionally the uptake of N_2O_5 on aerosol particles above the enhanced $ClNO_2$ layer could be inefficient given the low RH (<40%) which could account for some of the decoupling. The majority of $ClNO_2$ and Cl_2 observations during the intercepts of plume 2 occurred when the winds were out of the southwest at 226°. Given this general direction the point source is likely one of the coal-fired combustion sources such as the Arapahoe, Cherokee, or Valmont power plants (see Figure 1).

5.3.4 $ClNO_2$ yield estimates

We use several different approaches to inferring $ClNO_2$ yields from the observations. Each of these approaches requires assumptions, either due to the Eulerian sampling framework or incomplete measurement suite. We therefore refrain from reporting specific yield values and instead give a range of likely yields based on the combined results of all approaches.

Following the work of Wagner et al. (2012), we use the vertically resolved observations of total nitrate (aerosol phase NO_3^- + gas phase HNO_3) and $ClNO_2$ taken during the plume intercepts to derive an observation-based estimate of the $ClNO_2$ yield from reactions of N_2O_5 in the two plumes. Based on the relationship introduced in Reaction R1, in a nocturnal air mass evolving in time, $ClNO_2$ will be linearly related to the total amount of NO_3^- in the gas and particle phase produced by N_2O_5 reactions as shown below in in Eq. 2.

$$m = \frac{\Delta ClNO_2}{\Delta NO_3^-} = \frac{\phi_{ClNO_2}}{2 - \phi_{ClNO_2}} \quad (2)$$

$$\phi_{ClNO_2} = \frac{2m}{1+m} \quad (3)$$

The slope *m* of a regression line fitted to a scatter plot of $ClNO_2$ vs. total NO_3^- is then related to the molar yield of $ClNO_2$ per mole of N_2O_5 reacted, Eq. 3, subject to several assumptions. First, we neglect the production of HNO_3 or organic nitrates from NO_3 reactions with hydrocarbons due to the much colder temperatures and high NO_x conditions, which favors N_2O_5 over NO_3 (R3), when $ClNO_2$ was typically observed during NACHTT. Particulate NO_3^- has a sufficiently long lifetime that its concentration can be influenced by the previous day's photochemistry or even by NO_3^- production from the previous night. These effects likely bias our yield estimates low. Additionally, this approach assumes a constant N_2O_5 reaction probability and a constant $ClNO_2$ yield since the origin of the plume. In reality these quantities are unlikely to remain constant over the plume lifetime, and the apparent correlations may in fact represent variable chemical histories containing emissions from multiple sources of different ages and initial conditions that therefore could potentially result in variable intercepts and slopes. Changes in temperature and RH as well as the buildup of nitrate due to plume processing and the consumption of chloride to form $ClNO_2$ have the potential to further alter these quantities. However, given the data available these assumptions are a necessary simplification in order to obtain estimates of said parameters, but as a result these estimates are more representative of values averaged over the lifetime of the plume up to the time it was sampled as opposed to an instantaneous estimate.

In Figure 15 we show the nighttime relationship of $ClNO_2$ to total NO_3^- at different heights measured over the course of the study. Lines corresponding to ϕ_{ClNO_2} of 0.05, 0.15, 0.4, and 1.0 are drawn for illustrative purposes only given the caveats discussed above. In general, the figure demonstrates robustly that $ClNO_2$ and total NO_3^- measured at night were positively correlated (R = 0.35), with the slope and intercept varying significantly with height and from night-to-night as we show in Figure 15. The overall relationship in Figure 15 shows two populations: low elevations generally exhibiting a low yield (shallow slope), possibly due to the presence of daytime nitrate, and higher elevations exhibiting a comparatively higher yield (steeper slope). Vertical structure in the gas phase HNO_3 measurement was not as pronounced as that for aerosol phase NO_3^-, as such, most of the variation in the nitrate is driven by particulate nitrate. Though precautions were taken to avoid any time delays as a result of inlet effects, such as the use of a heated inlet, the reduced vertical structure may have resulted from the time response of the inlet for the HNO_3 instrument (see for example, Fehsenfeld et al. (1998)) Details regarding the HNO_3 measurement can be found in elsewhere (VandenBoer et al., 2013). However, reduced time response in HNO_3 is not expected to significantly bias the estimates considering that gas phase HNO_3 was largely constant with respect to a single profile.

Based on these relationships we estimate that the typical ϕ_{ClNO_2} aloft in this region during wintertime is 0.05 ± 0.15, consistent with box modeling of observations made from a nearby ground-based site (Thornton et al., 2010). In order to obtain this estimate, we only select data taken at heights >75 m with NO_2 values larger than 8 ppbv thereby removing surface effects and selecting data representative of urban conditions aloft. In general ϕ_{ClNO_2} for the surface layer is likely well below that for the air aloft considering the large total nitrate values and modest $ClNO_2$ levels measured near the surface.

We also apply this same $ClNO_2$ vs. total NO_3^- approach to the individual transects of plumes 1 and 2 discussed above. As shown in Figure 16a, these estimates give $\phi_{ClNO_2} \approx 0.3$ and $\phi_{ClNO_2} \approx 0.7$ for plume 1 and plume 2, respectively. Data below 100 m is omitted from the calculation of the estimated plume 1 yield shown in Figure 16a (left pane), and similarly, data below 85 m is omitted from the plume 2 yield estimate shown in Figure 16a (right pane). This precaution is taken to ensure effects of the ground surface do not influence these strictly in-plume estimates. As we outlined in the Methods section, the narrow extent of plume 2 in the vertical (<25 m in depth) and in time ($ClNO_2$ mixing ratios >500 pptv are only encountered during two successive vertical profiles), allow for few data points within the plume. That said, a similar ϕ_{ClNO_2} was obtained from another transect of the plume that took place 6 minutes prior to that described in Figure 16a (see Figure 17). Apart from this additional transect it is unlikely we sampled the plume during any of the other vertical profiles as the major characteristics defining plume 2 ($ClNO_2$ >500 pptv and elevated Cl_2) were not found in other profiles.

A related but alternative approach to infer a $ClNO_2$ yield is to determine the enhancements of both $ClNO_2$ and total NO_3^- within distinct plumes relative to the values outside of the plumes. As illustrated in Figure 16b, we use the enhancements of $ClNO_2$ and total NO_3^- in plume 1 and plume 2 as estimates of $\Delta ClNO_2$ and ΔNO_3^- in Eq. 2. The enhancements are determined by subtracting the background mixing ratios from the plume center defined by the maxima in $ClNO_2$ over the profile. Background mixing ratios of $ClNO_2$ and NO_3^- are determined by linear interpolations of data outside the plume (low in $ClNO_2$) which occur above and below the plume center as shown by the dotted lines in Figure 16b. This background interpolation, while uncertain, is necessary to remove enhancements in NO_3^- which are apparently unrelated to the plumes and are possibly residual NO_3^- from photochemical production the day before. Large

preexisting nitrate values if left completely unaccounted for would artificially drive the estimated $ClNO_2$ yields to low values. Calculating the relative enhancement of $ClNO_2$ to NO_3^- in the plumes (denoted by the grey shaded areas) gives ϕ_{ClNO_2} for plume 1 and 2 as 0.45 and 0.8, respectively. These values do not change significantly if a constant NO_3^- background, defined only by the high altitude NO_3^- values, is used instead of the interpolated values. This constant background approach assumes that any NO_3^- above the background at lower altitudes is the result of a nighttime NO_3^- source. The resulting ϕ_{ClNO_2} values for both plumes are similar to the other two approaches: 0.4 and 0.7 for plume 1 and plume 2, respectively.

In a third approach, we utilize the aerosol composition measurements provided by an aerosol mass spectrometer (AMS) mounted in the tower carriage to derive an estimate of ϕ_{ClNO_2}. Using the AIM thermodynamic aerosol model (available at http://www.aim.env.uea.ac.uk/aim/aim.php) and the measured RH and aerosol composition (shown for plumes 1 and 2 in Figure 18), we can obtain an estimate of the amount of particulate water present (Clegg et al., 1998). Given this estimate of aerosol water concentration and the measured aerosol chloride concentration, ϕ_{ClNO_2} can be estimated using Eq. 4 which is based on a number of laboratory studies estimating the relative rates of $ClNO_2$ vs. HNO_3 formation from N_2O_5 heterogeneous reactions (Behnke et al., 1997; Bertram and Thornton, 2009; Roberts et al., 2009). The uncertainty associated with this approach arises mainly from the aerosol chloride measurement, only non-refractory chloride is efficiently measured by the AMS, and the effect of the organic aerosol fraction on particulate water calculated by the thermodynamic aerosol model. We assume the organic species do not contribute to the water content of the aerosols. Moreover, these calculations represent instantaneous yields that assume all the chloride is available for reaction with N_2O_5, and that do not account for depletion of chloride or mixing and transport

prior to the measurement. The results of this approach for plumes 1 and 2 are shown in Figure 16c with estimated yields for plumes 1 and 2 of 0.32 and 0.98, respectively. Again the grey shaded regions are used to determine these in-plume yields.

$$\phi_{ClNO_2} \approx \frac{1}{1+\frac{[H_2O]}{450[Cl^-]}} \quad (4)$$

Results from the multiple ϕ_{ClNO_2} estimate approaches described above indicate the ϕ_{ClNO_2} ≈ 0.3 – 0.45 and ϕ_{ClNO_2} ≈ 0.7 – 1 for plumes 1 and 2, respectively. It is important to note that these yields are not representative of the entire vertical extent of the plume or a vertical profile but only for the conditions that give rise to the largest (>500 pptv) $ClNO_2$ values. That said, these ϕ_{ClNO_2} are similar to those found in polluted coastal regions and suggest that $ClNO_2$ production can be efficient within inland combustion plumes such as those associated with power generation. The plume 1 yield is of similar magnitude to the largest yield inferred from previous wintertime measurements in Denver/Boulder area (Thornton et al., 2010). The estimated yield for plume 2 indicates efficient $ClNO_2$ production comparable to what would be expected in polluted marine environments, though confined to a very narrow vertical extent.

5.3.5 Plume box modeling

That plumes 1 and 2 are well isolated from the ground surface and likely experience little nighttime vertical mixing represents conditions well suited for box model applications where the reactions are assumed to proceed in a static volume. We use a 0-D time dependent chemical box model to further investigate the nocturnal chemical processing within the two plumes that lead to

these largest $ClNO_2$ values of the study. A goal with this modeling is to determine whether the observations can be simulated using the above estimates of ϕ_{ClNO_2} and reasonable estimates of $\gamma_{N_2O_5}$ and plume age. Gas phase reaction rate constants in the model are taken from the most recent data available on the International Union of Pure and Applied Chemistry (IUPAC) kinetics database (http://www.iupac-kinetic.ch.cam.ac.uk). The model is given initial inputs of NO, O_3, aerosol surface area, temperature, and pressure, which are chosen so the model output matches observations taken during the two plume intercepts. The initial conditions are thus indicative of the chemical conditions at or near the emission source. We assume all NO_x is initially emitted as NO, which is subsequently oxidized by O_3 to NO_2, and that $\gamma_{N_2O_5}$ and ϕ_{ClNO_2} remain constant over the lifetime of the plume. Due to the cold plume temperatures (~0 °C), the equilibrium between N_2O_5, NO_3, and NO_2 (R3) is strongly shifted toward N_2O_5 (N_2O_5:NO_3 ~ 250:1 for typical plume NO_2 values). In addition, given the low abundance of biogenic VOC and other NO_3 sinks, we assume that N_2O_5 losses dominate over that of NO_3. The NO_3 lifetime in the model is arbitrarily set to 30 minutes. Model outputs are fairly insensitive to this assumption. For example, adjusting the NO_3 lifetime by a factor of 10 in either direction changes modeled N_2O_5 and $ClNO_2$ mixing ratios by less than 7%. The ϕ_{ClNO_2} is fixed to the yields calculated in section 3.4, while $\gamma_{N_2O_5}$ and the reaction time (plume age) are adjustable parameters that are varied to best match the observations of O_3, NO_2, N_2O_5, $ClNO_2$, and the NO_3^- enhancements shown in the plumes. A complete table of the reactions and rates used in the box model can be found in the Table 1.

A summary of the modeling results are shown in Table 1. The resulting $\gamma_{N_2O_5}$ is similar for both plumes at ~0.02 which falls within the range (<0.001 – 0.1) of $\gamma_{N_2O_5}$ reported from

laboratory studies on a variety of different particle types and for different temperatures; these values are comparable to larger observations of $\gamma_{N_2O_5}$ obtained from direct measurements on ambient particles, though these measurements were not taken during wintertime (Bertram et al., 2009; Hallquist et al., 2003; Hu and Abbatt, 1997; Mozurkewich and Calvert, 1988; Riedel et al., 2012b). The $\gamma_{N_2O_5}$ estimates are also of similar magnitude to those predicted by an iterative box model analysis that predicts $\gamma_{N_2O_5}$ using all of the observations taken during NACHTT (Wagner et al., 2013). For the select data used in that analysis, the distribution in $\gamma_{N_2O_5}$ was centered near 0.018. Given the moderate to high ϕ_{ClNO_2} estimated for the two plumes, these results are also conceptually consistent with our understanding of N_2O_5 heterogeneous chemistry in that similar factors have been shown to influence both $\gamma_{N_2O_5}$ and ϕ_{ClNO_2} (Bertram and Thornton, 2009; Riedel et al., 2012b; Roberts et al., 2009). While these estimates do place useful constraints on $\gamma_{N_2O_5}$ and ϕ_{ClNO_2}, the most robust constraint is the product of the two quantities because both can vary relative to each other to produce the same amount of $ClNO_2$ (see Eq. 1).

The resulting time required by the model to best match the observations is an indication of plume age. In both cases, this age is significantly less than the time since sunset. For plume 1 an age of ~4 hours is reasonable considering an ideal case in which the air within the plume is transported directly to the measurement site from central Denver with the same wind speed observed at the measurement site. This results in a processing time of ~4 hours. Similarly in the case of plume 2, given the wind speed and approximate direction within the plume, the transit time from the Valmont power plant to the site is estimated to be at least 2 hours, and the transit time from the Arapahoe power plant to the site is ~4 hours. An alternative option for the reaction/processing time is to run the model as if the plume originated at sunset which is also

shown in Table 1. However, using the constraints on ϕ_{ClNO_2} and the NO_3^- enhancements in the plumes, we were unable to match the observations, supporting the conclusion that these plumes were emitted well after sunset. Disregarding these constraints and using the time since sunset as the reaction time results in $\phi_{ClNO_2} = 0.06$ and $\gamma_{N_2O_5} = 0.022$ for plume 1 and $\phi_{ClNO_2} = 0.19$ and $\gamma_{N_2O_5} = 0.023$ for plume 2. Because the time since sunset is the maximum possible reaction time these ϕ_{ClNO_2} values can be considered lower limits for the two plumes.

The uncertainty in plume age contributes uncertainty in the model predictions. Brown et al. (2006) use observations of O_3 and NO_2 to approximate the age of nocturnal plumes. There is clearly a negative relationship between O_3 and NO_2 in plumes 1 and 2, which is consistent with nocturnal emission and/or processing, and in a Lagrangian sense that slope can be equated to age. However, the variations with height of the O_3 vs. NO_2 slope suggest wind shear or mixing effects on the O_3 and NO_2 relationship. Variations in time and space such as fresh injections into existing plumes and mixing complicate an age estimate based on this relationship. The clear dependences on height and time shown for the two plumes suggest that, while persistent $ClNO_2$ production can occur throughout the plume volume like plume 1, there may well be a set of distinct NO_x sources and injection heights with varying ages within a sampling period and vertical region.

NACHTT represents only the third time that $ClNO_2$ and Cl_2 have been measured simultaneously and presents an opportunity to investigate the proposed conversion of $ClNO_2$ to Cl_2 via heterogeneous chemistry (Mielke et al., 2011; Riedel et al., 2012a; Roberts et al., 2008). Using the model we add a heterogeneous loss of $ClNO_2$ to form Cl_2 with unit yield and adjust the corresponding aerosol reaction probability for $ClNO_2$ to reproduce the observed Cl_2 mixing ratios. The resulting aerosol reaction probability for $ClNO_2$ conversion to Cl_2 is 0.001, or less,

for the two plume cases which is about 6 times lower than that given in Roberts et al. (2008) for acidic aerosols (pH<2). Observationally constrained estimates of aerosol pH were made during NACHTT at 9 m (Young et al., 2013). While not directly comparable to the altitudes of plume 1 and 2, these estimates suggest pH >3, consistent with the low conversion rate of $ClNO_2$ to Cl_2 we infer from the model. Given the enhanced Cl_2 occurred only when sampling from a specific sector, and that aerosol pH was likely >3, we conclude it was more likely that the observed Cl_2 was co-emitted with $ClNO_2$ precursors rather than produced by $ClNO_2$ heterogeneous chemistry.

Finally we can use the box model to assess the maximum possible $ClNO_2$ production in plumes similar to those we characterized above. Assuming emission at sunset and chemical evolution over the entire night (~13 hours) based on the model parameters and constraints derived above, we estimate the maximum possible $ClNO_2$ produced could reach 2.5 to 4 ppbv. This estimate assumes a vertically static reaction volume. The previous, limited available data on plume transport at night suggests that mixing may be quite limited (Brown et al., 2012). The largest $ClNO_2$ values could be well downwind of the emission location by some 50 - 100 km, and past the NACHTT measurement location, with larger effects on the chemistry in these regions than inferred from our observations described in this paper.

5.4 Conclusions

Over the course of the study, $ClNO_2$ and Cl_2 were observed on most nights. Similar to measurements off the coast of Los Angeles, we conclude that Cl_2 is more likely the result of direct emissions rather than conversion from $ClNO_2$, which is produced only from N_2O_5 heterogeneous chemistry. Though the nocturnal atmosphere at this site was highly stratified, as expected for a winter time continental setting, mixing ratios of both species approached those

reported in the polluted marine boundary layer where the large chloride source from sea salt aerosol is more obvious than inland sources. All air masses enhanced in $ClNO_2$ were characterized by moderate to high RH (45 - 90%) and originated from the urban areas of Denver and the Front Range of the Rocky Mountains, as well as from regions with significant natural gas extraction activities. Enhanced Cl_2 mixing ratios were measured when air originated from a much narrower section of the Denver metro area.

Using the expected nocturnal relationship between $ClNO_2$ and total NO_3^- and the measured aerosol composition, we inferred a variable yield of $ClNO_2$ from N_2O_5 chemistry that spanned nearly the entire allowable range (0 - 1). The exact causes of this variability remain uncertain but likely involve, in part, the availability of aerosol chloride driven either by particle phase (low yields at low RH), or by partitioning of the chloride into a portion of the aerosol population with a smaller fraction of the available surface area. $ClNO_2$ production was most efficient within the plume of a combustion point source which we attribute to a local power plant. This finding raises the possibility that power generation is at least part of the wide-spread $ClNO_2$ production inferred by Thornton et al. (2010). Coal burning and water-cooling operations associated with power generation are recognized but uncertain sources of soluble chloride. Our measurements are strongly suggestive that the nocturnal processing of power plants plumes leads to $ClNO_2$ formation. Aircraft and modeling studies are needed to confirm this result and determine the implications for regional air quality and NO_x processing.

References

Alexander, B., Hastings, M. G., Allman, D. J., Dachs, J., Thornton, J. A., and Kunasek, S. A.: Quantifying atmospheric nitrate formation pathways based on a global model of the oxygen isotopic composition (delta(17)O) of atmospheric nitrate, Atmospheric Chemistry and Physics, 9, 5043-5056, doi: 10.5194/acp-9-5043-2009, 2009.

Anttila, T., Kiendler-Scharr, A., Tillmann, R., and Mentel, T. F.: On the reactive uptake of gaseous compounds by organic-coated aqueous aerosols: Theoretical analysis and application to the heterogeneous hydrolysis of N_2O_5, Journal of Physical Chemistry A, 110, 10435-10443, doi: 10.1021/jp062403c, 2006.

Behnke, W., George, C., Scheer, V., and Zetzsch, C.: Production and decay of $ClNO_2$, from the reaction of gaseous N_2O_5 with NaCl solution: Bulk and aerosol experiments, Journal of Geophysical Research-Atmospheres, 102, 3795-3804, doi: 10.1029/96jd03057, 1997.

Bertram, T. H., and Thornton, J. A.: Toward a general parameterization of N_2O_5 reactivity on aqueous particles: the competing effects of particle liquid water, nitrate and chloride, Atmospheric Chemistry and Physics, 9, 8351-8363, doi: 10.5194/acp-9-8351-2009, 2009.

Bertram, T. H., Thornton, J. A., Riedel, T. P., Middlebrook, A. M., Bahreini, R., Bates, T. S., Quinn, P. K., and Coffman, D. J.: Direct observations of N_2O_5 reactivity on ambient aerosol particles, Geophysical Research Letters, 36, doi: 10.1029/2009gl040248, 2009.

Brown, S. S., Neuman, J. A., Ryerson, T. B., Trainer, M., Dube, W. P., Holloway, J. S., Warneke, C., de Gouw, J. A., Donnelly, S. G., Atlas, E., Matthew, B., Middlebrook, A. M., Peltier, R., Weber, R. J., Stohl, A., Meagher, J. F., Fehsenfeld, F. C., and Ravishankara, A. R.: Nocturnal odd-oxygen budget and its implications for ozone loss in the lower troposphere, Geophysical Research Letters, 33, doi: 10.1029/2006gl025900, 2006.

Brown, S. S., Dube, W. P., Fuchs, H., Ryerson, T. B., Wollny, A. G., Brock, C. A., Bahreini, R., Middlebrook, A. M., Neuman, J. A., Atlas, E., Roberts, J. M., Osthoff, H. D., Trainer, M., Fehsenfeld, F. C., and Ravishankara, A. R.: Reactive uptake coefficients for N_2O_5 determined from aircraft measurements during the Second Texas Air Quality Study: Comparison to current model parameterizations, Journal of Geophysical Research-Atmospheres, 114, doi: 10.1029/2008jd011679, 2009.

Brown, S. S., Dube, W. P., Karamchandani, P., Yarwood, G., Peischl, J., Ryerson, T. B., Neuman, J. A., Nowak, J. B., Holloway, J. S., Washenfelder, R. A., Brock, C. A., Frost, G. J., Trainer, M., Parrish, D. D., Fehsenfeld, F. C., and Ravishankara, A. R.: Effects of NO_x control and plume mixing on nighttime chemical processing of plumes from coal-fired power plants, Journal of Geophysical Research-Atmospheres, 117, doi: 10.1029/2011jd016954, 2012.

Brown, S. S., Thornton, J. A., Keene, W. C., Pszenny, A. A. P., Sive, B. C., Wagner, N. L., Young, C. J., Riedel, T. P., Roberts, J. M., VandenBoer, T. C., Dube, W. P., Hubler, G., and Wolfe, D.: Nitrogen, Aerosol Composition and Halogens on a Tall Tower (NACHTT): Overview of a Wintertime Air Chemistry Field Study in the Front Range Urban Corridor of Colorado, Journal of Geophysical Research, submitted, 2013.

Chang, S. Y., and Allen, D. T.: Atmospheric chlorine chemistry in southeast Texas: Impacts on ozone formation and control, Environmental Science & Technology, 40, 251-262, doi: 10.1021/es050787z, 2006.

Chang, W. L., Bhave, P. V., Brown, S. S., Riemer, N., Stutz, J., and Dabdub, D.: Heterogeneous Atmospheric Chemistry, Ambient Measurements, and Model Calculations of N_2O_5: A Review, Aerosol Science and Technology, 45, 665-695, doi: 10.1080/02786826.2010.551672, 2011.

Clegg, S. L., Brimblecombe, P., and Wexler, A. S.: Thermodynamic Model of the System H^+–NH_4^+–Na^+–SO_4^{2-}–NO_3^-–Cl^-–H_2O at 298.15 K, The Journal of Physical Chemistry A, 102, 2155-2171, doi: 10.1021/jp973043j, 1998.

Deiber, G., George, C., Le Calve, S., Schweitzer, F., and Mirabel, P.: Uptake study of $ClONO_2$ and $BrONO_2$ by Halide containing droplets, Atmospheric Chemistry and Physics, 4, 1291-1299, doi: 10.5194/acp-4-1291-2004, 2004.

Dentener, F. J., and Crutzen, P. J.: Reaction of N_2O_5 on tropospheric aerosols - Impacts on the global distributions of NO_X, O_3, AND OH, Journal of Geophysical Research-Atmospheres, 98, 7149-7163, doi: 10.1029/92jd02979, 1993.

Fehsenfeld, F. C., Huey, L. G., Sueper, D. T., Norton, R. B., Williams, E. J., Eisele, F. L., Mauldin, R. L., and Tanner, D. J.: Ground-based intercomparison of nitric acid measurement techniques, Journal of Geophysical Research-Atmospheres, 103, 3343-3353, doi: 10.1029/97jd02213, 1998.

Finlayson-Pitts, B. J., Ezell, M. J., and Pitts, J. N.: Formation of chemically active chlorine compounds by reactions of atmospheric NaCl particles with gaseous N_2O_5 and $ClONO_2$, Nature, 337, 241-244, doi: 10.1038/337241a0, 1989.

Finley, B. D., and Saltzman, E. S.: Measurement of Cl_2 in coastal urban air, Geophysical Research Letters, 33, doi: 10.1029/2006gl025799, 2006.

Finley, B. D., and Saltzman, E. S.: Observations of Cl_2, Br_2, and I_2 in coastal marine air, Journal of Geophysical Research-Atmospheres, 113, doi: 10.1029/2008jd010269, 2008.

Folkers, M., Mentel, T. F., and Wahner, A.: Influence of an organic coating on the reactivity of aqueous aerosols probed by the heterogeneous hydrolysis of N_2O_5, Geophysical Research Letters, 30, doi: 10.1029/2003gl017168, 2003.

Gebel, M. E., and Finlayson-Pitts, B. J.: Uptake and reaction of $ClONO_2$ on NaCl and synthetic sea salt, Journal of Physical Chemistry A, 105, 5178-5187, doi: 10.1021/jp0046290, 2001.

Hallquist, M., Stewart, D. J., Stephenson, S. K., and Cox, R. A.: Hydrolysis of N_2O_5 on sub-micron sulfate aerosols, Physical Chemistry Chemical Physics, 5, 3453-3463, doi: 10.1039/b301827j, 2003.

Hu, J. H., and Abbatt, J. P. D.: Reaction probabilities for N_2O_5 hydrolysis on sulfuric acid and ammonium sulfate aerosols at room temperature, Journal of Physical Chemistry A, 101, 871-878, doi: 10.1021/jp9627436, 1997.

Kercher, J. P., Riedel, T. P., and Thornton, J. A.: Chlorine activation by N_2O_5: simultaneous, in situ detection of $ClNO_2$ and N_2O_5 by chemical ionization mass spectrometry, Atmospheric Measurement Techniques, 2, 193-204, doi: 10.5194/amt-2-193-2009, 2009.

Knipping, E. M., and Dabdub, D.: Impact of chlorine emissions from sea-salt aerosol on coastal urban ozone, Environmental Science & Technology, 37, 275-284, doi: 10.1021/es025793z, 2003.

Lawler, M. J., Sander, R., Carpenter, L. J., Lee, J. D., von Glasow, R., Sommariva, R., and Saltzman, E. S.: HOCl and Cl_2 observations in marine air, Atmospheric Chemistry and Physics, 11, 7617-7628, doi: 10.5194/acp-11-7617-2011, 2011.

Lopez-Hilfiker, F. D., Constantin, K., Kercher, J. P., and Thornton, J. A.: Temperature dependent halogen activation by N_2O_5 reactions on halide-doped ice surfaces, Atmospheric Chemistry and Physics, 12, 5237-5247, doi: 10.5194/acp-12-5237-2012, 2012.

Mielke, L. H., Furgeson, A., and Osthoff, H. D.: Observation of $ClNO_2$ in a Mid-Continental Urban Environment, Environmental Science & Technology, 45, 8889-8896, doi: 10.1021/es201955u, 2011.

Mozurkewich, M., and Calvert, J. G.: Reaction probability of N_2O_5 on aqueous aerosols, Journal of Geophysical Research-Atmospheres, 93, 15889-15896, doi: 10.1029/JD093iD12p15889, 1988.

Osthoff, H. D., Roberts, J. M., Ravishankara, A. R., Williams, E. J., Lerner, B. M., Sommariva, R., Bates, T. S., Coffman, D., Quinn, P. K., Dibb, J. E., Stark, H., Burkholder, J. B., Talukdar, R. K., Meagher, J., Fehsenfeld, F. C., and Brown, S. S.: High levels of nitryl chloride in the polluted subtropical marine boundary layer, Nature Geoscience, 1, 324-328, doi: 10.1038/ngeo177, 2008.

Phillips, G. J., Tang, M. J., Thieser, J., Brickwedde, B., Schuster, G., Bohn, B., Lelieveld, J., and Crowley, J. N.: Significant concentrations of nitryl chloride observed in rural continental Europe associated with the influence of sea salt chloride and anthropogenic emissions, Geophysical Research Letters, 39, doi: 10.1029/2012gl051912, 2012.

Pszenny, A. A. P., Keene, W. C., Jacob, D. J., Fan, S., Maben, J. R., Zetwo, M. P., Springer-Young, M., and Galloway, J. N.: Evidence of inorganic chlorine gases other than hydrogen chloride in marine surface air, Geophysical Research Letters, 20, 699-702, doi: 10.1029/93gl00047, 1993.

Pszenny, A. A. P., Fischer, E. V., Russo, R. S., Sive, B. C., and Varner, R. K.: Estimates of Cl atom concentrations and hydrocarbon kinetic reactivity in surface air at Appledore Island, Maine (USA), during International Consortium for Atmospheric Research on Transport and Transformation/Chemistry of Halogens at the Isles of Shoals, Journal of Geophysical Research-Atmospheres, 112, doi: 10.1029/2006jd007725, 2007.

Raff, J. D., Njegic, B., Chang, W. L., Gordon, M. S., Dabdub, D., Gerber, R. B., and Finlayson-Pitts, B. J.: Chlorine activation indoors and outdoors via surface-mediated reactions of nitrogen oxides with hydrogen chloride, Proceedings of the National Academy of Sciences of the United States of America, 106, 13647-13654, doi: 10.1073/pnas.0904195106, 2009.

Reff, A., Bhave, P. V., Simon, H., Pace, T. G., Pouliot, G. A., Mobley, J. D., and Houyoux, M.: Emissions Inventory of PM2.5 Trace Elements across the United States, Environmental Science & Technology, 43, 5790-5796, doi: 10.1021/es802930x, 2009.

Riedel, T. P., Bertram, T. H., Crisp, T. A., Williams, E. J., Lerner, B. M., Vlasenko, A., Li, S.-M., Gilman, J., de Gouw, J., Bon, D. M., Wagner, N. L., Brown, S. S., and Thornton, J. A.: Nitryl Chloride and Molecular Chlorine in the Coastal Marine Boundary Layer, Environmental Science & Technology, 46, 10463-10470, doi: 10.1021/es204632r, 2012a.

Riedel, T. P., Bertram, T. H., Ryder, O. S., Liu, S., Day, D. A., Russell, L. M., Gaston, C. J., Prather, K. A., and Thornton, J. A.: Direct N_2O_5 reactivity measurements at a polluted coastal site, Atmospheric Chemistry and Physics, 12, 2959-2968, doi: 10.5194/acp-12-2959-2012, 2012b.

Roberts, J. M., Osthoff, H. D., Brown, S. S., and Ravishankara, A. R.: N_2O_5 oxidizes chloride to Cl_2 in acidic atmospheric aerosol, Science, 321, 1059-1059, doi: 10.1126/science.1158777, 2008.

Roberts, J. M., Osthoff, H. D., Brown, S. S., Ravishankara, A. R., Coffman, D., Quinn, P., and Bates, T.: Laboratory studies of products of N_2O_5 uptake on Cl^- containing substrates, Geophysical Research Letters, 36, doi: 10.1029/2009gl040448, 2009.

Sarwar, G., and Bhave, P. V.: Modeling the effect of chlorine emissions on ozone levels over the eastern United States, Journal of Applied Meteorology and Climatology, 46, 1009-1019, doi: 10.1175/jam2519.1, 2007.

Spicer, C. W., Chapman, E. G., Finlayson-Pitts, B. J., Plastridge, R. A., Hubbe, J. M., Fast, J. D., and Berkowitz, C. M.: Unexpectedly high concentrations of molecular chlorine in coastal air, Nature, 394, 353-356, doi: 10.1038/28584, 1998.

Thornton, J. A., Braban, C. F., and Abbatt, J. P. D.: N_2O_5 hydrolysis on sub-micron organic aerosols: the effect of relative humidity, particle phase, and particle size, Physical Chemistry Chemical Physics, 5, 4593-4603, doi: 10.1039/b307498f, 2003.

Thornton, J. A., and Abbatt, J. P. D.: N_2O_5 reaction on submicron sea salt aerosol: Kinetics, products, and the effect of surface active organics, Journal of Physical Chemistry A, 109, 10004-10012, doi: 10.1021/jp054183t, 2005.

Thornton, J. A., Kercher, J. P., Riedel, T. P., Wagner, N. L., Cozic, J., Holloway, J. S., Dube, W. P., Wolfe, G. M., Quinn, P. K., Middlebrook, A. M., Alexander, B., and Brown, S. S.: A large atomic chlorine source inferred from mid-continental reactive nitrogen chemistry, Nature, 464, 271-274, doi: 10.1038/nature08905, 2010.

Tie, X. X., Emmons, L., Horowitz, L., Brasseur, G., Ridley, B., Atlas, E., Stround, C., Hess, P., Klonecki, A., Madronich, S., Talbot, R., and Dibb, J.: Effect of sulfate aerosol on tropospheric NO_x and ozone budgets: Model simulations and TOPSE evidence, Journal of Geophysical Research-Atmospheres, 108, doi: 10.1029/2001jd001508, 2003.

VandenBoer, T. C., Brown, S. S., Murphy, J. G., Keene, W. C., Young, C. J., Pszenny, A. A. P., Kim, S., Warneke, C., Gouw, J. A. d., Maben, J. R., Wagner, N. L., Riedel, T. P., Thornton, J. A., Wolfe, D. E., Dubé, W. P., Ozturk, F., Brock, C. A., Grossberg, N., Lefer, B., Lerner, B., Middlebrook, A. M., and Roberts, J. M.: Understanding the role of the ground surface in HONO vertical structure: High resolution vertical profiles during NACHTT-11, Journal of Geophysical Research, submitted, 2013.

Vogt, R., Crutzen, P. J., and Sander, R.: A mechanism for halogen release from sea-salt aerosol in the remote marine boundary layer, Nature, 383, 327-330, doi: 10.1038/383327a0, 1996.

Wagner, N. L., Riedel, T. P., Roberts, J. M., Thornton, J. A., Angevine, W. M., Williams, E. J., Lerner, B. M., Vlasenko, A., Li, S. M., Dube, W. P., Coffman, D. J., Bon, D. M., de Gouw, J. A., Kuster, W. C., Gilman, J. B., and Brown, S. S.: The sea breeze/land breeze circulation in Los Angeles and its influence on nitryl chloride production in this region, Journal of Geophysical Research-Atmospheres, 117, doi: 10.1029/2012jd017810, 2012.

Wagner, N. L., Riedel, T. P., Thornton, J. A., Dubé, W. P., Middlebrook, A. M., Sive, B., Brock, C. A., Young, C. J., Ozturk, F., Bahreini, R., Russo, R., Zhou, Y., Swarthout, R., Kim, S., and Brown, S. S.: N_2O_5 uptake coefficients determined from ambient wintertime measurements, Journal of Geophysical Research, submitted, 2013.

Wolfe, D. E., Welsh, D. C., Brown, S. S., and Wagner, N. L.: Summary of meteorological conditions during the 2011 Nitrogen, Aerosol Composition and Halogens on a Tall Tower (NACHTT) Experiment, Journal of Geophysical Research, submitted, 2013.

Young, A. H., Keene, W. C., Pszenny, A. A. P., Sander, R., Thornton, J. A., Riedel, T. P., and Maben, J. R.: Phase partitioning of soluble trace gases with size-resolved aerosols in near-surface continental air over northern Colorado, USA during winter, Journal of Geophysical Research, submitted, 2013.

Young, C. J., Washenfelder, R. A., Roberts, J. M., Mielke, L. H., Osthoff, H. D., Tsai, C., Pikelnaya, O., Stutz, J., Veres, P. R., Cochran, A. K., VandenBoer, T. C., Flynn, J., Grossberg, N., Haman, C. L., Lefer, B., Stark, H., Graus, M., de Gouw, J., Gilman, J. B., Kuster, W. C., and Brown, S. S.: Vertically Resolved Measurements of Nighttime Radical Reservoirs; in Los Angeles and Their Contribution to the Urban Radical Budget, Environmental Science & Technology, 46, 10965-10973, doi: 10.1021/es302206a, 2012.

Plume 1: February 26	
target O_3 (ppbv)	16.2
target NO_2 (ppbv)	17
target N_2O_5 (ppbv)	0.4335
target $ClNO_2$ (ppbv)	0.527
aerosol surface area ($\mu m^2 cm^{-3}$)	264
modeled time (hours)	3.3
initial O_3 (ppbv)	48
initial NO (ppbv)	20
ϕ_{ClNO2} (constrained)	0.38
γ_{N2O5}	0.024
time since sunset (hours)	10.7
initial O_3 (ppbv)	69
initial NO (ppbv)	35
ϕ_{ClNO2}	0.06
γ_{N2O5}	0.022

Plume 2: March 5	
target O_3 (ppbv)	24.5
target NO_2 (ppbv)	16.4
target N_2O_5 (ppbv)	0.907
target $ClNO_2$ (ppbv)	1.3
aerosol surface area ($\mu m^2 cm^{-3}$)	130
modeled time (hours)	4.4
initial O_3 (ppbv)	49
initial NO (ppbv)	22
ϕ_{ClNO2} (constrained)	0.85
γ_{N2O5}	0.02
time since sunset (hours)	10.3
initial O_3 (ppbv)	64
initial NO (ppbv)	31
ϕ_{ClNO2}	0.19
γ_{N2O5}	0.023

Table 5.1 Summary of box modeling constraints and results.

Reaction	k (cm^3 $molec^{-1}$ s^{-1})
$NO + O_3 \rightarrow NO_2 + O_2$	1.2e-14
$NO_2 + O_3 \rightarrow NO_3 + O_2$	1.5e-17
$NO_2 + NO_3 + M \rightarrow N_2O_5 + M$	1.4e-12
$NO + NO_3 \rightarrow 2NO_2$	2.8e-11
$N_2O_5 \rightarrow NO_2 + NO_3$	1.5e-3
$NO_3 \rightarrow$ "products"	5.0e-4
$N_2O_5 + HCl \rightarrow \phi ClNO_2 + (2 - \phi)HNO_3$	S_A / [2e-3 + 4/($\omega_{N2O5}\gamma_{N2O5}$)]
$ClNO_2 + HCl \rightarrow Cl_2 + HONO$	S_A / [2e-3 + 4/($\omega_{ClNO2}\gamma_{ClNO2}$)]

Table 5.2 Reactions and rate constants used in the chemical box model. S_A is the aerosol surface area in a volume of air (cm^2/cm^3). ω_{N2O5} and ω_{ClNO2} are the mean molecular speeds (cm/s) of an N_2O_5 molecule and $ClNO_2$ molecule, respectively. γ_{N2O5} and γ_{ClNO2} are the heterogeneous reaction probabilities of N_2O_5 and $ClNO_2$, respectively.

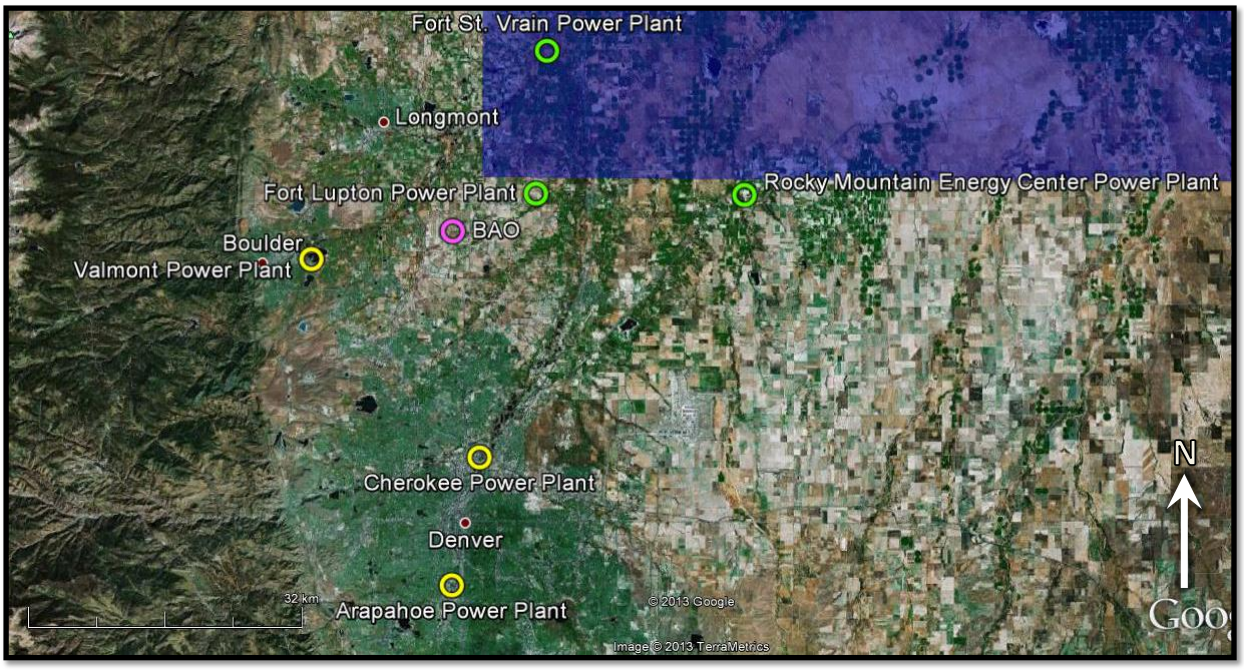

Figure 5.1 A map of important emission landmarks in the region surrounding the NACHTT measurement site. The measurement site is shown as an open pink circle. Small red dots illustrate the location of major cities, open yellow circles are coal-fired power plants, and open green circles are natural gas power plants. The blue shaded region represents areas with heavy natural gas and other hydrocarbon extraction activity.

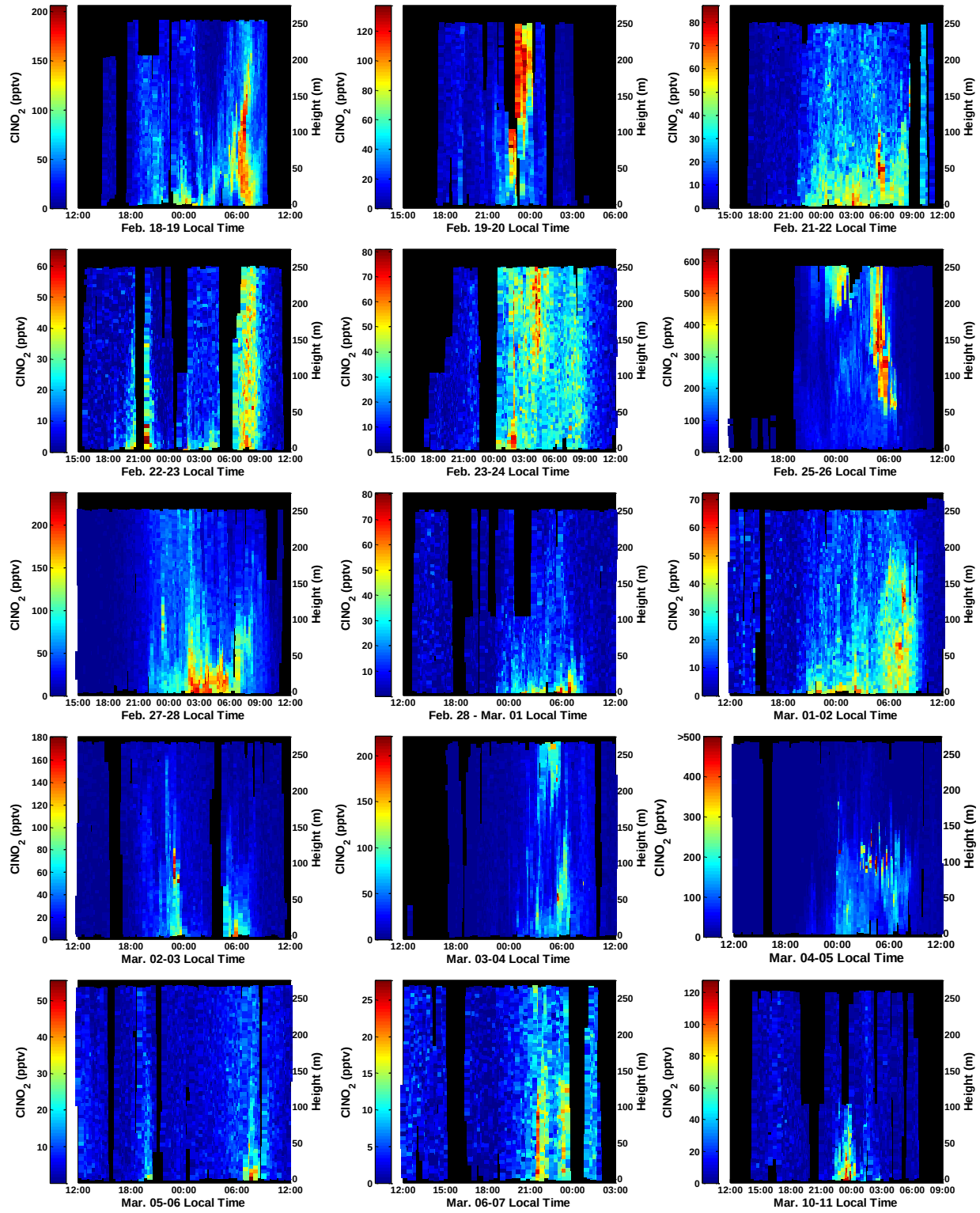

Figure 5.2 15-day overview of NACHTT vertical $ClNO_2$ profiles versus time of day. Mixing ratios are shown as colored squares. Black areas indicate no available measurements. Note the color scales vary between panels.

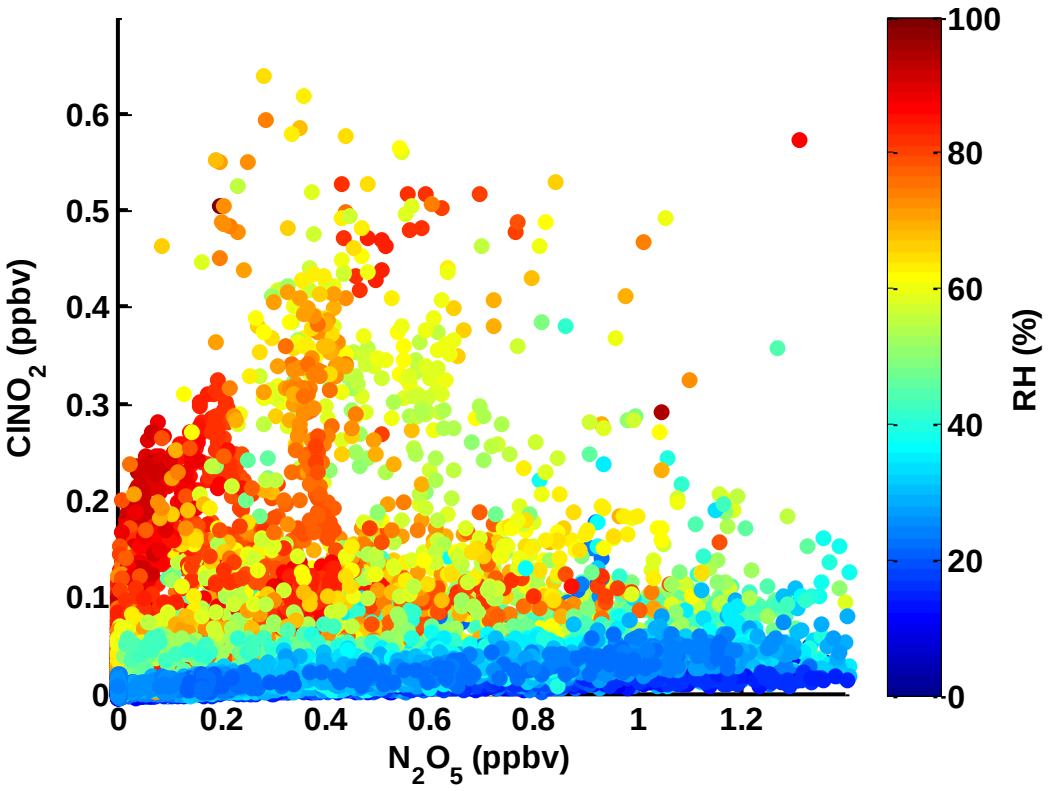

Figure 5.3 $ClNO_2$ mixing ratios vs. N_2O_5 mixing ratios scattered by the relative humidty for the NACHTT study period.

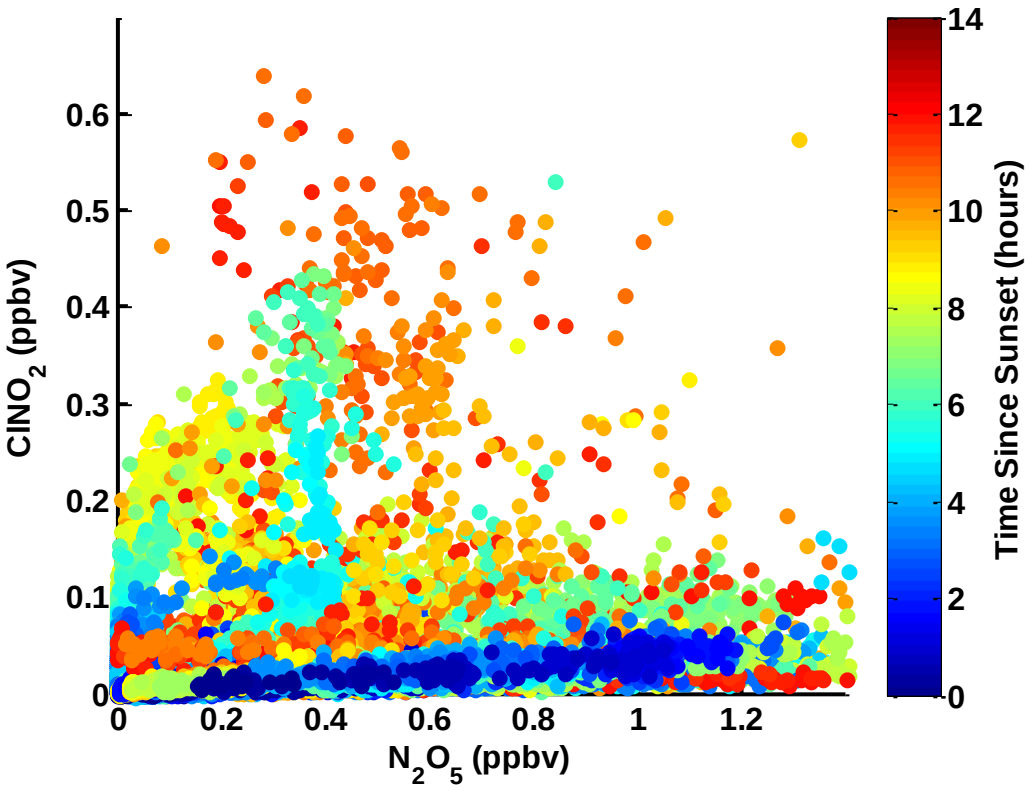

Figure 5.4 $ClNO_2$ mixing ratios vs. N_2O_5 mixing ratios scattered by the time since sunset for the NACHTT study period.

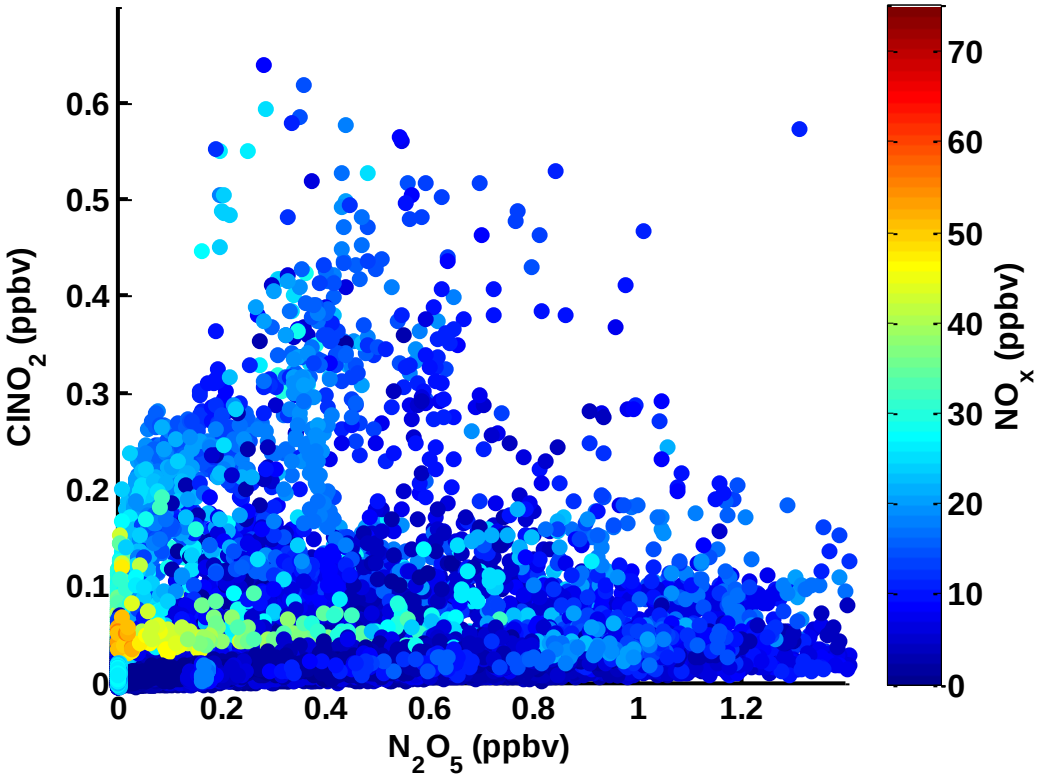

Figure 5.5 $ClNO_2$ mixing ratios vs. N_2O_5 mixing ratios scattered by NO_x mixing ratios for the NACHTT study period.

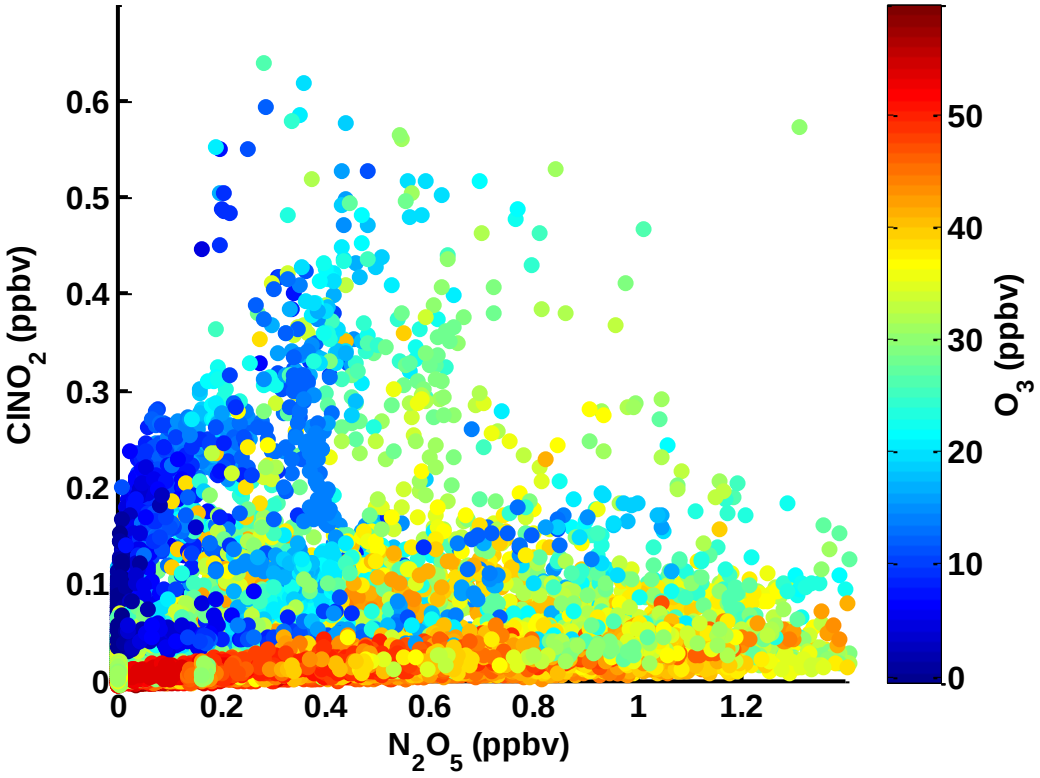

Figure 5.6 $ClNO_2$ mixing ratios vs. N_2O_5 mixing ratios scattered by ozone mixing ratios for the NACHTT study period.

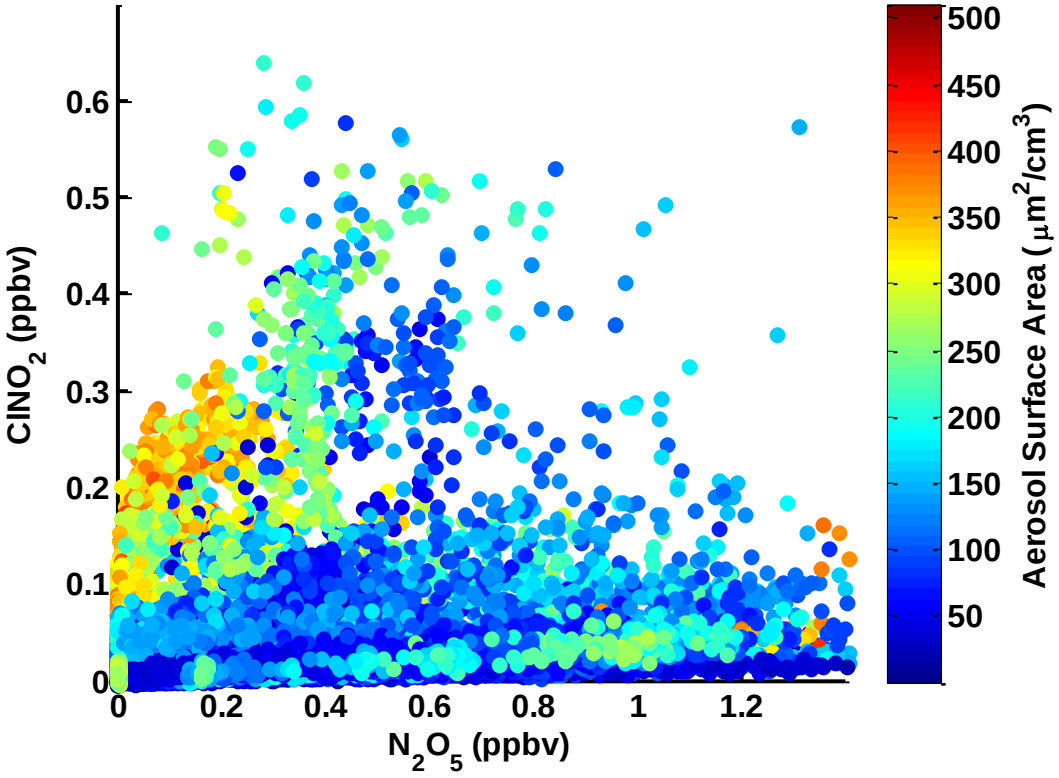

Figure 5.7 $ClNO_2$ mixing ratios vs. N_2O_5 mixing ratios scattered by aerosol surface area for the NACHTT study period.

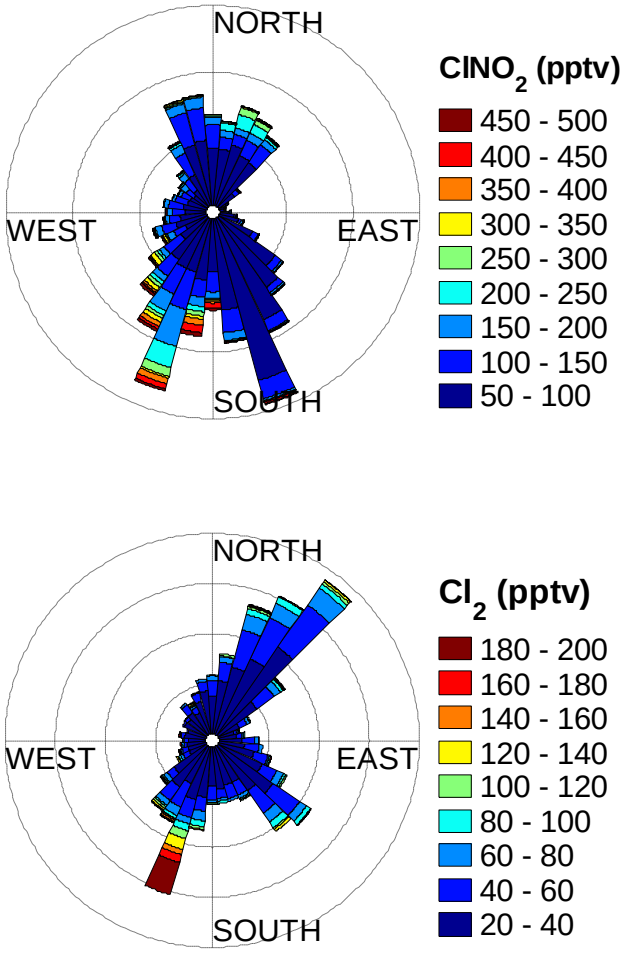

Figure 5.8 A wind rose showing the frequency of $ClNO_2$ (top) and Cl_2 (bottom) observations with wind direction colored by mixing ratios for the NACHTT study.

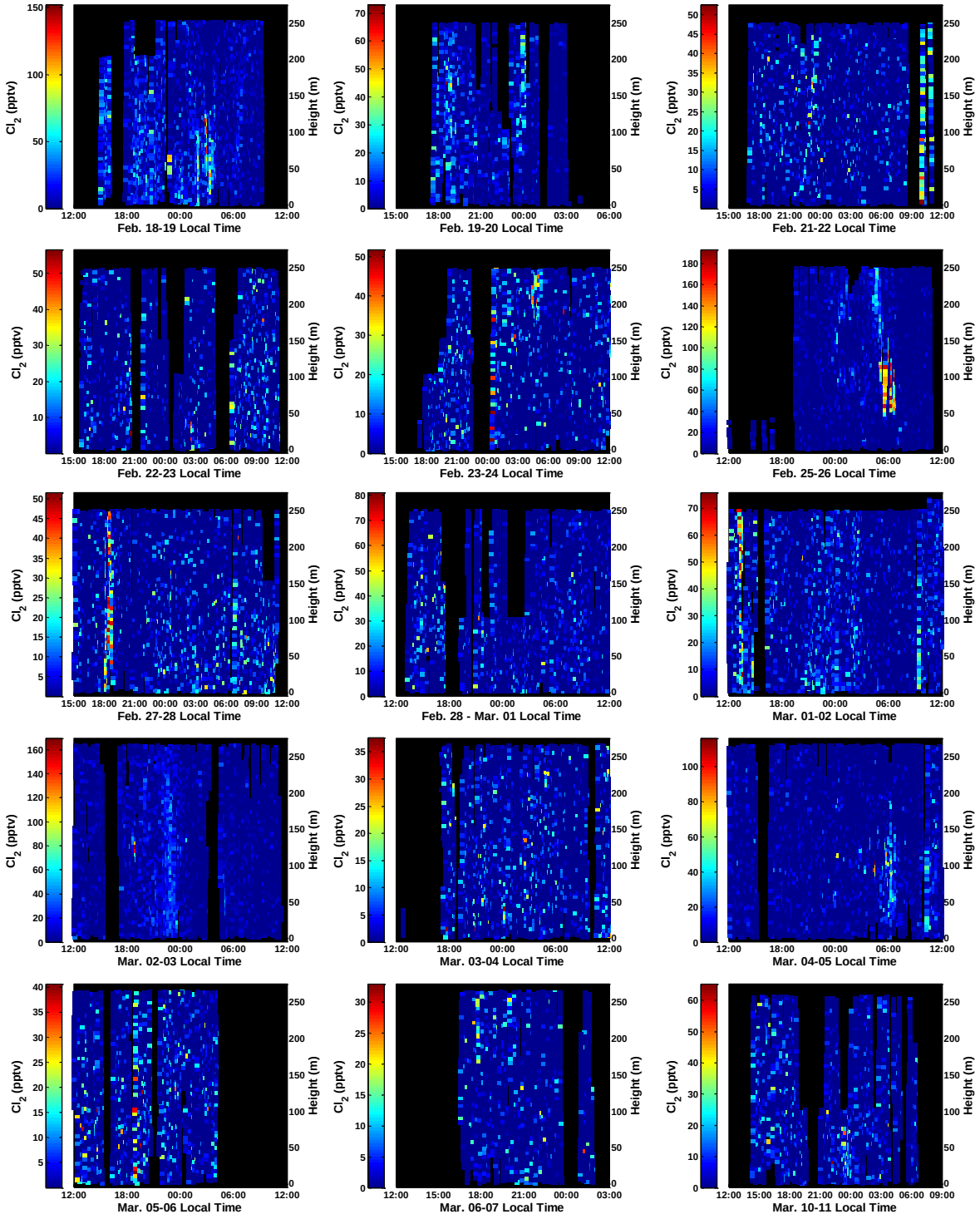

Figure 5.9 A summary of Cl_2 observations over 15 days during the NACHTT study. Vertical Cl_2 profiles versus time of day. Cl_2 mixing ratios are shown as colored squares. Black areas indicate no available measurements. Note the color scales vary between panels.

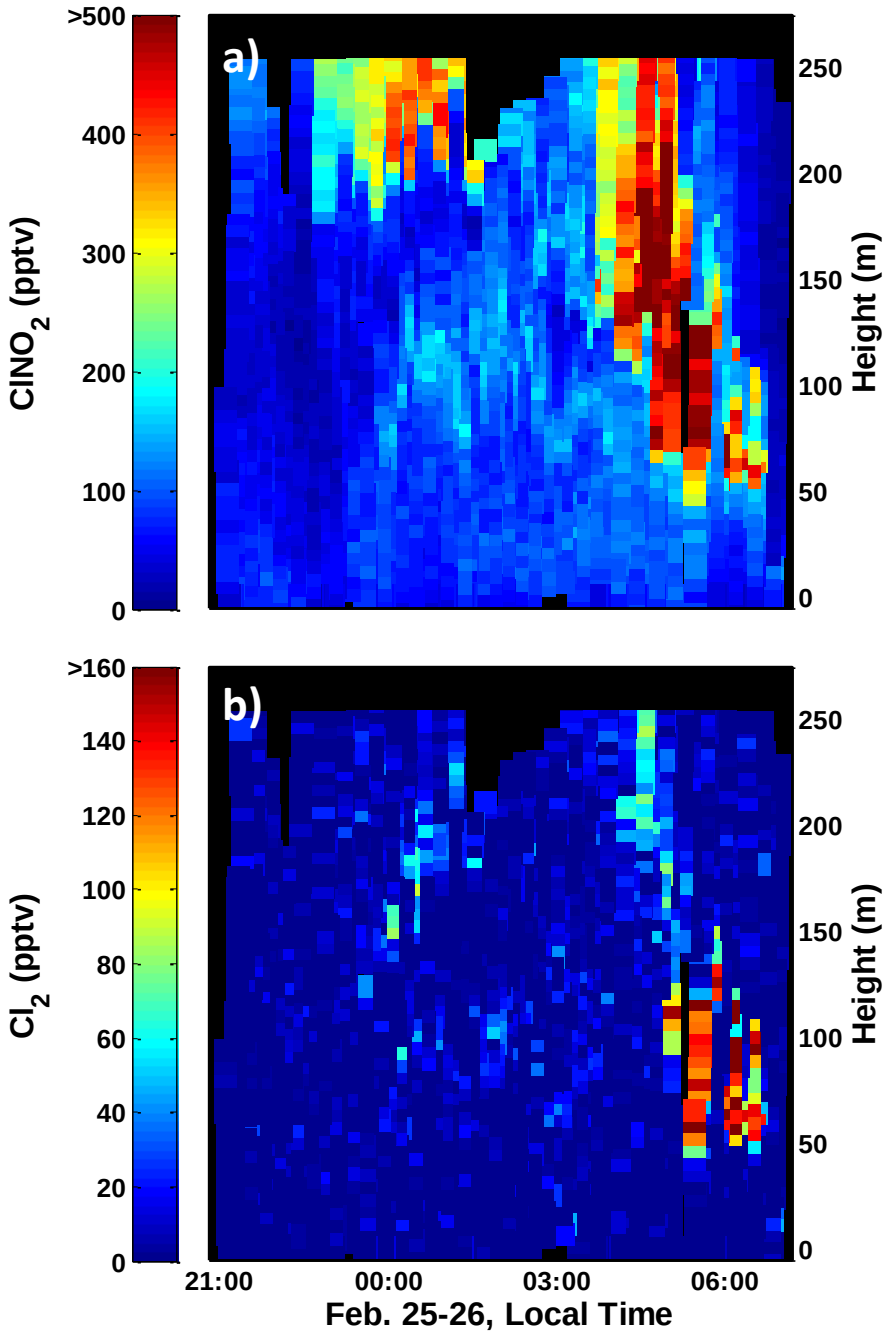

Figure 5.10 Vertical profiles versus time of day for a) $ClNO_2$ and b) Cl_2 mixing ratios during the time period around plume 1. Mixing ratios are shown as colored squares; the color scale for $ClNO_2$ saturates at 500 pptv while that for Cl_2 saturates at 160 pptv. Black areas indicate no available measurements.

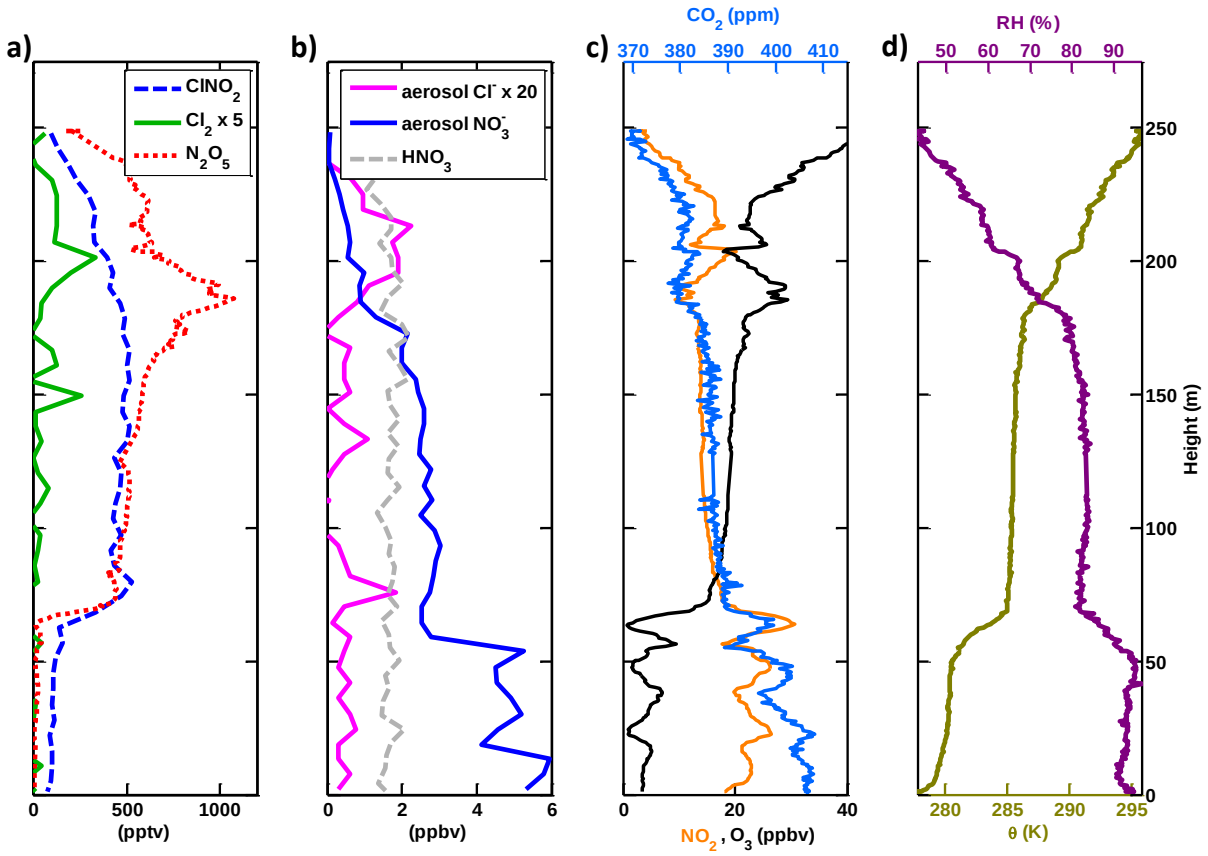

Figure 5.11 Observations taken during a plume 1 intercept. a) $ClNO_2$ (blue dashed line), Cl_2 x 5 (green solid line), and N_2O_5 (red dotted line) mixing ratios. b) aerosol phase Cl^- x 20 (pink solid line) and NO_3^- (blue solid line), gas phase HNO_3 (grey dashed line) c) CO_2 (cyan solid line, top x-axis), NO_2 (orange solid line, bottom x-axis), and O_3 (black solid line, bottom x-axis) mixing ratios. d) Relative humidity (RH (%), purple solid line) and potential temperature (θ (K), olive solid line).

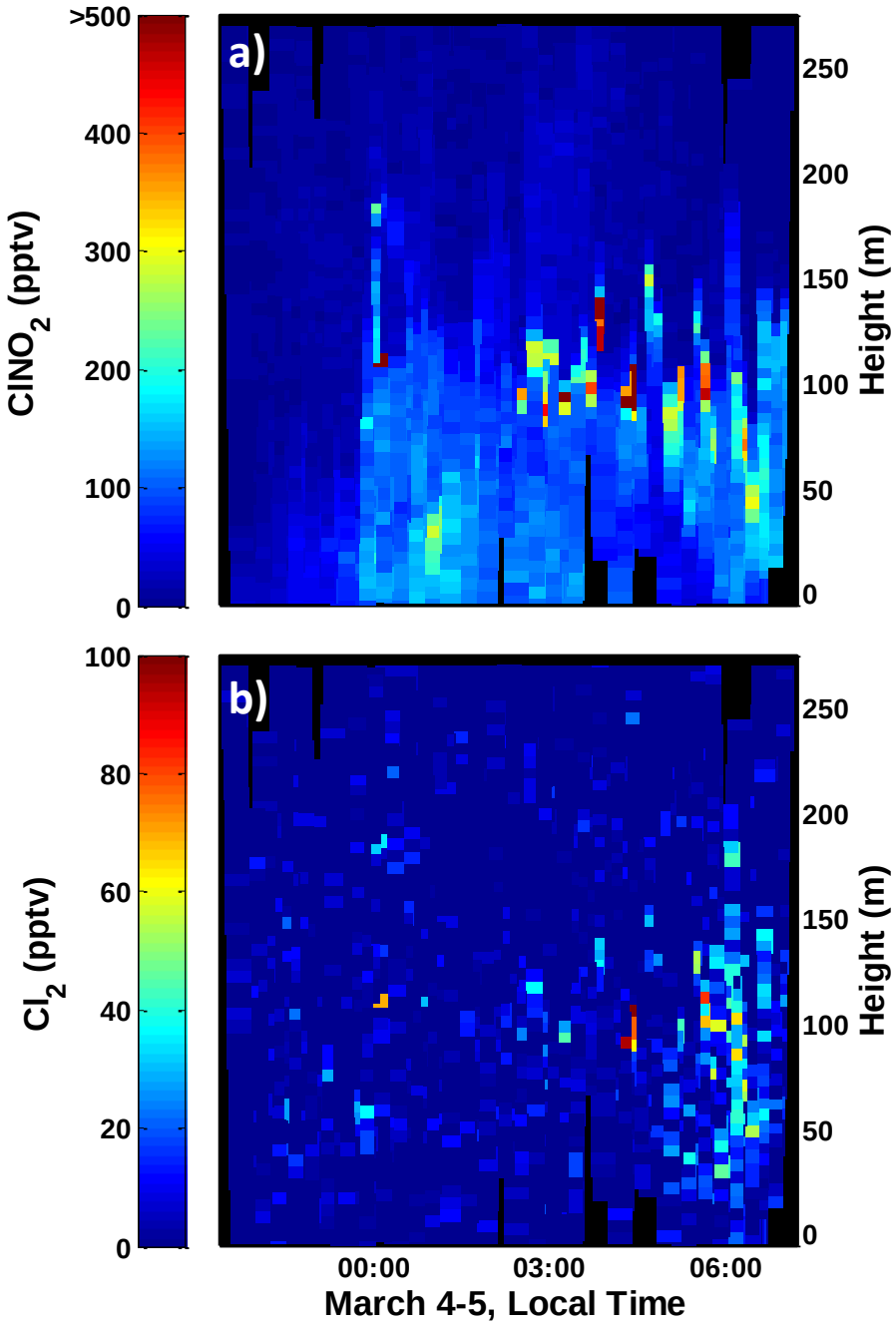

Figure 5.12 Vertical profiles versus time of day for a) $ClNO_2$ and b) Cl_2 mixing ratios during the time period around plume 2. Mixing ratios are shown as colored squares; the color scale for $ClNO_2$ saturates at 500 pptv while that for Cl_2 saturates at 100 pptv. Black areas indicate no available measurements.

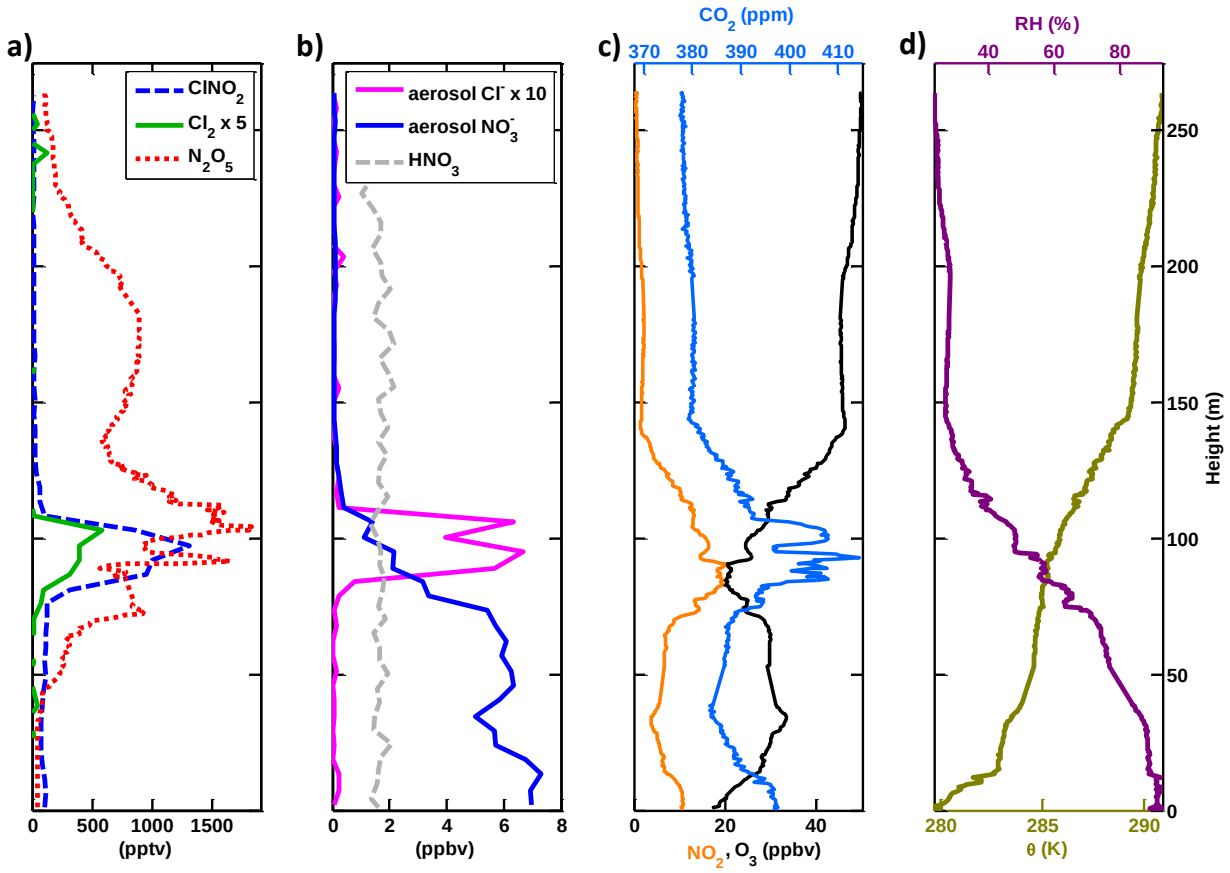

Figure 5.13 Observations taken during a plume 2 intercept. a) $ClNO_2$ (blue dashed line), Cl_2 x 5 (green solid line), and N_2O_5 (red dotted line) mixing ratios. b) aerosol phase Cl^- x 10 (pink solid line) and NO_3^- (blue solid line), gas phase HNO_3 (grey dashed line) c) CO_2 (cyan solid line, top x-axis), NO_2 (orange solid line, bottom x-axis), and O_3 (black solid line, bottom x-axis) mixing ratios. d) Relative humidity (RH (%), purple solid line) and potential temperature (θ (K), olive solid line).

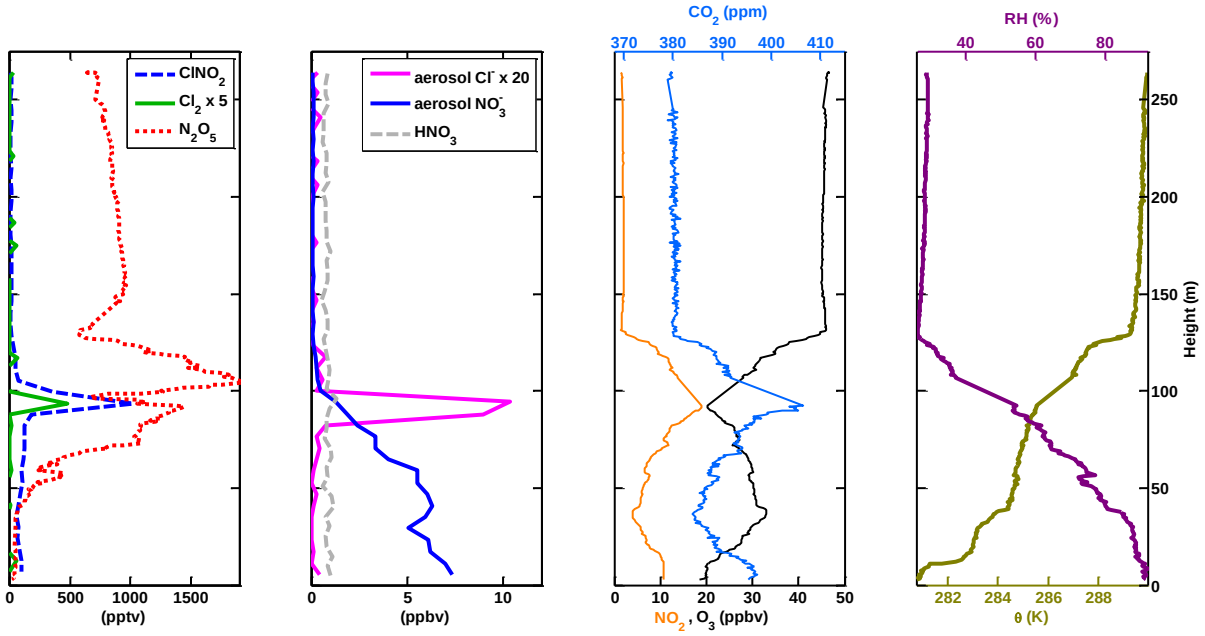

Figure 5.14 Observations taken during a vertical profile (04:04 – 04:12) prior to plume 2. $ClNO_2$ (blue dashed line), Cl_2 x 5 (green solid line), and N_2O_5 (red dotted line) mixing ratios. Aerosol phase Cl^- x 20 (pink solid line) NO_3^- (blue solid line), and gas phase HNO_3 (grey dashed line). CO_2 (cyan solid line, top x-axis), NO_2 (orange solid line, bottom x-axis), and O_3 (black solid line, bottom x-axis) mixing ratios. Relative humidity (RH (%), purple solid line) and potential temperature (θ (K), olive solid line).

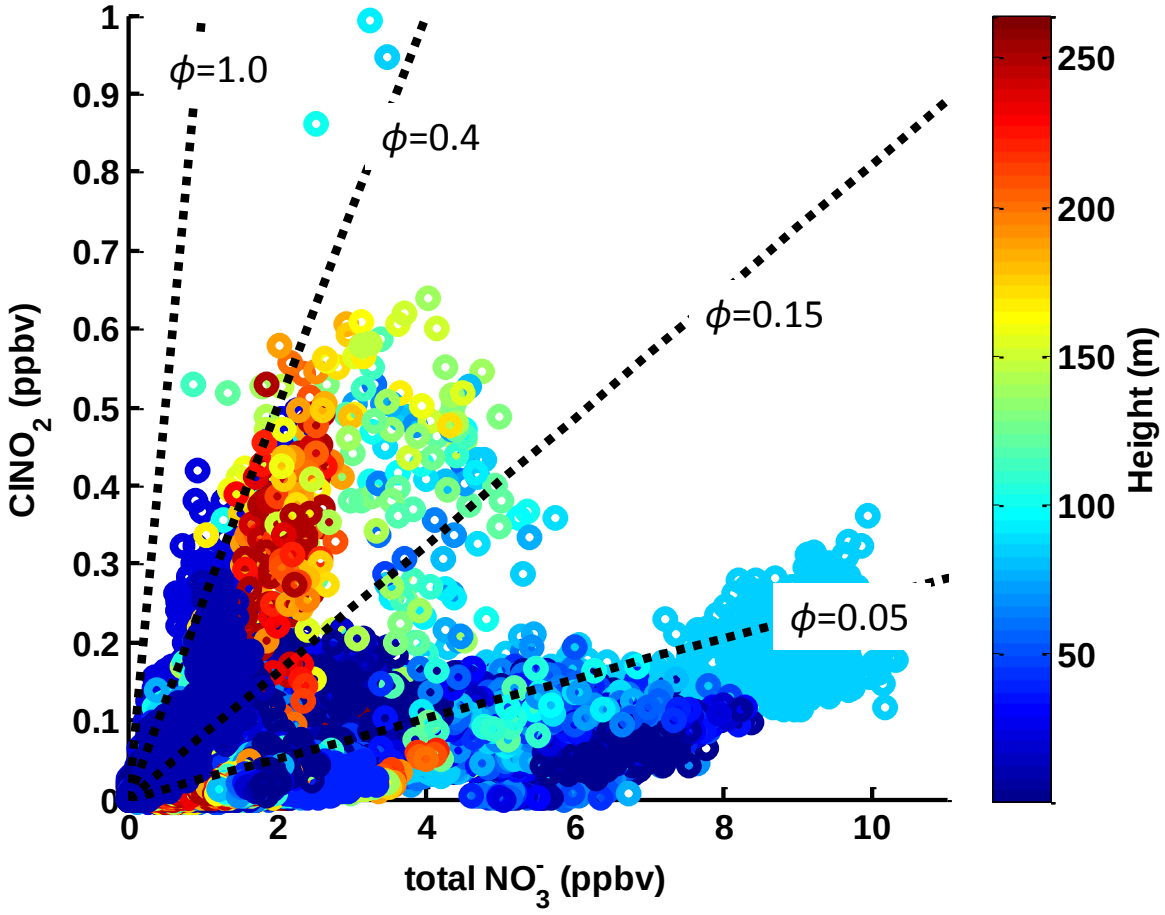

Figure 5.15 $ClNO_2$ mixing ratios are plotted versus total nitrate (HNO_3(g) + aerosol phase NO_3^-) mixing ratios illustrating the positive relationship between the two species that varied significantly with height over the course of the study. Each point is colored by the height at which the measurement was taken. Lines corresponding to various approximate $ClNO_2$ yields, based on Eq. 2, are drawn through the origin for illustrative purposes only.

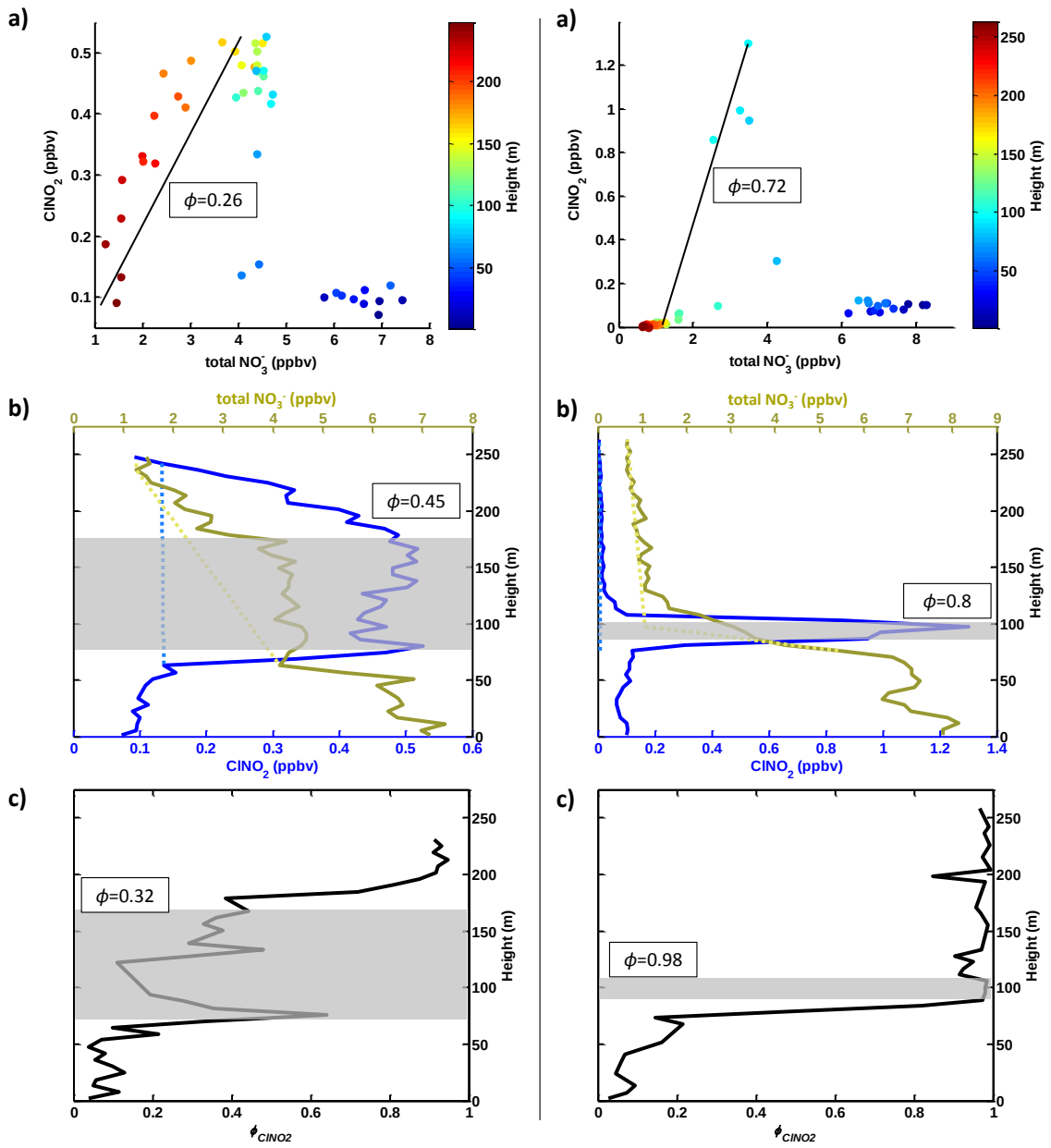

Figure 5.16 Summary of $ClNO_2$ yield estimate approaches for plume 1 (left pane) and plume 2 (right pane). a) $ClNO_2$ mixing ratios are plotted versus total nitrate (HNO_3(g) + aerosol phase NO_3^-) mixing ratios for the single transect. Each point is colored by the height at which the measurement was taken. The slope of the solid black lines, which are least squares linear fits to data in the plumes (data below 100 m are omitted from the plume 1 fit; data below 85 m are omitted from the plume 2 fit), together with Eq. 3 are used to estimate the in-plume $ClNO_2$ yield shown next to the line. b) Vertical profile of $ClNO_2$ mixing ratios and total nitrate mixing ratios. In estimating the given $ClNO_2$ yield for the plume, the dotted lines are used as background values to determine the in-plume (shaded region) enhancements of $ClNO_2$ and total nitrate. c) Height versus estimated $ClNO_2$ yields obtained from aerosol composition data and aerosol thermodynamic modeling. The stated yield represents the average of the yields over the shaded region.

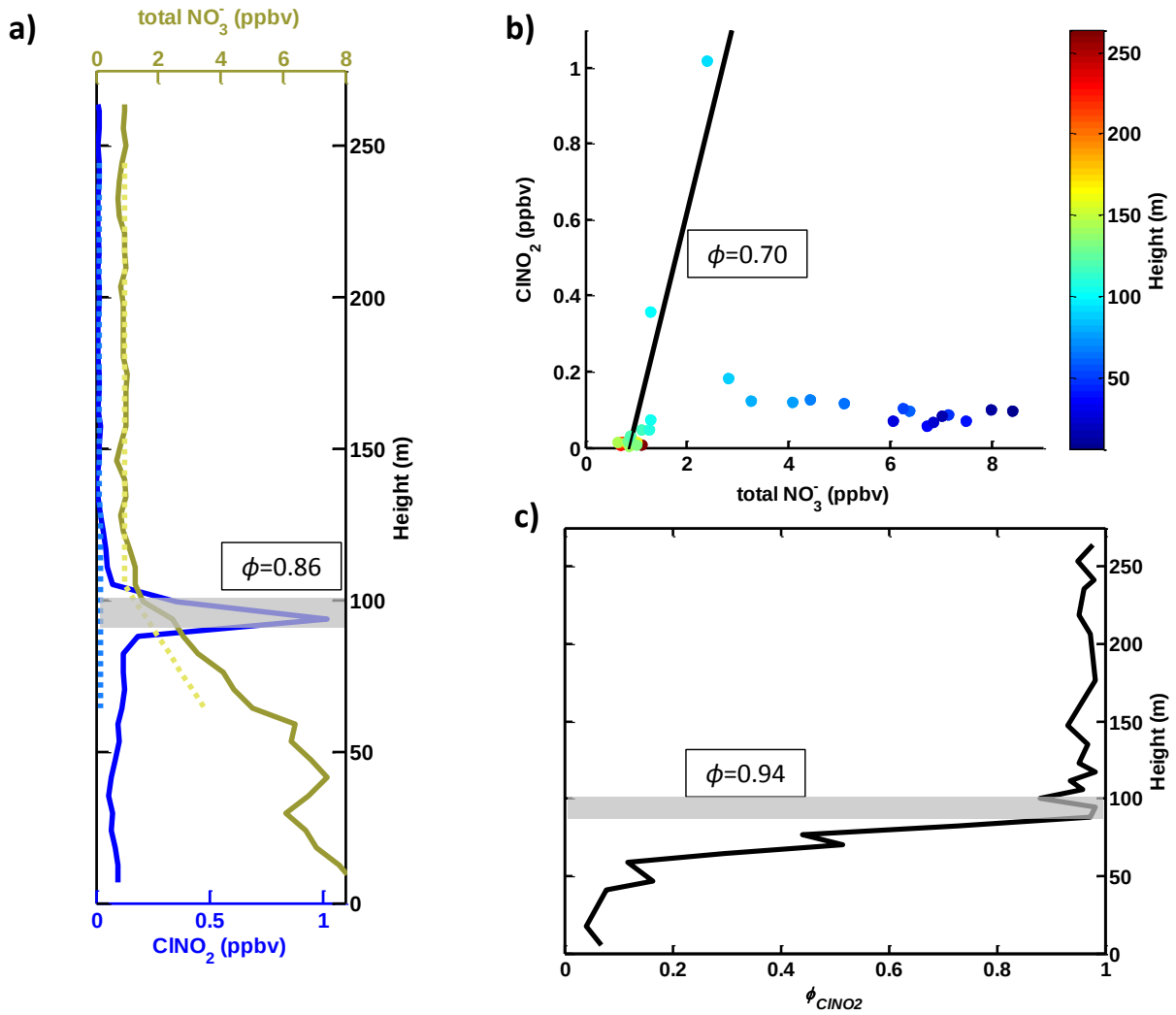

Figure 5.17 Additional data taken from a vertical profile (04:04 – 04:12) prior to plume 2. a) Vertical profile of $ClNO_2$ mixing ratios and total nitrate mixing ratios. In estimating the given $ClNO_2$ yield for the plume, the dotted lines are used as background values to determine the in-plume (shaded region) enhancements of $ClNO_2$ and total nitrate. b) $ClNO_2$ mixing ratios are plotted versus total nitrate (HNO_3(g) + aerosol phase NO_3^-) mixing ratios for the single transect. Each point is colored by the height at which the measurement was taken. The slope of the solid black lines, which are least squares linear fits to data in the plumes (data below 90 m are omitted from the fit), together with Eq. 3 (main text) are used to estimate the in-plume $ClNO_2$ yield shown next to the line. c) Height versus estimated $ClNO_2$ yields obtained from aerosol composition data and aerosol thermodynamic modeling. The stated yield represents the average of the yields over the shaded region.

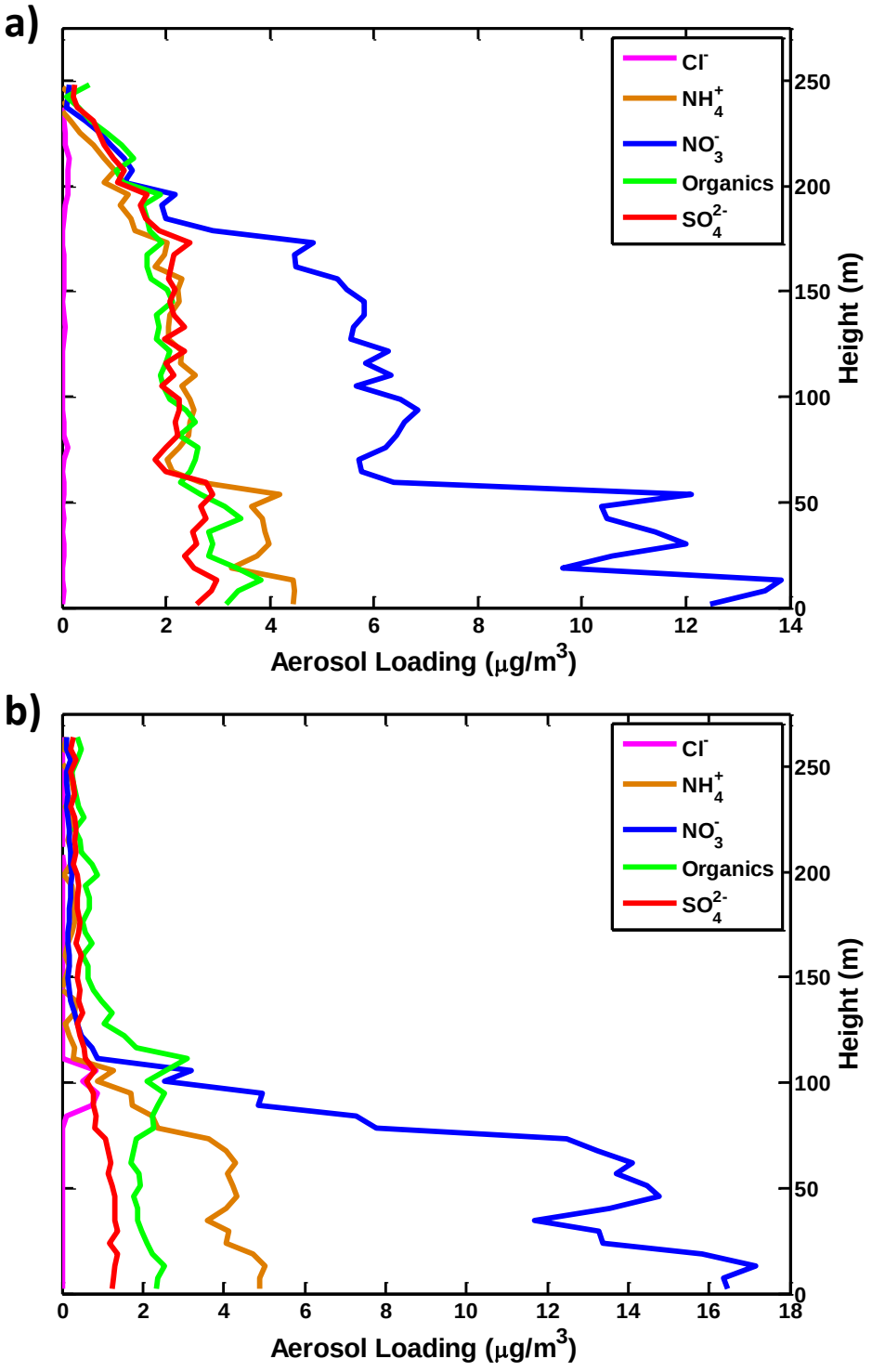

Figure 5.18 AMS-measured particle composition loadings for a) plume 1 and b) plume 2.

Chapter 6

An MCM Modeling Study of Nitryl Chloride ($ClNO_2$) Impacts on Oxidation, Ozone Production, and Nitrogen Oxide Partitioning in Polluted Continental Outflow

6.1 Introduction

Atomic chlorine atoms (Cl·) are highly reactive, often having rate constants for reactions with volatile organic compounds (VOC) that are factors of 10 to 100 larger than the hydroxyl radical, OH, which is considered the atmosphere's primary initiator of oxidation. As a result, the presence of Cl· can lead to shorter lifetimes for VOC and an enhanced radical pool which can potentially enhance the production of ozone, especially in polluted areas. The global tropospheric Cl· budget remains uncertain with a large range in recent studies (~15 – 40 Tg Cl yr^{-1}) developed from indirect means (Allan et al., 2007; Platt et al., 2004) as tropospheric Cl· concentrations are not presently measurable by existing methods. There are a number of potential Cl· sources in the troposphere, the major of which are outlined in Reactions R1 – R5.

$$HCl + OH \rightarrow Cl\bullet + H_2O \quad \text{(R1)}$$

$$Cl_2 + h\nu \rightarrow 2Cl\bullet \quad \text{(R2)}$$

$$BrCl + h\nu \rightarrow Cl\bullet + Br\bullet \quad \text{(R3)}$$

$$ClNO + h\nu \rightarrow Cl\bullet + NO \quad \text{(R4)}$$

$$ClNO_2 + h\nu \rightarrow Cl\bullet + NO_2 \quad \text{(R5)}$$

The reaction of hydrochloric acid (HCl) with the hydroxyl radical (OH) is a daytime source of Cl·. Typical HCl mixing ratios in the troposphere vary from 100 – 5000 pptv with the highest found in polluted regions with direct HCl emissions from industrial processes and acid displacement of aqueous chloride by HNO_3 and H_2SO_4. Cl· formed by HCl + OH tend to peak around midday with the peak in OH formed from $O(^1D) + H_2O$. Additionally, the oxidation of many VOC by Cl· proceeds via a hydrogen abstraction to form HCl, thus recycling Cl·.

Photolysis of molecular chlorine (Cl_2) produces two Cl· and has been the focus of many Cl· investigations since it was first measured in ambient air (Finley and Saltzman, 2006, 2008; Lawler et al., 2011; Riedel et al., 2012a; Spicer et al., 1998). Cl_2 mixing ratios are often on the order of tens of pptv with maximum reported mixing ratios near 100 – 200 pptv. There are direct emissions Cl_2 whose sources can be related to processes associated with power generation, water treatment, and oil refineries (Sarwar and Bhave, 2007). In addition, Cl_2 can be formed in situ through multiphase chemistry involving chlorine nitrate ($ClONO_2$) and hypochlorous acid (HOCl). These species can photolyze to reform Cl· or ClO or react on acidic, chloride-containing particles to form Cl_2. In heavily polluted air the majority of ClO will react with NO, in a null cycle producing a Cl· and NO_2 rather than going on to form Cl_2.

BrCl photolysis to form Cl· and atomic bromine is also thought to be an important Cl· source especially in polar regions where reported ambient mixing ratios are on the order of tens of pptv (Buys et al., 2013; Foster et al., 2001; Spicer et al., 2002). To our knowledge there have been no reported observations of BrCl in ambient air outside of polar regions (Finley and Saltzman, 2008). BrCl can form through heterogeneous reactions of $BrONO_2$ and HOBr on

acidic, chloride-containing particles in an analogous manner to the Cl_2 formation reactions described above or through reactions $ClONO_2$ and HOCl on acidic, bromide-containing particles.

Nitrosyl chloride (ClNO) has recently been proposed as a potential Cl· source (Raff et al., 2009). These theoretical and laboratory studies have yet to be confirmed by field measurements of ClNO in ambient air, but mixing ratios in the ppbv range are predicted by regional model calculations in polluted marine areas.

Since its proposed formation by Finlayson-Pitts et al. (1989) and first observation in ambient air by Osthoff et al. (2008), nitryl chloride ($ClNO_2$) has been observed during a number of different field studies worldwide with nighttime maximum mixing ratios ranging from tens of pptv to over 2 ppbv (Kercher et al., 2009; Mielke et al., 2011; Osthoff et al., 2008; Phillips et al., 2012; Riedel et al., 2012a; Thornton et al., 2010; Young et al., 2012). These observations have occurred in both continental and marine locations illustrating the importance of $ClNO_2$ as a Cl· source in a variety of different environments. $ClNO_2$ represents a Cl· source with clear anthropogenic origins as it is formed at night by reactions involving NO_x (NO_2 + NO), ozone, and chloride containing aerosols. Anthropogenic activities associated with power generation, motor vehicle use, and agriculture now dominate the global NO_x source. Natural sources of NO_x such as microbial activity, lightning, and wildfires are also significant globally, at the 25% level, but the impact of these NO_x sources on $ClNO_2$ formation remain unknown. At night, a fraction of NO_x is converted into $ClNO_2$ through Reactions R6 – R8. The branching ratio between $ClNO_2$ and HNO_3 formation in Reaction R8, commonly referred to as the $ClNO_2$ yield (ϕ_{ClNO_2}), is determined by the efficiency of $ClNO_2$ formation from heterogeneous reactions of N_2O_5. This and the N_2O_5-particle reaction probability (γ) are uncertain quantities that can vary significantly

depending on a number of factors such as particulate water, chloride, nitrate, and organic content (Bertram and Thornton, 2009; McNeill et al., 2006; Mentel et al., 1999; Thornton et al., 2003).

$$NO_2 + O_3 \rightarrow NO_3 + O_2 \quad \text{(R6)}$$

$$NO_3 + O_3 \leftrightarrow N_2O_5 \quad \text{(R7)}$$

$$N_2O_5 + Cl^- + H^+ \xrightarrow{\gamma} \phi_{ClNO_2} ClNO_2 + (2 - \phi_{ClNO_2}) HNO_3 \quad \text{(R8)}$$

Here we examine the effects of $ClNO_2$ formation as predicted by a detailed box model which incorporates the Master Chemical Mechanism and is constrained by ground and ship-based ambient measurements taken during the CalNex 2010 field study. We use the model to assess the impact of $ClNO_2$ on the Cl· budget, hydrogen oxide and organic peroxy radical abundance (RO_x = OH + HO_2 + RO_2), NO_x lifetime and partitioning, and the net ozone production rate. In the presence of high NO_x, all of these quantities or processes are linked through photochemical oxidation of VOC. As shown in Reactions R9 – R12 the oxidation of a hydrocarbon (RH) is initiated by reaction with OH or Cl· to form the organic peroxy radical (RO_2). In a high NO_x environment, the dominant fate of RO_2 is to react with NO. The dominant channel of this reaction leads to a closed shell oxygenated hydrocarbon (OVOC), hydroperoxyl radical (HO_2) and NO_2, while the minor channel leads to an alkyl nitrate ($RONO_2$). If the RO_2 is an acyl peroxy radical, then reaction with NO_2 produces acyl peroxy nitrates (APN) such as peroxy acetyl nitrate (PAN). NO also reacts with HO_2 to form NO_2 and OH. This radical chain thereby net produces ~ $2O_3$ via NO_2 photolysis for every VOC oxidation.

$$RH + OH \rightarrow RO_2 + H_2O \quad \text{(R9)}$$

$$RH + Cl\bullet \rightarrow RO_2 + HCl \quad \text{(R10)}$$

$$RO_2 + NO \rightarrow OVOC + HO_2 + NO_2 \quad \text{(R11a)}$$

$$RO_2 + NO \rightarrow RONO_2 \quad \text{(R11b)}$$

$$RO_2 + NO_2 \leftrightarrow APN \quad \text{(R12)}$$

From the above discussion, we expect that $ClNO_2$ acts similarly, though not exactly the same, as an OH source such as that from nitrous acid (HONO) photolysis or $O(^1D) + H_2O$. Under high NO_x, where the radical pool is terminated via cross reactions between RO_x and NO_x, a higher production rate of HO_x or Cl· will nearly linearly increase the ozone production rate (Daum et al., 2000; Kleinman, 2005). Moreover, at high NO, production of an RO_2 by Cl· attack directly increases the steady state concentration of OH and HO_2 due to the rapid cycling between OH, HO_2 and RO_2. However, the increased RO_2 due to Cl· arises from a potentially different pool of hydrocarbons than that from OH given the large differences in RH abundance and relative reactivity towards OH and Cl·. Moreover, $ClNO_2$ photolysis predominantly occurs in the first few hours after sunrise, well before the maximum OH production rate from $O(^1D) + H_2O$ and before the maximum in the NO/NO_2. Thus, the full impact of $ClNO_2$ on ozone production, VOC lifetime and NO_x abundance and partitioning may not be the same as simply scaling the daytime average HO_x production rate.

6.2 Measurements and Model Description

We chose to constrain a box model using data taken during the CalNex field study which occurred in May and June of 2010 in the southern California region (Ryerson et al., 2013). There were multiple measurement platforms involved in CalNex, two of which recorded both $ClNO_2$

and extensive VOC measurements: the Research Vessel *Atlantis* and a ground site located on the California Institute of Technology campus in Pasadena, CA. Though the R/V *Atlantis* sampled in many locations along the southern California coast, we focus on the measurements made in and around Los Angeles urban outflow due to the added constraints provided by the Pasadena ground site measurements. $ClNO_2$ mixing ratios in the nocturnal outflow from the Los Angeles region were commonly over 500 pptv with maximums on the order of 2 ppbv (Riedel et al., 2012a).

Cl· chemistry was incorporated into an existing model framework described in Wolfe and Thornton (2011) which is based on the Master Chemical Mechanism version 3.2 (MCM) developed at the University of Leeds (more information available at http://mcm.leeds.ac.uk/MCM) (Bloss et al., 2005; Jenkin et al., 1997; Jenkin et al., 2003; Saunders et al., 2003). Use of the MCM allows for explicit tracking of approximately 2800 chemical species and about 9000 different reactions with reaction rate constants constrained by the International Union of Pure and Applied Chemistry (IUPAC) kinetics database (http://www.iupac-kinetic.ch.cam.ac.uk).

In total, 44 of the VOC measured at the Pasadena site are used to constrain the model. However, certain VOC, such as ethanol (median value = 8.2 ppbv) and acetone (median value = 3.8 ppbv), measured at the Pasadena ground site appeared to often be dominated by local emissions. In order to more generally represent an urban air mass in the model, ground site VOC measurements were scaled by those measured on the R/V *Atlantis*. A smaller number of VOC were measured aboard the R/V *Atlantis*, so species not represented in the R/V *Atlantis* dataset were scaled by species of similar structure. For example, methanol was measured with median levels of approximately 6 ppbv and 1 ppbv at the ground site and on the ship, respectively. Ethanol, however, was only measured at the ground site. In order to estimate ethanol levels in the

urban outflow that the R/V *Atlantis* sampled, the ground site ethanol mixing ratios were simply scaled down by 1/6. For a complete list of the measured VOC used in the model see Table 1.

VOC and HCl mixing ratios are held to their ship-scaled diurnal profiles for a 69 hour "spin-up" period. NO_2, O_3, and CO are held to mean values measured at the ground site during this spin-up period. In addition, we fix methane at a mixing ratio of 1.8 ppmv. The box model does not attempt to replicate the effects of meteorology and thus the processes of dilution and deposition are not accurately incorporated. To maintain reasonable concentrations of the many modeled species which were not constrained by observations, we apply a continuous dilution rate of 1.5% per hour to all species. Formaldehyde and nitric acid have an additional dilution rate of 30% per hour in order to keep the mixing ratios at levels relevant to those sampled during the CalNex study (<6 ppbv) (Warneke et al., 2011). The sensitivity of the results to this additional loss rate is minor (<20% adjustments to the Cl· budget), and the need for this additional loss is likely related to our neglect of deposition for intermediate organic oxidation products and of HNO_3 itself. Isoprene, alpha-pinene, beta-pinene, and limonene are allowed to freely evolve at night during the spin-up period to avoid unrealistic conditions where fast reactions such as oxidation by NO_3 were capable of proceeding with an unlimited source of these reactive species. At hour 69, which represents sunset on the third day, all species are released from constraints and the chemistry evolves freely for another 27 hours. We use the final 24-hours of a model run as the analysis period. All figures and calculations described here are performed on the model output from this period.

A number reactions critical toward Cl· production and reactivity are not included in the MCM. Version 3.2 of the MCM only includes Cl· reactions with alkanes. In order to accurately represent the chemistry, multiple mechanisms were added to the model framework. These

include the Reactions R1 – R3, R8, R13 – R21, and a number of VOC + Cl· reaction

$$Cl\bullet + O_3 \rightarrow ClO + O_2 \quad \text{(R13)}$$

$$ClO + NO_2 \rightarrow ClONO_2 \quad \text{(R14)}$$

$$ClO + HO_2 \rightarrow HOCl + O_2 \quad \text{(R15)}$$

$$ClONO_2 + h\nu \rightarrow Cl\bullet + NO_3 \quad \text{(R16)}$$

$$ClONO_2 + h\nu \rightarrow ClO + NO_2 \quad \text{(R17)}$$

$$HOCl + h\nu \rightarrow Cl\bullet + OH \quad \text{(R18)}$$

$$ClONO_2 + H^+ + Cl^- \xrightarrow{\gamma} Cl_2 + HNO_3 \quad \text{(R19)}$$

$$HOCl + H^+ + Cl^- \xrightarrow{\gamma} Cl_2 + H_2O \quad \text{(R20)}$$

$$ClO + NO \rightarrow Cl\bullet + NO_2 \quad \text{(R21)}$$

mechanisms where VOC = methanol, ethanol, isopropanol, ethene, propene, formaldehyde, ethanal, propanal, acetone, benzene, styrene, o-xylene, toluene. Several of these added mechanisms are shown in detail in Figures 1 – 5. Additionally, our revised mechanism explicitly tracks gas-phase HCl formation that results from hydrogen atom abstraction VOC oxidation reactions. Unique to the added alkene reaction mechanisms is that the major pathway involves the addition of chlorine to the double bond rather than the typical hydrogen abstraction pathway (Atkinson et al., 2004). This pathway leads to chlorinated products which might be detectable as tracers of Cl· chemistry in future studies. As we show below, such compounds could be another avenue for Cl· recycling. Reactions of Cl· with isoprene, which also produces unique chlorinated

products, were not included in the model framework given its modest <1% contribution to total Cl· reactivity in the modeled Los Angeles outflow and the large increase in complexity when incorporating said mechanism (Fan and Zhang, 2004; Tanaka et al., 2003). Instead the products of Cl· + isoprene were simply tracked as a single generic specie with no chemical losses. However, in areas where isoprene is a more significant contributor to Cl· reactivity, it would be necessary to include a more explicit isoprene oxidation mechanism to accurately capture the effects Cl·, especially to assess any chlorinated products that might form from these reactions. In such locations the products of chlorine initiated isoprene oxidation are likely more pronounced than in the Los Angeles region.

Aerosol reaction probabilities in the model are set to 0.01 for N_2O_5, $ClONO_2$, and HOCl (R8, R19, R20). γ = 0.01 is within the typical range of N_2O_5 reaction probabilities measured on ambient aerosol (<0.001 – 0.03) during various field studies (Bertram et al., 2009; Riedel et al., 2012b). Laboratory measurements of $ClONO_2$ and HOCl uptake under stratospheric and tropospheric conditions on sulfuric acid, sodium chloride, and sodium bromide particles and pure water droplets generally report γ values <0.06 for $ClONO_2$ and HOCl (Deiber et al., 2004; Hanson and Ravishankara, 1994; Hanson et al., 1994). We assume that reactions of $ClONO_2$ and HOCl on aerosol particles produce only Cl_2 with unit efficiency. Unit yield is unlikely except possibly on sea salt particles which represented <40% of the surface area in the Los Angeles region during the CalNex study. Given that Cl_2 production from heterogeneous reactions of $ClONO_2$ and HOCl is proportional to the product of γ and the yield, we use γ = 0.01 and a 100% yield on all particles in the model.

To examine the effects of $ClNO_2$ formation, we vary the $ClNO_2$ yield between 50% and 0% in successive model runs, which produce a with-$ClNO_2$ case and a without-$ClNO_2$ case. A

50% yield results in ~1.5 ppbv of $ClNO_2$ as shown in Figure 6 which is typical of the Los Angeles outflow conditions encountered during CalNex. We also performed a series of model runs where HONO was constrained to observations made at the Pasadena ground site. Its abundance otherwise is determined only by the reaction of OH + NO, HONO + OH, and the photolysis of HONO. Most of our main conclusions reported here are relatively insensitive to HONO. Moreover, the likely different relative vertical profiles of $ClNO_2$ and HONO throughout the nocturnal and evolving daytime boundary layer make our primary focus on $ClNO_2$ a reasonable simplification for a box model (Young et al., 2012).

6.3 Results and Discussion

6.3.1 Cl-atom Budget

These modeling studies indicate that integrated over a typical day in the Los Angeles outflow, $ClNO_2$ is likely the major driver of Cl· evolution. Neither HCl + OH or multiphase chemistry involving $ClONO_2$ and HOCl to produce Cl_2 are competitive with the $ClNO_2$ source. Moreover, this picture is consistent with that derived solely from observations in this region (Riedel et al., 2012a). Figure 6 shows the Cl· concentration predicted by the model during the 24-hour analysis period for both the with-$ClNO_2$ and without-$ClNO_2$ cases. When $ClNO_2$ formation is included, the Cl· concentration reaches a maximum at ~7 AM (2 hours after model sunrise) with a value of 1.08×10^5 molecules per cm^3. A substantially different picture results from the without-$ClNO_2$ case where the maximum Cl· concentration occurs around noon and only reaches 0.2×10^5 molecules per cm^3. The assumptions made about the aerosol reaction probabilities of $ClONO_2$ and HOCl partially drive the late afternoon Cl· profile, which as a result is more uncertain. However, this afternoon Cl· concentration profile is not especially sensitive to the

assumed reaction probabilities. For example, increasing the reaction probabilities of $ClONO_2$ and HOCl by a factor of ten to 0.1 does not substantially change the 24-hour profile. The maximum in Cl· concentration is increased by ~10% still occurring in the early morning hours after sunrise (~7 AM), and the integrated Cl· concentration over the entire day is enhanced by only 20%. Additionally, the choice of 0.01 for a $ClONO_2$ and HOCl reaction probability and a 100% Cl_2 yield is likely more realistic as the formation of Cl_2 from these reactions is unlikely to be the sole product (Caloz et al., 1996; Santschi and Rossi, 2005). That said, it appears that to fully understand the impact of Cl· chemistry in coastal urban areas, the fate of $ClONO_2$ especially needs to be better constrained.

The Cl· evolution largely follows that of the dominant source terms, the modeled diurnal evolution of which we compare in Figure 7. In the absence of $ClNO_2$ formation (Figure 7a), the bulk of the Cl· are a result of HCl + OH production channel, and the maximum in Cl· production rate of $0.5x10^6$ molecules per cm^3 per second coincides with the maximum production from the HCl + OH channel. In the with-$ClNO_2$ case (Figure 7b), the maximum Cl· production rate occurs at 7 AM with a value of $3.4x10^6$ molecules cm^{-3} s^{-1} corresponding to the maximum contribution from $ClNO_2$ photolysis. The $ClNO_2$ production channel represents 56% of Cl· production over the course of the entire day, leading to nearly 3.7 times as many Cl· produced relative to the without-$ClNO_2$ case. By noon, $ClNO_2$ is largely depleted under the clear-sky model conditions, and other Cl· production channels like the reaction of HCl with OH and the photolysis of Cl_2 from HOCl and $ClONO_2$ heterogeneous chemistry become more dominant. These production channels involving multi-phase Cl-recycling to form Cl_2 show significant enhancements when $ClNO_2$ formation is included. For example, Cl· production from $ClONO_2$ photolysis, HOCl photolysis, and Cl_2 photolysis are enhanced by 3.3, 2.2, and 3.3, respectively over the without-

$ClNO_2$ case. To some extent these enhancements should be expected considering the larger Cl· pool available for recycling reactions when $ClNO_2$ formation is allowed, but they give indication of the degree of indirect coupling between $ClNO_2$ and Cl_2 via the increased formation of reactive chlorine reservoirs like $ClONO_2$ and HOCl. During CalNex, molecular chlorine was also measured along with $ClNO_2$ (Riedel et al., 2012a). Observations of nighttime and early morning Cl_2 were typically in the 5 – 50 pptv range. Modeled Cl_2 levels are of similar magnitude to these observations, as well as previous observations of Cl_2 in this region (Finley and Saltzman, 2006, 2008), and show a morning enhancement with slightly elevated levels throughout the day but only with the inclusion of $ClNO_2$ (see Figure 8).

The use of a comprehensive chemical mechanism such as the MCM illustrates a potentially important but heretofore overlooked source of Cl· in polluted regions. In the with-$ClNO_2$ case, the reaction of OH with formyl chloride (CHOCl), produced from Cl· attack of alkenes, becomes a noticeable Cl· source during the afternoon. In fact, because we possibly overestimate the actual multi-phase recycling of $ClONO_2$ and HOCl to form Cl_2, Cl· release from such acid chlorides may be more important than these multiphase processes. This result suggests observations of acid chlorides would be as beneficial as Cl_2 in polluted regions. HONO has a noticeable impact on the afternoon Cl· budget via photolysis to form OH followed by the reaction of OH + HCl. Constraining the model to the measured HONO diurnal profile leads to an 60% ($1.4x10^7$ to $2.26x10^7$ molecules per cm^3) increase in the daily maximum OH concentration and a similar increase in the integrated Cl· formation rate from OH + HCl. Multi-phase recycling via $ClONO_2$ and HOCl are also increased as a result of the larger Cl· concentrations. However, as discussed by Young et al. (2012), afternoon and daytime HONO concentrations are fairly

uncertain, so we suspect that the perturbations to afternoon Cl· throughout the boundary layer are likely more similar to the box model predictions without the incorporation of measured HONO.

We also investigate the formation potential of chlorinated products at potentially detectable quantities resulting from the Cl· oxidation of VOC. These species could represent "tracers" of Cl· chemistry and the extent to which Cl· oxidation reactions are occurring. This has been investigated previously in Houston using ship based measurements of potential products from Cl· oxidation of isoprene (Riemer et al., 2008). As stated above, chlorinated products of Cl· reactions with isoprene are not included these model investigations and are likely of minor importance to total Cl· reactivity in the Los Angeles region. Within our model framework, Cl· addition reactions with ethene and propene can produce chlorinated products such as chloroacetaldehyde, formyl chloride, 2-chloropropanal, 2-chloroperoxypropionyl nitrate (2-chloroPPN), chloroperoxyacetyl nitrate (CLETPAN), and chloroacetone. As with most of the previously mentioned effects, these enhancements are most obvious in the early part of the day when Cl· and VOC concentrations are highest in the model. As we show in Figure 9, morning enhancements are typically on the order of a 5-30 pptv above the background generated during the spin-up period. Chloroacetaldehyde and formyl chloride exhibit the largest enhancements. Interestingly, the photolysis of formyl chloride was shown in Figure 7b to represent a significant source of Cl·, comparable in magnitude to that predicted from HOCl photolysis.

In a polluted region such as the Los Angeles basin and outflow, Cl· produced by the above processes will be net lost primarily through reactions with VOC. These reactions produce organic peroxy radicals which through reactions with NO subsequently form HO_x. As such, Cl· in polluted regions have similar impacts to an increased HO_x source. The effect of incorporating Cl· chemistry is not the same as simply increasing the HO_x production rate because of the

different temporal evolution of Cl· chemistry and the different reactivity towards VOC of Cl· compared to OH. Cl· reactivity determined by the observationally constrained model is illustrated in Figure 10, where it is broken into Cl· reactions with methane, alkanes, alkenes, alcohols, carbonyls (aldehydes and ketones), and ozone. Other Cl· + VOC reactions such as reactions with aromatics are not shown as they were not a significant sink of Cl· relative to the species listed. In the morning (7 AM), the bulk of reactivity is due to reactions with a variety of alkanes which comprise 42% of the 44 sec^{-1} total reactivity. Later in the day (3 PM) as the VOC are consumed in the model and O_3 maximizes, the reaction with O_3 to form ClO is the dominant Cl· sink and represents about 60% of the 39 sec^{-1} total reactivity. However, the majority of ClO (77% at 7 AM and 67% at 3 PM) will react with NO to give NO_2 and Cl· that can terminally react with VOC. That is to say that only 23 – 33% of the Cl· + O_3 eventually goes on to form $ClONO_2$ and HOCl. Over the course of the day no single VOC dominates the Cl· reactivity (see Figure 11). Methane is consistently about 10% of the total. This implies that all VOC reactive towards Cl· are relevant when trying to estimate the total reactivity and that only using a small subset may significantly underestimate the total. This behavior is different from that of OH, the reactivity of which is often dominated by a few VOC or inorganic species such as CO and NO_2 in highly polluted regions (Kato et al., 2011; Ren et al., 2003).

6.3.2 Impact on RO_x and NO_x

The effects of $ClNO_2$ formation described above lead to important and unique impacts on processes relevant to tropospheric air quality. As described above, Cl· produced by $ClNO_2$ photolysis will react with VOC to produce organic peroxy radicals during morning hours. The RO_2 will primarily react with NO under the polluted conditions to form HO_2 and a closed-shell

oxygenated VOC or an alkyl nitrate. Alternatively, given the large NO_2/NO ratio during the morning, enhanced peroxy nitrate formation is possible via reaction of acyl peroxy radicals with NO_2. The HO_2 produced via RO_2 + NO also reacts with NO to form OH, which in turn reacts with VOC to form RO_2. The radical chain length of this cycle tends to be somewhat short in the morning given higher concentrations of NO_x leading to termination via OH + NO_2 to form HNO_3 which is efficiently lost to wet and dry deposition. That said, Cl· will enhance the abundance of morning time RO_x (OH + HO_2 + RO_2) as illustrated in Figure 12 which will lead to enhanced O_3 production rates relative to a model run without $ClNO_2$.

Figure 12a shows the HO_x production rate (P_{HOx}) for both the with- and without-$ClNO_2$ cases. A nearly factor of 2.2 increase occurs in the early morning hours around 7 AM when Cl· production from $ClNO_2$ photolysis is the major Cl· source. P_{HOx} remains elevated throughout the day relative to the without-$ClNO_2$ case likely due to the larger ozone values in the with-$ClNO_2$ case, thus illustrating that the $ClNO_2$ influence persists for more than just the early morning hours. The 24-hour integrated HO_x production rate for the with- and without-ClNO2 cases is 75 ppbv and 62 ppbv, respectively. Uncertainties in modeling HONO have the largest impact on the quantifying the perturbation of $ClNO_2$ to P_{HOx}. Constraining modeled HONO to the diel average values measured at the ground site results in the same overall pattern of $ClNO_2$ effects on P_{HOx} described above, just at a reduced magnitude – i.e. the inclusion $ClNO_2$ formation increases P_{HOx} by ~35% in the morning, with moderate enhancements to P_{HOx} sustained throughout the day resulting in an integrated P_{HOx} of 116 ppbv and 105 ppbv for the with- and with-out ClNO2 cases, respectively. These two extremes in terms of HONO are likely both representative – the latter HONO-rich case being representative of near surface chemistry while the former HONO-

poor case being more representative of the residual boundary layer aloft of the surface which dominants the column-average radical budget as described by Young et al. (2012).

Figure 12b shows the effects of $ClNO_2$ on the concentrations OH, HO_2, the sum over all 717 organic peroxy radicals (RO_2), and the sum of 140 acyl peroxy nitrates (APNs) predicted by the model. The enhancement ratio of the with-$ClNO_2$ case relative to the without-$ClNO_2$ case is shown. Inclusion of $ClNO_2$ formation results in significant changes in HO_x (OH and HO_2) with 190% and 220% enhancements during the morning hours in OH and both HO_2 and RO_2, respectively. In remote low-NO_x regions, Cl· and OH are largely uncoupled such that the presence of one does not largely impact the abundance of the other. This condition then allows indirect quantification of Cl· abundance by comparing VOC which have different reaction rate constants for reaction with OH and Cl· (i.e., Platt et al. (2004) and Allan et al. (2007)). However, the presence of additional Cl· from $ClNO_2$ in a polluted region has the potential to significantly increase OH via the above mechanism, especially in the morning hours. Constraining modeled HONO again lowers the magnitude of these $ClNO_2$ induced morning perturbations to 25 and 50% increases in OH and the sum of HO_2 and RO_2, respectively. Again, while even these HONO-rich perturbations are significant, these findings, together with the vertically resolved estimates of Young et al. (2012), further imply strong vertical gradients in the effects of $ClNO_2$ on morning oxidant evolution.

$ClNO_2$ formation and photolysis has implications for the reactive nitrogen budget as well as Cl· sources. $ClNO_2$ is relatively unreactive at night, thereby building up and allowing transport of NO_x downwind of the urban core with morning photolysis of $ClNO_2$ analogous to thermal decomposition of acyl peroxy nitrates such as PAN. In addition to this direct impact on the NO_x transport, we find significant perturbations to acyl peroxy nitrate formation occur in the with-

$ClNO_2$ case (see Figure 12b). A 50% enhancement in total APN occurs before noon, and the enhancement remains elevated at around 10% for the remainder of the day. This $ClNO_2$ induced perturbation to APN formation largely persists even when measured HONO values are incorporated. Additionally, the sum of alkyl nitrates is also enhanced by 15% before noon with individual alkyl nitrates enhanced up to 60% in the with-$ClNO_2$ case. Increasing the partitioning of NO_x into reservoirs such as APN is important in that it implies a greater potential for export of NO_x to remote regions. In fact, while $ClNO_2$ formation extends the lifetime of NO_x through the night, our model suggests faster OH + NO_2, APN formation, and alkyl nitrate formation during the subsequent day largely offset this effect, such that NO_x is ~6% lower from sunrise until noon in the with-$ClNO_2$ than in the without-$ClNO_2$ case.

6.3.3 Impact on the Ozone Production Rate and Odd-Oxygen

The previously stated effects on HO_x and RO_2 directly influence ozone production which we illustrate in Figure 12c. Over the entire model day the difference between the integrated ozone production rate with 1.5 ppbv $ClNO_2$ and the integrated ozone production rate without $ClNO_2$ is about 12 ppbv. The majority of this enhancement takes place over the first 5 hours after sunrise where at 6:30 AM the ozone production rate in enhanced by ~200%. The pre-noon ozone mixing ratios relative to the without-$ClNO_2$ case are increased by ~20% with a ~10% increase over the remainder of the day including peak ozone which occurs at about 5 PM. This is a large enough absolute enhancement to influence predictions of attainment of air quality standards in polluted coastal regions. The enhancement in ozone production scales nearly linearly with the $ClNO_2$ yield for this region, as expected, given that the ozone production rate is approximately linear with the primary radical source in a high NO_x environment like Los Angeles. Constraining

modeled HONO to the observations results in a 9 ppbv enhancement in the integrated ozone production rate due to $ClNO_2$.

The above result is also interesting to consider in terms of the impact of nocturnal nitrogen oxide chemistry on the odd-oxygen budget. Defining O_x as the sum of O_3 and NO_2, our model predicts that N_2O_5 reactions on aerosol particles transform 9 ppbv O_x at night. If we neglect $ClNO_2$ formation, this 9 ppbv O_x is permanently lost due to nitrate formation from N_2O_5 hydrolysis. However, incorporating $ClNO_2$ formation, with a yield (branching ratio) of 50%, results in up to 12 ppbv O_x produced the subsequent day compared to the case where $ClNO_2$ formation is neglected. Thus, due to $ClNO_2$ formation and its daytime impact on oxidants and ozone, nighttime N_2O_5 chemistry does not net destroy O_x but is in fact potentially a net source, or at least a null cycle, for the Los Angeles region conditions we simulate here.

While not directly comparable, our results appear generally consistent with a recent 3D CMAQ modeling study of $ClNO_2$ effects on ozone and particulate nitrate (Sarwar et al., 2012). In the Los Angeles region, the CMAQ modeling showed roughly a 2 – 4 ppbv increase in daytime ozone per ppbv $ClNO_2$ photolyzed, with maxima approaching 8 ppbv/ppbv. Likely important in setting the actual ozone enhancement is, among other possibilities, the mixing of background marine air with the polluted core and the model predicted vertical distribution of $ClNO_2$. These issues will be important to test with observations for validating model representations of this process.

6.4 Summary and Conclusions

These model outputs suggest that $ClNO_2$ photolysis is likely a major $Cl\cdot$ source, if not the dominant source, under conditions similar to those sampled in the Los Angeles region during

CalNex 2010. The impact of $ClNO_2$ on potential daytime halogen atom recycling is substantial, with significant enhancements predicted on other Cl· reservoirs like $ClONO_2$, HOCl, and Cl_2. Relative to model runs without $ClNO_2$ formation, the presence of $ClNO_2$ causes significant and non-negligible perturbations in HO_x, RO_2, APN, and ozone production. Relative to a model without $ClNO_2$ formation and heterogeneous HONO production, incorporating $ClNO_2$ perturbed the integrated total radical and ozone production rates by 20%, with perturbations in RO_x and APN >100%. Moreover, we show that given these effects, the impact of N_2O_5 reactions on aerosol particles is not a net sink of odd-oxygen but instead a net source for the polluted coastal conditions we model here. The absolute magnitude of the perturbations in these quantities and processes relative to a model that does not include $ClNO_2$ will ultimately depend upon the presence of HONO and the abundance of $ClNO_2$ and HONO vertically as well as seasonally. Given that the only vertically resolved $ClNO_2$ and HONO observations in the Los Angeles basin (and elsewhere for that matter) suggest $ClNO_2$ is far more important an oxidant source in a column average sense (Young et al., 2012), the upper end of the impacts of $ClNO_2$ we present here may in fact be representative for polluted coastal regions in summer.

We conclude by noting that during winter, in locations such as the Northeastern U.S., the role of $ClNO_2$ may be substantially more important to the total radical budget given that $O(^1D)$ production and H_2O vapor concentrations can both be factors of 5 lower than presented here, resulting in significantly lower OH abundances while $ClNO_2$ approaches similar concentrations (Kercher et al., 2009). This idea is consistent with the apparently important role of $ClNO_2$ at inland locations during wintertime as illustrated by recent studies at the Uintah Basin, Utah (Edwards et al., 2013).

References

Allan, W., Struthers, H., and Lowe, D. C.: Methane carbon isotope effects caused by atomic chlorine in the marine boundary layer: Global model results compared with Southern Hemisphere measurements, Journal of Geophysical Research: Atmospheres, 112, D04306, doi: 10.1029/2006jd007369, 2007.

Atkinson, R., Baulch, D. L., Cox, R. A., Crowley, J. N., Hampson, R. F., Hynes, R. G., Jenkin, M. E., Rossi, M. J., and Troe, J.: Evaluated kinetic and photochemical data for atmospheric chemistry: Volume I - gas phase reactions of Ox, HOx, NOx and SOx species, Atmos. Chem. Phys., 4, 1461-1738, doi: 10.5194/acp-4-1461-2004, 2004.

Bertram, T. H., and Thornton, J. A.: Toward a general parameterization of N_2O_5 reactivity on aqueous particles: the competing effects of particle liquid water, nitrate and chloride, Atmospheric Chemistry and Physics, 9, 8351-8363, doi: 10.5194/acp-9-8351-2009, 2009.

Bertram, T. H., Thornton, J. A., Riedel, T. P., Middlebrook, A. M., Bahreini, R., Bates, T. S., Quinn, P. K., and Coffman, D. J.: Direct observations of N_2O_5 reactivity on ambient aerosol particles, Geophysical Research Letters, 36, doi: 10.1029/2009gl040248, 2009.

Bloss, C., Wagner, V., Jenkin, M. E., Volkamer, R., Bloss, W. J., Lee, J. D., Heard, D. E., Wirtz, K., Martin-Reviejo, M., Rea, G., Wenger, J. C., and Pilling, M. J.: Development of a detailed chemical mechanism (MCMv3.1) for the atmospheric oxidation of aromatic hydrocarbons, Atmos. Chem. Phys., 5, 641-664, doi: 10.5194/acp-5-641-2005, 2005.

Buys, Z., Brough, N., Huey, L. G., Tanner, D. J., von Glasow, R., and Jones, A. E.: High temporal resolution Br_2, BrCl and BrO observations in coastal Antarctica, Atmospheric Chemistry and Physics, 13, 1329-1343, doi: 10.5194/acp-13-1329-2013, 2013.

Caloz, F., Fenter, F. F., and Rossi, M. J.: Heterogeneous Kinetics of the Uptake of $ClONO_2$ on NaCl and KBr, The Journal of Physical Chemistry, 100, 7494-7501, doi: 10.1021/jp953099i, 1996.

Daum, P. H., Kleinman, L., Imre, D. G., Nunnermacker, L. J., Lee, Y. N., Springston, S. R., Newman, L., and Weinstein-Lloyd, J.: Analysis of the processing of Nashville urban emissions on July 3 and July 18, 1995, Journal of Geophysical Research: Atmospheres, 105, 9155-9164, doi: 10.1029/1999jd900997, 2000.

Deiber, G., George, C., Le Calve, S., Schweitzer, F., and Mirabel, P.: Uptake study of $ClONO_2$ and $BrONO_2$ by Halide containing droplets, Atmospheric Chemistry and Physics, 4, 1291-1299, doi: 10.5194/acp-4-1291-2004, 2004.

Edwards, P. M., Young, C. J., Aikin, K., deGouw, J. A., Dubé, W. P., Geiger, F., Gilman, J. B., Helmig, D., Holloway, J. S., Kercher, J., Lerner, B., Martin, R., McLaren, R., Parrish, D. D., Peischl, J., Roberts, J. M., Ryerson, T. B., Thornton, J., Warneke, C., Williams, E. J., and Brown, S. S.: Ozone photochemistry in an oil and natural gas extraction region during winter: simulations of a snow-free season in the Uintah Basin, Utah, Atmos. Chem. Phys. Discuss., 13, 7503-7552, doi: 10.5194/acpd-13-7503-2013, 2013.

Fan, J., and Zhang, R.: Atmospheric Oxidation Mechanism of Isoprene, Environmental Chemistry, 1, 140-149, doi: 10.1071/en04045, 2004.

Finlayson-Pitts, B. J., Ezell, M. J., and Pitts, J. N.: Formation of chemically active chlorine compounds by reactions of atmospheric NaCl particles with gaseous N_2O_5 and $ClONO_2$, Nature, 337, 241-244, doi: 10.1038/337241a0, 1989.

Finley, B. D., and Saltzman, E. S.: Measurement of Cl_2 in coastal urban air, Geophysical Research Letters, 33, doi: 10.1029/2006gl025799, 2006.

Finley, B. D., and Saltzman, E. S.: Observations of Cl_2, Br_2, and I_2 in coastal marine air, Journal of Geophysical Research-Atmospheres, 113, doi: 10.1029/2008jd010269, 2008.
Foster, K. L., Plastridge, R. A., Bottenheim, J. W., Shepson, P. B., Finlayson-Pitts, B. J., and Spicer, C. W.: The role of Br_2 and BrCl in surface ozone destruction at polar sunrise, Science, 291, 471-474, doi: 10.1126/science.291.5503.471, 2001.
Hanson, D. R., and Ravishankara, A. R.: Reactive uptake of $ClONO_2$ onto sulfuric-acid due to reaction with HCl and H_2O, Journal of Physical Chemistry, 98, 5728-5735, doi: 10.1021/j100073a026, 1994.
Hanson, D. R., Ravishankara, A. R., and Solomon, S.: Heterogeneous reactions in sulfuric-acid aerosols - a framework for model-calculations, Journal of Geophysical Research-Atmospheres, 99, 3615-3629, doi: 10.1029/93jd02932, 1994.
Jenkin, M. E., Saunders, S. M., and Pilling, M. J.: The tropospheric degradation of volatile organic compounds: A protocol for mechanism development, Atmospheric Environment, 31, 81-104, doi: 10.1016/s1352-2310(96)00105-7, 1997.
Jenkin, M. E., Saunders, S. M., Wagner, V., and Pilling, M. J.: Protocol for the development of the Master Chemical Mechanism, MCM v3 (Part B): tropospheric degradation of aromatic volatile organic compounds, Atmospheric Chemistry and Physics, 3, 181-193, 2003.
Kato, S., Sato, T., and Kajii, Y.: A method to estimate the contribution of unidentified VOCs to OH reactivity, Atmospheric Environment, 45, 5531-5539, doi: 10.1016/j.atmosenv.2011.05.074, 2011.
Kercher, J. P., Riedel, T. P., and Thornton, J. A.: Chlorine activation by N_2O_5: simultaneous, in situ detection of $ClNO_2$ and N_2O_5 by chemical ionization mass spectrometry, Atmospheric Measurement Techniques, 2, 193-204, doi: 10.5194/amt-2-193-2009, 2009.
Kleinman, L. I.: The dependence of tropospheric ozone production rate on ozone precursors, Atmospheric Environment, 39, 575-586, doi: 10.1016/j.atmosenv.2004.08.047, 2005.
Lawler, M. J., Sander, R., Carpenter, L. J., Lee, J. D., von Glasow, R., Sommariva, R., and Saltzman, E. S.: HOCl and Cl_2 observations in marine air, Atmospheric Chemistry and Physics, 11, 7617-7628, doi: 10.5194/acp-11-7617-2011, 2011.
McNeill, V. F., Patterson, J., Wolfe, G. M., and Thornton, J. A.: The effect of varying levels of surfactant on the reactive uptake of N_2O_5 to aqueous aerosol, Atmospheric Chemistry and Physics, 6, 1635-1644, doi: 10.5194/acp-6-1635-2006, 2006.
Mentel, T. F., Sohn, M., and Wahner, A.: Nitrate effect in the heterogeneous hydrolysis of dinitrogen pentoxide on aqueous aerosols, Physical Chemistry Chemical Physics, 1, 5451-5457, doi: 10.1039/a905338g, 1999.
Mielke, L. H., Furgeson, A., and Osthoff, H. D.: Observation of $ClNO_2$ in a Mid-Continental Urban Environment, Environmental Science & Technology, 45, 8889-8896, doi: 10.1021/es201955u, 2011.
Osthoff, H. D., Roberts, J. M., Ravishankara, A. R., Williams, E. J., Lerner, B. M., Sommariva, R., Bates, T. S., Coffman, D., Quinn, P. K., Dibb, J. E., Stark, H., Burkholder, J. B., Talukdar, R. K., Meagher, J., Fehsenfeld, F. C., and Brown, S. S.: High levels of nitryl chloride in the polluted subtropical marine boundary layer, Nature Geoscience, 1, 324-328, doi: 10.1038/ngeo177, 2008.
Phillips, G. J., Tang, M. J., Thieser, J., Brickwedde, B., Schuster, G., Bohn, B., Lelieveld, J., and Crowley, J. N.: Significant concentrations of nitryl chloride observed in rural continental

Europe associated with the influence of sea salt chloride and anthropogenic emissions, Geophysical Research Letters, 39, doi: 10.1029/2012gl051912, 2012.
Platt, U., Allan, W., and Lowe, D.: Hemispheric average Cl atom concentration from $^{13}C/^{12}C$ ratios in atmospheric methane, Atmos. Chem. Phys., 4, 2393-2399, doi: 10.5194/acp-4-2393-2004, 2004.
Raff, J. D., Njegic, B., Chang, W. L., Gordon, M. S., Dabdub, D., Gerber, R. B., and Finlayson-Pitts, B. J.: Chlorine activation indoors and outdoors via surface-mediated reactions of nitrogen oxides with hydrogen chloride, Proceedings of the National Academy of Sciences of the United States of America, 106, 13647-13654, doi: 10.1073/pnas.0904195106, 2009.
Ren, X. R., Harder, H., Martinez, M., Lesher, R. L., Oliger, A., Simpas, J. B., Brune, W. H., Schwab, J. J., Demerjian, K. L., He, Y., Zhou, X. L., and Gao, H. G.: OH and HO_2 chemistry in the urban atmosphere of New York City, Atmospheric Environment, 37, 3639-3651, doi: 10.1016/s1352-2310(03)00459-x, 2003.
Riedel, T. P., Bertram, T. H., Crisp, T. A., Williams, E. J., Lerner, B. M., Vlasenko, A., Li, S.-M., Gilman, J., de Gouw, J., Bon, D. M., Wagner, N. L., Brown, S. S., and Thornton, J. A.: Nitryl Chloride and Molecular Chlorine in the Coastal Marine Boundary Layer, Environmental Science & Technology, 46, 10463-10470, doi: 10.1021/es204632r, 2012a.
Riedel, T. P., Bertram, T. H., Ryder, O. S., Liu, S., Day, D. A., Russell, L. M., Gaston, C. J., Prather, K. A., and Thornton, J. A.: Direct N_2O_5 reactivity measurements at a polluted coastal site, Atmospheric Chemistry and Physics, 12, 2959-2968, doi: 10.5194/acp-12-2959-2012, 2012b.
Riemer, D. D., Apel, E. C., Orlando, J. J., Tyndall, G. S., Brune, W. H., Williams, E. J., Lonneman, W. A., and Neece, J. D.: Unique isoprene oxidation products demonstrate chlorine atom chemistry occurs in the Houston, Texas urban area, Journal of Atmospheric Chemistry, 61, 227-242, doi: 10.1007/s10874-009-9134-5, 2008.
Ryerson, T. B., Andrews, A. E., Angevine, W. M., Bates, T. S., Brock, C. A., Cairns, B., Cohen, R. C., Cooper, O. R., de Gouw, J. A., Fehsenfeld, F. C., Ferrare, R. A., Fischer, M. L., Flagan, R. C., Goldstein, A. H., Hair, J. W., Hardesty, R. M., Hostetler, C. A., Jimenez, J. L., Langford, A. O., McCauley, E., McKeen, S. A., Molina, L. T., Nenes, A., Oltmans, S. J., Parrish, D. D., Pederson, J. R., Pierce, R. B., Prather, K., Quinn, P. K., Seinfeld, J. H., Senff, C. J., Sorooshian, A., Stutz, J., Surratt, J. D., Trainer, M., Volkamer, R., Williams, E. J., and Wofsy, S. C.: The 2010 California research at the Nexus of air quality and climate change (CalNex) field study, Journal of Geophysical Research: Atmospheres, n/a-n/a, doi: 10.1002/jgrd.50331, 2013.
Santschi, C., and Rossi, M. J.: The heterogeneous interaction of HOCl with solid KBr substrates: The catalytic role of adsorbed halogens, Physical Chemistry Chemical Physics, 7, 2599-2609, doi: 10.1039/b503071d, 2005.
Sarwar, G., and Bhave, P. V.: Modeling the effect of chlorine emissions on ozone levels over the eastern United States, Journal of Applied Meteorology and Climatology, 46, 1009-1019, doi: 10.1175/jam2519.1, 2007.
Sarwar, G., Simon, H., Bhave, P., and Yarwood, G.: Examining the impact of heterogeneous nitryl chloride production on air quality across the United States, Atmospheric Chemistry and Physics, 12, 6455-6473, doi: 10.5194/acp-12-6455-2012, 2012.
Saunders, S. M., Jenkin, M. E., Derwent, R. G., and Pilling, M. J.: Protocol for the development of the Master Chemical Mechanism, MCM v3 (Part A): tropospheric degradation of non-

aromatic volatile organic compounds, Atmospheric Chemistry and Physics, 3, 161-180, 2003.
Spicer, C. W., Chapman, E. G., Finlayson-Pitts, B. J., Plastridge, R. A., Hubbe, J. M., Fast, J. D., and Berkowitz, C. M.: Unexpectedly high concentrations of molecular chlorine in coastal air, Nature, 394, 353-356, doi: 10.1038/28584, 1998.
Spicer, C. W., Plastridge, R. A., Foster, K. L., Finlayson-Pitts, B. J., Bottenheim, J. W., Grannas, A. M., and Shepson, P. B.: Molecular halogens before and during ozone depletion events in the Arctic at polar sunrise: concentrations and sources, Atmospheric Environment, 36, 2721-2731, doi: 10.1016/s1352-2310(02)00125-5, 2002.
Tanaka, P. L., Allen, D. T., McDonald-Buller, E. C., Chang, S., Kimura, Y., Mullins, C. B., Yarwood, G., and Neece, J. D.: Development of a chlorine mechanism for use in the carbon bond IV chemistry model, Journal of Geophysical Research: Atmospheres, 108, 4145, doi: 10.1029/2002jd002432, 2003.
Thornton, J. A., Braban, C. F., and Abbatt, J. P. D.: N_2O_5 hydrolysis on sub-micron organic aerosols: the effect of relative humidity, particle phase, and particle size, Physical Chemistry Chemical Physics, 5, 4593-4603, doi: 10.1039/b307498f, 2003.
Thornton, J. A., Kercher, J. P., Riedel, T. P., Wagner, N. L., Cozic, J., Holloway, J. S., Dube, W. P., Wolfe, G. M., Quinn, P. K., Middlebrook, A. M., Alexander, B., and Brown, S. S.: A large atomic chlorine source inferred from mid-continental reactive nitrogen chemistry, Nature, 464, 271-274, doi: 10.1038/nature08905, 2010.
Warneke, C., Veres, P., Holloway, J. S., Stutz, J., Tsai, C., Alvarez, S., Rappenglueck, B., Fehsenfeld, F. C., Graus, M., Gilman, J. B., and de Gouw, J. A.: Airborne formaldehyde measurements using PTR-MS: calibration, humidity dependence, inter-comparison and initial results, Atmos. Meas. Tech., 4, 2345-2358, doi: 10.5194/amt-4-2345-2011, 2011.
Wolfe, G. M., and Thornton, J. A.: The Chemistry of Atmosphere-Forest Exchange (CAFE) Model – Part 1: Model description and characterization, Atmos. Chem. Phys., 11, 77-101, doi: 10.5194/acp-11-77-2011, 2011.
Young, C. J., Washenfelder, R. A., Roberts, J. M., Mielke, L. H., Osthoff, H. D., Tsai, C., Pikelnaya, O., Stutz, J., Veres, P. R., Cochran, A. K., VandenBoer, T. C., Flynn, J., Grossberg, N., Haman, C. L., Lefer, B., Stark, H., Graus, M., de Gouw, J., Gilman, J. B., Kuster, W. C., and Brown, S. S.: Vertically Resolved Measurements of Nighttime Radical Reservoirs; in Los Angeles and Their Contribution to the Urban Radical Budget, Environmental Science & Technology, 46, 10965-10973, doi: 10.1021/es302206a, 2012.

Pasadena (GC-MS)	R/V Atlantis (GC-FID)	R/V Atlantis (PTR-ToF-MS)	median (pptv)	1σ
methanol	methanol		1220	180
ethanol			1540	200
isopropanol			320	50
ethanal	ethanal		370	150
methacrolein			10	10
propanal			90	20
butanal			20	4
ethane			3120	440
propane		propane	1940	330
i-butane		i-butane	510	70
n-butane		n-butane	1200	190
i-pentane			780	100
n-pentane		n-petane	350	40
hexane			250	30
nonane			40	2
decane			36	2
undecane			34	4
ethene		ethene	900	100
propene		propene	250	60
cis-2-butene			10	2
1-butene		1-butene	25	5
2-methylpropene			80	20
1,3-butadiene			44	17
trans-2-butene			33	7
ethyne		ethyne	320	40
propylbenzene			15	1
isopropylbenzene			5	1
benzaldehyde			40	8
benzene	benzene	benzene	65	5
ethylbenzene			25	2
o-methylethylbenzene			4	1
1,3,5-trimethylbenzene			10	3
phenylethene			14	2
1,2,4-trimethylbenzene			25	5
o-xylene			30	3
toluene	toluene	toluene	140	13
1,2,3-trimethylbenzene			8	2
methylvinylketone			16	25
acetone	acetone		740	260
methylethylketone			53	27
alphapinene			13	8
betapinene			8	4
limonene			9	7
isoprene			30	180

Table 6.1 VOC measured during CalNex 2010 at the Pasadena, CA, ground site and aboard the R/V *Atlantis* and used as model constraints. Medians and standard deviations (1σ) for the diurnal values used in the model are also given.

Figure 6.1 Methanol oxidation mechanism by atomic chlorine added to the model reactions.

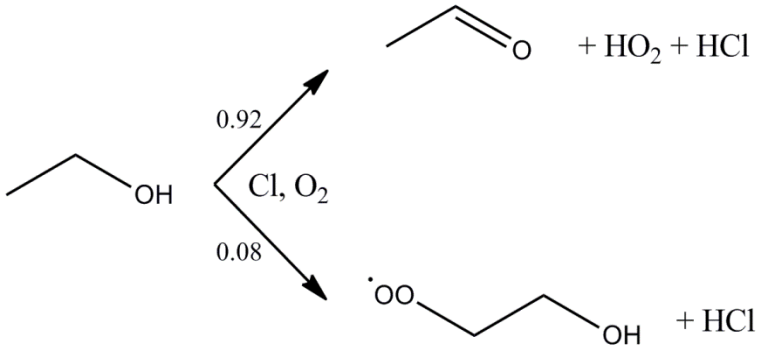

Figure 6.2 Ethanol oxidation mechanism by atomic chlorine added to the model reactions.

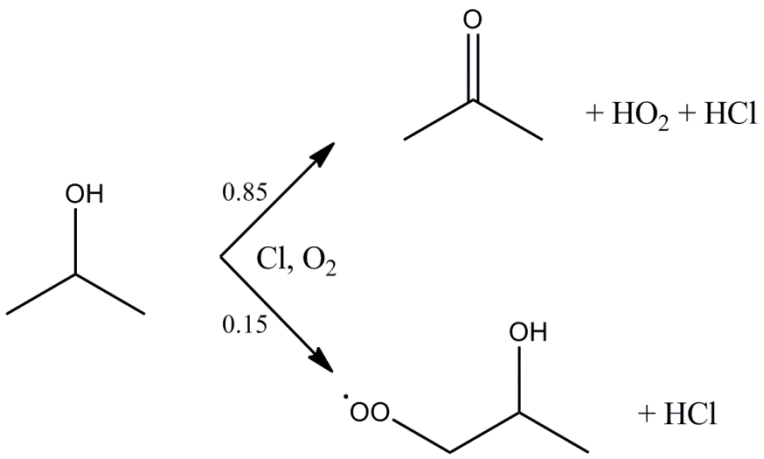

Figure 6.3 Isopropanol oxidation mechanism by atomic chlorine added to the model reactions.

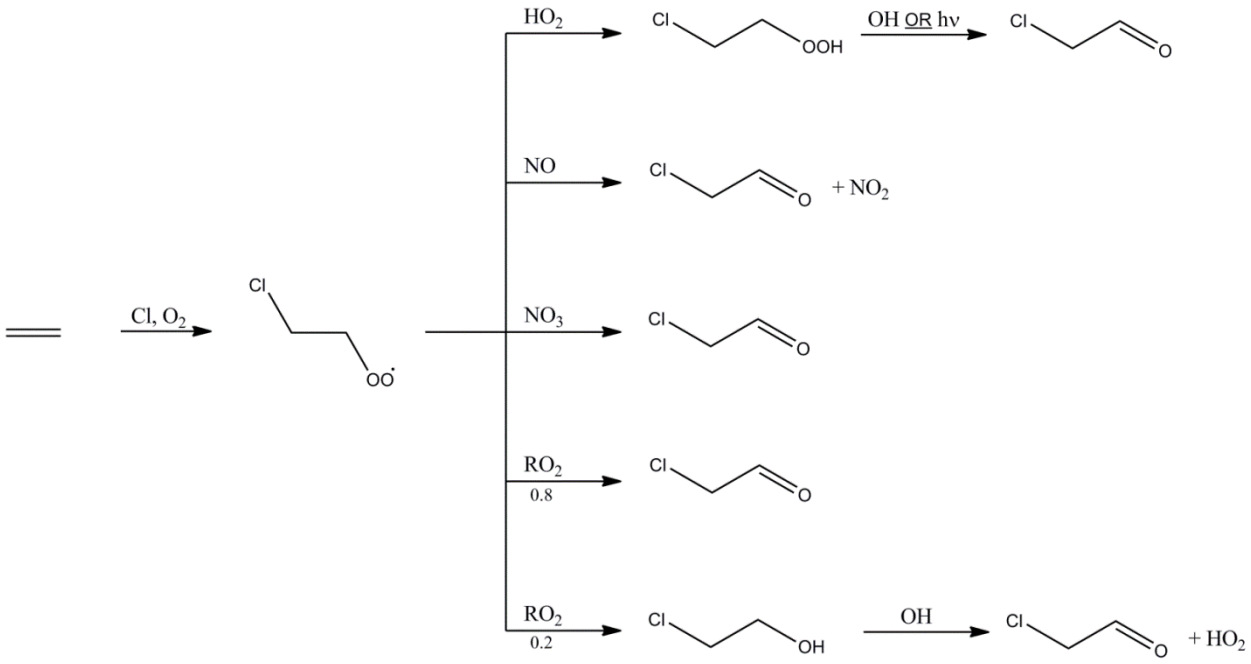

Figure 6.4 Ethene oxidation mechanism by atomic chlorine added to the model reactions.

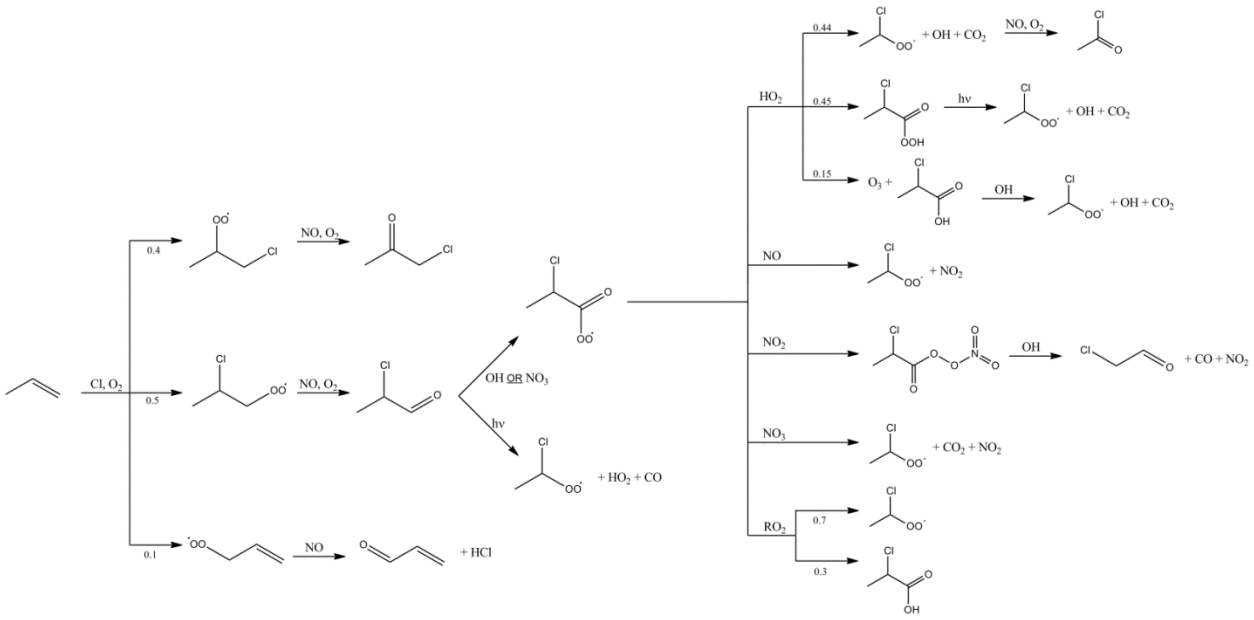

Figure 6.5 Propene oxidation mechanism by atomic chlorine added to the model reactions.

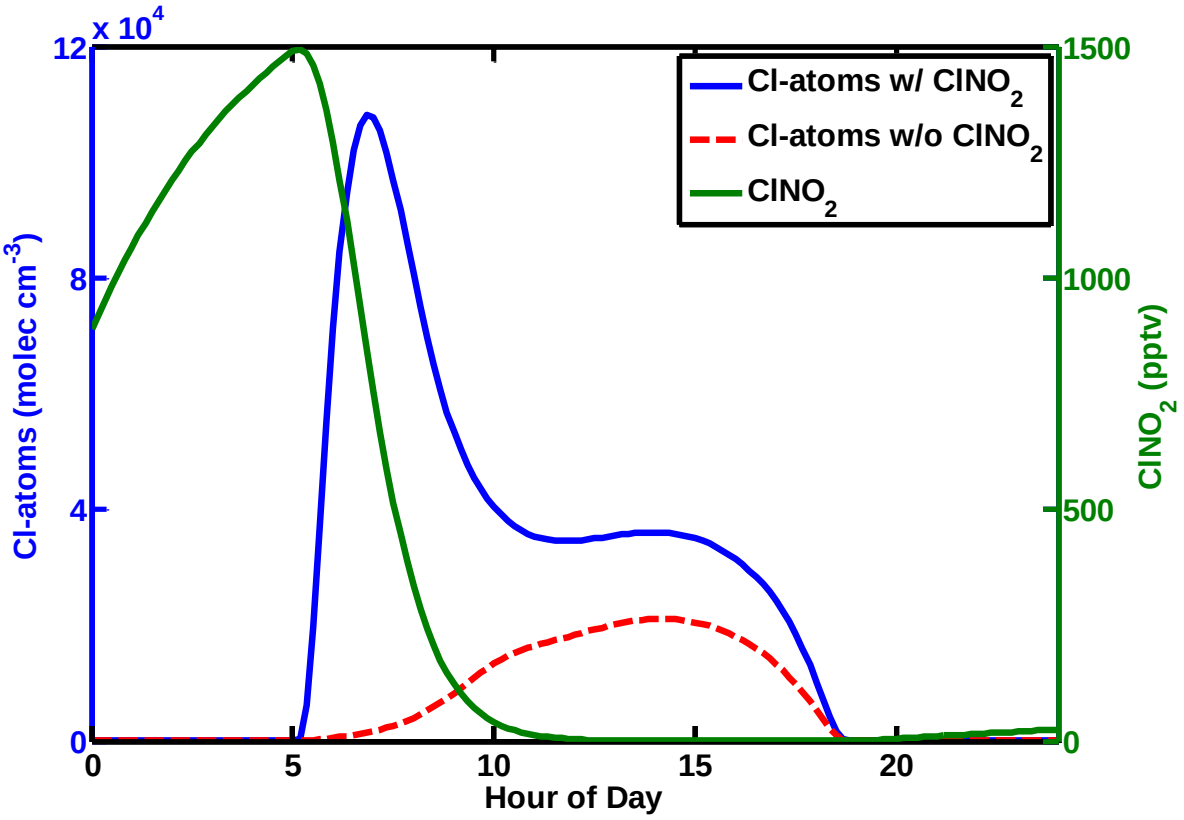

Figure 6.6 Output for the analysis period of a model run showing $ClNO_2$ mixing ratios (heavy green line, right y-axis) and Cl· concentrations for the case including $ClNO_2$ formation (heavy blue line, left y-axis) and the case excluding $ClNO_2$ formation (dashed red line, left y-axis).

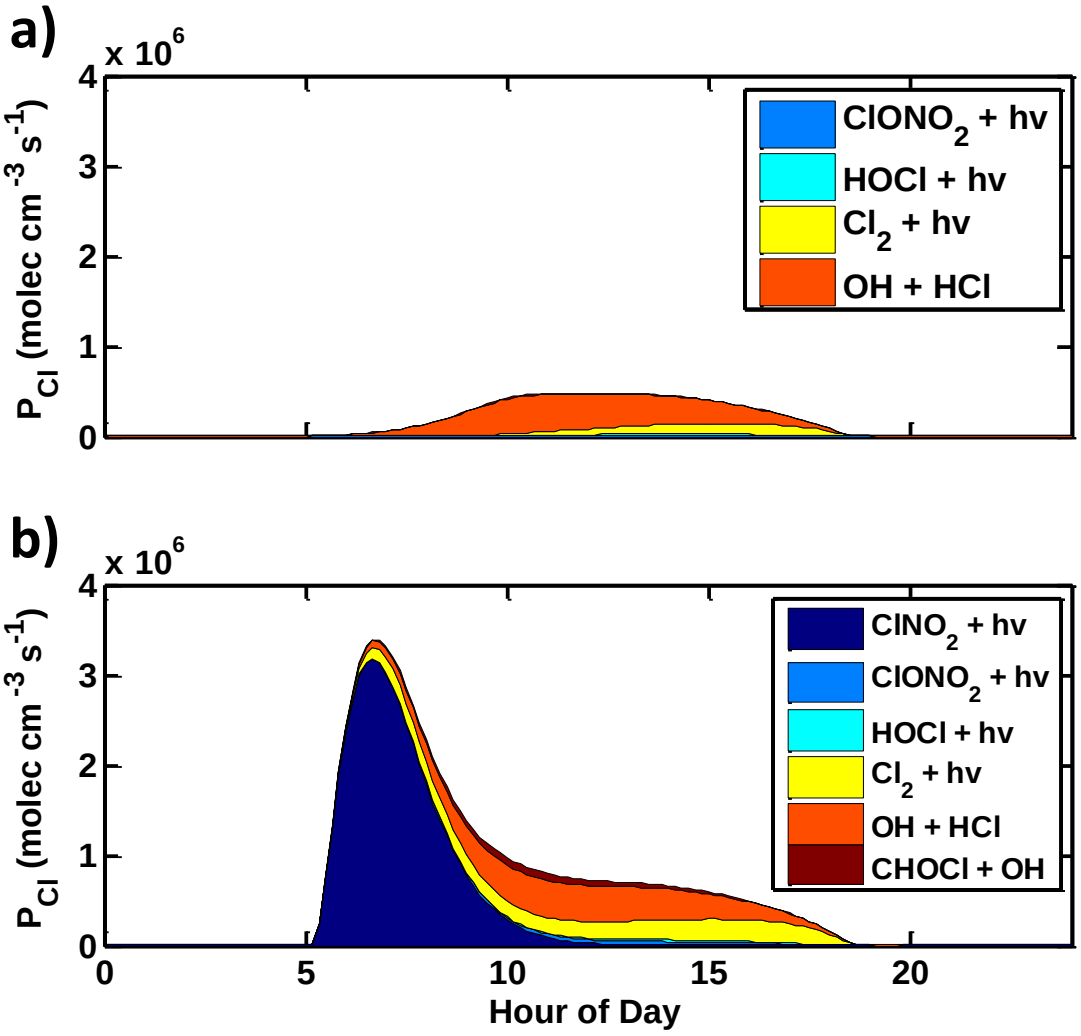

Figure 6.7 Model output of Cl· production channels a) without $ClNO_2$ formation (top) and b) with $ClNO_2$ formation (bottom).

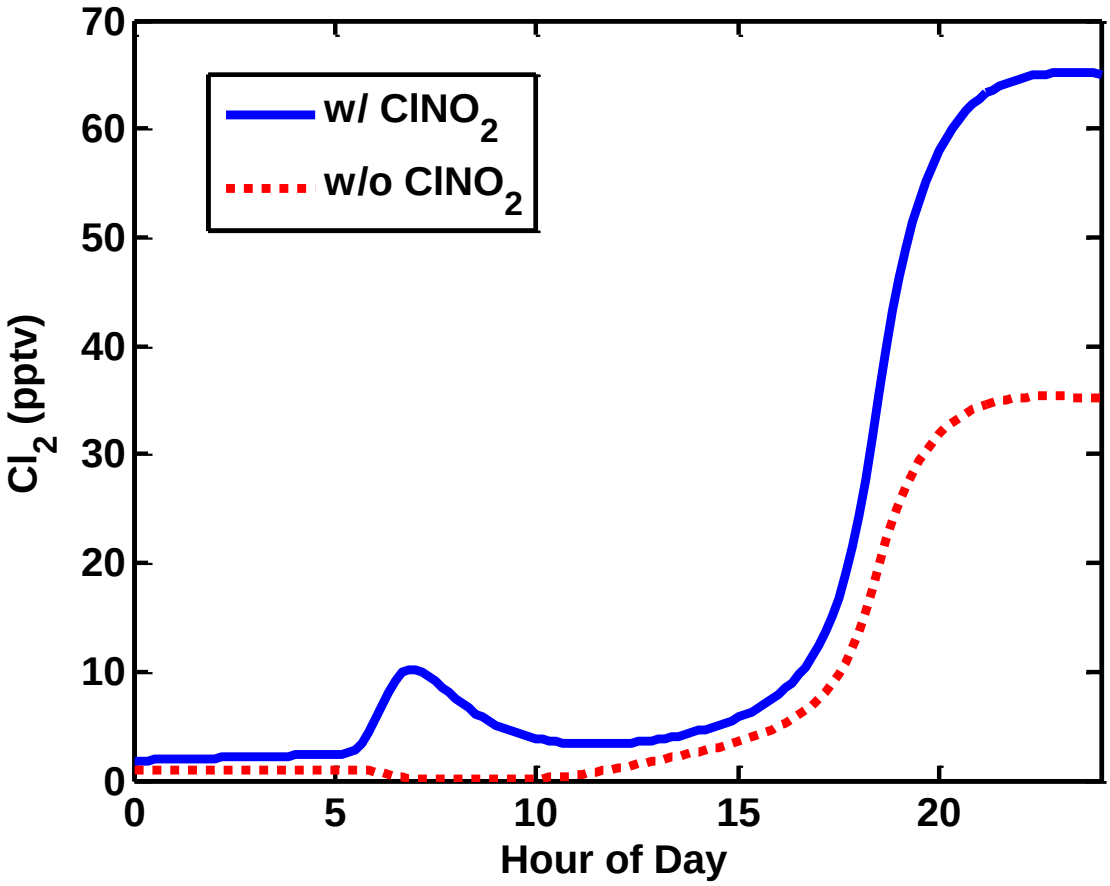

Figure 6.8 Effects of $ClNO_2$ on the molecular chlorine (Cl_2) levels during a model run.

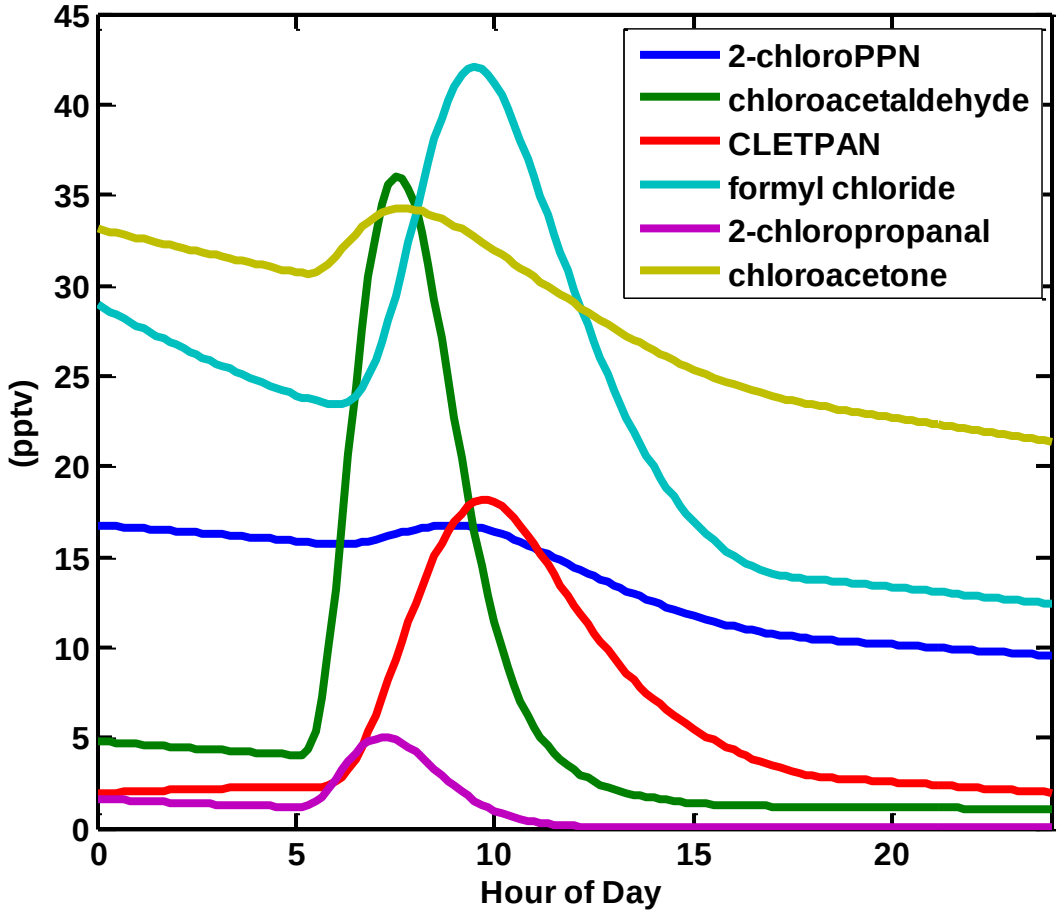

Figure 6.9 Modeled enhancements in chlorinated species resulting from the inclusion of $ClNO_2$ formation.

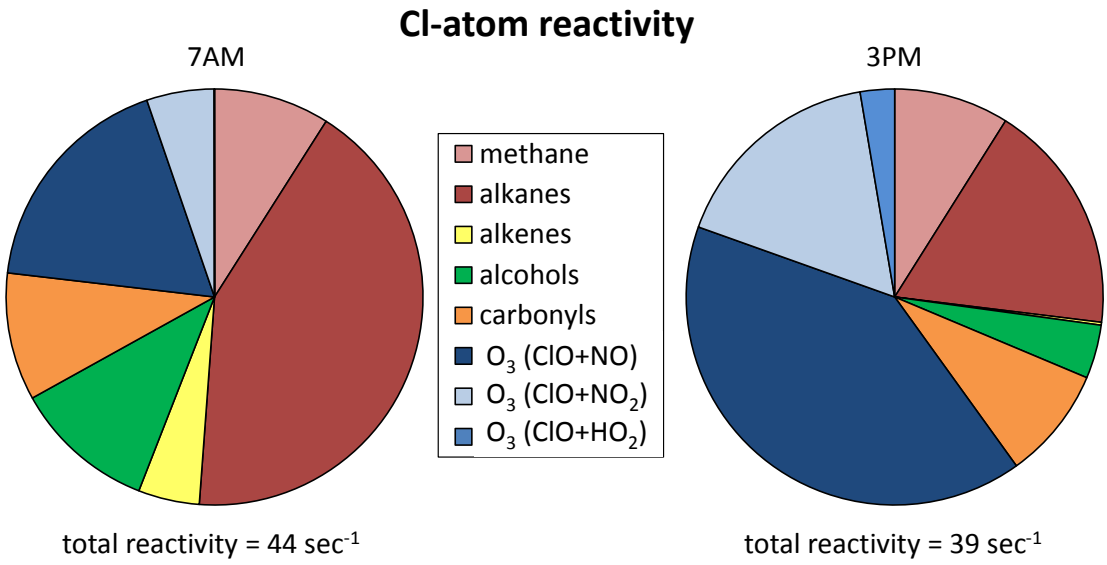

Figure 6.10 Modeled Cl· reactivity at 7 AM (left) and 3 PM (right) grouped by reactant types.

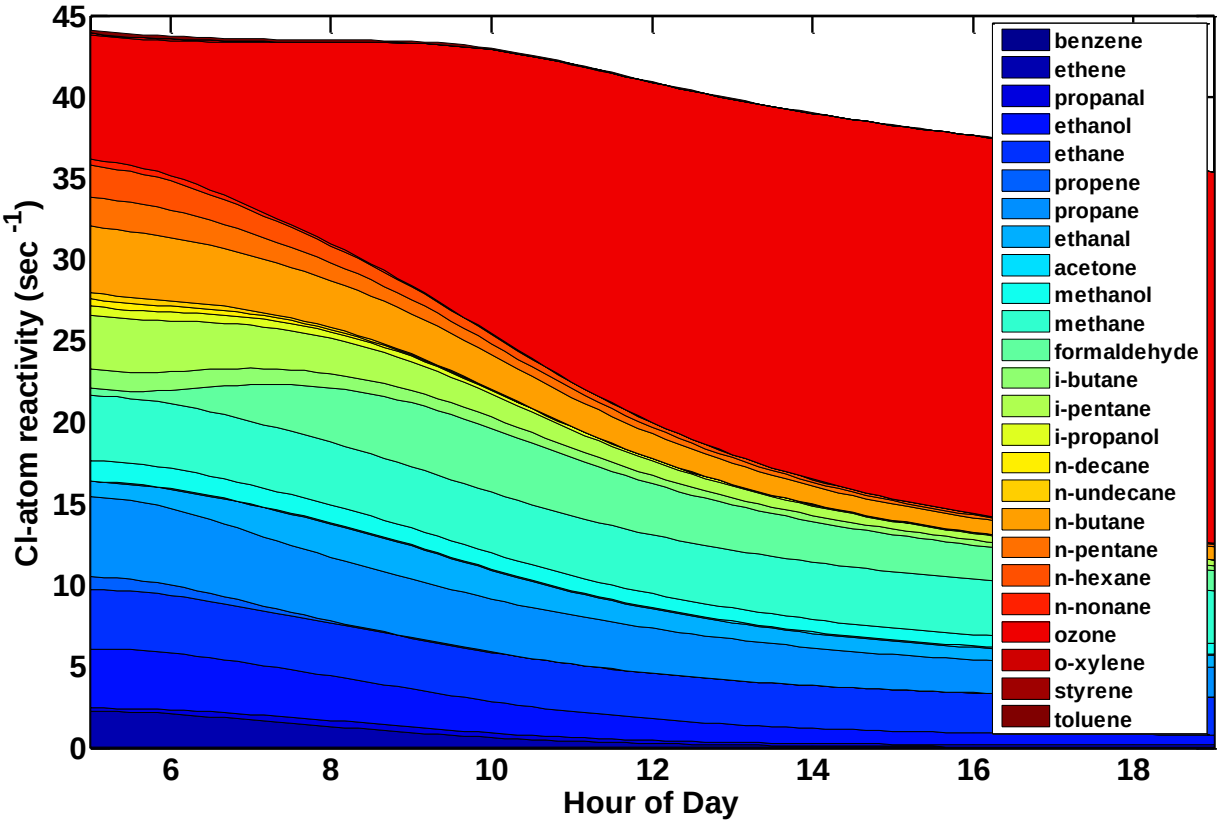

Figure 6.11 Speciated Cl-atom reactivity over the course of a model day.

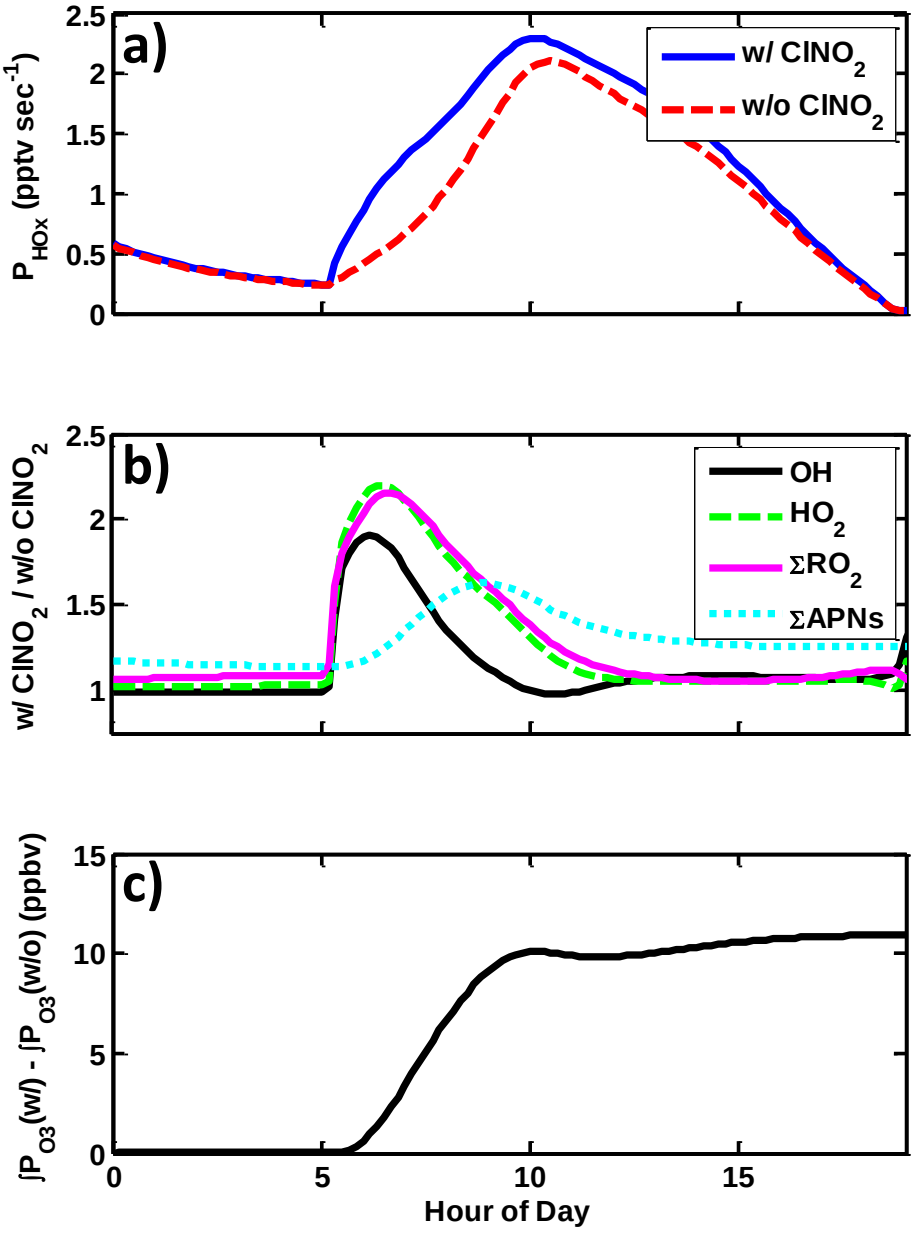

Figure 6.12 a) the HO_x production rate with $ClNO_2$ formation (solid blue line) and without $ClNO_2$ formation (dashed red line). b) The enhancement ratio of the hydroxyl radical (solid black line), hydroperoxyl radical (dashed green line), sum of organic peroxy radicals (solid pink line), and sum of acyl peroxy nitrates (dotted cyan line) for the with-$ClNO_2$ case relative to the without-$ClNO_2$ case. c) The difference between the integrated ozone production rate with $ClNO_2$ formation and the integrated ozone production rate without $ClNO_2$ formation.

Chapter 7

Conclusions

In the years since I have started my graduate work, nitryl chloride has gone from a theorized nocturnal NO_x reservoir likely confined to marine environments at mixing ratios of a few tens of pptv to a chemical measured in ambient air at a growing number of coastal and inland locations with mixing ratios exceeding 1 ppbv. The majority of these observations were taken using a chemical ionization mass spectrometry measurement technique I helped to develop. As shown in Chapter 2, our observations of $ClNO_2$ in Boulder, CO – about 1400 km from any source of sea salt – on nearly every night that the NO_x-rich urban plume was sampled coupled with estimates of $ClNO_2$ formation over the contiguous United States took this chemistry from primarily coastal phenomena to that of global importance. Despite these advances, uncertainties still remain concerning the reactivity of N_2O_5, the distribution of chloride mass across the particle size distribution, and inland sources of HCl and particulate chloride. Ultimately these limit the accuracy of our extrapolations and support the need for better constraints on N_2O_5 reactivity, quantitative single particle composition measurements, and measurements of gas phase acid concentrations and their partitioning to particles. Nonetheless, our approaches suggest that between 1 – 5 Tg Cl from $ClNO_2$ could be produced each year across the U.S. alone which, as we said, is similar to that estimated for global marine boundary layer regions. These estimates indicate that $ClNO_2$ potentially plays a substantial role in the global chlorine atom budget, much larger than was previously thought, with implications for the role of anthropogenic activities on the tropospheric halogens.

In an effort to reduce some of the uncertainties I just described, direct measurements of N_2O_5 reactivity on ambient aerosol particles were made during September 2009 and described in Chapter 3. Measurements were performed at the Scripps Institution of Oceanography (SIO) Pier facility located in La Jolla, CA, using a recently developed custom flow reactor and the particle modulation technique with measurements of aerosol particle size distributions and non-refractory composition. The pseudo-first order rate coefficients derived from this technique and the particle surface area concentrations were used to determine the population average N_2O_5-aerosol reaction probabilities, $\gamma(N_2O_5)$, with a time resolution of approximately 50 minutes. Air quality models used to guide policy decisions must simplify these complex reactions for the ease of computation. These parameterizations, as with any atmospheric model framework, need to be verified by ambient observations to ensure such models accurately represent the processes at work. We compare these data to a recent N_2O_5 reactivity parameterization that utilizes aerosol composition measurements and an aerosol thermodynamic model. The parameterization captures several aspects of the measurements well with similar general trends over the time series. However, the parameterization persistently overestimates the measurements by a factor of 1.5 – 3 and fails to illustrate the same small scale variability. Assuming chloride is internally mixed across the particle population leads to the largest overestimates. Removing this assumption only partially reduces the discrepancies, suggesting that other unaccounted for particle characteristics can suppress $\gamma(N_2O_5)$ are important, such as organic coatings or non-aqueous particles. Given the immense number of potential VOC present in the atmosphere at a given location and the variety in their reactivity and particle partitioning, assessing the role organic species in the gas and particle phases represents one of the single most challenging aspects of modern atmospheric chemistry. How organics behave in and affect the particle phase state of aerosols has large

potential effects on $\gamma(N_2O_5)$. A complete parameterization that takes into account all of these variables is the ultimate goal. That said, the relative variability in $\gamma(N_2O_5)$ with nitrate (termed the "nitrate effect") was well represented in the parameterization when compared to the ambient observations. This relative change in measured $\gamma(N_2O_5)$ as a function of particle nitrate loading appears to be consistent with expectations based on laboratory data from which such parameterizations are developed, providing direct support for the atmospheric importance of the nitrate effect.

The magnitude and sources of chlorine atoms in marine air remain highly uncertain but have potentially important consequences for air quality in polluted coastal regions. In Chapter 4 we discuss the continuous measurements of ambient $ClNO_2$ and Cl_2 concentrations taken from May 15 to June 8 aboard the Research Vessel *Atlantis* during the CalNex 2010 field study which help gage the most important sources of chlorine atoms in polluted marine environments. In the Los Angeles region, $ClNO_2$ was more ubiquitous than Cl_2 during most nights of the study period. The maxima in both species were observed in the Los Angeles urban outflow only a few miles off the coast. While Cl_2 and $ClNO_2$ have been proposed to be directly linked via heterogeneous chemistry, the majority of the correlation between Cl_2 and $ClNO_2$ was likely due to similar source regions. At other times, however, there was little to no correlation between the two, implying distinct and varying sources. Well-confined Cl_2 plumes were observed due west of Los Angeles, largely independent of $ClNO_2$, providing support for local industrial emissions of reactive chlorine. These observations of $ClNO_2$ and Cl_2 as well as observations of HCl were used to constrain a simple box model that predicts their relative importance as chlorine atom sources in the polluted marine boundary layer. In contrast to the emphasis of previous marine studies in

which consider Cl_2 the main source of chlorine atoms, $ClNO_2$ and HCl are dominant primary chlorine atom sources for the Los Angeles basin.

From the discussions above it is apparent that regions with strong anthropogenic activity have large $ClNO_2$ formation potential. This includes inland regions due to transport or local emissions of soluble chloride. Chapter 5 detailed the NACHTT field study, where we recorded the first wintertime vertically resolved $ClNO_2$ and Cl_2 measurements taken on a 300 meter tall tower located at NOAA's Boulder Atmospheric Observatory in Weld County, CO, during February and March of 2011. Gas and particle phase measurements aboard the tower carriage allowed for a detailed description of the chemical state of the nocturnal atmosphere as a function of height. Apart from a sparse number of summertime airplane measurements, these observations show the first significant vertical structures in $ClNO_2$ and Cl_2. In particular we select two distinct combustion plume events where $ClNO_2$ mixing ratios surpassed 500 pptv well aloft of the nocturnal surface layer. From these events we infer efficient $ClNO_2$ production from N_2O_5-aerosol reactions using observational constraints and box modeling. The derived yields in these plumes suggest $ClNO_2$ production comparable to that of marine regions. These yields show substantial night-to-night and within night variability which correlates well with ambient relative humidity and suggest that the most efficient continental $ClNO_2$ formation likely occurs in combustion plumes where N_2O_5 precursors and chloride are coemitted.

Finally, in Chapter 6 we examine the potential fate of the chlorine atoms liberated by $ClNO_2$ formation and the overall impact of $ClNO_2$ on regional photochemistry. This is accomplished through the incorporation of $ClNO_2$ production, photolysis, and subsequent chlorine atom reactions into an existing Master Chemical Mechanism (MCM version 3.2) box model framework using observational constraints from the CalNex 2010 field study introduced

in Chapter 4. Chlorine atom reactions with a set of alkenes and alcohols, and the simplified multiphase chemistry of N_2O_5, $ClNO_2$, HOCl, $ClONO_2$, and Cl_2, none of which are part of the MCM, were added to the mechanism. Relative to model runs excluding $ClNO_2$ formation, the presence of $ClNO_2$ produces marked changes important to oxidants, ozone, and nitrogen oxide partitioning, all of which can have large potential effects on air quality. Modeled chlorine atoms from $ClNO_2$ were found to react predominantly with a large suite of volatile organic compounds (VOC) to produce more organic peroxy radicals in the morning hour. In the presence of several ppbv of NO_x, these perturbations lead to similar enhancements in HO_x. Neglecting contributions from HONO, the total integrated daytime radical source is 17% larger when including $ClNO_2$ which in turn leads to a similar enhancement in integrated ozone production of 15%. VOC and NO_x lifetimes are shorter in the model run that includes $ClNO_2$ formation, primarily due to enhanced morning OH. These results also challenge the fundamental idea that reactions of nocturnal NO_x species represent a net sink for odd-oxygen. $ClNO_2$ formation in the model was shown to have the potential to reduce the efficiency of nocturnal loss reactions to the point that nocturnal reactions could potentially result in a net source of odd-oxygen. Additionally, potentially detectable levels of chlorine containing organic compounds are predicted to form as a result of chlorine addition to alkenes, which may be useful in identifying times of active chlorine atom chemistry. The effects implied by these model studies illustrate the same general message as all of the findings outlined in this dissertation: $ClNO_2$ is an important component of nocturnal NO_x and should be considered in model studies as its effects can be far reaching. Not only is it a significant reservoir of NO_x, but the activation of reactive chlorine atoms can influence a number of important tropospheric chemical reactions. In order to appropriately understand the effects of

$ClNO_2$, it is also critical that the heterogeneous reaction kinetics of N_2O_5, which precede and as a result are inherently tied to any $ClNO_2$ formation, be better constrained.

While predicted effects based on ambient concentrations and modeling of $ClNO_2$ appear to be substantial, these predictions, as with all atmospheric chemistry phenomena, need to be further probed and demonstrated through field observations and atmospheric chemical models in order to confirm such effects. The challenge in dealing with chlorine atoms is that they cannot be measured directly given their low concentrations and short chemical lifetime in ambient air. As such, indirect measurements must be employed. The MCM modeling described above highlights one potential avenue that might confirm active chlorine atom chemistry resulting from $ClNO_2$. Predawn measurements of $ClNO_2$ concentrations coupled with co-located morning enhancements of chlorinated species or HCl would represent a particularly strong case. Similar measurements of other predicted enhancements to OH, HO_2, RO_2, etc. would also be beneficial. Incorporation of $ClNO_2$ formation, photolysis, and subsequent chlorine atom chemistry into large scale chemical and air quality models is also a necessary step toward assessing the importance of this chemistry. Whether or not such models can include these reactions and still accurately predict and reproduce preexisting observations remains to be seen.

Appendix

List of Coauthors/Contributors

Portions of Chapter 2 were previously published with the following authors:

J. A. Thornton[2], J. P. Kercher[1], T. P. Riedel[1,2], N. L. Wagner[3], J. Cozic[3,4], J. S. Holloway[3,4], W. P. Dubé[3,4], G. M. Wolfe[1,2], P. K. Quinn[5], A. M. Middlebrook[3], B. Alexander[2], S. S. Brown[3]

Chapter 3 was previously published with the following authors:

T. P. Riedel[1,2], T. H. Bertram[6], O. S. Ryder[6], S. Liu[7], D. A. Day[7,4], L. M. Russell[7], C. J. Gaston[7], K. A. Prather[6,7], J. A. Thornton[2]

Chapter 4 was previously published with the following authors:

T. P. Riedel[1,2], T. H. Bertram[6], T. A. Crisp[6], E. J. Williams[3,4], B. M. Lerner[3,4], A. Vlasenko[8], S.-M. Li[8], J. Gilman[3,4], J. de Gouw[3,4], D. M. Bon[3,4,9], N. L. Wagner[3,4], S. S. Brown[3], J. A. Thornton[2]

Chapter 5 has been submitted for publication with the following authors:

T. P. Riedel[1,2], N. L. Wagner[3,4], W. P. Dubé[3,4], A. M. Middlebrook[3], C. J. Young[10], F. Öztürk[11], R. Bahreini[12], T. C. VandenBoer[13], D. E. Wolfe[3], E. J. Williams[4], J. M. Roberts[3], S. S. Brown[3], J. A. Thornton[1,2]

Chapter 6 is in preparation for publication with the following authors:

T. P. Riedel[1,2], G. M. Wolfe[14], K. Danas[2], J. B. Gilman[3,4], W. C. Kuster[3,4], J. A. de Gouw[3,4], D. M. Bon[3,4], A. Vlasenko[8], S.-M. Li[8], E. J. Williams[3,4], B. M. Lerner[3,4], P. R. Veres[3,4], J. M. Roberts[3], J. S. Holloway[4], B. Lefer[15], J. A. Thornton[2]

Coauthor/Contributor Affiliations

[1]Department of Chemistry, University of Washington, Seattle, Washington, USA

[2]Department of Atmospheric Sciences, University of Washington, Seattle, Washington, USA

[3]NOAA Earth System Research Laboratory, Boulder, Colorado, USA

[4]Cooperative Institute for Research in Environmental Sciences, University of Colorado, Boulder, Colorado, USA

[5]NOAA Pacific Marine Environmental Laboratory, Seattle, Washington, USA

[6]Department of Chemistry and Biochemistry, University of California, San Diego, California, USA

[7]Scripps Institution of Oceanography, San Diego, California, USA

[8]Air Quality Research Division, Science and Technology Branch, Environment Canada, Canada

[9]Department of Chemistry and Biochemistry, University of Colorado, Boulder, Colorado, USA

[10]Department of Chemistry, Memorial University of Newfoundland, St. Johns, Newfoundland, Canada

[11]Environmental Engineering Department, Abant Izzet Baysal University, Bolu, Turkey

[12]Department of Environmental Sciences, University of California Riverside, Riverside, CA, USA

[13]Department of Chemistry, University of Toronto, Toronto, Ontario, Canada

[14]Joint Center for Earth Systems Technology, University of Maryland, Baltimore County, Baltimore, Maryland, USA

[15]Department of Earth and Atmospheric Sciences, University of Houston, Houston, Texas, USA

Vita

Theran P. Riedel was born in central Wisconsin. Named after a Wisconsin Badgers' ice hockey defenseman, hockey was his primary focus from a very young age until he graduated high school. At the University of Wisconsin – Eau Claire his focus turned to academics and Green Bay Packers football. Here in 2007, Theran received a degree in Chemistry with a minor in Geology. After being introduced to intricacies of research by Professor Marc McEllistrem, graduate school seemed like a logical next step. Lured to the Pacific Northwest by the North Cascades and the extraordinary summers, Theran chose to continue studying chemistry at the University of Washington in Seattle. After an exceptionally enjoyable course taught by his future advisor, Joel Thornton, during his first quarter of graduate school, it was clear that atmospheric chemistry would be his new focus. Though his loyalty to the Green Bay Packers and a newly cultivated interest in ultimate frisbee always represented welcomed distractions, Theran graduated with a Ph.D. in Chemistry in 2013.